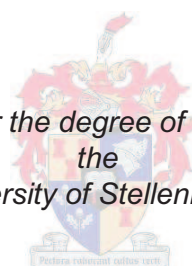


**Novel electrospun fibres of
amphiphilic organic-inorganic graft
copolymers of poly(acrylonitrile)-graft-
poly(dimethylsiloxane) for silicone
composite reinforcement**

by

Gareth Michael Bayley

*Dissertation presented for the degree of PhD (Polymer Science) at
the
University of Stellenbosch*



Promoter: Prof. Peter Edward Mallon

Faculty of Natural Sciences
Department of Chemistry and Polymer Science

December 2011

Declaration

By submitting this thesis/dissertation electronically, I declare that the entirety of the work contained therein is my own, original work, that I am the sole author thereof (save to the extent explicitly otherwise stated), that reproduction and publication thereof by Stellenbosch University will not infringe any third party rights and that I have not previously in its entirety or in part submitted it for obtaining any qualification.

December 2011

Copyright © 2011 University of Stellenbosch

All rights reserved

Abstract

Novel silicone nanocomposites were prepared using poly(acrylonitrile) (PAN) based reinforcing fibres as well as multi-walled carbon nanotubes (MWCNTs). Compatibility of the fibre fillers with the silicone matrix required the synthesis of novel amphiphilic, organic–inorganic graft copolymers of PAN and poly(dimethylsiloxane) (PAN-g-PDMS). These fibre precursor materials were synthesised via the “grafting through” technique using conventional free radical copolymerisation. The PDMS macromonomer content in the feed was varied from 5 wt% to 25 wt% and the molecular weights of the macromonomer were 1000 g.mol⁻¹ and 5000 g.mol⁻¹. The solvent medium of the precipitation reaction was optimised at a volume ratio of 98% benzene to 2% dimethylformamide (DMF). Successful incorporation of PDMS yielded graft copolymer blend materials of PAN-g-PDMS, blended with PAN homopolymer and unreacted PDMS macromonomer. A gradient elution profile was developed to track the successful removal of the PDMS macromonomer via hexane extraction. The gradient profile showed that as the PDMS content in the feed increased, the number of graft molecules in the blend increased relative to the number of PAN homopolymer molecules. The crystallisability of the PAN segments was shown to decrease as the PDMS content increased. The synthesised polymer was used as precursor material for the electrospinning of fibre fillers. The electrospinning of the precursor material was successfully achieved using 100% DMF as electrospinning solution medium. The amphiphilic nature of the precursor material in DMF resulted in self-assembled aggregate structures in the electrospinning solution. An increasing PDMS content was shown to affect the aggregation of the precursor material, and resulted in an increase in the solution viscosity. The “gel-like” solutions limited the achievable fibre morphological control when altering conventional electrospinning parameters such as voltage, tip-to-collector distance, and solution concentrations. The rapid evaporation and stretching of the solution during electrospinning, combined with the phase segregated amphiphilic molecules in solution and the crystallisation of the PAN segments resulted in (non-equilibrium morphology) fully porous fibres. The crystallinity was shown to decrease after electrospinning of the fibre precursor materials. Successful incorporation of surface oxidised MWCNTs into the electrospun fibres was achieved. The content of nanotubes was varied from 2 wt% to 32 wt%. The MWCNTs reduced the mean fibre diameters by acting as cross-linkers between the PAN segments and increasing the solution conductivity. The nanotubes dispersed well throughout the porous structure of the fibres and aligned in the direction of the fibre axis. Fabrication of silicone composites containing non-woven and aligned fibre mats (with 8 wt% MWCNTs in the fibres, and without) was successfully

achieved. The compatibilisation of the PDMS surface segregated domains allowed excellent dispersion and interaction of the PAN based fibre fillers with the silicone matrix. Mechanical analysis showed improved properties as the PDMS content in the fibre increased. The highest PDMS content fibres did, however, exhibit decreased properties. This was ascribed to increased PDMS (soft and weak) content, decreased crystallinity and increased fibre diameter (lower interfacial area). Dramatic improvements in strength, stiffness, strain and toughness were achieved. The most significant result was an increase in strain of 470%. The mechanical results correlated with results of SEM analysis of the fracture surfaces. The dramatic improvements in properties were a result of the fibre strength and ductility, as well as the mechanism of composite failure.

Opsomming

Nuwe silikonnanosamestellings is berei deur gebruik te maak van poli(akrilonitriël) (PAN) gebaseerde versterkende vesels wat multi-ommuurde koolstof nanobuisies bevat het. Versoenbaarheid van die vesels met die silikonmatriks het die sintese van nuwe amfiliese, organies–anorganiese ent-kopolimere van PAN en poli(dimetiëlsiloksaan) (PAN-g-PDMS) benodig. Die vesel voorloper materiaal is deur middel van 'n "ent-deur" vryeradikaal-kopolimerisasie gesintetiseer. Die inhoud van die PDMS makromonomeer in die reaksie het gewissel vanaf 5% tot 25%. Die gebruik van twee verskillende molekulêre massas makromonomeer is bestudeer (1000 en $5000 \text{ g}\cdot\text{mol}^{-1}$). Die optimale oplosmiddelmengsel vir die neerslagreaksie was 'n volume verhouding van 98% benseen tot 2% dimetiëlfornamied (DMF). Suksesvolle insluiting van PDMS het versnitmateriale van PAN-g-PDMS kopolimere gemeng met PAN homopolimere en ongereageerde PDMS makromonomeer gelewer. 'n Gradiënt-eluering-chromatografiese profiel is ontwikkel om die suksesvolle verwydering van die PDMS makromonomeer via heksaanekstraksie te bepaal. Die gradiëntprofiel het aangetoon dat indien die PDMS inhoud in die reagent verhoog is, die aantal entmolekules relatief tot PAN homopolimeermolekules ook verhoog het. 'n Toename in PDMS inhoud het egter 'n afname in kristallasie van die PAN segmente tot gevolg gehad. Die gesintetiseerde polimeer is gebruik as die beginmateriaal vir die elektrospinning van veselvallers. Die elektrospinning van die beginmateriaal was suksesvol wanneer 100% DMF as elektrospinningoplosmiddel gebruik is. Die amfiliese aard van die beginmateriaal in DMF lei tot outokonstruksie van aggregeatstrukture in die elektrospinningoplossing. Toenemende PDMS inhoud beïnvloed die outokonstruksie van die molekules in oplossing en het gelei tot 'n toename in die oplossings se viskositeit. Die "gelagtige" oplossings beperk die haalbare vesel se morfologiese beheerbaarheid wanneer konvensionele elektrospinning parameters soos elektriese spanning, punt-tot-versamelaar afstand, en oplossingkonsentrasies gewysig word. Die vinnige verdamping en strek van die oplossing tydens elektrospinning, gekombineer met die fase-geskeide amfiliese molekules in oplossing en die kristallasie van die PAN segmente, het gelei tot (nie-ewewig morfologie) volledige poreuse vesels. Die kristalliniteit van die veselbeginmateriaal het afgeneem nadat elektrospinning toegepas is. Die insluiting van die oppervlak-geoksideerde multi-ommuurde koolstof nanobuisies in die elektrogespinde vesels was suksesvol. Die inhoud van die nanobuisies het gewissel van 2 wt% tot 32 wt%. Die nanobuisies het die gemiddelde veseldeursnit verminder deur op te tree as kruisbinders tussen die PAN segmente van die molekules. Die nanobuisies was goed versprei deur die poreuse struktuur van die vesels en dit was gerig in die rigting van die vesel-as.

Bereiding van die silikonsamestellings bestaande uit nie-geweefde en gerigte veseloppervlakke (met en sonder 8 wt% multi-ommuurde koolstof nanobuisies in die vesel) was suksesvol. Die versoenbaarheid tussen die oppervlak van die PDMS-geskeide gebiede en die silikonmatriks laat uitstekende verspreiding en interaksie van die PAN-gebaseerde veselvullers met die silikonmatriks toe. Meganiese analise het aangetoon dat die fisiese eienskappe verbeter het namate die PDMS inhoud in die vesel vermeerder het. Die vesels met die hoogste PDMS inhoud het egter verswakke eienskappe getoon. Dit is toegeskryf aan 'n verhoogde PDMS inhoud (sag en swak), 'n afname in kristalliniteit en 'n verhoogde veseldeursnit (laer grensoppervlakke). Dramatiese verbeterings in sterkte, styfheid, verlengbaarheid, vervorming en taaiheid is bereik. Die mees betekenisvolle gevolg was 'n toename in die verrekking van 470%. Die meganiese resultate is gekorreleer met SEM ontleding van die brekingsoppervlakke. Die veselkrag en vervormbaarheid, sowel as die meganisme van die splyting van die samestellings, het tot die dramatiese verbeterings in die meganiese eienskappe gelei.

Acknowledgments

Firstly, I would like to thank my supervisor Prof P.E. Mallon, for all the support, guidance and opportunities he has afforded me during this project. Thank you for always having an open door!

I thank the following people for their tireless work in analysing my samples. Jean McKenzie and Elsa Malherbe for their friendliness and great help with NMR analysis. Mohamed Jaffe from UCT for TEM analysis and the pleasant chats while scanning for those sometimes elusive images.

Thanks to Prof. Mikael Hedenqvist from KTH, Swedish Royal Institute of Technology, for arranging use of their FE-SEM instrument and tensile testing equipment.

Thomas Blomveldt from KTH, Swedish Royal Institute of Technology, is thanked for his invaluable assistance with the FE-SEM instrument.

I would like to give a special thanks to all the staff at the department of polymer science, Calvin, Deon, Oom Hennie, Aneli and Erinda for all their help throughout the past few years.

The NRF and the Harry Crosley foundation are thanked for bursary funding during this research project.

Thanks to all my fellow lab-mates in Lab 134 (Physical lab), really a great group of people to work with. Special thanks to my close friends for their ready supply of lighter moments! Maggie, Elana, Nadine, Liesl, Ashwell, Aimée, Pritish, Gareth H, Lindie, William, Jacques, Morné.

The good friends I made at KTH are also appreciated, Hasan, Sohail, Peter K, Thomas, Sung-Woo, Richard, Soheil and Peter B.

Last but not least, I would like to thank my parents for their support, patience and understanding, especially during the trying times! Thanks also go to the rest of my family, Grant, Neil and Cheré for always listening and at least “feigning interest” in what I was doing!

List of Contents

Glossary	v
List of figures	viii
List of tables	xiv
CHAPTER 1	
1.1 INTRODUCTION	2
1.2 OBJECTIVES	5
1.3 REFERENCES	7
CHAPTER 2	
2.1 GRAFT COPOLYMERS	10
2.1.1 SYNTHESIS OF GRAFT COPOLYMERS	11
2.1.1.1 Grafting onto approach	11
2.1.1.2 Grafting from approach	13
2.1.1.3 Grafting through approach	14
2.1.2 AMPHIPHILIC GRAFT COPOLYMERS IN SOLUTION	16
2.2 ELECTROSPINNING	21
2.2.1 POLYMER SOLUTION PARAMETERS	23
2.2.1.1 Molecular weight, solution viscosity and surface tension:	23
2.2.1.2 Solution conductivity and solvent dielectric properties	24
2.2.2 PROCESSING PARAMETERS	24
2.2.2.1 Voltage and tip to collector distance (TCD)	24
2.2.2.2 Feed-rate of polymer solution	25
2.2.2.3 Needle spinneret diameter	25
2.2.2.4 Temperature	25
2.2.3 AMBIENT PARAMETERS	25
2.2.3.1 Humidity, pressure and atmosphere	25

2.2.4	ALIGNED FIBRES BY COLLECTOR MODIFICATION	26
2.2.5	SPECIAL EXAMPLES OF ELECTROSPUN FIBRES	27
2.2.5.1	Porous and hollow nanofibres	27
2.2.5.2	Electrospun emulsions and amphiphilic solutions.	28
2.2.5.3	Electrospun fibres containing functional materials or fillers	29
2.3	POLYMER NANOCOMPOSITES	31
2.3.1	PARTICULATE FILLERS	32
2.3.2	SHEET FILLERS (PLATELETS)	33
2.3.3	FIBROUS FILLERS	34
2.3.3.1	Carbon nanotubes	34
2.3.3.1.1	Carbon nanotube structure	35
2.3.3.1.2	Carbon nanotube synthesis	36
2.3.3.1.2.a	Laser ablation:	36
2.3.3.1.2.b	Arc-discharge:	37
2.3.3.1.2.c	Chemical vapour deposition:	37
2.3.3.1.3	Carbon nanotube functionalization	37
2.3.3.1.4	Carbon nanotube filled nanocomposites	39
2.3.3.1.4.a	Melt blending	39
2.3.3.1.4.b	In situ polymerisation	40
2.3.3.1.4.c	Solution blending	41
2.3.3.1.4.d	Other blending methods	42
2.3.3.1.5	Carbon nanotube alignment in composites	42
2.3.3.1.6	Carbon nanotube composite properties	44
2.3.3.1.7	CNT filled electrospun fibre nanocomposites	46
2.3.3.2	Electrospun nanofibres as composite fillers	48
2.4	REFERENCES	52
CHAPTER 3		
3.1	SYNTHESIS	66
3.1.1	MATERIALS	66
3.1.2	SYNTHESIS OF POLYACRYLONITRILE-GRAFT-POLYDIMETHYLSILOXANE COPOLYMERS	66

3.1.3	EXTRACTION OF HOMO-PDMS	67
3.1.4	MODIFICATION OF MULTI-WALLED CARBON NANOTUBES	67
3.1.5	SILICONE MATRIX PREPARATION AND CURING	68
3.2	CHARACTERISATION	68
3.2.1	SIZE EXCLUSION CHROMATOGRAPHY (SEC)	68
3.2.2	GRADIENT ELUTION CHROMATOGRAPHY (GEC)	69
3.2.3	NUCLEAR MAGNETIC RESONANCE (NMR)	69
3.2.4	STATIC CONTACT ANGLE MEASUREMENTS	69
3.2.5	SCANNING ELECTRON MICROSCOPY (SEM) AND FIELD EMISSION SEM (FE-SEM)	70
3.2.6	TRANSMISSION ELECTRON MICROSCOPY (TEM)	70
3.2.7	ATTENUATED TOTAL REFLECTANCE (ATR) FOURIER TRANSFORM INFRA-RED (FT-IR)	71
3.2.8	RHEOLOGY MEASUREMENTS	71
3.2.9	MECHANICAL TESTING ON INSTRON:	71
3.2.10	WIDE ANGLE X-RAY DIFFRACTION (WAXD)	71
3.3	ELECTROSPINNING APPARATUS	72
3.4	REFERENCES	73
CHAPTER 4		
4.1	NOVEL PAN-GRAFT-PDMS COPOLYMER FIBRE FILLER PRECURSOR MATERIAL	75
4.1.1	SYNTHESIS OF THE FIBRE FILLER PRECURSOR MATERIAL	75
4.1.2	CHARACTERISATION OF THE FIBRE FILLER PRECURSOR MATERIAL	79
4.1.2.1	Gradient chromatography	79
4.1.2.2	WAXD of the fibre filler precursor material	81
4.2	PRODUCTION OF THE REINFORCING FIBRE FILLERS VIA ELECTROSPINNING	86
4.2.1	ELECTROSPINNING PROCEDURE AND RESULTANT FIBRE MORPHOLOGICAL VARIATION	86
4.2.1.1	Effect of PDMS content on solution properties and final fibre morphology	87
4.2.1.2	Effect of PAN-g-PDMS Concentration	89
4.2.1.3	Voltage and tip-to-collector distance effects	91
4.2.1.4	Amphiphilic solution effects on porous fibre filler morphology	94
4.2.1.5	Effect of MWCNTs on the electrospun amphiphilic solutions.	104

4.2.1.5.1	Electrospinning of the MWCNT filled PAN-g-PDMS solutions:	105
4.2.1.5.2	Porous morphology of the MWCNT filled PAN-g-PDMS solutions	108
4.3	REFERENCES	114
CHAPTER 5		
5.1	PREPARATION OF THE FIBRE FILLED SILICONE NANO/COMPOSITES	118
5.1.1	CHOICE OF PAN-G-PDMS COPOLYMERS AS FILLER MATERIALS	118
5.1.2	SUMMARY OF THE FIBRE FILLERS PREPARED	119
5.1.3	CONTACT ANGLE DETERMINATIONS OF THE FIBRE FILLERS	120
5.1.4	VARIABLES STUDIED IN THE PRODUCTION OF THE FIBRE FILLED SILICONE COMPOSITES	122
5.1.5	PRODUCTION OF THE FILLED SILICONE COMPOSITES	123
	5.1.5.1 Aligned fibre filler collection	124
	5.1.5.2 Composite preparation and curing	125
5.1.6	INVESTIGATION OF FIBRE DISTRIBUTION IN THE SILICONE ELASTOMER COMPOSITES	128
5.1.7	MECHANICAL PROPERTIES OF THE FILLED SILICONE ELASTOMER COMPOSITES	129
5.1.8	SUMMARY OF THE SILICONE NANO/COMPOSITES AND COMPARISON TO LITERATURE	144
5.2	REFERENCES	147
CHAPTER 6		
6.1	CONCLUSIONS	151
6.2	PROSPECTS FOR FUTURE WORK	154
APPENDIX A		157

Glossary

Notations

B	full width at half maximum
$\chi_{bb,s}$	monomer-monomer interaction parameter of the backbone
$\chi_{br,s}$	monomer-monomer interaction parameter of the branches
$D_{\text{crystallisation}}$	degree of crystallisation
$\Delta L/L_0$	elongation (strain)
E	Young's modulus
ϵ_{max}	maximum strain at break
G'	storage modulus
G''	loss modulus
k_{11}	rate constant of monomer 1 adding to monomer 1
k_{12}	rate constant of monomer 2 adding to monomer 1
k_{21}	rate constant of monomer 1 adding to monomer 2
k_{22}	rate constant of monomer 2 adding to monomer 2
L	coherence length
λ	X-ray wavelength
M^*	monomer at end of a growing chain
M_n	number average molecular weight
θ	Bragg diffraction angle
r_1	reactivity ratio of monomer 1
r_2	reactivity ratio of monomer 2
σ_{max}	maximum stress at break
$\nu_{bb,s}$	excluded volume parameter of graft backbone in solution
$\nu_{bbr,s}$	excluded volume parameter of graft branches in solution
ω	angular frequency
W_{max}	maximum energy at break/toughness
W_{PAN}	weight fraction PAN

Abbreviations

ABS	acrylonitrile-butadiene-styrene
AFM	atomic force microscopy
AIBN	azobisisobutyronitrile
ali	aligned
AN	acrylonitrile
ATR-FTIR	attenuated total reflectance fourier transform infra-red
ATRP	atom transfer radical polymerisation

BIS-GMA	2,20-bis-[4-(methacryloxypropoxy)-phenyl]-propane
BuLi	butyl lithium
CaCO ₃	calcium carbonate
CNT	carbon nanotube
CVD	chemical vapour deposition
DMF	N,N dimethylformamide
DMSO	dimethylsulfoxide
Dox	doxorubicin hydrchloride
EEMA	1-(ethoxy)ethyl methacrylate
EtTrp	tryptophan ethyl ester
FE-SEM	field emission scanning electron microscopy
FTIR	fourier transform infra red
FWHM	full width at half maximum
GEC	gradient elution chromatography
GMA	glycidal methacrylate
H ₂ O ₂	hydrogen peroxide
H ₂ SO ₄	sulfuric acid
HA	hydroxyapatite
HNO ₃	nitric acid
KMnO ₄	potassium permanganate
MeOH	methanol
MMP-PDMS	mono-methacryloxypropyl terminal poly(dimethylsiloxane)
MWCNT	multi-walled carbon nanotube
NaNO ₃	soudium nitrate
NMR	nuclear magetic resonance
nw	non-woven
PAN	poly(acrylonitrile)
PBI	poly(benzimidazole)
PBS	poly(butylene succinate)
PCL	poly(ε-caprolactone)
PDI	polydispersity index
PDMS	poly(dimethylsiloxane)
PE	polyethylene
PEG	poly(ethylene glycol)
PEGMA	poly(ethylene glycol) methyl ethyl methacrylate
PEO	poly(ethylene oxide)
PLA	poly(lactic acid)
PLGA	poly(lactide-co-glycolide)
PMMA	poly(methyl methacrylate)
PNIPAm	poly(N-isopropylacrylamide)
POSS	polyhedral oligosilsesquioxane
PPP	poly(phosphazene)
PSS	poly(styrene sulfonate)
PU	polyurethane
PVA	poly(vinyl acetate)

PVOH	poly(vinyl alcohol)
PVP	poly(vinyl pyrrolidone)
RAFT	reversible addition fragmentation chain transfer
RH	relative humidity
SBR	styrene-butadiene rubber
SDS	sodium dodecyl sulphate
SEC	size exclusion chromatography
SEM	scanning electron microscopy
SiO ₂	silica
SWCNT	single-walled carbon nanotube
TCD	tip-to-collector distance
TEGDMA	tri(ethylene glycol) dimethacrylate
TEM	transmission electron microscopy
THF	tetrahydrofuran
TiO ₂	titanium dioxide
TMEDA	tetramethylenediamine
VD ₂	2-vinyl-2,4,4,6,6-pentamethylcyclotrisiloxane
WAXD	wide angle X-ray diffraction
XRD	X-ray diffraction
ZrO ₂	zirconium dioxide

List of Figures

CHAPTER 2

Figure 2.1 : Illustration of the three grafting approaches (a) grafting onto, (b) grafting from and (c) grafting through. 12

Figure 2.2 : Plot illustration of possible micellar structures for sparsely grafted short grafts as a function of solvent quality for the backbone and branches, represented by excluded volume parameters $\upsilon_{bb,s}$ and $\upsilon_{br,s}$, respectively, where χ is the monomer-monomer interaction parameter and the dashed line represents non-select solvent quality $\upsilon_{bb,s} = \upsilon_{br,s}$ 17

Figure 2.3 : Schematic illustration of the changes in micellar structure as the solvent conditions change from good to the backbone but progressively worse for the branches and vice-versa. 18

Figure 2.4 : Diagrammatic representation of an electrospinning setup with a control feed pump, high voltage supply, polymer solution reservoir and grounded collector plate. 21

Figure 2.5 : Three main classes of filler dimensions with aspect ratio (surface area to volume) formulae. 31

Figure 2.6 : Schematic diagram showing the hexagonal lattice of a grapheme sheet and how the concept of the chiral vector. 36

Figure 2.7 : Diagrammatic illustration of covalent modification of CNTs versus adsorption or polymer wrapping, both used for CNT dispersion. 38

Figure 2.8 : The wedge with a semi-angle α . Polar coordinates r (radial) and ε (polar angle) are used to describe the position of a rod centre. Spherical angular coordinate's θ and φ are used to characterize the orientation of the rod-like particle AB. Also the corresponding Cartesian coordinates x , y and z are included. Obtained from reference. 43

CHAPTER 3

Figure 3.1 : Synthesis of the novel PAN-g-PDMS copolymers via free radical copolymerisation 67

Figure 3.2 : Image of water drop showing the height and radius used in determination of the contact angle (θ) 70

CHAPTER 4

Figure 4.1 : Synthesis of the novel PAN-g-PDMS copolymers via free radical copolymerisation. 75

Figure 4.2 : Gradient profile of THF:DMF mobile phase vs. elution time for the gradient chromatographic separation of the PAN-g-PDMS copolymers. (DMF/THF mobile phase, Si 300 Å, 5 µm, 1 ml.min⁻¹, 30 °C) 89

Figure 4.3 : Gradient elution chromatographic overlays of the various PAN-g-PDMS / homo-PAN polymer blend, where (a) shows the 1000g.mol⁻¹ PDMS and (b) the 5000 g.mol⁻¹ PDMS grafts. (DMF/THF mobile phase, Si 300 Å, 5 µm, 1 ml.min⁻¹, 30 °C) 80

Figure 4.4 : WAXD patterns of (a) PAN and (b) PDMS-g-PAN / PAN blend with 25 wt% PDMS (19.4 wt%, 1000 g.mol⁻¹), highlighting the various crystalline and amorphous regions according to the Gupta et. al. method. 82

Figure 4.5 : WAXD patterns of the various (a) 1000 g.mol⁻¹ and (b) 5000 g.mol⁻¹ PDMS containing graft copolymer PAN-homopolymer blends. 83

Figure 4.6 : Degree of crystallisation values as a function of PDMS content, overlaid with the FWHM of the dominant PAN crystallisation peak at 17° for (a) the 1000 g.mol⁻¹ and (b) 5000 g.mol⁻¹ PDMS series. 85

Figure 4.7 : Viscosity versus shear rate for the precursor PAN-g-PDMS / PAN copolymer blend materials in DMF (15 wt%) for the 1000 g.mol⁻¹ (solid squares) series and two samples from the 5000 g.mol⁻¹ PDMS series (open squares). 87

Figure 4.8 : Mean fibre diameter as a function of PDMS (wt%) content in the PAN-g-PDMS copolymer series for the 1000g.mol⁻¹ and 5000g.mol⁻¹ copolymer series. 89

Figure 4.9 : SEM images and corresponding diameter distribution diagrams of (a) 13 wt% polymer, (b) 15 wt% polymer and (c) 18 wt% polymer (4.8 wt% PDMS, 1000 g.mol⁻¹) in DMF with the TCD (20 cm), feed-rate (0.008 ml.min⁻¹) and the voltage (15 kV) in all cases. 90

Figure 4.10 : Mean fibre diameter as a function of PDMS content (wt%) and TCD distance for (a) the 1000 g.mol⁻¹ PDMS and (b) the 5000 g.mol⁻¹ PDMS series. 92

Figure 4.11 : Mean fibre diameter as a function of PDMS content (wt%) and potential voltage applied for (a) the 1000 g.mol⁻¹ and (b) the 5000 g.mol⁻¹ PDMS series. 93

Figure 4.12 : Typical TEM images obtained from identical dilute concentration solutions in DMF of various PAN-g-PDMS fibre precursor materials (a) 4.8 wt% PDMS (1000 g.mol⁻¹), (b) 11.4 wt% PDMS (1000 g.mol⁻¹), (c) 16.3 wt% PDMS (1000 g.mol⁻¹) and (d) 19.4 wt% PDMS (1000 g.mol⁻¹). 95

Figure 4.13 : Oscillating rheological analysis of the 19.3 wt% PDMS (1000 g.mol⁻¹) fibre precursor material, presenting the typical storage (G') and loss moduli (G'') obtained as a function of angular frequency (ω). 97

Figure 4.14 : FE-SEM images of (a) homo-PAN, (b) homo-PAN, (c) 4.8 wt% PDMS (1000 g.mol⁻¹), (d) 11.4 wt% PDMS (1000 g.mol⁻¹), (e) 16.3 wt% PDMS (1000 g.mol⁻¹) and (f) 19.4 wt% PDMS (1000 g.mol⁻¹), corresponding TEM images obtained from evaporation from dilute solution (100% DMF) as insets set on the same scale. 98

Figure 4.15 : FE-SEM images of (a) 8.5 wt% PDMS (5000 g.mol⁻¹), (b) 8.5 wt% PDMS (5000 g.mol⁻¹), (c) 13.1 wt% PDMS (5000 g.mol⁻¹) and (d) 13.1 wt% PDMS (5000 g.mol⁻¹), corresponding TEM images obtained from evaporation from dilute solution (100% DMF) as insets. 100

Figure 4.16 : Cross-sectional views of an 11.4 wt% PDMS (1000g.mol⁻¹) containing electrospun fibre. 101

Figure 4.17 : WAXD diffraction patterns of the electrospun fibres of PAN-g-PDMS/PAN copolymer blends for the 1000 g.mol⁻¹ series and two 5000 g.mol⁻¹ samples used for filler production. 102

Figure 4.18 : WAXD overlays of the 16.3 wt% PDMS (1000 g.mol⁻¹) in fibre form and fibre precursor powder form (normalized to the 17° peak). 103

Figure 4.19 : Comparison of (a) the degree of crystallinity and (b) the FWHM values of the electrospun fibres and the fibre precursor materials (1000 g.mol⁻¹ PDMS series). 104

Figure 4.20 : Mean fibre diameter as a function of MWCNT content (wt%) for two different PDMS content copolymer blends (11.4 and 16.3 wt% PDMS, 1000 g.mol⁻¹), spun at optimum concentrations: 13.5 wt% PAN-g-PDMS (2 wt% MWCNT), 12 wt% PAN-g-PDMS (4 wt% MWCNT), 10 wt% PAN-g-PDMS (8 wt% MWCNT) and 8,5 wt% PAN-g-PDMS (16 and 32 wt% MWCNT) in DMF. 106

Figure 4.21 : Mean fibre diameter as a function of PDMS content (wt%) in the copolymer blends containing 8 wt% MWCNTs for (a) the 1000 g.mol⁻¹ and (b) 5000 g.mol⁻¹ series. 107

Figure 4.22 : Typical TEM images obtained from dilute solution in DMF of various PAN-g-PDMS copolymers (a) 4.8 wt% PDMS (1000 g.mol⁻¹), (b) 11.4 wt% PDMS (1000 g.mol⁻¹), (c) 16.3 wt% PDMS (1000 g.mol⁻¹) and (d) 19.4 wt% PDMS (1000 g.mol⁻¹) containing 8 wt% MWCNTs. 109

Figure 4.23 : FE-SEM images of (a) homo-PAN, (b) 4.8 wt% PDMS (1000 g.mol⁻¹), (c) 11.4 wt% PDMS (1000 g.mol⁻¹) and (d) 16.3 wt% PDMS (1000 g.mol⁻¹), all containing 8 wt% MWCNTs, corresponding TEM images obtained from evaporation from dilute solution (100% DMF) as insets. 110

Figure 4.24 : TEM images obtained from MWCNT containing fibres (8 wt%) embedded in an epoxy resin and then microtomed showing the MWCNT dispersion. 111

Figure 4.25 : WAXD pattern overlays of the raw fibre precursor, electrospun fibre and electrospun fibre filled with 8 wt% MWCNTs for the 16.3 wt% PDMS copolymer blend (1000 g.mol⁻¹ PDMS). 112

CHAPTER 5

Figure 5.1 : Mean fibre diameter and contact angle as a function of PDMS incorporation for (a) the unfilled fibres and (b) the MWCNT (8 wt%) filled fibres. 121

Figure 5.2 : SEM images of (a) aligned fibre mat of 4.8 wt% PDMS unfilled, (b) non-woven mat of 4.8 wt% PDMS unfilled, (c) aligned mat of 4.8 wt% PDMS (8 wt% MWCNT) and (d) non-woven mat of 4.8 wt% PDMS (8 wt% MWCNT) electrospun fibres (1000 g.mol⁻¹ PDMS). 124

Figure 5.3 : Mean fibre diameter of filled and unfilled fibres collected on the rotating drum versus the stationary collector. 125

Figure 5.4 : Stepwise guide of how the silicone elastomer composites were prepared. 126

Figure 5.5 : Typical optical images of (a) MWCNTs directly added to the silicone film, (b) fibre filled silicone composite and (c) fibre filled silicone composite with 8 wt% MWCNTs in the fibre fillers and 1.2 wt% to the silicone matrix. 127

Figure 5.6 : Typical fibre distribution in the silicone elastomer matrix observed using SEM at two different magnifications (a) and (b). 128

Figure 5.7 : Summary of the tensile stress-strain curves of the 11.4 wt% PDMS (1000 g.mol^{-1}) nonwoven and aligned fibre composites with and without 8 wt% MWCNTs. 129

Figure 5.8 : Comparison of the tensile test specimens just prior to fracture for (a) unfilled silicone, (b) aligned fibre filler, (c) aligned fibre filler with 8 wt% MWCNT, (d) non-woven fibre filler with 8 wt% MWCNT and (e) non-woven fibre filler, with all the fibres containing (11.4 wt% PDMS, 1000 g.mol^{-1}). 130

Figure 5.9 : FE-SEM images of non-woven fibre filled silicone composite fracture surfaces of (a) and (b) 4.8 wt% PDMS, (c) and (d) 11.4 wt% PDMS and (e) and (f) 16.3 wt% PDMS containing copolymer fibres (1000 g.mol^{-1}) after tensile failure. 134

Figure 5.10 : Diagrammatic representation of the shear lag model for modeling the pull-out behaviour of a ductile fibre in a brittle matrix as proposed in work by Hsueh. 135

Figure 5.11 : FE-SEM images of non-woven fibre filled silicone composite fracture surfaces of 11.4 wt% PDMS containing copolymer fibres (1000 g.mol^{-1}) containing 8 wt% MWCNT after tensile failure. 137

Figure 5.12 : Typical optical microscopy images of (a) and (b) tensile fractured unfilled silicone composites and (c) and (d) tensile fractured non-woven composite sample specimen. 138

Figure 5.13 : SEM images of a surface crack present on a tensile fractured non-woven sample specimen at different magnifications. 139

Figure 5.14 : FE-SEM images of aligned fibre filled silicone composite fracture surfaces of (a) and (b) 11.4 wt% PDMS and (c) and (d) 16.3 wt% PDMS containing copolymer fibres (1000 g.mol^{-1} series) after tensile failure. 140

Figure 5.15 : FE-SEM images of aligned fibre filled silicone composite fracture surfaces of 11.4 wt% PDMS containing fibres (1000 g.mol^{-1}) with 8wt% MWCNTs after tensile failure. 141

APPENDIX A

Figure A.1: Maximum strain at break ($\Delta L/L_0$) (ϵ_{\max}) for the various composites, where the x-axis represents the PDMS content variation and the y-axis represents the filled, unfilled, non-woven and aligned fibre composites. 156

Figure A.2: Maximum stress at break (σ_{\max}) (MPa) for the various composites, where the x-axis represents the PDMS content variation and the y-axis represents the filled, unfilled, non-woven and aligned fibre composites. 156

Figure A.3: Young's modulus or stiffness (E) (MPa) for the various composites, where the x-axis represents the PDMS content variation and the y-axis represents the filled, unfilled, non-woven and aligned fibre composites. 157

Figure A.4: Maximum energy (toughness) at break (J) for the various composites, where the x-axis represents the PDMS content variation and the y-axis represents the filled, unfilled, non-woven and aligned fibre composites. 157

Figure A.5: Young's modulus (stiffness) (MPa) for the various composites, where the x-axis represents the PDMS content variation and the y-axis represents the MWCNT filled (8 wt%, 16 wt% and 32 wt%) non-woven and aligned fibre composites. 158

Figure A.6 : Maximum strain at break ($\Delta L/L_0$) (ϵ_{\max}) for the various MWCNT containing composites, where the x-axis represents the PDMS content variation and the y-axis represents the various MWCNT filled, non-woven and aligned fibre composites. 158

Figure A.7 : Maximum stress at break (σ_{\max}) (MPa) for the various MWCNT containing composites, where the x-axis represents the PDMS content variation and the y-axis represents the various MWCNT filled, non-woven and aligned fibre composites. 159

Figure A.8 : Maximum energy (W_{\max}) at break (J) for the various MWCNT containing composites, where the x-axis represents the PDMS content variation and the y-axis represents the various MWCNT filled, non-woven and aligned fibre composites. 159

Figure A.9 : FE-SEM images of the tensile fracture surface of 4.8 wt% (1000 g.mol^{-1}) PDMS content non-woven fibre filled silicone composites. 160

Figure A.10 : FE-SEM images of the tensile fracture surface of 4.8 wt% (1000 g.mol^{-1}) PDMS content aligned fibre filled silicone composites. 161

Figure A.11 : FE-SEM images of the tensile fracture surface of 11.4 wt% (1000 g.mol^{-1}) PDMS content non-woven fibre filled silicone composites. 162

Figure A.12 : FE-SEM images of the tensile fracture surface of 11.4 wt% (1000 g.mol^{-1}) PDMS content aligned fibre filled silicone composites. 163

Figure A.13 : FE-SEM images of the tensile fracture surface of 16.3 wt% (1000 g.mol^{-1}) PDMS content non-woven fibre filled silicone composites. 164

Figure A.14 : FE-SEM images of the tensile fracture surface of 11.4 wt% (1000 g.mol^{-1}) PDMS content aligned fibre filled silicone composites. 165

Figure A.15 : FE-SEM images of the tensile fracture surface of 4.8 wt% (1000 g.mol^{-1}) PDMS content non-woven fibre filled silicone composite (with 8 wt% MWCNTs in the fibres). 166

Figure A.16 : FE-SEM images of the tensile fracture surface of 4.8 wt% (1000 g.mol^{-1}) PDMS content aligned fibre filled silicone composite (with 8 wt% MWCNTs in the fibres). 167

Figure A.17 : FE-SEM images of the tensile fracture surface of 11.4 wt% (1000 g.mol^{-1}) PDMS content non-woven fibre filled silicone composite (with 8 wt% MWCNTs in the fibres). 168

Figure A.18 : FE-SEM images of the tensile fracture surface of 11.4 wt% (1000 g.mol^{-1}) PDMS content aligned fibre filled silicone composite (with 8 wt% MWCNTs in the fibres). 169

Figure A.19 : FE-SEM images of the tensile fracture surface of 16.3 wt% (1000 g.mol^{-1}) PDMS content non-woven fibre filled silicone composite (with 8 wt% MWCNTs in the fibres). 170

Figure A.20 : FE-SEM images of the tensile fracture surface of 16.3 wt% (1000 g.mol^{-1}) PDMS content aligned fibre filled silicone composite (with 8 wt% MWCNTs in the fibres). 171

List of Tables

CHAPTER 2

Table 2.1 : A summary of the parameters affecting the electrospinning of polymer solutions. 22

Table 2.2 : A comparison of the performances of SWCNT and MWCNT filled composites prepared using different approaches 45

CHAPTER 4

Table 4.1 : PDMS macromonomer incorporation in the PAN-g-PDMS copolymers at different reaction medium compositions, and for different macromonomer lengths. 77

Table 4.2 : Summary of the crystalline and amorphous regions of a series of PDMS-g-PAN copolymer (1000 g.mol^{-1} PDMS and 5000 g.mol^{-1}) blends with PAN, the calculated degree of crystallinity, FWHM and the coherence length (L). 84

Table 4.3 : Summary of the crystalline and amorphous regions of a series of electrospun fibres of PDMS-g-PAN copolymer (1000 g.mol^{-1} PDMS) blends with PAN, the calculated degree of crystallinity and the coherence length (L) 102

CHAPTER 5

Table 5.1 : Comparison of electrospinning conditions for the respective unfilled PAN-g-PDMS and MWCNT filled graft copolymers, including the mean fibre diameters obtained. 119

Table 5.2 : A summary of the various composites prepared in this work, where (NW) refers to the non-woven mats and (Ali) refers to the Aligned fibre mats. The columns and rows highlighted from A - G are added to clarify the variables studied. 122

Table 5.3: A summary of the mechanical properties of the reinforced silicone films, filled with non-woven as well as aligned fibre mats, prepared by the electrospinning of PAN-g-PDMS copolymer with varying PDMS content and 0 wt% MWCNT. 131

Table 5.4: A summary of the mechanical properties of the reinforced silicone films, filled with non-woven as well as aligned fibre mats, prepared by the electrospinning of PAN-g-PDMS copolymer with varying PDMS content and 8 wt% MWCNT. 132

Table 5.5: Summary of the mechanical properties of the reinforced silicone films, filled with non-woven as well as aligned fibre mats, prepared by the electrospinning of PAN-g-PDMS copolymer with varying PDMS content and 16 wt% MWCNTs. 142

Table 5.6: Summary of the mechanical properties of the reinforced silicone films, filled with non-woven as well as aligned fibre mats, prepared by the electrospinning of PAN-g-PDMS copolymer with varying PDMS content and 32 wt% MWCNTs. 143

Table 5.7 : Summation of the best performing silicone nano/composites prepared in this project according to the measured mechanical results after tensile testing 145

Chapter 1

Introduction and objectives

1.1 Introduction

The field of nanotechnology has grown to be one of the most important and highly studied areas of polymer and material science to date. The broad range of applications for nanomaterials vary from microelectronics to biomaterials, drug release, mini-emulsion particles, fuel cell research, self-assembling of polymeric nano-layers, nanofibre electrospinning and nanocomposite reinforcement. The development of nanocomposites is a sub-field of nanotechnology that has demanded much interest in recent years^{1,2}. By the incorporation of nano-sized fillers, new properties can be afforded to existing polymer matrices. These include increased mechanical properties, improved barrier properties, altering of optical properties among others. Filler types vary from silicas³, exfoliated natural clays⁴ and carbon black⁵ to carbon nanotubes⁶⁻⁸. The aim in this study is to produce novel silicone nanocomposites reinforced with poly(acrylonitrile) based copolymeric electrospun fibres. Incorporation of MWCNTs into the fibre fillers as a means of distributing them in the silicone matrix is also investigated. A major challenge to overcome when working with fillers is the distribution of the fillers in the matrix. Poor distribution can lead to agglomeration of filler particles or void formation between the filler surfaces and the matrix leading to inferior material performance¹. Nanofibres present particular problems in this regard and for this reason there is not much work published on the use of nanofibres as fillers. Kim *et al.*⁹ used polybenzimidazole nanofibres to reinforce epoxy and rubber matrices. Also, recent work by Swart *et al.*¹⁰ used polymethylmethacrylate-graft-polydimethylsiloxane copolymers to electrospin fibre fillers for silicone matrices. In this work we used novel graft copolymers of polyacrylonitrile-graft-polydimethylsiloxane (PAN-g-PDMS) to electrospin our fibre fillers. Immiscibility of the polymers leads to nano-phase segregation and with its lower surface energy, PDMS tends to surface segregate^{11,12}. PDMS domains can act as compatibilisers between the PAN fibres and the silicone matrix. Electrospinning is a widely used technique in the production of nano/fibres.

Electrospinning has gained interest in the last few years as a facile and versatile technique to produce nanometric scaled fibres. Discovered and patented by Formhals¹³ in 1934 this simple technique was revived by Reneker and Chun¹⁴ in the 1990's where they showed that various kinds of polymer solutions could be electrospun to produce nanofibres. A variety of books¹⁵ and reviews¹⁶⁻²⁰ on the electrospinning of various polymers and composites have been published since then. The ability to obtain nano-scaled fibres leads to the production of fibre mats with extremely high aspect ratios and this aspect lends itself to various

applications including: filtration²¹, tissue scaffolds^{22,23}, drug delivery²⁴, wound dressing²⁵, protective clothing²⁶ and as is the case in this project, composite reinforcement^{19,27}.

An interesting aspect which has not received much attention is the electrospinning of copolymer materials. Much work has been published on the coaxial-spinning of different homopolymers rendering fibres with interesting phase morphologies (see reviews²⁸⁻³⁰), but the study of copolymers where the different constituent molecules are covalently bonded has not received as much interest. Ma and co-workers³¹ investigated the electrospinning of block copolymers of polystyrene and poly(dimethylsiloxane) (PDMS) in the production of superhydrophobic materials. Swart *et al.*³² studied the electrospinning of graft copolymers of PDMS and polymethylmethacrylate, where they were able to switch between superhydrophobic and superhydrophilic fibre mats. Macrophase segregation of immiscible polymers or particle additives as mentioned previously can be used to tailor-make fibres suited for specific end-functions. Copolymers allow us to produce phase-segregated morphologies where the disparate phases are covalently bound producing a much more stable and robust material.

A special case of copolymers, amphiphilic copolymers, can self-assemble into a variety of aggregate structures in solution, including micelles (spherical or rod-like), lamellar, vesicular or complicated network structures³³. These various assemblies can be manipulated by choice of solvents, solution pH, temperature, molecular structure among others. Amphiphilic block copolymers have received much attention in these cases where they offer a multitude of applications in the medicinal³⁴ or micro reactor³⁵ fields. Not much attention has, however, been paid to the behavior of amphiphilic graft copolymers as potential self-assembling molecules³⁶⁻³⁹. Electrospinning of these materials is also a relatively new topic in this area. This study investigates the electrospinning of amphiphilic graft copolymers of polyacrylonitrile and poly(dimethylsiloxane) (PAN-g-PDMS). PDMS in its own is an interesting material to study due to its unique properties, unfortunately due to a very low glass transition temperature this material cannot be electrospun. The electrospinning of PAN on the other hand has been widely studied⁴⁰⁻⁴³. Combination of these two materials in the form of a novel copolymer, can allow the production of novel fibres with the strength of the PAN and the interesting surface properties of elastomeric PDMS. There are a number of parameters that affect the electrospinning process¹⁵ not the least of which are solution conductivity, surface tension and viscoelasticity of the spinning solutions. PAN and PDMS do not share a common solvent that is suitable for electrospinning unlike most other systems that have been investigated. The amphiphilic graft copolymer molecules have the potential to act as micelles where the PAN segments are in solution and the PDMS segments group

together in the immiscible core. This type of emulsion electrospinning has not been widely studied but has gained much interest in the biological field of drug delivery^{44,45}, where it has been shown that core sheath nanofibres can be obtained by elongation of the emulsion spheres along the fibre axis and eventual de-emulsification^{46,47}. Immiscibility of the polymers induces nano-phase segregation and with its lower surface energy, PDMS tends to surface segregate, which lends interesting properties and possible advantages to the final fibre product. Enhanced surface hydrophobicity can be achieved, due to the presence of the PDMS domains. The fibres can also be used as fillers in matrices that are traditionally not suited for PAN, such as silicone elastomers, where the PDMS domains can act as compatibilisers.

The inclusion of various additives to the solutions can alter parameters, for example, solution conductivity and viscosity can be modified by the addition of salts⁴⁸, conductive particles (eg. nanotubes^{49,50}) or magnetic particles⁵¹, among others. These particles not only affect the electrospinning procedure, but also the properties of the final electrospun fibre. First reported by Iijima⁵² in 1990, MWCNT's are outstanding candidates for polymer reinforcement⁵³ due to their excellent mechanical integrity as well as electrical conductivity properties. There are a number of articles^{49,50,54} and reviews⁵⁵⁻⁵⁷ on the subject. The electrospinning of PAN containing MWCNTs has also been well documented in literature⁵⁸⁻⁶⁰, however, the distribution of MWCNTs in silicone as well as their alignment is limited by the weak interaction between the nanotubes and the matrix. Surface modification methods and the use of surfactants can and have been used to improve the distribution of these composite systems. This project will look at incorporating the MWCNTs into the electrospun fibre fillers, thereby indirectly distributing the nanotubes throughout the silicone matrix. It has been shown that simple surface oxidised MWCNTs interact strongly with PAN through the formation of charge transfer complexes⁵⁹. Alignment of MWCNTs has been shown to occur due to electrostatic and high shear interactions during the electrospinning process⁵⁹. Ensuring a good distribution of the MWCNTs in the electrospun fibres and in turn a good distribution of the fibres in the silicone matrix, will allow the production of silicone elastomer composites containing well dispersed and even aligned MWCNTs. The work in this project will look at using nanofibres and multi-walled carbon nanotubes (MWCNTs) to reinforce silicone elastomer films.

1.2 Objectives

The chief objectives in this project focus on the development of an electrospun fibre filler that can be successfully used for the reinforcement of cross-linked silicone films. The first aim is to produce a fibre filler precursor material that exhibits superior physical properties capable of reinforcing the silicone matrix. The fibre precursor material also has to possess functionality that allows compatibilisation with the silicone matrix. Polyacrylonitrile (PAN) was selected as the robust semi-crystalline base material for the fabrication of the fibre fillers. Poly(dimethylsiloxane) (PDMS) was selected as the polymer component to endow compatibility with the silicone matrix. The first objective is the successful synthesis of the novel PAN-graft-PDMS copolymers via the grafting through (macromonomer) technique. A sequential series of graft copolymer materials must be synthesised with varying PDMS content, as well as PDMS graft length. Electrospinning requires a certain minimum molecular weight to ensure successful fibre production, so molecules of sufficient molar mass must be synthesised. Characterisation to determine the PDMS graft incorporation of the fibre filler precursor material is also essential. The effect of the PDMS on the crystallinity of the PAN segments must also be studied as this has implications on the integrity of the final fibre filler.

The next objectives include the successful fabrication of the fibre fillers using polymer solution electrospinning. The incompatibility of these novel graft copolymers results in the development of amphiphilic character in solution. The solution properties of the fibre precursor material in the electrospinning solution must be examined. The novelty of these amphiphilic graft copolymers requires a study of the electrospinning parameters on the fibre morphology. The effect of graft content on the electrospinning parameters and their effect on fibre morphology also have to be examined. The phase segregation behaviour of the graft copolymers as well as the changes in crystallinity of the material during the non-equilibrium electrospinning process must be investigated. The production of electrospun fibres containing a varying content of MWCNTs must be obtained. The effect of MWCNTs on the electrospinning process must also be investigated. The interaction and distribution of the MWCNT nano-fillers in the electrospun fibres must be studied.

The final objectives relate to the production of the filled silicone composites. A series of composites must be prepared containing fibre fillers with varying PDMS content. Possible surface segregation of PDMS domains must be investigated as a means to compatibilise the PAN based fibres with the silicone matrix. The fibre filler reinforcing mats must also be varied from non-woven to aligned fibre mats. The effects of the PDMS content as well as the fibre arrangement (non-woven or aligned) must be studied. Fibre fillers containing various

amounts of MWCNTs must also be studied as possible reinforcing fillers. The mechanical properties together with fracture surface analysis must be used to investigate the behaviour of the prepared silicone composites.

In summation, the main objectives of this research endeavour are as follows:

1. The synthesis and characterisation of novel PAN-g-PDMS graft copolymers that can be electrospun to form fibres, as well as, interact with MWCNTs and interact with the silicone matrix.
2. Fully investigate the effect of the electrospinning parameters on the electrospinning of the novel PAN-g-PDMS copolymers.
3. Investigate how the aggregation of the phase segregated amphiphilic molecules together with the crystallisation of the PAN segments and non-equilibrium electrospinning process combine to affect the final fibre morphology.
4. Study the effect of MWCNTs on the electrospinning of the novel graft copolymer materials at various loadings, as well as their distribution in the fibres and silicone matrix.
5. Investigate the mechanical properties of the silicone composites using tensile testing and correlate this to the fracture surfaces of the tensile test specimens to gain insight into the reinforcement or failure mechanism of the composites. Understanding of how the fibre filler arrangement (aligned or non-woven) affect the composite properties, as well as the MWCNT loading.

1.3 References

- (1) Balazs, A. C., Emrick, T., Russell, T. P. *Science* **2006**, *314*, (5802), 1107-1110.
- (2) Paul, D. R., Robeson, L. M. *Polymer* **2008**, *49*, (15), 3187-3204.
- (3) Yuan, Q. W., Mark, J. E. *Macromol. Chem. Phys.* **1999**, *200*, (1), 206-220.
- (4) Sengupta, R., Chakraborty, S., Bandyopadhyay, S., Dasgupta, S., Mukhopadhyay, R., Auddy, K., Deuri, A. S. *Polym. Eng. Sci.* **2007**, *47*, (11), 1956-1974.
- (5) Huang, J. *Adv. Polym. Technol.* **2002**, *21*, (4), 299-313.
- (6) Breuer, O., Sundararaj, U. *Polym. Compos.* **2004**, *25*, (6), 630-645.
- (7) Ahir, S. V., Huang, Y. Y., Terentjev, E. M. *Polymer* **2008**, *49*, (18), 3841-3854.
- (8) Coleman, J. N., Khan, U., Blau, W. J., Gun'ko, Y. K. *Carbon* **2006**, *44*, (9), 1624-1652.
- (9) Kim, J., Reneker, D. H. *Polym. Compos.* **1999**, *20*, (1), 124-131.
- (10) Swart, M., Olsson, R. T., Hedenqvist, M. S., Mallon, P. E. *Polym. Eng. Sci.* **2010** *50*, (11), 2143-2152.
- (11) Chen, X., Gardella Jr, J.A., Kumler, P.L. *Macromolecules* **1993**, *26*, 3778-3783.
- (12) Chen, X., Gardella Jr, J.A., Kumler, P.L. *Macromolecules* **1992**, *25*, 6631-6637.
- (13) Formhals A, (1934) Schreiber-Gastell R *Process and apparatus for preparing artificial threads*. US patent 1975504.
- (14) Reneker, D. H., Chun, I. *Nanotech.* **1996**, *7*, (3), 216-223.
- (15) Ramakrishna, S., Fujihara, K., Teo, W. E., Lim, T. C., Ma, Z. *An Introduction to Electrospinning and Nanofibers*. World Scientific: London, **2005**.
- (16) Reneker, D. H., Yarin, A. L. *Polymer* **2008**, *19*, 2387-2425.
- (17) Li, D., Xia, Y. *Adv. Mater. (Weinheim, Ger.)* **2004**, *16*, (14), 1151-1170.
- (18) Subbiah, T., Bhat, G. S., Tock, R. W., Parameswaran, S., Ramkumar, S. S. *J. Appl. Polym. Sci.* **2005**, *96*, (2), 557-569.
- (19) Huang, Z. M., Zhang, Y. Z., Kotaki, M., Ramakrishna, S. *Compos. Sci. Technol.* **2003**, *63*, (15), 2223-2253.
- (20) Zhang, Y., Lim, C. T., Ramakrishna, S., Huang, Z. M. *J. Mater. Sci.-Mater. M.* **2005**, *16*, 933-946.
- (21) Tsai, P. P., Schreuder-Gibson, H., Gibson, P. J. *Electrost.* **2002**, *54*, (3-4), 333-341.
- (22) Matthews, J. A., Wnek, G. E., Simpson, D. G., Bowlin, G. L. *Biomacromolecules* **2002**, *3*, (2), 232-238.
- (23) Stephens, J. S., Casper, C. L., Chase, D. B., Rabolt, J. F. *Polym. Prepr.* **2003**, *44*, (2), 91.

-
- (24) Kenawy, E., Bowlin, G. L., Mansfield, K., Layman, J., Simpson, D. G., Sanders, E. H., Wnek, G. E. *J. Controlled Release* **2002**, *81*, (1-2), 57-64.
- (25) Kenawy, E., Layman, J. M., Watkins, J. R., Bowlin, G. L., Matthews, J. A., Simpson, D. G., Wnek, G. E. *Biomaterials* **2003**, *24*, (6), 907-913.
- (26) Gibson, P., Schreuder-Gibson, H., Rivin, D. *Colloids Surf., A* **2001**, *187-188*, 469-481.
- (27) Neppalli, R., Marega, C., Marigo, A., Bajgai, M. P., Kim, H. Y., Causin, V. *Eur. Polym. J.* **2010**, *46*, 968-976.
- (28) Chakraborty, S., Liao, I. -, Adler, A., Leong, K. W. *Adv. Drug Delivery Rev.* **2009**, *61*, (12), 1043-1054.
- (29) Loscertales, I. G., Barrero, A., Guerrero, I., Cortijo, R., Marquez, M., Gaain-Calvo, A. M. *Science* **2002**, *295*, (5560), 1695-1698.
- (30) Moghe, A. K., Gupta, B. S. *Polym. Rev.* **2008**, *48*, (2), 353-377.
- (31) Ma, M., Hill, R. M., Lowery, J. L., Fridrikh, S. V., Rutledge, G. C. *Langmuir* **2005**, *21*, (12), 5549-5554.
- (32) Swart, M., Mallon, P. E. *Pure Appl. Chem.* **2009**, *81*, (3), 495-511.
- (33) Alexandridis, P. *Curr. Opin. Colloid Interface Sci.* **1996**, *1*, (4), 490-501.
- (34) Jones, M. -, Leroux, J. -. *Eur. J. Pharm. Biopharm.* **1999**, *48*, (2), 101-111.
- (35) Persigehl, P., Jordan, R., Nuyken, O. *Macromolecules* **2000**, *33*, (19), 6977-6981.
- (36) Borisov, O. V., Zhulina, E. B. *Macromolecules* **2005**, *38*, (6), 2506-2514.
- (37) Wittgren, B., Wahlund, K., Derand, H., Wesslen, B. *Macromolecules* **1996**, *29*, (1), 268-276.
- (38) Wang, C., Li, G., Guo, R. *Chem. Commun.* **2005**, (28), 3591-3593.
- (39) Zhang, J. X., Qiu, L. Y., Zhu, K. J. *Macromol. Rapid Commun.* **2005**, *26*, (21), 1716-1723.
- (40) Fang, J., Wang, H., Niu, H., Lin, T., Wang, X. *Macromol. Symp.* **2010**, *287*, 155-161.
- (41) Yang, T., Yao, Y., Lin, Y., Wang, B., Xiang, R., Wu, Y., Wu, D. *Appl. Phys. A: Mater. Sci. Process.* **2010**, *98*, (3), 517-523.
- (42) Zhang, W., Wang, Y., Sun, C. *J. Polym. Res.* **2007**, *14*, (6), 467-474.
- (43) Fennessey, S. F., Farris, R. J. *Polymer* **2004**, *45*, (12), 4217-4225.
- (44) Xu, X., Yang, L., Xu, X., Wang, X., Chen, X., Liang, Q., Zeng, J., Jing, X. *J. Control. Release* **2005**, *108*, 33-42.
- (45) Qi, H., Hu, P., Xu, J., Wang, A. *Biomacromolecules* **2006**, *7*, 2327-2330.
- (46) Xiaoqianga, L., Yana, S., Shuipinga, L., Lianjianga, T., Xiumeia, M., Ramakrishnad, S. *Colloid surface B* **2010**, *75*, 418-424.
- (47) Xu, X., Zhuang, X., Chen, X., Wang, X., Yang, L., Jing, X. *Macromol. Rapid Comm.* **2006**, *27*, 1637-1642.

- (48) Qin, X., Wang, S. *Mater. Lett.* **2008**, *62*, (8-9), 1325-1327.
- (49) Mazinani, S., Ajji, A., Dubois, C. *Polymer* **2009**, *50*, 3329-3342.
- (50) Vaisman, L., Wachtel, E., Wagner, H. D., Marom, G. *Polymer* **2007**, *48*, (23), 6843-6854.
- (51) Zhang, D., Karki, A. B., Rutman, D., Young, D. P., Wang, A., Cocke, D., Ho, T. H., Guo, Z. *Polymer* **2009**, *50*, (17), 4189-4198.
- (52) Iijima, S. *Nature* **1991**, *354*, (6348), 56-58.
- (53) Moniruzzaman, M., Winey, K. I. *Macromolecules* **2006**, *39*, (16), 5194-5205.
- (54) Titchenal, N.L., Naguib, N., Ye, H., Gogotsi, Y., Liu, J., Ko, F.K. *Abstracts of papers 226th ASC national meeting, NY, USA*, **2003**, 1-573.
- (55) Xie, X., Mai, Y., Zhou, X. *Mater. Sci. Eng., R* **2005**, *R49*, (4), 89-112.
- (56) Thostenson, E. T., Li, C., Chou, T. *Compos. Sci. Technol.* **2005**, *65*, (3-4), 491-516.
- (57) Thostenson, E. T., Ren, Z., Chou, T. *Compos. Sci. Technol.* **2001**, *61*, (13), 1899-1912.
- (58) Hou, H., Ge, J. J., Zeng, J., Li, Q., Reneker, D. H., Greiner, A., Cheng, S. Z. D. *Chem. Mater.* **2005**, *17*, (5), 967-973.
- (59) Ge, J. J., Hou, H., Li, Q., Graham, M. J., Greiner, A., Reneker, D. H., Harris, F. W., Cheng, S. Z. D. *J. Am. Chem. Soc.* **2004**, *126*, (48), 15754-15761.
- (60) Ji, J., Sui, G., Yu, Y., Liu, Y., Lin, Y., Du, Z., Ryu, S., Yang, X. *J. Phys. Chem. C* **2009**, *113*, (12), 4779-4785.

Chapter 2

Historical and literature review

This chapter aims to provide a brief yet comprehensive review of the past and current state of literature on the various aspects related to this study. The various aspects include graft copolymer synthesis, solution behaviour of amphiphilic materials, electrospinning, and nanocomposite materials, focusing on various filler types.

2.1 Graft copolymers

Graft copolymers, especially hybrid and amphiphilic materials, are gaining importance in modern day applications. This is because many scientists are investigating new ways of synthesising high performance materials from existing monomers and materials¹. Hybrid polymers are polymer chains that consist of organic and inorganic segments. The synthesis of organic/inorganic hybrid materials is an area of growing interest as the useful properties of disparate components can be combined into a single material. The fact that the inorganic polymers have totally different properties to their organic counterparts, lends these materials interesting properties. The opposing properties of most hybrid materials lead to block immiscibility within the material substrate. This leads to the formation of nanophase segregated morphologies¹. One can also control these morphologies to a certain extent using “living” anionic polymerisation methods to produce these block copolymers. A review by Matyjaszewski *et. al.*¹ covered the synthesis of hybrid materials with varying chain architectures. There are a variety of possible copolymer structures, ranging from conventional block copolymers², where the different polymer segments are grouped together along the backbone. Star copolymers³ consist of different polymer chains (arms) connected to a central core. Graft copolymers³⁻⁵ are an important class of hybrid and amphiphilic materials, where the backbone consists of one type of polymer and the pendant side chains another. Depending on the choice of materials one can synthesise materials that have interesting properties in solution, which can affect the morphology of the polymers even after solvent removal. The following section will present a brief overview of amphiphilic graft copolymers, as this was the polymer system chosen to study in this project.

2.1.1 Synthesis of graft copolymers

There are numerous methods to synthesise graft copolymers, each suited to the desired polymer components or final structure of the copolymer molecule. There are three general approaches in the synthesis of graft copolymers, namely, grafting onto, grafting from and grafting through^{2,3,5}. Figure 2.1 summarises the three different methods diagrammatically.

2.1.1.1 Grafting onto approach

Figure 2.1 (a) illustrates the grafting onto approach which utilises a coupling reaction between preformed and functionalised polymer backbones and pendant arms. In this case the backbone bears functionality (reactive sites) along its length and is mixed with the pendant grafts that bear a complementary functionality.

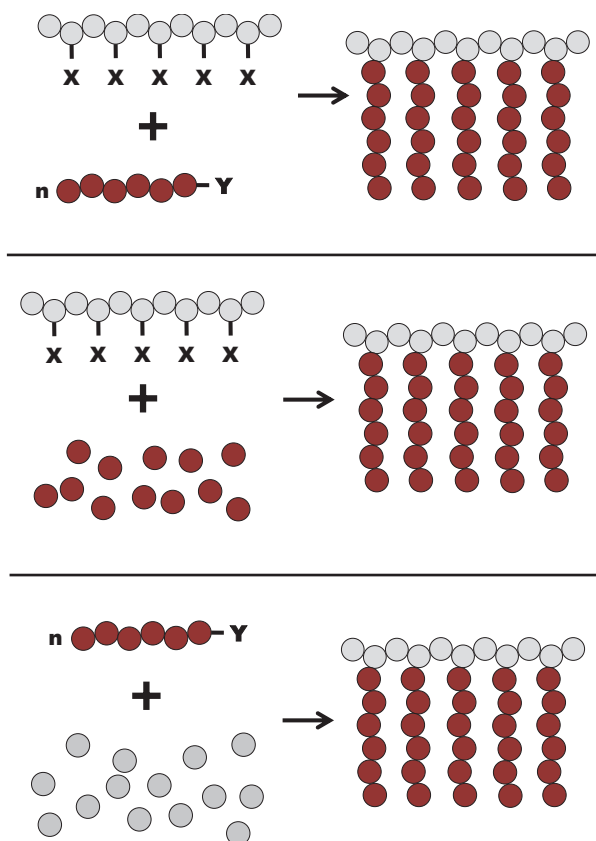


Figure 2.1 : Illustration of the three grafting approaches (a) grafting onto, (b) grafting from and (c) grafting through.

The number and density of the reactive sites along the backbone molecule determines the grafting density. The functionalised backbone can be synthesised using post-polymerisation techniques to introduce functionality, or more commonly, by the introduction of a comonomer with suitable functionality during backbone polymerisation. Backbone functionality is usually electrophilic in nature (anhydrides, esters, and pyridine or halide groups)⁶. Pendant graft arms are usually prepared using anionic polymerisation due to the ease of endcapping with a variety of functionalities. Other controlled radical polymerisation techniques such as reversible addition fragmentation chain transfer (RAFT) can also be used to prepare grafts

with desired functionality. Polybutadiene is well suited to this technique, as it contains unsaturations along its backbone which can be used for the attachment of pendant groups. An example by Xenidou and Hadjichristidis⁷ showed how to prepare poly(butadiene-g-styrene) copolymers using anionic polymerisation. The unsaturated 1,2-additions along the backbone were modified using a hydrosilylation reaction to render chlorosilane moieties, which were subsequently reacted with living anionic polystyrene molecules. Subsequent work by the same group⁴ prepared comb polymers using the same method and then used catalytic hydrogenation to prepare polyethylene combs with well defined structure. Zhang and Ruckenstein⁸ prepared amphiphilic graft copolymers of poly(methyl methacrylate) (PMMA) as backbone and polystyrene as pendant grafts. The backbone was prepared via anionic copolymerisation of 1-(ethoxy)ethyl methacrylate (EEMA) and glycidyl methacrylate (GMA). Living polystyrene anions were then added which reacted with the epoxy groups in the GMA comonomer. The EEMA was then hydrolysed to realise the PMMA-g-polystyrene copolymers with well defined structure. Hirao and Ryu⁹ synthesised polystyrene comb polymers with almost one graft per monomer unit using a backbone with benzyl halide functionality and highly reactive polystyrene anions as branches. Partially chloromethylated or bromomethylated polystyrenes are widely used as backbones in the synthesis of graft copolymers with poly(2-vinyl pyridene)¹⁰ and poly(ethylene oxide)¹¹ as a route to synthesising amphiphilic graft copolymers.

2.1.1.2 Grafting from approach

Figure 2.1 (b) is a diagrammatic representation of this technique. The backbone acts as a macro-initiator in this case with multiple initiation sites for the polymerisation of the pendant grafts. Depending on the number of active initiation sites, one can synthesise the graft copolymer with different branching densities. Depending on the initiation functionality, a variety of approaches can be used to grow the grafts. One can initiate anionic polymerisation of the grafts from a selection of functional groups including allylic, benzylic or aromatic C-H bonds. An example of this is the use of polyisoprene and polybutadiene along with butyl lithium (BuLi) and tetramethylenediamine (TMEDA) as chelating agent. In this case one can produce polyisoprene-g-polystyrene or polybutadiene-g-polystyrene as shown in a number of studies¹²⁻¹⁴. Work by Chen *et. al.*¹⁵ used the RAFT process to grow their pendant grafts in a controlled manner. In this case they used poly(vinylidene fluoride) as the backbone and after ozone pretreatment the peroxides that were generated were used for the thermal initiation of poly(ethylene glycol) methyl ether methacrylate PEGMA. These amphiphilic graft copolymers were then studied as microfiltration membranes. A review by Jenkins and Hudson¹⁶ looks at using controlled radical techniques to grow pendant grafts from chitin and

chitosan backbones using different “grafting from” approaches. This method does not allow direct chromatographic analysis of the components as with the grafting onto technique where the separate components can be analysed individually. It has, however, been shown in literature that, depending on the functionality, the branches can be severed from the backbone and then separately analysed¹⁷.

2.1.1.3 Grafting through approach

This technique is also known as the macromonomer approach. Figure 2.1 (c) illustrates this type of graft copolymerisation. In this case the graft copolymer is synthesised by copolymerising conventional low molecular weight monomer with higher molecular weight macromonomers, hence the name macromonomer method. The macromonomers are preformed and depending on the technique used to synthesise them, one can achieve a variety of end functionality. The desired functionality often relies on the choice of comonomer used. While the macromonomer form the pendant grafts, the backbone is formed *in situ*. Depending on the ratio between the comonomers, different branching densities can be obtained. It must be noted that this type of copolymerisation depends heavily on the reactivity ratios (r_1 and r_2) of the constituent comonomers. These reactivity constants determine the randomness of the graft incorporation along the backbone. The first order Markov (terminal model) model of copolymerisation can be used to study the behaviour of the copolymerisation. This is valid for radical, carbocation and carbanion active centers. It must be noted that in this model, it is solely the last incorporated monomer unit that determines which monomer unit will be added next. There are four fundamental equations:



where M^* indicates the monomer at the end of a growing polymer chain, and the footnote denotes whether it is monomer one or monomer two. Now the reactivity ratios of each monomer can be written as follows:

$$r_1 = k_{11}/k_{12} \quad 2.5$$

$$r_2 = k_{22}/k_{21} \quad 2.6$$

It can be seen from equations 2.5 and 2.6 that the reactivity ratio of each monomer is the likelihood that the same monomers will be incorporated consecutively as opposed to incorporation of a different monomer each time. If r_1 were to be larger than unity, then monomer one would be preferentially incorporated after the addition of monomer one. If r_1 was smaller than unity then monomer two would be preferentially incorporated after the addition of monomer one. The same can be said for monomer two and its reactivity. From this information it is apparent that if $r_1 > 1$ and $r_2 < 1$, then monomer one will be incorporated preferentially until the monomer is exhausted before monomer two is incorporated. This would yield a linear block copolymer of polymer one block polymer two. Due to the factors mentioned earlier which affect the reactivity ratios, it is extremely difficult to find two monomers that can undergo such a polymerisation, and there are invariably “errors” along the length of the chain, or the synthesis of gradient block copolymers.

An article by Chonnowski *et. al.*¹⁸ used the idea of reactivity ratios to prepare gradient block copolymers of vinylmethylsiloxane and dimethylsiloxane. The monomers used were hexamethylcyclotrisiloxane (D_3) along with 2-vinyl-2,4,4,6,6-pentamethylcyclotrisiloxane (VD_2), with reactivity ratios of 0.22 and 8.1 respectively. After anionic polymerisation of these monomers, it was found that the first section of the chains were majority VD_2 , but as the VD_2 monomer headed for exhaustion there was an increase in D_3 incorporation. The last sections of the chains were mainly D_3 units. This gave a gradient distribution of monomer incorporation. Williamson *et. al.*¹⁹ copolymerised 1,3-cyclohexadiene and styrene with reactivity ratios of 0.022 and 0.024, respectively. They determined the reactivity ratios using Fourier transform infra-red spectroscopy (FTIR) combined with Mayo-Lewis graphical plots. In the case of this grafting technique, direct polymerisation of the macromonomers can be used to prepare dense graft copolymer brushes with pendant groups on every repeating monomer unit.²⁰ The RAFT technique as well as atom transfer radical polymerisation (ATRP) can also be used to control the length of the synthesised copolymer backbones as shown in work by Shinoda and Matyjaszewski²¹. Other work by the same group²² showed that PMMA-g-poly(dimethyl siloxane) (PDMS) graft copolymers could be synthesised by copolymerising MMA and methacrylate functional PDMS macromonomers using RAFT and ATRP and conventional radical copolymerisation. It was shown that ATRP presented homogeneously distributed grafts, RAFT gave gradient distribution of the grafts and conventional free radical

polymerisation gave heterogeneously distributed branches. This grafting approach along with using conventional free radical copolymerisation is a facile technique to synthesise a variety of graft copolymers. It was thus chosen as the technique to synthesise the polymers in this work.

2.1.2 Amphiphilic graft copolymers in solution

This class of graft copolymer consists of a backbone and grafts that have different solubilities in certain solvents. The reason for discussing this class of materials is due to the fact that the hybrid copolymers prepared in this work are amphiphilic in nature. It is obvious that the behaviour of the amphiphilic graft copolymers in solution is essential when it comes to electrospinning, as this technique generally uses polymer solutions to produce fibres. A simplified summary of amphiphilic graft copolymers in solution will be presented.

Amphiphilic copolymers have the capability to self-assemble into a wide variety of aggregate structures in certain solvents. Typically, micellisation can occur where the segments that are not solubilised by the solvent tend to stick together and collapse, while the soluble components typically surround the collapsed core as a shell or corona. Micellisation includes the formation of spherical micelles, rod like micelles, vesicles or even lamellae²³⁻²⁹. Amphiphilic block copolymers have been extensively studied from a theoretical and experimental viewpoint^{23,30-38}, due to their ability to form well defined structures in solution. There has not been as much attention paid to amphiphilic graft copolymers, as these systems present a more complicated behaviour in solution^{23,39-44}. Like the linear analogues, these graft copolymers tend to be sensitive to chemical and physical stimuli, responsive to changes in light, pH, temperature and solvent composition^{23,45-49}. Some theoretical studies have been conducted by Zhang *et. al.*²⁹ using self-consistent field theory in two dimensions. Borisov and Zhulina⁴² also presented a theoretical model for predicting the behaviour of densely and sparsely grafted copolymers, where the backbone was insoluble in the solvent system. Work by Halperin³⁹ and Semenov *et. al.*⁵⁰ studied models for the behaviour of graft copolymers in solution, where the self-assembly occurred in a solvent that was inferior for the backbone and good for the branches. Experimental work by Kikuchi and Nose^{40,41}, studied the formation of unimolecular micelle formation in PMMA-g-polystyrene in solvent systems that were good for the backbone and poor for the branches⁴⁰, as well poor for the backbone and good for the branches⁴¹. Their graft copolymers were also focused on using sparsely grafted short graft branches. Figure 2.2 reconstructed from reference^{40,41} highlights these two different solvent polymer interactions.

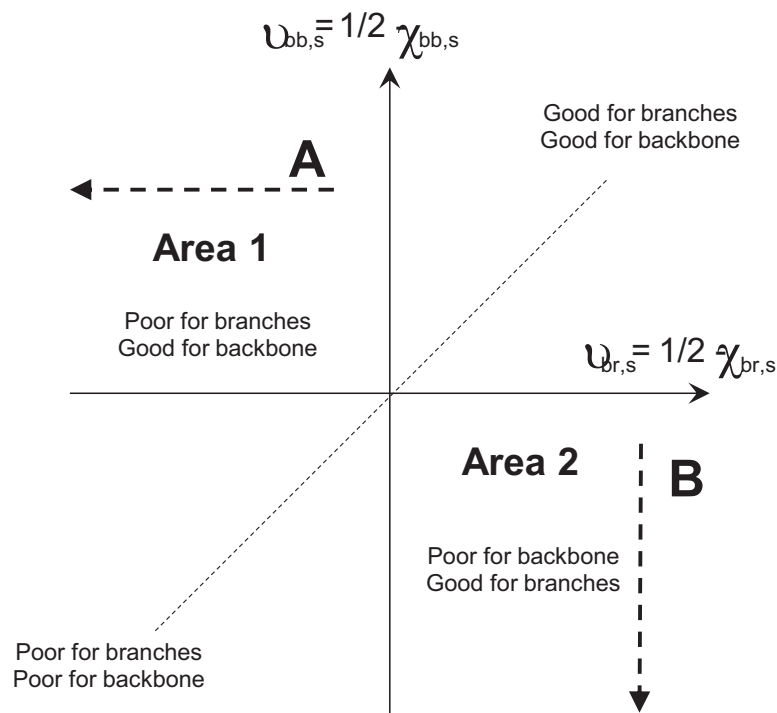


Figure 2.2 : Illustration of possible micellar structures for sparsely grafted short grafts as a function of solvent quality for the backbone and branches, represented by excluded volume parameters $v_{bb,s}$ and $v_{br,s}$, respectively, where χ is the monomer-monomer interaction parameter and the dashed line represents represent non-selective solvent quality $v_{bb,s} = v_{br,s}$.^{40,41}

From Figure 2.2, one can see that excluded volume parameters are used to indicate the solvent quality with regards to the backbone and branches according to the following equations respectively^{40,41}.

$$v_{bb,s} = \frac{1}{2} - \chi_{bb,s} \quad (2.7)$$

$$v_{br,s} = \frac{1}{2} - \chi_{br,s} \quad (2.8)$$

The dashed line indicates the region where the solvent is non-selective and indicates the transition from globule to coil for linear polymers occurs. It must be noted in Figure 2.2, area one corresponds to the region where the solvent is poor for the branches but good for the backbone. The dashed line marked A represents a condition where the solvent quality to the backbone remains good ($v_{bb,s} > 0$) but the solvent quality becomes gradually poorer for the branches from $v_{br,s} = 0$ (Θ condition) to $v_{br,s} \ll 0$. This causes changes in the molecular behaviour in solution as shown in Figure 2.3. In contrast, the dashed line B in area two,

looks at conditions where the solvent remains good for the branches ($\nu_{br,s} > 0$), but becomes poorer for the backbone from $\nu_{bb,s} = 0$ to $\nu_{bb,s} \ll 0$.

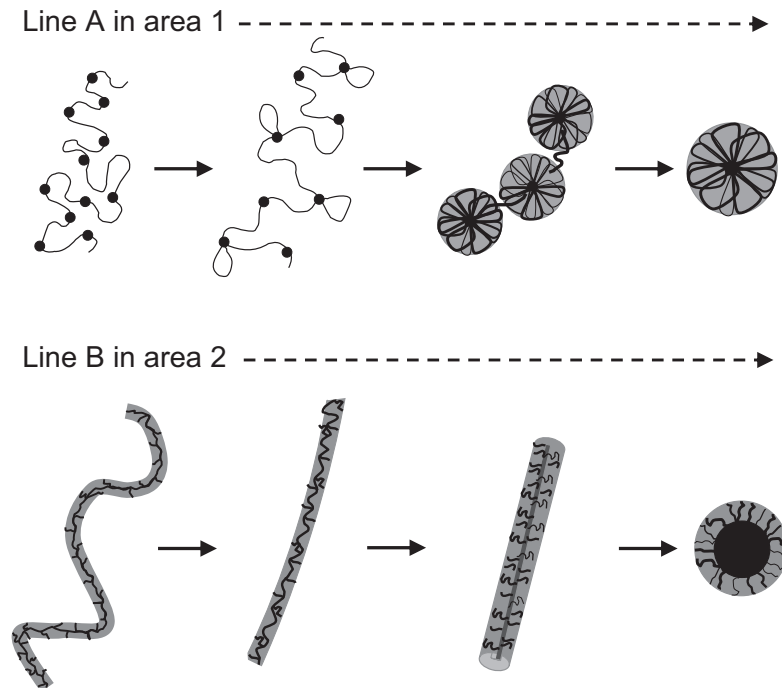


Figure 2.3 : Schematic illustration of the changes in micellar structure as the solvent conditions change from good for the backbone but progressively worse for the branches and vice-versa^{40,41}.

In Figure 2.3^{40,41} the series according to dashed line A, shows that as the solvent for the branches becomes progressively poorer, the branches tend to stick together in clusters. As they stick together, the backbone branches which are in solution tend to form petal-like loops around the branch core. The number of petals and size thereof is determined by the branching density and the distances between the branches as well as solvent quality. The poorest solvent quality yields unimolecular micelle formation. One can also see that a string of connected micelles can also be formed at intermediate solvent quality for the branches. It has been theorised by Seminov⁵⁰ that the formation of a collapsed network chain of flowers is possible which can form a compact sphere. Flexible strings of flower like micelles are proposed by Halperin³⁹ for alternating multi-block copolymers. When the number of loops (petals) increases the string of micelles can become extremely rigid. This results in the formation of a rigid rod-like structure. It was shown by Kikuchi and Nose⁴⁰, that as the branch density increases, the number of petals (loops) increases leading to a more rigid rod-like arrangement of agglomerated micelles. Decreasing temperature showed the same trend.

In contrast, the dashed line B in Figure 2.3^{40,41} illustrates the changes in micellar structure as the solvent quality becomes progressively poorer for the backbone and remains good for the branches. The backbone tends to collapse out of solution and the formation of worm-like chain or rod micelles (bottle-brush structure) ensues. At poorer backbone solvent conditions, rod-like micelles are formed, with a collapsed core of the backbone polymer and a corona of branches around the outside of the core. At even poorer solvent conditions the formation of spherical micelles persist, where the backbone chains form the large core, and the outer branches form the corona shell. Borisov and Zhulina⁴² showed that when the branches are significantly shorter than the backbone spacers between the grafts, one can also obtain strings of “crew-cut” micelles, where the corona is present as a very thin shell of short graft branches. Similar micelles are also formed with rod-like structures and even lamellae “disc-like” morphologies.

Work by Zhang, Qiu and Zhu⁵¹ studied amphiphilic graft copolymers having a polyphosphazene (PPP) backbone and tryptophan ethyl ester (EtTrp) as hydrophobic group and poly(N-isopropylacrylamide) (PNIPAm) as the hydrophilic groups. They compared copolymers with varying hydrophobic to hydrophilic group ratios. According to the copolymer composition and organic solvent employed, a variety of supramolecular aggregates were obtained, from network, nanospheres, high-genus particles to macrophage-like aggregates. Wang, Li and Guo⁵² studied graft copolymers of chitooligosaccharides as hydrophilic backbones with polycaprolactones as the hydrophobic grafts. In this case the backbone was kept short while the branches were synthesised to be much longer in comparison. By changing the length of the branches and the amount of water in the common solvent, they were able to form an array of different morphologies ranging from spheres, petal-like spheres, rods and vesicles to complicated networks of cylindrical micelles. Very interesting work by Kikuchi and Nose^{40,41}, mentioned earlier, studied PMMA-g-polystyrene copolymers in various solvents. The one paper focused on studying the case where the backbone was solvated and branches were not, using a acetonitrile / acetoacetic acid ethyl ether solution mixture⁴⁰. The subsequent paper looked at the reversed conditions using iso-amyl acetate⁴¹. They found the formation of strings of petal-like spheres, as well as strings of spheres with short branches as the outer shell depending on the solvent conditions. Rigid rod-like structures were also formed depending on the grafting density and temperature of the solutions. The stringing together of the micelles presented a route to a lightly cross-linked gel formation. Breitenkamp and Emrick⁵³ used amphiphilic graft copolymers along with cross-metathesis to produce novel polymer capsules. They used poly(ethylene glycol) (PEG) grafted polyolefins with backbone unsaturation to form capsules around oil emulsion

particles in a aqueous solution. The hydrophobic olefin backbone associated with the oil phase while the PEG remained in the water phase forming a polymer layer around the oil droplet. They then used *bis*-octene PEG to crosslink the molecules at the oil-water interface to form the capsule using a ring opening cross metathesis reaction. Depending on the branching density, branch length to backbone length ratio, solvent quality and sensitivity, it is clear that a wide variety of possible aggregated structures in solution is possible. This section serves as a brief overview of amphiphilic graft copolymers in solution, and it must be noted that various combinations of these aforementioned structures and modifications thereof are possible when looking at experimentally obtained structures.

2.2 Electrospinning

The ability to create polymeric fibres with submicron diameters opens an entirely different class of materials with exceptionally high aspect ratios (surface to volume)⁵⁴. This can in turn lend superior mechanical properties to the polymeric material with regards to modulus and tensile strength, more so than any other form of the material. There are various methods found in literature that enable the production of such nanofibres. These include, fibre drawing⁵⁵, template synthesis^{56,57}, phase separation⁵⁸, self-assembly⁵⁹⁻⁶¹ and of course electrospinning⁵⁴. Of these techniques, electrospinning offers the most advantages as it is a relatively simple technique. There is a wide range of materials that can be processed using electrospinning, long continuous nanofibres can be achieved and this technique has the ability to be scaled up. The relative ease of this technique lead to the decision of using it to prepare the polymeric fibres in this study. Electrospinning is a technique that allows the production of nanofibres through an electrically charged polymer solution or melt.

Figure 2.4 illustrates a simple diagram of a typical electrospinning setup.

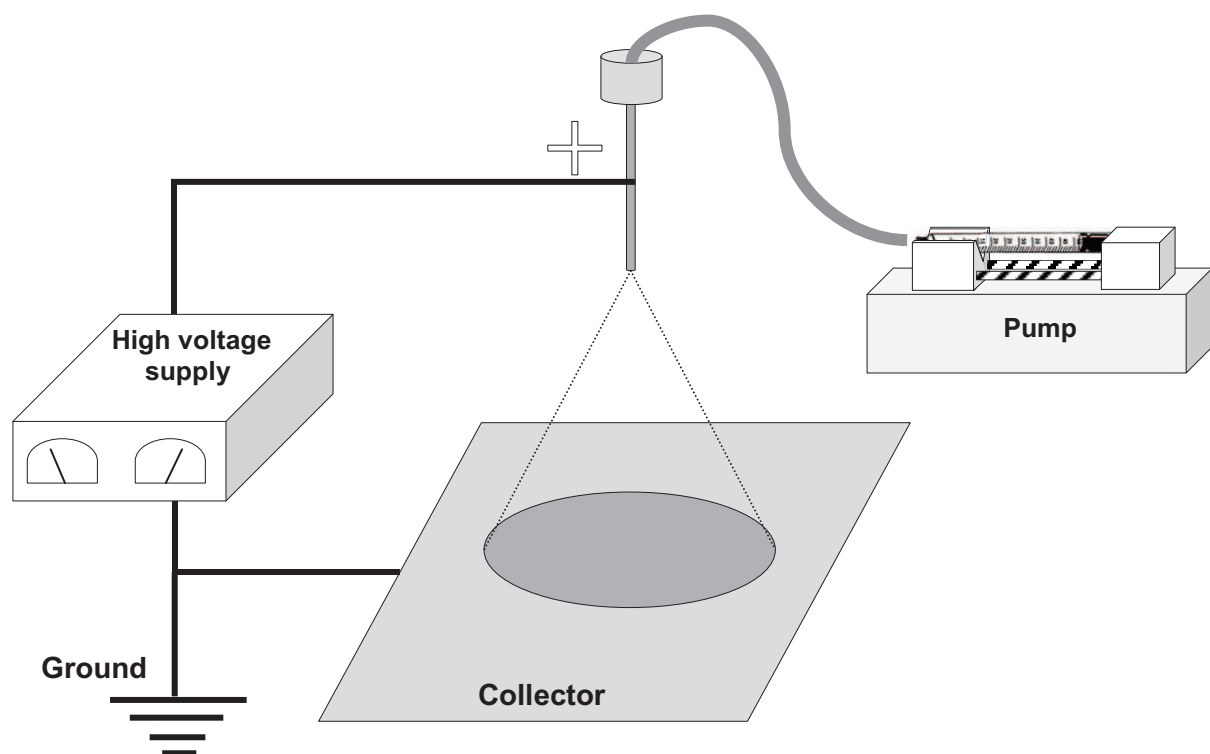


Figure 2.4 : Diagrammatic representation of an electrospinning setup with a control feed pump, high voltage supply, polymer solution reservoir and grounded collector plate.

The polymer solution (or melt) is contained in the reservoir (syringe) and is fed to the steel needle tip (spinneret) by a pump. A high voltage is then applied to the tip of the needle and a grounded collector plate is placed a certain distance from the needle. The potential difference between the spinneret and the collector plate induces an electrostatic charge gradient. The charged droplet of polymer solution at the needle tip then deforms into what is called a Taylor cone⁶². When the forces built over the droplet overcome the surface tension of the solution, the polymer solution forms a jet that stretches and whips from the charged needle tip to the grounded collector plate. The solvent evaporates during this stretching of the polymer jet and ultrafine polymer fibres are collected on the earthed collector. The bending of the fibre jet as it accelerates towards the target collector results in the reduction of the fibre diameter, every time this whipping action occurs.

This technique dates back to 1934 when Formhals published a series of patents (1934 to 1944)⁶³⁻⁶⁹ on the electrospinning of polymer solutions to produce continuous fibre filaments. Until 1993, not much work had been published on using this technique to produce ultra-thin fibres. The group of Reneker did, however, study the use of electrospinning to produce fibres from a range of polymeric materials in the 1990's^{70,71}. This catalysed a revived interest in this technique. Since then, the electrospinning technique has become a widely used and studied processing method of polymer materials. It will not be attempted to give a detailed review of the electrospinning technique, as there are numerous reviews⁷¹⁻⁷⁵ and excellent books⁵⁴ which fully discuss this process in great detail. A brief overview of the parameters affecting the electrospinning of various polymers will be presented with a focus on the facets directly affecting the work presented in this dissertation. Table 2.1 highlights the various parameters that affect the electrospinning process.

Table 2.1 : A summary of the parameters affecting the electrospinning of polymer solutions.

General Parameters affecting the electrospinning process		
Polymer solution parameters	Processing parameters	Ambient Parameters
<ul style="list-style-type: none"> • Molecular weight • Solution viscosity 	<ul style="list-style-type: none"> • Feed-rate • Tip to collector distance 	<ul style="list-style-type: none"> • Atmosphere • Humidity
<ul style="list-style-type: none"> • Surface tension • Solution conductivity 	<ul style="list-style-type: none"> • Voltage • Diameter of pipette 	<ul style="list-style-type: none"> • Pressure
<ul style="list-style-type: none"> • Di-electric effect of solvent 	<ul style="list-style-type: none"> • Temperature 	

As can be seen, there are three main factors, the polymer solution properties, processing conditions and the ambient conditions. As a general rule (also in this work), one aims to eliminate the ambient effects, by working in a laboratory with a relatively stable climate. A brief overview of how the various processing conditions can affect the final fibre morphology is presented below.

2.2.1 Polymer solution parameters

These properties directly affect the resultant fibre morphology and play the biggest factor in reducing the appearance of beading along the fibre axis as well as the amount of stretching and the resultant fibre diameter.

2.2.1.1 Molecular weight, solution viscosity and surface tension:

These three parameters have been grouped together in this discussion as they work concurrently in affecting the electrospinning process. When a polymer sample with a high molecular weight is dissolved at the same concentration as a lower molecular weight version of the polymer, the viscosity is higher in the case of the higher molecular weight sample. For electrospinning to occur, the polymer sample must be of sufficient molecular weight and the solution of sufficient viscosity, as chain entanglements between the molecules are essential. This indicates that there is a boundary condition of polymer concentration for the production of smooth fibres⁷⁶. Without adequate chain entanglements, continuous fibre jets cannot be achieved which invariably leads to electrospaying. It was also shown by Shenoy *et. al.*⁷⁷ that insufficient entanglements lead to jet breaks and beading along the fibre axis. One can increase the viscosity of low molecular weight polymer solutions by increasing the concentration of the solutions. This increases chain entanglements and can yield smooth fibres. It must, however, be noted that if the viscosity is too high, pumping of the solution can become problematic as well as drying of the polymer solution at the spinneret tip⁷⁸. If the viscosity is too low and there is not enough interaction of the solvent molecules with the polymer, the surface tension increases and causes the solvent molecules to bunch together along the fibre axis resulting in bead formation. One can add surfactants and solvents that reduce surface tension to assist in the production of smooth fibres, if the surface tension dominates the electrospinning system. It must also be mentioned that the higher the concentration the thicker the fibres, due to less stretching as shown in work by Deitzel *et. al.*⁷⁹. In this work they showed a power-law relationship between concentration and fibre diameter for the poly(ethylene oxide) (PEO) system under investigation.

2.2.1.2 Solution conductivity and solvent dielectric properties

Ions increase the charge carrying capacity of the polymer solutions, resulting in a larger tension within the polymer jet in an electric field. The addition of salts can aid in increasing the solution conductivity and decrease beading, as the polymer jet is stretched to a larger extent due to the larger solution charge. Increasing the bending instability results in greater stretching and a narrowing of the fibre diameter is achieved, as shown by Zhong and colleagues⁷⁸. Certain solvents also have higher dielectric properties which then eliminate the need to add salts. DMF is an excellent example with a conductivity reading of 1.09 mS.m^{-1} . This was shown in work by Jarusuwannapoom *et. al.*⁸⁰ where they investigated 18 different solvents for the electrospinning of polystyrene fibres.

2.2.2 Processing parameters

These parameters summarise the effect of external forces acting on the polymer solutions. These affect the morphology of the final fibres to a significant, but lesser extent, than the solution parameters discussed previously.

2.2.2.1 Voltage and tip to collector distance (TCD)

It has been found that the effects of voltage and working distance are linked in that decreasing of the tip-to-collector distance mimics the effect of increasing the applied voltage to a certain extent. This phenomenon was shown in work by Li *et. al.*⁷³ as well as Demir and co-workers⁸¹. By increasing the voltage and charge on the polymer solution, the droplet distorts to form a Taylor cone. Depending on the shape and stability of this jet initiating site, the fibre morphology will be affected⁷⁶. At too high a voltage beaded fibres can be obtained which is in contrast to the idea that greater stretching leads to smoother fibres. Deitzel⁷⁶ and Zhong⁷⁸ showed that the beads may be due to increased instability in the jet as the Taylor cone recedes into the spinneret. This can be due to the drawing of the material from the spinneret being faster than the feed-rate of the polymer solution. Further studies also showed contradicting results. In work by Buchko *et. al.*⁸² studying biocompatible protein based fibres and Megelski *et.al.*⁸³ studying polystyrene fibres, the increased voltage lead to greater bending instability, stretching and a decrease in the fibre diameter. Zhao and colleagues⁸⁴, however, found an increase in fibre diameter as the voltage increased due to faster acceleration and essentially a shorter flight time. TCD tends to cause an increase in fibre diameter as the distance is decreased. Shorter flight times and an increase in the apparent electrical field lead to less stretching of the polymer jet. It is also shown by Buchko *et. al.*⁸² that by decreasing the TCD by a critical amount, one experiences insufficient

evaporation of the solvent, resulting in wet polymer collecting on the grounded plate and the formation of an interconnected mesh.

2.2.2.2 Feed-rate of polymer solution

Lower feed-rates result in less polymer solution being drawn from the needle tip. This results in thinner fibres as the volume of material being stretched is less⁷⁸. The jet may also take a longer time to dry if the solution being drawn is too much, resulting in interconnected fibre meshes.

2.2.2.3 Needle spinneret diameter

The smaller the diameter of the needle, the smaller the drop of solution at the tip and the higher the surface tension of the drop. Therefore, a greater force is required for jet formation which results in a slower moving jet with more time to stretch and thin. Depending on the viscosity of the solution, there may be a limiting orifice size before pumping of the solution becomes too difficult.

2.2.2.4 Temperature

Increased temperature has the combined effect of decreasing the viscosity of the solution and increasing the evaporation rate as shown by Demir *et. al.*⁸¹, resulting in fibres with increased diameter uniformity.

2.2.3 Ambient parameters

Collectively, this set of parameters refers to the external or environmental conditions in which one chooses to electrospin.

2.2.3.1 Humidity, pressure and atmosphere

In humid environments, water droplets may accumulate on the surface of the electrospinning jet which can result in pore formation as shown by Megelski and co-workers⁸³. Lower humidity can also increase the facility of solvent evaporation during electrospinning. At very low pressures electrospinning is inhibited due to direct discharge of the charges. At moderately low pressures, the solution tends to flow out of the needle tip resulting in unstable jet initiation. Certain atmospheres tend to break down in the presence of a strong electric field which can hinder electrospinning. Baumgarten⁸⁵ found that by spinning in an atmosphere with a high breakdown voltage, one can obtain fibres with diameters different to those electrospun in air.

2.2.4 Aligned fibres by collector modification

The alignment of electrospun nanofibres can be achieved using a variety of different approaches, each with their own advantages and disadvantages. Depending on the amount of fibres and mesh dimensions needed, a suitable method must be selected. Following are a few techniques one can use to align electrospun fibres.

The rotating drum⁸⁶⁻⁸⁸ is possibly the most widely used technique due to the facile setup and ability to collect thick fibre meshes with well aligned fibres. Instead of a stationary grounded electrode, a grounded rotating drum is used around which the fibres are wound. A disadvantage of this technique is fibre breakage, if the rotation speed is too high. Optimisation according to the polymer system being collected and the speed at which the fibres are being spun is necessary.

Variations of the rotating drum method include the rotating wire drum⁸⁹ and the rotating drum surrounded by wound wire⁹⁰. Advantages of these systems are improved fibre alignment compared to the conventional rotating drum. Drawbacks of these techniques include non-uniform fibre alignment over the entire wire drum and un-even collection of fibres on the wire wound drum. Fibres tend to concentrate on the wire being wound around the drum. Thick fibre meshes are also not possible to collect on the rotating wire drum.

Other rotating collector methods include the rotating tube with knife edge lower electrodes and the knife edge controlled spinning methods^{91,92}. The latter method also uses a rotating drum, but knife edges are used to control the fibre jet, allowing a more concentrated collection of fibres on the rotating collectors. These techniques allow improved alignment of fibres and also control the deposition areas of the fibres on the rotating tubes. Thicker fibre mats can also be electrospun using these collectors. Problems with these techniques arise from the fact that negative counter electrodes are needed which can complicate the setup.

The rotating disc collector^{93,94} allows excellent fibre alignment and control over fibre deposition. A drawback of this technique is that as the collected fibre mesh becomes thicker, the control over alignment decreases. This method also has limited aligned sample collection area, due to the narrow disc edge used to collect the fibres.

The parallel electrode setup⁹⁵ is another method used to collect aligned fibres, but it is a stationary collector. Fibres tend to align between the two electrodes and are easily transferable to various substrates. A high degree of fibre alignment is possible using this technique. A disadvantage is the fact that fibre meshes of limited length are achievable,

limited by the distance between the electrodes. It is also not possible to collect thick mats of aligned fibres.

Other variations on the above mentioned techniques are available, suited specifically for the system under study. The use of negative electrodes, combination electrodes or multiple electrodes are all possible, but one has to make sure which approach is best for the desired fibre mesh format one wishes to achieve.

2.2.5 Special examples of electrospun fibres

Following is a brief discussion of a few interesting examples where electrospinning is able to produce fibres with varying surface structure (increased aspect ratio) as well as new tailor made properties. There is an enormous amount of information available, but the choice of examples are related and limited to the type of polymer studied in this project.

2.2.5.1 Porous and hollow nanofibres

The morphology of nanofibres can be controlled by varying the parameters during the electrospinning process. Beaded fibres can be produced conventionally as mentioned previously, which can dramatically alter the appearance of nanofibres. There are other approaches available to produce fibres with even greater morphological differences, including the production of porous and even hollow nanofibres. Production of such fibres can dramatically increase the available surface area of the nanofibres. Work by Bognitzki *et. al.*⁹⁶ and Megelski *et. al.* showed that the mechanism of pore formation on a polymer film cast from solution can also be applied to the formation of pores on nanofibre surfaces. This mechanism is a function of solvent type, polymer species and electrospinning parameters. During the convective evaporation of solvent from the electrospun fibre or cast film, the solution becomes thermodynamically unstable. This results in segregation of polymer rich domains and solvent rich domains in the polymer solution. The polymer rich domains then dry and solidify before the polymer poor domains, which in turn leads to pore formation. It is clear that the solvent vapour pressure is critical in determining the formation of pores in the final product. Megelski and colleagues⁸³ studied four different polymer types, which they electrospun from a variety of solvents with different vapour pressures. The use of less volatile solvents such as dimethyl formamide (DMF) resulted in a decrease in pore formation. They also found that the humidity played an important role in the formation of pores on the surface. During rapid evaporation of solvent there is an accompanying cooling effect as the fibre travels from the spinneret to the collector. During this cooling, moisture in the atmosphere condenses on the fibre surface creating beaded fibres. As the fibres dry

and solidify the water droplets leave behind physical imprints on the surface of the fibres⁹⁷. It must be noted this type of porosity is limited to the surface of the fibres only. Later work by Casper *et. al.*⁹⁸ studied polystyrene electrospinning from tetrahydrofuran (THF) at different humidities. They found that smooth fibre surfaces persisted at humidities lower than 25%, while above 30% pore formation occurred. Increasing the humidity lead to increased pore number, distribution and size. When electrospinning higher molecular weight polystyrene, the fibre structure remained the same but the formation of larger pores with greater size distribution occurred. Another method to produce porous fibres is by the electrospinning of two different polymer types followed by removal of one of the phases. Unlike the previously mentioned techniques, this method allows the formation of fully porous fibres, not only at the surface. Wendorff *et. al.*⁹⁹ studied blends of poly(lactic acid) (PLA) with poly(vinyl pyrrolidone) (PVP), where they selectively removed one of the components after fibre production. They found that at a 50/50 ratio of PLA to PVP, that the best porous fibres were obtained.

Hollow fibres can also lead to a dramatic increase in available surface area. A common way to achieve this is by coaxial spinning^{54,75,100,101} of different polymer types. This process enables one to produce nanofibres with a core consisting of one material and a shell consisting of another. Selective removal of the polymer core allows the production of nanofibres with hollow interiors. Work by Li and Xia¹⁰², electrospun PVP fibres containing titania precursor together with an oil as core. After removal of the core oil using octane, the fibres were calcined creating hollow TiO₂ nanofibres. Larsen and colleagues¹⁰³ demonstrated the polymer free production of SiO₂ and ZrO₂ nanotubes by electrospinning an aged sol together with an immiscible liquid oil (glycerine, olive oil). After removal of the oil, hollow nanotubes were obtained.

2.2.5.2 Electrospun emulsions and amphiphilic solutions.

The electrospinning of such polymer solutions opens a new door to the production of nanofibres with improved or additional functionality. Work by Kim *et. al.*¹⁰⁴ studied the electrospinning of an amphiphilic copolymer of poly(vinyl alcohol) (PVA) with polyhedral oligosilsesquioxane (POSS) macromonomers. In the dry state PVA has good mechanical properties, but in biological applications were it can come into contact with water, it dissolves. By combining the hydrophobic POSS macromonomer with the hydrophilic PVA they aimed to prevent the electrospun fibres of PVA from solubilisation in water. They found that at a molar ratio of POSS of 4.7, the as spun amphiphilic fibres did not dissolve, but swelled in water. Hadjiargyrou and co-workers¹⁰⁵ electrospun fibres of poly(lactide-co-

glycolide) (PLGA) to produce a scaffold for the release of a hydrophilic drug. Incorporation of an amphiphilic block copolymer poly(ethylene glycol)-block-poly(lactic acid) PEG-b-PLA, allowed a slower release of the drug up to a period of one week. Other work by Kim, Lee and Knowles¹⁰⁶ prepared amphiphilic solutions of PLA and hydroxyapatite (HA) by the use of surfactant to disperse the hydrophilic HA powder and the hydrophobic PLA in chloroform. Electrospinning of this solution enabled excellent distribution of the ceramic HA and cell growth was successful on this fibre scaffold. Work by Xu *et. al.*¹⁰⁷ used emulsion electrospinning of a water in oil system. They had an aqueous solution containing a solvated anti-cancer drug doxorubicin hydrochloride (Dox). The oil phase consisted of an amphiphilic block copolymer of PEG-b-PLLA dissolved in chloroform. Drop-wise addition of the aqueous solution with agitation yielded a stable emulsion that was later electrospun. It was found that the drug was encapsulated in the amphiphilic polymer fibres and was released over time. Emulsion electrospinning can also yield core-sheath structures, similar to those obtained from coaxial spinning, but via a single spinneret. Xu and colleagues¹⁰⁸ electrospun a water in oil emulsion, where the water phase contained dissolved PEG. The oil phase consisted of chloroform with an amphiphilic copolymer of PEG-b-PLLA in solution. Definite core-sheath fibres were formed with a core of PEG and a PLLA shell. Core-sheath formation was ascribed to stretching and evaporation induced de-emulsification. In principle, this technique can be applied to any pair of water-soluble polymer and hydrophobic (or amphiphilic) polymer. Lin and co-workers¹⁰⁹ looked at reinforcing a dental resin system of 2,20-bis-[4-(methacryloxypropoxy)-phenyl]-propane/ tri (ethylene glycol) dimethacrylate BIS-GMA/TEGDMA. They looked at using electrospun core-shell fibres of PAN (core) and poly(methyl methacrylate) (PMMA) (shell) by blending of the two polymers. They aimed to increase the interfacial adhesion between the fibre filler and the methacrylate based dental resin by the use of a PMMA outer shell. The incorporation of 7.5 wt% core shell nanofibres was shown to increase the flexural strength by 18.7 %, elastic modulus by 14.1 % and the fracture energy by 64.8 %. From this handful of examples it is clear that the electrospinning of emulsions with emphasis on the use of amphiphilic copolymers is a relatively new and exciting area. The ability to create fibres that can be used as scaffolds for tissue engineering or drug release requires the use of polymers that have multiple properties in solution or in the final solid state.

2.2.5.3 Electrospun fibres containing functional materials or fillers

A variety of particles can be added to electrospinning solutions for incorporation in the final fibre structure. The incorporation of multi-walled carbon nanotubes MWCNTs is an area of growing importance and is discussed at a later stage in this literature review chapter. There

are, however, a variety of different materials one can add to nanofibres to alter or improve final fibre properties. Greiner *et. al.*¹¹⁰ added palladium diacetate to a PLA solution to increase conductivity and assist in thinner fibre formation. Annealing of these samples yielded fibres containing palladium nanoparticles. Reneker and Hou¹¹¹ incorporated iron salts into an electrospun solution of PAN. After carbonisation of the PAN, the resultant carbon nanofibres contained iron nanoparticles due to reduction of the iron salts during the carbonisation process. These iron nanoparticles were then used as catalytic sites for the growth of carbon nanotubes from the carbon nanofibres. Work by Zhang *et. al.*¹¹² incorporated Fe₃O₄ nanoparticles in PAN fibres to produce nanofibre sheets with magnetic properties. Various drugs can also be incorporated into nanofibres enabling slow release of the medicinal agents^{105,107}. It must be noted that in the case of the additives not being soluble in the polymer system, two phase systems (blends or emulsions) can be used to allow incorporation as shown by Sanders and colleagues¹¹³. Once again, there is a vast array of possible materials that can be added to electrospun nanofibres, which are outside the scope of this discussion. A recommended review article by Huang and co-workers⁷² looks at the state of nanofibre composite trends and advancements. Other reviews¹¹⁴⁻¹¹⁶ are also available which give brief overviews of the different properties nanofibre composites offer.

2.3 Polymer nanocomposites

The term nanocomposite refers to a class of materials where one or more of the components in the composite are of nano-scaled dimensions. Usually this refers to systems, where one has a polymer matrix that is filled with nano-scaled filler agents, be they particles, sheets or fibrous materials. Usually, the physical properties of the composite materials differ greatly from the properties of the disparate components. The difference between conventional micron-sized fillers and their nano-scaled analogues is the remarkable increases in aspect ratios when using fillers of a nano-scaled dimension. The interfacial area between the filler particles and the polymer matrix is greatly enhanced allowing more effective load transfer to the filler particles and usually far superior physical performance is achievable even at lower loadings¹¹⁷⁻¹²⁰. Attempting to present a detailed discussion on nanocomposites is challenging as the amount of literature available is considerable. A brief overview of the more common types of nano-scaled composite fillers will be given, focusing on the materials under study in this work, namely, MWCNTs and nano-fibres. Below in Figure 2.5 one can view the three main classes of composite fillers, particulate, sheets and fibres/fibroids with their aspect ratio formulae¹¹⁹.

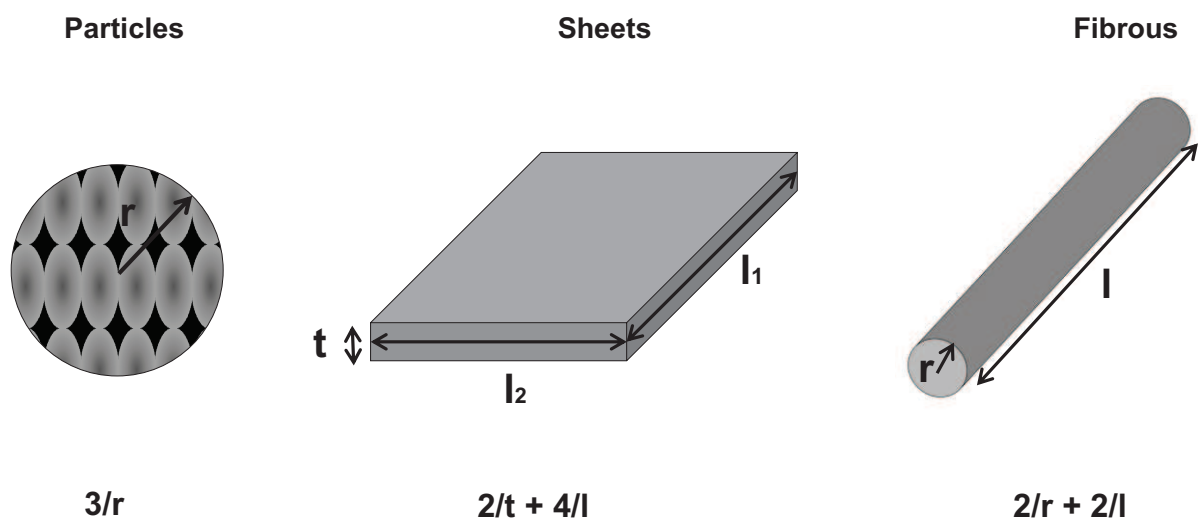


Figure 2.5 : Three main classes of filler dimensions with aspect ratio (surface area to volume) formulae¹¹⁹.

One can see from Figure 2.5 how a decrease to nano dimensions can drastically increase the aspect ratios of these filler types.

2.3.1 Particulate fillers

There are a variety of fillers of this type including SiO₂ particles^{121,122}, aluminium particles¹²³, alumina particles^{124,125}, metal oxides¹²⁶, calcium carbonate (CaCO₃)¹²⁷ and carbon black¹²⁸. The review article by Zou *et. al.*¹²² is a very comprehensive compilation on the preparation, characterisation, properties and applications of silica (SiO₂) based nanocomposites which are one of the most widely studied particulate fillers for nanocomposite preparation. As is widely known, for fillers to be useful in the reinforcement of polymer matrices there needs to be a degree of interaction between the filler surface and the polymer matrix. This interfacial adhesion allows not only, better load transfer from the matrix to the filler particles, but also aids in the distribution of the particles throughout the matrix. It is known that agglomeration of filler particles generally leads to a decrease in composite properties. There are a variety of ways in which to prepare polymer nanocomposites. Vollenburg *et. al.*¹²⁵ used physical mixing to incorporate alumina and glass beads in polystyrene, polycarbonate and poly(styrene acrylonitrile) copolymers. They dispersed the polymer in a polar solvent and added the filler and mixed thoroughly for a few hours. The solution was then dried and additional polymer was added to produce varying filler content. They showed good results with the alumina beads ranging from 35 to 400 nm in size. Chan and colleagues¹²⁷ used melt mixing to disperse 40 nm sized CaCO₃ particles in stabilised polypropylene. They obtained good dispersions at lower filler content, but at loadings higher than 13 wt% agglomeration of the particles occurred. To increase the dispersion of the particles, surface modification can be performed as was done by Rong *et. al.*¹²⁹. In this case irradiation polymerisation of polystyrene was used to graft the polymer to the surface of the SiO₂ filler particles. This greatly increased the dispersion of the fillers in the polypropylene matrix using conventional compounding techniques and also increased the mechanical properties. As summarised briefly above, the most common ways of composite preparation include melt blending, solvent blending and mechanical extrusion mixing methods. In the case of silica particles other techniques such as cryo-milling used by Li *et. al.*^{130,131} to disperse silica particles in a poly(ethylene terephthalate) matrix can be used. Ball-milling was also shown to increase fumed silica dispersion in PMMA matrices as shown by Gonza'lez-Benito *et. al.*¹³² where, the properties of the final composite were related to the time spent milling the components. The review article by Zou *et. al.*¹²² investigates other methods of silica nanocomposite fabrication where the dispersion methods allow strong interaction between the silica nanoparticles and the matrix. The use of *in situ* functionalised polymerisation as well as sol-gel techniques to produce the nanocomposites are presented. Carbon black is also a widely known filler commonly used in the manufacturing of car tyres. As with the previously

mentioned fillers, dispersion is key in composite material enhancement. Work by Patel and Lee¹³³ investigated the aggregate size of the carbon black particles and found a relationship between the dynamic and mechanical properties of the nanocomposite and the degree of agglomeration. The review article by Jan-Chan Huang¹²⁸ focuses on the conductive nature of this filler and presents a detailed overview of the electrical properties that carbon black can offer a composite. It is also shown that at higher content (as required for electrical conductivity) poorer mechanical performance is observed due to uneven dispersion of the filler particles. Improving dispersion and interaction via surface modification can be used, as presented in the review by Tsubokawa¹³⁴. There is a plethora of information regarding particulate fillers which is difficult to fully discuss in this brief summary, but one should have a basic understanding of the factors influencing composite fabrication, dispersion and property modification.

2.3.2 Sheet fillers (platelets)

There are only two main filler materials that have been widely studied in this class, namely, graphite sheets and exfoliated clay sheets. Both of these filler types exist as layered materials. To fully utilise these materials one needs to separate these layers by introducing polymer molecules that can push the layers apart¹³⁵. Intercalated clay composites are obtained when the clay platelets are pushed apart by the presence of polymer material penetrating the gallery spacings between the sheets. When the layers are fully separated from each other we have what is known as “exfoliated clay”. The most commonly used clays are montmorillonite, saponite and synthetic mica. The following recent reviews¹³⁵⁻¹³⁷ present comprehensive summaries of the latest developments in the production of clay nanocomposites. The revolutionary work of the Toyota group¹³⁸ revived interest in this class of nanocomposites where they showed that increased mechanical performance and barrier properties could be achieved by the inclusion of small amounts of montmorillonite clay in nylon-6 matrices. The addition of clay can enhance the following properties of the composite matrix including; increased moduli and strength¹³⁹⁻¹⁴¹, flame retardancy¹⁴², heat resistance¹⁴³, decreased gas permeability¹⁴⁴⁻¹⁴⁶ and increased biodegradability¹⁴⁷ in the case of biodegradable polymers. Graphite sheets also enable enhanced mechanical properties greater than that of the clay composites including¹¹⁹ increased modulus, tensile strength and thermal conductivity, with an increased electrical conductivity. The percolation threshold for exfoliated graphite sheets has been shown to be 1 wt% and work by Zheng *et. al.*¹⁴⁸ showed that lower thresholds could be achieved in high density polyethylene based nanocomposites. Once again interaction between the sheets and the polymer matrix is essential for dispersion

of the particles. In the case of clay platelets, the surfaces are highly hydrophilic (containing hydrated Na^+ and K^+ ions) and interact well with hydrophilic polymers like poly(ethylene oxide) and poly(vinyl alcohol). One must modify the surface of the clays to facilitate interaction with other organic polymers. Modification can be done via ion exchange using cationic surfactants (generally: primary, secondary, tertiary alkylammonium or alkylphosphonium cations)^{135,137}. Large molecules like these surfactants increase the gallery spacing allowing a larger surface area to be exposed to the polymer matrix. One can even use these cations as initiation sites for polymerisation to increase the interaction with the polymer matrix^{149,150}. Work by Samakande *et. al.*¹⁵¹ showed how cationic exchange with reversible addition chain fragmentation transfer (RAFT) agents allowed the controlled bulk polymerisation of polystyrene which remained tethered to the clay surfaces and lead to full exfoliation of the clay platelets. Later work by Samakande and colleagues¹⁵² used the same tethered RAFT technique to polymerise polystyrene using mini-emulsion.

2.3.3 Fibrous fillers

In this class of fillers focus will be directed to the materials used in this study, namely, electrospun fibres as well as carbon nanotubes, specifically single and multi-walled carbon nanotubes (MWCNTs).

2.3.3.1 Carbon nanotubes

One can include various additives to electrospinning solutions to alter parameters, for example, solution conductivity and viscosity can be modified by the addition of salts¹⁵³, conductive particles (eg. nanotubes¹⁵⁴⁻¹⁵⁶) or magnetic particles¹¹², among others. Earlier nanocomposites used carbon blacks, carbon nanofibres, silicas and clays as nano filler materials. The use of carbon nanotubes (CNTs) was more recently exploited. First reported by Iijima¹⁵⁷ in 1991, MWCNT's are outstanding candidates for polymer reinforcement¹⁵⁸ due to their excellent mechanical integrity as well as electrical conductivity and thermal properties. Ajayan *et al.*¹⁵⁹ first reported the use of carbon nanotubes as fillers in their 1994 paper published in *Science*, where they produced arrays of aligned carbon nanotubes by cutting of an embedded resin. Due to the remarkable properties of these materials they add considerable value to the field of polymer nanocomposites, however, there are numerous challenges to face when working with this class of materials. Most known preparations of nanotubes yield products with varying aspect ratios, diameters, chirality as well as different amounts of impurities and structural irregularities. This makes reproducible comparisons between various batches challenging not to mention comparisons to literature examples of

other investigators. The practical transference of nanotube properties to that of the polymer matrix under investigation is also extremely challenging and requires astute strategies of filler functionalization and sample preparation. There are a number of reviews which look at nanocomposites focusing on the development of carbon nanotube systems.¹⁶⁰⁻¹⁶³ Firstly, I will discuss a few fundamental aspects of carbon nanotubes regarding their structure, properties, synthesis techniques and modification for use as fillers.

2.3.3.1.1 Carbon nanotube structure

There are two different types of carbon nanotubes (CNT), single-walled carbon nanotubes (SWCNT) and the type studied in this project, multi-walled carbon nanotubes (MWCNT). Simplistically, they can be described as graphitic sheets that have been rolled up to form a seamless tube or cylinder, where one sheet gives rise to a SWCNT and multiple sheets creating a MWCNT. The distances between the graphitic shells of the MWCNTs are 0.34 nm^{157,162}. The covalently bonded carbons constituting the nanotube monolayers are sp² hybridised (one *s*-orbital and two *p*-orbitals) and form a hexagonal lattice as seen in Figure 2.6¹⁶⁴. The strong in-plane covalent bond is known as the σ -bond, and the remaining *p*-orbital perpendicular to the plane gives rise to the π -bond. The π -bonds are responsible for the interactions between the graphitic monolayers as well as the electrical conductivity of the nanotubes. The structure of a CNT can further be described in the form of a chiral vector. When rolling up a single sheet, the orientation of the graphitic lattice with respect to the tubes' longitudinal axis, gives rise to this chiral vector $\vec{C}_h = na_1 + ma_2$. Based on this there are three types of SWCNT structures, namely: armchair CNTs (*n, n*), zig-zag CNTs (*n, 0*) and chiral CNTs (*n, m*). These structures are illustrated in Figure 2.6¹⁶⁵. It must be noted that the electronic properties of the CNTs are strongly linked to the chirality of the nanotubes¹⁶⁶. The nanotube diameter and chiral angle can be calculated according to the following equations¹⁶⁴:

$$d_{CNT} = \frac{a\sqrt{n^2+m^2+nm}}{\pi} \quad (2.9)$$

$$\cos \theta = \frac{2n+m}{2\sqrt{n^2+m^2+nm}} \quad (2.10)$$

The diameters of MWCNTs depend on the inside diameter as well as the number of concentric graphitic shells, which may vary from 1 to 20. This does increase the diameter of the MWCNTs which lead to a decrease in the aspect ratio, or surface to volume ratio.

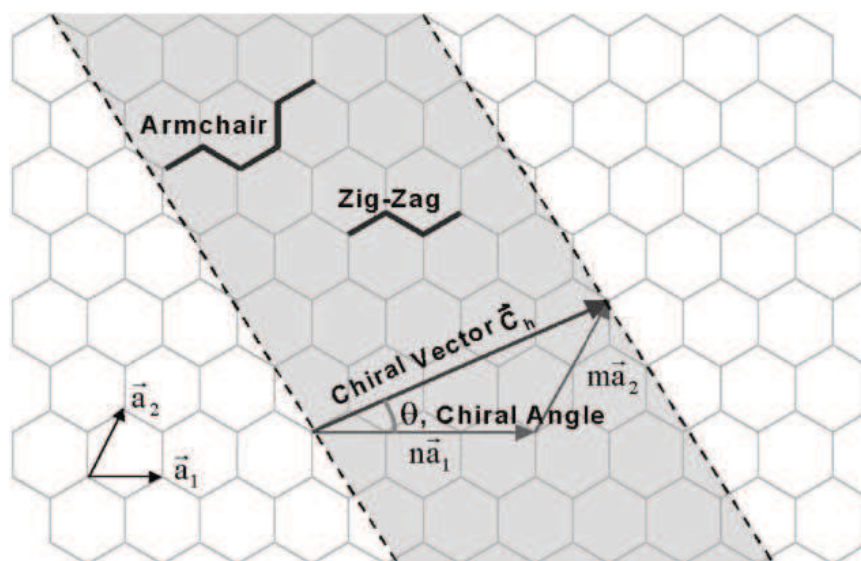


Figure 2.6 : Schematic diagram showing the hexagonal lattice of a grapheme sheet and how the concept of the chiral vector¹⁶⁵.

Peigney *et. al.*¹⁶⁷ calculated the theoretical surface areas of the different types of nanotubes, where SWCNTs showed values of $1315 \text{ m}^2 \cdot \text{g}^{-1}$. Values for the MWCNTs varied from this to several ten square meters per gram.

The production of CNTs invariably lead to a mixture of products with varying lengths, diameters and impurity content. Depending on the technique used, different product properties are attained.

2.3.3.1.2 Carbon nanotube synthesis

The three most common methods of CNT production are laser ablation, arc-discharge and chemical vapour deposition. There are numerous reviews^{164,168} and articles dealing with these methods, and a brief summary is presented in the following section.

2.3.3.1.2.a Laser ablation:

In this process a laser directed onto a piece of graphite causes carbon atoms to evaporate during irradiation. This process takes place in a heated furnace at a temperature of $1200 \text{ }^\circ\text{C}$, and makes use of a pulsed laser. In the production of SWCNTs the graphite target usually contains a transition metal catalyst (Ni, Co, Yt)¹⁶⁹. The evaporated carbon then gets carried by an inert gas flow to a condensation unit where the MWCNT CNTs are formed¹⁷⁰. This method was developed by Smalley and co-workers¹⁷¹ at Rice University. Unfortunately, this process presents low yields and is not economically viable for large scale production.

2.3.3.1.2.b *Arc-discharge:*

This process uses two graphite electrodes between which an electrical arc is generated in an inert atmosphere at low pressures¹⁷². In this case, carbon atoms are evaporated at the anode and then condense at the cathode to produce the MWCNTs along with graphite sheets^{157,173}. The addition of metal catalysts (Ni, Fe, Co, Cr) enables the production of SWCNTs¹⁷⁴. CNTs produced using this method tend to contain fewer defects, but are comparatively short. This method is not suitable for large scale production due to economic reasons.

2.3.3.1.2.c *Chemical vapour deposition (CVD):*

Endo *et. al*¹⁷⁵. was among the first groups to develop this method of CNT production. This technique is used to produce CNTs on a large scale. Although the CNTs contain more structural defects when produced using this technique, they still maintain sufficient properties for various applications. Another benefit is that much longer CNTs can be produced this way which makes it advantageous for electrical conductivity purposes. In this process gaseous carbon sources (hydrocarbons) are used to grow the CNTs off of a metal catalyst which acts as a nucleation site¹⁷⁶. The catalyst can be supplied directly into the reactor or on a substrate or formed *in situ*, as is the case when using ferrocene¹⁷⁷. Reaction temperatures are in the range of 700 – 1000 °C. Both SWCNTs and MWCNTs can be produced using this method, and better control over CNT structure is possible when compared to the previously mentioned techniques¹⁷⁸.

2.3.3.1.3 **Carbon nanotube functionalization**

One of the challenges when working with CNTs is the disruption of aggregation of the nanotubes. Strong van der Waals forces between the CNTs cause them to agglomerate and form CNT bundles or ropes which can reduce the mechanical enhancement that these materials offer polymer composites^{116,165,179} by poor solubilisation with solution or polymer matrices leading to uneven dispersion and load transfer¹⁸⁰. Bundles refer to non-crystalline collections of SWCNTs as well as MWCNTs. Ropes^{181,182} specifically refer to SWCNTs, where the packing is such that a hexagonal lattice structure is formed. As shown by Salvetat *et.al.*¹⁸² this can cause slipping and a decrease in composite properties. Moderate dispersion is possible using ultrasonication in certain solvents such as dimethylformamide (DMF), however, most suspensions are unstable and short lived. Nanotube functionalisation has been shown as an effective tool for the de-agglomeration of CNT bundles. Functionalisation can not only assist in the solubilisation of nanotubes in solvents, but also prevents agglomeration and interaction with other chemical moieties such as polymer molecules.

Figure 2.7 compares two functionalisation methods (a) covalent bonding and (b) adsorption or polymer wrapping. The fact that CNTs are more susceptible to covalent reactions due to their chemical structure (misalignment of the π -orbitals of the sp^2 hybridised carbon atoms)¹⁸³ than flat graphite sheets makes them ideal candidates for chemical modification. Two major approaches are used in CNT functionalisation, the “open end” approach¹⁸⁴ and the direct “side-wall” attachment method¹⁸⁵. The “open end” functionalisation method which usually involves refluxing in concentrated nitric acid introduces carboxylic acid functionality to the surface of the nanotubes, but can be destructive^{186,187}. Usually such modification leads to a decrease in the CNT length as well as disruption of the π -conjugation in the nanotubes leading to a dramatic decrease in the conductivity. The carboxylic functionality can be converted to other reactive functionalities using standard chemical procedures and is discussed in detail in the review by Sun *et. al.*¹⁸⁴. Sun and colleagues¹⁸⁸⁻¹⁹⁰ have shown how it is possible to functionalise (and solubilise) CNTs of any length by esterification of the carboxylic functionality as well as de-functionalisation via hydrolysis. It has also been shown in work by Ge *et. al.*¹⁹¹ that the carboxylic functionalities, without further modification, obtained after oxidation allows a strong interaction with polyacrylonitrile (PAN) via formation of a charge transfer complex. They also found that after sonication, the MWCNTs remained in suspension for up to 4 days.

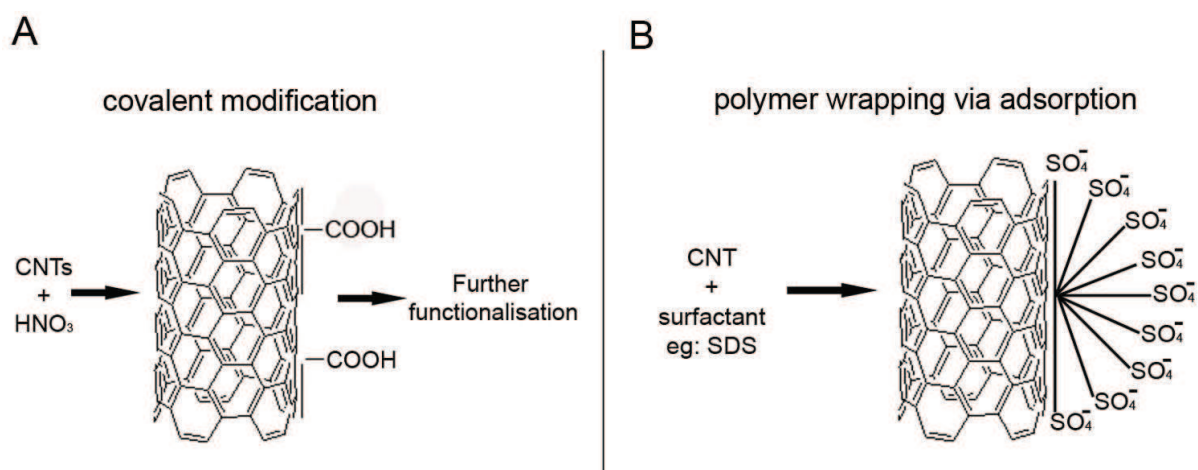


Figure 2.7 : Diagrammatic illustration of covalent modification of CNTs versus adsorption or polymer wrapping, both used for CNT dispersion.

The direct covalent attachment of functional groups to the CNT surfaces is the second general method¹⁸⁵ used to functionalise CNTs. There are many approaches that have been studied, including fluorination (Michelson and colleagues^{192,193}), hydrogenation (Pekker *et.*

*al.*¹⁹⁴) using the Birch reduction in ammonia, and 1,3 dipolar cycloadditions shown by the group of Hirsch¹⁹⁵. Holzinger *et. al.*¹⁹⁶ also showed various reactions involving the use of nitrenes, carbenes and radicals. Other modification methods involve the adsorption of molecules to the surface of the nanotubes instead of covalent bonding. Work by Smalley *et. al.*¹⁹⁷ showed the “polymer wrapping” technique, where a close association with poly(vinyl pyrrolidone) PVP and poly(styrene sulfonate) PSS yielded SWCNTs that were water soluble. By changing the solvent type, the CNTs could be reversibly unwrapped. Star and co-workers also investigated the polymer wrapping technique to successfully solubilise CNTs in different organic solvents. An additional method that has been studied to solubilise and prevent the agglomeration of CNTs non-covalently is by introducing surfactants. O’Connell and colleagues¹⁹⁸ used ultrasonication of raw SWCNTs with sodium dodecyl sulphate (SDS) as surfactant to obtain individual micellularly wrapped nanotubes for fluorescence analysis. Islam *et. al.*¹⁹⁹ used sodium dodecylbenzene sulfonate to solubilise CNTs in water. They managed to disrupt bundle formation and produce individually wrapped nanotubes in solution. They proposed that the alkyl chain groups of the surfactant molecules adsorb along the axis of the nanotube surface. The benzene groups allowed better spacing for the SO₃⁻ charged groups hence a better dispersion. The review article by Meng, Fu and Lu²⁰⁰ presents a comprehensive overview of functionalised nanotubes and their use in modern applications. After the brief background in CNTs and the discussion of various ways in which to modify CNTs to limit agglomeration and allow solubilisation or miscibility with other solvents and polymers, I will now discuss a few different methods generally used to produce CNT nanocomposites.

2.3.3.1.4 Carbon nanotube filled nanocomposites

This section will summarise some of the major methods used to produce CNT filled polymer nanocomposites. The three most widely used approaches include melt blending, *in situ* polymerisation and solution blending. A brief overview of a few other techniques which have also been used to produce this class of nanocomposites will be presented.

2.3.3.1.4.a Melt blending

Melt blending is the most commonly used industrial technique for the production of CNT nanocomposites. This method uses high temperatures and shearing forces to disperse the CNTs in the polymer matrix. Conventional extrusion, blow moulding and injection moulding techniques can be used in the composite preparation which makes it industrially viable^{116,201,202}. Drawbacks of this technique include high viscosity at high CNT loadings as well as poorer dispersion characteristics. These issues make it difficult to produce

composites with high CNT loadings using the melt blending method. It has been shown that nanotubes tend to retain their high aspect ratios even after high temperature shearing^{201,203-205}, which is an advantage over previously used micro-fibrous fillers, with very little breakage. They can even align in the direction of melt flow²⁰⁶.

An early study by Jin and co-workers²⁰⁷ mixed PMMA with MWCNTs (26 wt%) at 200°C thereafter it was compression moulded to form sample films which showed adequate dispersions despite the high MWCNT concentration. Further work²⁰⁸ showed that compatibilisation with the PMMA matrix could be achieved by using MWCNTs coated with poly(vinylidene fluoride). Two publications by Andrews *et. al.*^{202,209} showed the melt processing behaviour of MWCNTs with different polymers including high impact polystyrene, polypropylene and acrylonitrile-butadiene-styrene (ABS) rubber. They found increased dispersion of the MWCNTs with increased shearing/mixing energy. Increased mixing time or shearing speed resulted in better dispersion but at a cost of decreasing the length of the MWCNTs by a quarter its original length due to mechanical breakage. Other successful examples of melt blending include work by Zhang *et. al.*^{210,211} where they dispersed MWCNTs in Nylon-6.

2.3.3.1.4.b *In situ* polymerisation

Fabrication using this process entails the suspension of CNTs in a monomer solution after which polymerisation takes place. In most cases, functionalised nanotubes are used to aid in the dispersion of the CNTs in the solution. One can also covalently bond the nanotubes to the polymer matrix by making use of condensation reactions. A large amount of *in situ* studies are for systems making use of epoxy resins^{203,212-215}. Interesting work by Schadler *et. al.*²⁰³ showed that the MWCNT composites they made displayed improved performance in the compression testing than the tensile testing. They ascribed this phenomenon to the fact that in tensile testing only the outer layers of the MWCNTs took load, while in compression the entire nanotube carried load. Moniruzzaman and co-workers²¹⁵ presented a novel way of grafting SWCNTs to epoxy resin molecules by heat treatment prior to curing. At 0.05 wt% loading they found significantly improved flexural properties. Early work by Jia *et. al.*²¹⁶ synthesised MWCNT filled PMMA composites showing increased mechanical properties, but later work by Velasco-Santos and colleagues²¹⁷ used chemically modified MWCNTs to process with PMMA and obtained a storage modulus increase of 1135% with 1 wt% loading. MWCNTs functionalised with carboxyl groups, were shown to form a charge transfer complex with ϵ -caprolactam in work by Zhao *et. al.*²¹⁸ which assisted in the dispersion and interaction of the MWCNTs in the final polyamide-6 matrix after polymerisation of the ϵ -

caprolactam. Similar charge transfer complexation has been found to occur between carboxylate MWCNTs and PAN as shown by Ge and co-workers¹⁹¹. It can be seen that *in situ* polymerisation blending of CNTs into composites present a very attractive route to excellent dispersion, interaction and property enhancement characteristics, whether the MWCNTs are covalently or non-covalently modified.

2.3.3.1.4.c Solution blending

This method is the most widely used technique in preparing polymer composites, as it is useful to prepare samples of smaller scales as well as relatively simple to perform. The main steps in this route are CNT dispersion in a suitable solvent, followed by the addition of the polymer matrix which is then allowed to solubilise. The composite can then be cast out of solution. As mentioned previously, solubilisation of CNTs are challenging and require surface modification via covalent or non-covalent functionalising. This has been discussed in the previous section so I refer you back to the techniques used. To prevent the formation of CNT bundles in solution, one also needs to ultrasonicate the nanotubes, but this does cause damage, usually reducing the lengths of the CNTs²¹⁹. One needs to optimise the sonication time relative to the CNT breakage or the aspect ratios may drop too low, reducing the property enhancements possible. Jin and co-workers²²⁰ performed earlier work where MWCNTs were dispersed via sonication in chloroform. After addition of the polymer to the solution, further sonication was performed before solvent film casting. Reasonable dispersions were achieved. Many groups have used this and similar approaches where the pre-dispersed CNTs are mixed further with pre-dissolved or dry polymer^{221,222}. Work by Ruan *et. al.*²²³ used mechanical mixing and sonication to disperse the CNTs but incorporated the polymer under reflux for toughening polyethylene (PE) composites.

Surfactants have been used for solution blending to disperse the nanotubes in solution²²⁴⁻²²⁶, but the surfactants remain in the composites after solvent removal which can be problematic. Sundararajan and colleagues²²⁷ found that the surfactant TritonX-100 induced crystallisation of the polycarbonate matrix, which affect the opacity and impact properties of the material. Thermal conductivities of composites can also be affected as shown by Bryning *et. al.*²²⁸ where the surfactant containing SWCNT epoxy composites exhibited increased interfacial thermal resistance.

A further challenge is the agglomeration of CNTs as the solvent evaporates. Methods to reduce this evaporation time and decrease the effect of CNT bundling have been studied, and they include spin casting²²⁹⁻²³¹ (solution dropped onto a high speed rotating substrate) and drop casting²³² (solution is dropped onto a heated substrate). Other methods exist, as

shown by Singh *et. al.*²³³ where they took a partially dried sample and then increased the heating rate rapidly, allowing a final rapid solvent evaporation (wet annealing). Du and colleagues²³⁴ developed a coagulation method, where the MWCNT polymer solutions are added to a non-solvent in excess. The CNTs are then entrapped by the polymer as they precipitate out of solution preventing CNT agglomeration. Another more recently used method is electrospinning (whipping of the solution jet leads to rapid solvent evaporation). In this case excellent dispersions can be attained along with alignment of the CNTs in the direction of the fibre axis. For more detail on electrospinning materials with nanotubes I refer you back to the electrospinning section on composite nanofibres. This method of solution blending and electrospinning is the approach used in this project to produce MWCNT filled PAN-g-PDMS nanofibres.

2.3.3.1.4.d Other blending methods

Some methods such as pan milling²³⁵ and twin screw pulverisation²³⁶ allow composite preparation in the solid state. Another promising technique is the use of emulsion polymerisation, where the CNTs are dispersed in solvent (water) and the latex particles are then added to this solution²³⁷⁻²⁴¹. Subsequent freeze drying produces composite materials with excellent nanotube dispersions. Other techniques look at using the CVD method of CNT production where they grow arrays of nanotubes in polymer substrates, as shown in the following work using PDMS substrates^{242,243}. Work has also been done where the CVD process was used to grow CNTs on the surface of carbon fibres, which were subsequently embedded in a polymer matrix²⁴⁴. This field appears to be continually growing where newer methods are always under study with the ambition to produce composites with greater filler dispersion and improved properties.

2.3.3.1.5 Carbon nanotube alignment in composites

The alignment of carbon nanotubes is an interesting field, and a variety of methods exist that can achieve this. I shall summarise a few of these techniques. Raravikar *et. al.*²⁴⁵ prepared PMMA composites containing aligned arrays of CNTs, by growing nanotubes using the CVD process and then impregnating these arrays with the monomer. After *in situ* polymerisation composites were obtained with aligned nanotubes. Another method to achieve alignment is by *in situ* polymerisation under an electric field as shown by Kimura and colleagues²⁴⁶. They showed that alignment of MWCNTs in a polyester matrix could be achieved by polymerisation in the presence of a magnet. The degree of alignment depended on the magnetic anisotropy of the MWCNTs and the resistance against Brownian motion and the solution viscosity. Spin coating of composite films can also result in alignment, as illustrated

by Pradhan and co-workers²⁴⁷. This method was shown to rely on the fluid flow of the composite solutions as evaporation takes place. Blown bubble films have also been shown to align nanowires and nanotubes. Yu *et. al.*²⁴⁸ used epoxy based suspensions to blow bubbles, where the stretching and expansion of the suspension induced alignment of the nanotubes in the direction of the expansion. Tian *et. al.*²⁴⁹ used pulsed gas alignment with downward tilt and atomic force microscopy (AFM) manipulation to produced aligned SWCNT composites. Of the techniques, the most commonly used techniques are mechanical stretching²²⁰ and fibre spinning^{250,251}, notably electrospinning²⁵²⁻²⁵⁵. Mechanical stretching of polymers allow alignment due to the stretching of the polymer matrix. In the melt and solution electrospinning techniques, the nanotubes are also oriented with the flow of polymer molecules during drawing, extrusion or electrospinning. Alignment of MWCNTs was achieved using electrospinning in this project so a brief illustration of this process will be given. Dror *et. al.*²⁵² have presented a model for the behaviour of rod-like particles in an electrospinning solution. Figure 2.8 obtained from reference²⁵² presents a schematic of their model.

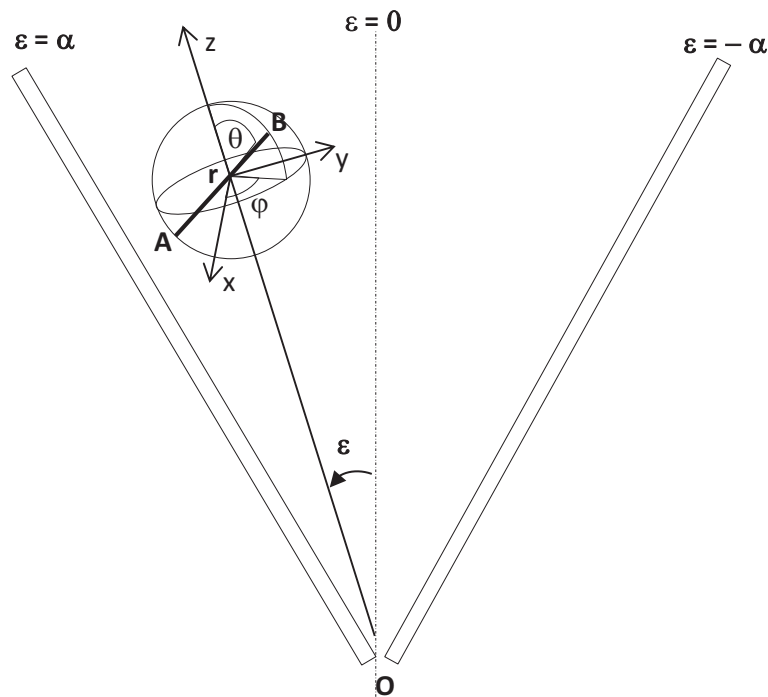


Figure 2.8 : The wedge with a semi-angle α . Polar coordinates r (radial) and ϵ (polar angle) are used to describe the position of a rod centre. Spherical angular coordinate's θ and φ are used to characterize the orientation of the rod-like particle AB. Also the corresponding Cartesian coordinates x , y and z are included. Obtained from reference²⁵².

This model considers the planar sink flow in a wedge, also known as Hamel flow²⁵⁶. This wedge model was chosen as a simplified version of a Taylor cone, from which the polymer jet originates. Shown in Figure 2.8 a small rod-like particle (AB) is drawn towards the sink point O by the flow of the material. While its centre moves along the streamline ($\varepsilon = \text{constant}$), the particle is rotated by the flow. For a more in depth explanation of the model, one can view the reference for more detail. They did, however, find that the rod-like particles aligned with the stream line as they were drawn towards the tip of the wedge. Initially un-oriented, this model implies that the nanotubes are oriented towards the tip of the Taylor cone and are aligned as they enter the electrospinning jet. As can be seen there are a variety of possible techniques to align CNTs in polymer composites, and one should have a clear understanding of which technique to use in relation to the composite you wish to prepare.

2.3.3.1.6 Carbon nanotube composite properties

After the brief overview discussing the various aspects of nanotube functionalisation and the subsequent methods used to prepare the composites using either unmodified or modified CNTs, a brief summary of the properties that carbon nanotubes lend to polymer composites will be presented.

The excellent mechanical integrity of CNTs, offers enhanced mechanical properties to composite materials. Recent work by Lau and Hui²⁵⁷ has also shown that during crack propagation CNTs aligned perpendicular to the crack can bridge the crack face and slow down the propagation. Many studies have been performed in this regard, but we shall just refer to a few of these cases. Work by Dalton *et. al.*²⁵⁸ spun poly(vinyl alcohol) fibres containing 60 wt% SWCNTs and obtained a tensile strength of 1.8 GPa, which is comparable to that of spider silk. Generally, by increasing the CNT content in a polymer, one obtains increased modulus values as well as increased strength of the material. This is, however, not always the case as bundling of CNTs can lead to a dramatic decrease in the expected material properties. One also has the added problem of an increasing viscosity as the nanotube concentrations are increased, resulting in poorer dispersion and incomplete wetting of the CNTs. Work by Schadler and colleagues²⁰³ has shown that slippage occurs between the outer shells of bundled CNTs as the forces between nanotubes are not as strong as those between individual nanotubes and the polymer matrix. This does depend on the nanotube matrix interaction/interface, but in most cases this interaction is stronger. Liao and co-workers²⁵⁹ showed that CNT-matrix interaction/adhesion character in the absence of atomic bonding between the two, is as a result of electrostatic van der Waals forces and the

stress arising from the different thermal expansion coefficients between the two components. There is an on-going effort to fully explain the behaviour between the nanotubes and the polymer matrices at the interfacial regions.

It should be clear at this stage that the introduction of functionality on the surfaces of the nanotubes goes a long way in increasing the interaction and dispersion of the nanotubes in various polymer mediums. Whether the stronger interaction be as a result of the formation of charge transfer complexes between the functionalised CNTs and polymer material as in the case of work by Ge¹⁹¹ and Zhao²¹⁸, or by the entangling of molecules grafted/adsorbed onto the CNT surface and the polymer matrix molecules, functionalisation is key to producing composites with maximum property enhancement. Work by Geng *et. al.*²⁶⁰ looked at fluorinated SWCNTs in PEO matrices and found increased tensile modulus (145%) and yield strength (300%) with only 1 wt% loading of the nanotubes. Gao and colleagues²⁶¹ looked at using carboxylated SWCNTs in the presence of ϵ -caprolactam (similar to Zhao *et. al.*²¹⁸) to polymerise the nylon-6 matrix *in situ* and obtain SWCNTs with grafted nylon molecules. Increases in the tensile modulus (153%) and strength (103%) were observed at 1 wt% SWCNT loading. Attempting to summarise all the mechanical reports that have been published over the years is outside the scope of this introduction. A comprehensive summary of various works focusing on using tensile modulus as a benchmark is presented in a paper by Coleman *et. al.*¹¹⁴ They summarised the material according to composite preparation categories. I have included Table 2.2¹¹⁴ summarising the performances of SWCNT and MWCNT filled composites produced using different methods.

Table 2.2 : A comparison of the performances of SWCNT and MWCNT filled composites prepared using different approaches¹¹⁴.

	Solution	Melt	Melt (fibre)	Epoxy	In situ polymerisation	Functionalised
Mean dY/dVf (Gpa)	309	23	128	231	430	157
Median dY/dVf (Gpa)	128	11	38	18	60-150	115
Max dY/dVf (Gpa) SWCNT	112	68	530	94	960	305
Max dY/dVf (Gpa) MWCNT	1244	64	36	330	150	380
Max Y (Gpa)	7	4.5	9.8	4.5	167	29
Max s (Gpa)	348	80	1032	41	4200	107

It is obvious from their comprehensive summary that nanotubes which are functionalised provided the best performance. It is also shown that in most cases increases in modulus and

strength are generally observed, but this occurs with a decrease in strain at break. The melt prepared MWCNT composites do show excellent values, however, these values were obtained from PVA based composites²⁶² which are biased due to their inherent high crystallinity compared to the other composite polymers. The melt (fibre) processed materials also provided better results than the conventional melt blended polymers, due to alignment effects of the fibre drawn melts.

Owing to their unique structure CNTs are electrically conductive as expressed in the review by Lu and Chen²⁶³. A large amount of literature on the subject exists, too broad for the scope of this introductory chapter. This project does not focus on electrical conductivity properties of nanotubes and their conductance in polymers, but due to the enormity of this field it is worth noting. Many studies have shown that nanotubes lend conductive properties to polymers matrices when used as fillers^{191,264-266}. Composites of this nature can satisfy applications in the field of electronics and sensor development²⁶⁷. A certain limit has to be reached with regards to the amount of CNTs loaded into a material before the material becomes conductive. This limit is known as the percolation threshold. The formation of a three dimensional network of CNT fillers occurs at this point. A jump in the conductivity of the composite by several orders of magnitude usually occurs at this critical point. The percolation threshold is determined by a variety of different parameters. The longer the nanotubes the lower the percolation threshold as found by Bai and Allaoui²⁶⁸. Dispersion also affects the threshold, where increased dispersion generally leads to a lower percolation threshold. Alignment of nanotubes in a composite tends to increase the percolation threshold as there are less contact points between the filler particles due to their orientation as shown by Du *et. al.*²⁶⁹ The functionalisation of CNTs can also lead to a disruption of the CNT network structure causing defects which can result in lower conductance of the material.

2.3.3.1.7 CNT filled electrospun fibre nanocomposites

This section will specifically focus on a few examples of CNT filled nanocomposites prepared via the electrospinning technique. CNT incorporation can once again be used to increase the mechanical properties of electrospun fibres as well as introduce new functionality to the fibres such as electrical conductivity. A number of research groups are investigating this approach. One can deduce from the previous discussions on the incorporation of CNTs, interaction with the polymer matrix is very important to aid in dispersion of the nanotubes as well as interaction with the matrix leading to enhanced properties. Ko *et. al.*²⁷⁰ investigated the orientation of nanotubes in electrospun fibres relative to different polymers where the interaction between the CNTs and polymer species differed. They found that electrospun

PAN fibres from DMF solution containing SWCNTs resulted in alignment of the nanotubes in the direction of the fibre axis. It was, however, noted that spinning the same SWCNTs using poly(lactic acid) (PLA) as the matrix polymer, resulted in fibres with random orientation and inhomogeneous dispersion of the nanotube fillers. This difference was as a result of limited interaction between the SWCNTs and PLA and the stronger interaction between the SWCNTs and PAN. It has been shown by Ge and co-workers¹⁹¹ that a charge transfer complex is formed between PAN and CNTs which results in the strong interaction between the two components. Sen and colleagues²⁷¹ electrospun SWCNTs in polystyrene and obtained fibres with diameters of 50-100nm, but the nanotubes although orientated in the direction of the fibres, were agglomerated as bundles. They then electrospun polyurethane (PU) fibres using "as prepared" SWCNTs and ester functionalised SWCNTs. They found that the ester functionalised nanotubes produced composites with decreased agglomeration, increased dispersion and increased mechanical properties. The tensile strength of the functionalised SWCNT composites was 104% better than the unfilled PU fibres, whereas the "as prepared" SWCNTs only exhibited a 46% increase. Salalha *et. al.*²⁵⁵ electrospun PEO fibres using SWCNTs that had been dispersed in water using an amphiphilic copolymer of styrene and sodium maleate. They found that depending on the CNT dispersion prior to polymer addition, the dispersion of single SWCNTs aligned in the fibre direction increased. The CNT incorporation was also found not to affect the crystallisation of the polymer. Further work by the same group²⁵² presented a theoretical model that described the behaviour of rod-like particles in electrospun solutions and also studied the effect of surfactant dispersed MWCNTs on the crystallisation of the PEO fibre matrix. They found significant disruption of the crystal orientation in the nanofibres due to the presence of the MWCNTs, which is in contrast to the results they obtained for the SWCNT filled PEO fibres.

There are a number of publications studying the strong interaction between oxidised CNTs and PAN^{191,253-255,264-266,272}. Work published by Ge *et. al.*¹⁹¹ used UV/vis spectroscopy to highlight the charge transfer complex formed between the negatively charged (-CN) functional groups on the PAN backbone and the surface oxidised MWCNTs. They also found axial orientation and good dispersion of the MWCNTs along the fibre axis resulting in increased mechanical properties. The tensile moduli of the compressed composite fibre sheets were enhanced to 10.9 and 14.5 GPa at MWCNT loadings of 10 and 20 wt% respectively. The composites also showed decreased heat shrinkage with a decrease in the thermal expansion coefficient by more than an order of magnitude for the 20 wt% loaded fibres. The conductivity of these fibres were also increased to 1 S/cm. Hou and co-workers²⁵⁴ studied the same system and also found increased mechanical properties, especially the

modulus which increased with nanotube loading (up to 20wt%). The tensile strength, however, reached a maximum (5 wt% 80MPa) at lower loadings and then decreased (37.1 MPa at 20 wt%). Very recent work by Ji *et. al.*²⁵³ studied PAN-MWCNT electrospun nanofibres, after hot stretching. At 2 wt% MWCNT loading they found dramatic increases in tensile modulus and strength of 204.5% and 320.7% respectively. They also showed that a Raman mapping method can be successfully used to study the alignment and distribution of the MWCNTs in the fibres. Other studies focus on the electrical conductivity of CNTs and its effect on the electrospun fibres^{191,264-266}. In most cases, electrical conductivity of the fibre composites are enhanced and the increased conductivity of the spinning solutions allow finer fibres to be electrospun with reductions in beading. Like the other composites, interaction between the CNTs and matrix is a necessity if one plans to incorporate well dispersed CNTs that can enhance the properties of electrospun fibre nanocomposites. The inherent interaction between PAN and carbon nanotubes makes this polymer an ideal choice for electrospinning well-structured polymer nanocomposite fibres.

2.3.3.2 Electrospun nanofibres as composite fillers

As explained earlier, electrospinning can yield fibres in the submicron range. One can also spin a vast variety of polymers which allows the production of nanofibres with a plethora of properties based on the properties of the material electrospun. The ability to produce fibres with such narrow diameters relative to their lengths, means that we are able to produce materials with extremely high aspect ratios compared to other traditional fillers such as carbon black, silica and more recently carbon nanotubes. It is, however, interesting to notice that very little work is available in open literature on the use of electrospun nanofibres as fillers for polymer matrices.

Prior to the pioneering work by Kim and Reneker²⁷³ this field of work was absent from literature. In their work they studied using electrospun fibres of polybenzimidazole (PBI) as reinforcing fillers for epoxy resin as well as styrene-butadiene rubbers (SBR). They electrospun sheets of the nanofibres with average diameter of 300 nm and then impregnated them in a compression mould with the uncured epoxy resin before curing. The SBR rubber films were created by milling sheets of the nanofibres with the SBR resin prior to curing in a compression mould. The fibre incorporation was varied between 3 and 15 %. Mechanical test showed an increasing trend of mechanical properties as the fibre content was increased. The modulus of the material increased (from 4.25 to 5.4 GPa) as well as the energy (93.4 to 363.0 J.m⁻²). As the fibres were aligned on a rotating collector, they tested both the axial and transverse fibre composite properties, which showed significantly different degrees of

enhancement. The filled SBR rubber composites showed a ten-fold increase in the modulus and a doubling of the fracture stress. The elongation at break was, however, lower than that for the unfilled matrix.

Bergshoef and Vancso²⁷⁴ also studied nanofibres filled composites at the same time as Kim and Reneker (1999) where they looked at creating transparent nanocomposites using electrospun nylon-4,6 nanofibres to reinforce epoxy resin. The fibre diameters varied from 50 to 200 nm and were impregnated into the epoxy film. The film was shown to be transparent due to the diameter of the fibre fillers, as well as reinforced. The modulus increased substantially (2.5 to 91 MPa) and the stress at break (0.82 to 2.4 MPa) followed the same trend, however, the elongation of the material decreased drastically (80 to 3 %). The fibres also remained unmodified as there was sufficient adhesion between the nylon nanofibres and the phenolic epoxy matrix. Later work by Tang and Liu²⁷⁵ also studied producing nanofibres reinforced composites with an aim to produce transparent composite films. They used cellulose nanofibres to reinforce poly(vinyl alcohol) (PVOH) films. They found the optimum fibre filler incorporation to be 40 wt% with regards to the PVOH matrix. The reinforcement was shown to increase the modulus of the composite by 600 % as well as the mechanical strength by 50 %. The films also remained 75 % transparent to visible light at this filler content. The elongation at break was again, shown to decrease noticeably. Concurrent work by this group²⁷⁶ showed that similar trends were observed when reinforcing films obtained from soybean protein isolate with electrospun cellulose nanofibres. In this case the filler content was increased from 0 to 20 wt%.

Pinho *et. al.*²⁷⁷ investigated biocompatible reinforced polymer systems using a degradable particulate filled matrix, poly(butylene succinate) (PBS) microfibrils melt extruded with electrospun chitosan fibre meshes. They compared PBS filled with chitosan particles (50 wt%) to PBS filled with chitosan particles and chitosan nanofibres meshes (0.05 wt%). The strain was shown to decrease (10.6 to 7.6 %) while the composites showed increased stress (6.2 to 6.9 MPa) and modulus (175.6 to 295.7 MPa) values.

Interestingly, other work focusing on nanofibres filled composites was investigated in the dental resin reinforcement field. Fong²⁷⁸ used electrospun fibre meshes of nylon-6 to reinforce the dental methacrylate of 2,20-bis-[4-(methacryloxypropoxy)-phenyl]-propane/ tri (ethylene glycol) dimethacrylate BIS-GMA/TEGDMA. The addition of 5 wt% fibre mesh moderately increased the flexural strength by 36 %, elastic modulus by 26 % and the fracture energy by 42 %. They suggested that the fibres deflected the crack propagation. Lin and co-workers¹⁰⁹ also looked at reinforcing the same dental resin system, but they looked at using electrospun core-shell fibres of PAN (core) and poly(methyl methacrylate) (PMMA)

(shell). They aimed to increase the interfacial adhesion between the fibre filler and the methacrylate based dental resin by the use of a PMMA outer shell. The incorporation of 7.5 wt% core shell nanofibres was shown to increase the flexural strength by 18.7 %, elastic modulus by 14.1 % and the fracture energy by 64.8 %. Work by Griswold *et. al.*²⁷⁹ studied a variety of different electrospun fibre mats (PVOH, PLLA and nylon-6) as reinforcing fillers for Hybrane (DSM) dental formulations. They found that the PVOH nanofibres showed improved compression strength (30 %) and reduced shrinkage (50 %) values at contents of 0.05 wt%. The other composites showed little improvement or a reduction in mechanical properties.

Work by Han *et. al.*²⁸⁰ investigated the use of cellulose fibres to reinforce PBS matrices, using a melt mixing method to produce the composites. They did show that there is a measure of reinforcement, but did not present detailed mechanical analysis. Very recent work by the group of Causin²⁸¹ also used a melt mixing method to produce composites in a compression mould. They studied the reinforcement of poly(ϵ -caprolactone) (PCL) using electrospun nylon-6 nanofibres. Unlike the previously mentioned studies, where increases in modulus and fracture strength were obtained at a loss of the strain, they found increased modulus values as well as increased ductile behaviour. They varied the fibre filler content from 3 and 5 to 8 wt% but found that at 3 wt%, the modulus increased (353 to 530 MPa) along with the strain at break (467 % to 601 %). They also found that better interfacial adhesion took place between the matrix and the finer nanofibres.

Recently published work by our group²⁸² looked at improving the mechanical properties of silicone elastomer films using electrospun graft copolymers of PMMA-graft-PDMS with varying PDMS content. To our knowledge there is no literature available investigating the use of electrospun nanofibres as reinforcing fillers for silicone elastomer matrices. A major problem is the interfacial adhesion between the matrix and the fibres. As discussed above, previous work relies on sufficient interaction between the chosen matrix and the fibre fillers. Lin and co-workers¹⁰⁹ did, however, modify their PAN fibres by creating a core shell morphology where the PMMA shell acted as a compatibiliser with the methacrylate based dental resin. The technique used by our group was the novel approach of introducing a compatibilising element covalently bonded to the desired fibre filler material. The results obtained from the PMMA-g-PDMS nanofibre fillers showed an increase in modulus as the mol% PDMS increased in the graft copolymer. There was also an increase in properties as the fibre filler content was increased. The 3.9 mol% PDMS copolymer showed a maximum increase in modulus from 0.67 to 7.62 MPa (11 fold increase). The elongation at break also increased dramatically from 42 % to 114 %. Unlike the previous work in this field (except for

Causin), increases in the strain at break were achieved along with increases in the modulus and tensile stress.

2.4 References

- (1) Pyun, J., Matyjaszewski, K. *Chem. Mater.* **2001**, *13*, 3436-3448.
- (2) Hadjichristidis, N., Pitsikalis, M., Iatrou, H. *Adv. Polym. Sci.* **2005**, *189*, 1-124.
- (3) Hadjichristidis, N., Pitsikalis, M., Pispas, S., Iatrou, H. *Chem. Rev.* **2001**, *101*, (12), 3747-3792.
- (4) Hadjichristidis, N., Xenidou, M., Iatrou, H., Pitsikalis, M., Poulos, Y., Avgeropoulos, A., Sioula, S., Paraskeva, S., Velis, G., Lohse, D. J., Schulz, D. N., Fetters, L. J., Wright, P. J., Mendelson, R. A., Garcia-Franco, C. A., Sun, T., Ruff, C. J. *Macromolecules* **2000**, *33*, (7), 2424-2436.
- (5) Hadjichristidis, N., Iatrou, H., Pitsikalis, M., Mays, J. *Prog. Polym. Sci.* **2006**, *31*, 1068-1132.
- (6) Pitsikalis, M., Pispas, S., Mays, J. W., Hadjichristidis, N. *Adv. Polym. Sci.* **1998**, *135*, 1-137.
- (7) Xenidou, M., Hadjichristidis, N. *Macromolecules* **1998**, *31*, (17), 5690-5694.
- (8) Zhang, H., Ruckenstein, E. *Macromolecules* **2000**, *33*, (3), 814-819.
- (9) Ryu, S. W., Hirao, A. *Macromolecules* **2000**, *33*, (13), 4765-4771.
- (10) Pitsikalis, M., Sioula, S., Pispas, S., Hadjichristidis, N., Cook, D. C., Li, J., Mays, J. W. *J. Polym. Sci., Part A: Polym. Chem.* **1999**, *37*, (23), 4337-4350.
- (11) Candau, F., Afchar-Taromi, F., Rempp, P. *Polymer* **1977**, *18*, (12), 1253-1257.
- (12) Falk, J. C., Hoeg, D. F., Schlott, R. J., Pendleton, J. F. *J. Macromol. Sci., Chem.* **1973**, *7*, (8), 1669-1676.
- (13) Falk, J. C., Schlott, R. J., Hoeg, D. F., Pendleton, J. F. *Rubber Chem. Technol.* **1973**, *46*, (4), 1044-1054.
- (14) Falk, J. C., Schlott, R. J., Hoeg, D. F. *J. Macromol. Sci., Chem.* **1973**, *7*, (8), 1647-1662.
- (15) Chen, Y., Ying, L., Yu, W., Kang, E. T., Neoh, K. G. *Macromolecules* **2003**, *36*, (25), 9451-9457.
- (16) Jenkins, D. W., Hudson, S. M. *Chem. Rev.* **2001**, *101*, (11), 3245-3273.
- (17) Ruckenstein, E., Zhang, H. *Macromolecules* **1999**, *32*, (19), 6082-6087.
- (18) Chonnowski, J., Cypryk, M., Fortuniak, W., Rozga-Wijas, K., Scibiorek, M. *Polymer* **2002**, *43*, 1993-2001.
- (19) Williamson, D.T., Buchanan, T.D. Elkins, C., Long, T.E. *Macromolecules* **2004**, *37*, 4505-4511.
- (20) Ederle, Y., Isel, F., Grutke, S., Lutz, P. J. *Macromol. Symp.* **1998**, *132*, 197-206.
- (21) Shinoda, H., Miller, P.J., Matyjaszewski, K. *Macromolecules* **2001**, *34*, 3186-3194.
- (22) Shinoda, H., Matyjaszewski, K. *Macromolecules* **2003**, *36*, 4772-4778.

-
- (23) Tuzar Z, Kratochivil P. Micelles of block and graft copolymers in solutions. In: Matijevic E, editor. *Surface and Colloid Science* New York: Plenum Press; **1993**, 1-83.
- (24) Zhang, L., Eisenberg, A. *Science* **1995**, 268, (5218), 1728-1731.
- (25) Zhang, L., Yu, K., Eisenberg, A. *Science* **1996**, 272, (5269), 1777-1779.
- (26) Riess, G. *Prog. Polym. Sci.* **2003**, 28, (7), 1107-1170.
- (27) Jain, S., Bates, F. S. *Science* **2003**, 300, (5618), 460-464.
- (28) Zhang, L., Lin, J., Lin, S. *J. Phys. Chem. B* **2007**, 111, (31), 9209-9217.
- (29) Zhang, L., Lin, J., Lin, S. *J. Phys. Chem. B* **2007**, 111, (31), 9209-9217.
- (30) Balsara, N. P., Tirrell, M., Lodge, T. P. *Macromolecules* **1991**, 24, (8), 1975-1986.
- (31) Halperin, A. *Macromolecules* **1987**, 20, (11), 2943-2946.
- (32) Halperin, A., Tirrell, M., Lodge, T. P. *Adv. Polym. Sci.* **1992**, 100, 31-71.
- (33) Honda, C., Hasegawa, Y., Hirunuma, R., Nose, T. *Macromolecules* **1994**, 27, (26), 7660-7668.
- (34) Honda, C., Sakaki, K., Nose, T. *Polymer* **1994**, 35, (24), 5309-5318.
- (35) Marques, C., Joanny, J. F., Leibler, L. *Macromolecules* **1988**, 21, (4), 1051-1059.
- (36) Raspaud, E., Lairez, D., Adam, M., Carton, J. *Macromolecules* **1994**, 27, (11), 2956-2964.
- (37) Wu, G., Chu, B. *Macromolecules* **1994**, 27, (7), 1766-1773.
- (38) Zhou, Z., Chu, B., Peiffer, D. G. *Macromolecules* **1993**, 26, (8), 1876-1883.
- (39) Halperin, A. *Macromolecules* **1991**, 24, (6), 1418-1419.
- (40) Kikuchi, A., Nose, T. *Macromolecules* **1996**, 29, (21), 6770-6777.
- (41) Kikuchi, A., Nose, T. *Polymer* **1996**, 37, (26), 5889-5896.
- (42) Borisov, O. V., Zhulina, E. B. *Macromolecules* **2005**, 38, (6), 2506-2514.
- (43) Borisov, O. V., Halperin, A. *Curr. Opin. Colloid Interface Sci.* **1998**, 3, (4), 415-421.
- (44) Price, C., Woods, D. *Polymer* **1973**, 14, (3), 82-86.
- (45) Iwasaki, Y., Akiyoshi, K. *Macromolecules* **2004**, 37, (20), 7637-7642.
- (46) Pispas, S., Hadjichristidis, N., Mays, J. W. *Macromolecules* **1996**, 29, (23), 7378-7385.
- (47) Sunintaboon, P., Ho, K. M., Li, P., Cheng, S. Z. D., Harris, F. W. *J. Am. Chem. Soc.* **2006**, 128, (7), 2168-2169.
- (48) Virtanen, J., Baron, C., Tenhu, H. *Macromolecules* **2000**, 33, (2), 336-341.
- (49) Virtanen, J., Tenhu, H. *Macromolecules* **2000**, 33, (16), 5970-5975.

-
- (50) Semenov, A. N., Joanny, J., Khokhlov, A. R. *Macromolecules* **1995**, *28*, (4), 1066-1075.
- (51) Zhang, J. X., Qiu, L. Y., Zhu, K. J. *Macromol. Rapid Commun.* **2005**, *26*, (21), 1716-1723.
- (52) Wang, C., Li, G., Guo, R. *Chem. Commun.* **2005**, (28), 3591-3593.
- (53) Breitenkamp, K., Emrick, T. *J. Am. Chem. Soc.* **2003**, *125*, (40), 12070-12071.
- (54) Ramakrishna, S., Fujihara, K., Teo, W. E., Lim, T. C., Ma, Z. *An Introduction to Electrospinning and Nanofibres*. World Scientific: London, **2005**.
- (55) Ondarcuhu, T., Joachim, C. *Europhys. Lett.* **1998**, *42*, (2), 215-220.
- (56) Feng, L., Li, S., Li, H., Zhai, J., Song, Y., Jiang, L., Zhu, D. *Angew. Chem., Int. Ed.* **2002**, *41*, (7), 1221-1223.
- (57) Martin, C. R. *Chem. Mater.* **1996**, *8*, (8), 1739-1746.
- (58) Ma, P. X., Zhang, R. *J Biomed Mater Res* **1999**, *46*, (1), 60-72.
- (59) Liu, G., Ding, J., Qiao, L., Guo, A., Dymov, B. P., Gleeson, J. T., Hashimoto, T., Saijo, K. *Chem.--Eur. J.* **1999**, *5*, (9), 2740-2749.
- (60) Whitesides, G. M., Grzybowski, B. *Science* **2002**, *295*, (5564), 2418-2421.
- (61) Niece, K. L., Hartgerink, J. D., Donners, J. J. J. M., Stupp, S. I. *J. Am. Chem. Soc.* **2003**, *125*, (24), 7146-7147.
- (62) Reneker, D. H., Yarin, A. L. *Polymer* **2008**, *19*, 2387-2425.
- (63) Formhals, A., Schreiber-Gastell R (1934) *Process and apparatus for preparing artificial threads*. US patent 1975504.
- (64) Formhals, A., Schreiber-Gastell R (1934) *Apparatus for producing artificial filaments from material such as cellulose acetate*. US patent 1975504.
- (65) Formhals, A., Schreiber-Gastell R, (1938) *Electrical spinning of fibres from solutions*. US patent 2123992.
- (66) Formhals, A., Schreiber-Gastell R (1938) *Electrical spinning of fibres such as those produced from cellulose acetate*. US patent 2116942.
- (67) Formhals, A., Schreiber-Gastell R, (1940) *Artificial threads*. US patent 2187306.
- (68) Formhals, A., Alien Property Custodian (1943) *Apparatus for producing artificial fibres from fibre-forming liquids by an "electrical spinning" method*. US patent 2323025.
- (69) Formhals, A., Alien Property Custodian (1944) *Spinner for synthetic fibres*. US patent 2349950.
- (70) Reneker, D. H., Chun, I. *Nanotechnology* **1996**, *7*, (3), 216-223.
- (71) Doshi, J., Reneker, D. H. *J. Electrostat.* **1995**, *35*, (2&3), 151-160.
- (72) Huang, Z. M., Zhang, Y. Z., Kotaki, M., Ramakrishna, S. *Compos. Sci. Technol.* **2003**, *63*, (15), 2223-2253.

-
- (73) Li, D., Xia, Y. *Adv. Mater.* **2004**, *16*, (14), 1151-1170.
- (74) Subbiah, T., Bhat, G. S., Tock, R. W., Parameswaran, S., Ramkumar, S. S. *J. Appl. Polym. Sci.* **2005**, *96*, (2), 557-569.
- (75) Teo, W. E., Ramakrishna, S. *Nanotechnology* **2006**, *17*, (14), R89-R106.
- (76) Deitzel, J. M., Kleinmeyer, J., Harris, D., Beck Tan, N. C. *Polymer* **2001**, *42*, (1), 261-272.
- (77) Shenoy, S. L., Bates, W. D., Frisch, H. L., Wnek, G. E. *Polymer* **2005**, *46*, (10), 3372-3384.
- (78) Zong, X., Kim, K., Fang, D., Ran, S., Hsiao, B. S., Chu, B. *Polymer* **2002**, *43*, (16), 4403-4412.
- (79) Deitzel, J. M., Kleinmeyer, J. D., Hirvonen, J. K., Beck Tan, N. C. *Polymer* **2001**, *42*, (19), 8163-8170.
- (80) Jarusuwannapoom, T., Hongrojjanawiwat, W., Jitjaicham, S., Wannatong, L., Nithitanakul, M., Pattamaprom, C., Koombhongse, P., Rangkupan, R., Supaphol, P. *Eur. Polym. J.* **2005**, *41*, (3), 409-421.
- (81) Demir, M. M., Yilgor, I., Yilgor, E., Erman, B. *Polymer* **2002**, *43*, (11), 3303-3309.
- (82) Buchko, C. J., Chen, L. C., Shen, Y., Martin, D. C. *Polymer* **1999**, *40*, (26), 7397-7407.
- (83) Megelski, S., Stephens, J. S., Chase, D. B., Rabolt, J. F. *Macromolecules* **2002**, *35*, (22), 8456-8466.
- (84) Zhao, S., Wu, X., Wang, L., Huang, Y. *J. Appl. Polym. Sci.* **2004**, *91*, (1), 242-246.
- (85) Baumgarten, P. K. *J. Colloid Interface Sci.* **1971**, *36*, (1), 71-79.
- (86) Chew, S. Y., Wen, J., Yim, E. K. F., Leong, K. W. *Biomacromolecules* **2005**, *6*, (4), 2017-2024.
- (87) Matthews, J. A., Wnek, G. E., Simpson, D. G., Bowlin, G. L. *Biomacromolecules* **2002**, *3*, (2), 232-238.
- (88) Wannatong, L., Sirivat, A., Supaphol, P. *Polym. Int.* **2004**, *53*, (11), 1851-1859.
- (89) Katta, P., Alessandro, M., Ramsier, R. D., Chase, G. G. *Nano Lett.* **2004**, *4*, (11), 2215-2218.
- (90) Bhattarai, N., Edmondson, D., Veiseh, O., Matsen, F. A., Zhang, M. *Biomaterials* **2005**, *26*, (31), 6176-6184.
- (91) Teo, W. E., Kotaki, M., Mo, X. M., Ramakrishna, S. *Nanotechnology* **2005**, *16*, (6), 918-924.
- (92) Teo, W. E., Ramakrishna, S. *Nanotechnology* **2005**, *16*, (9), 1878-1884.
- (93) Xu, C. Y., Inai, R., Kotaki, M., Ramakrishna, S. *Biomaterials* **2003**, *25*, (5), 877-886.
- (94) Inai, R., Kotaki, M., Ramakrishna, S. *Nanotechnology* **2005**, *16*, (2), 208-213.
- (95) Li, D., Wang, Y., Xia, Y. *Nano Lett.* **2003**, *3*, (8), 1167-1171.
- (96) Bognitzki, M., Czado, W., Frese, T., Schaper, A., Hellwig, M., Steinhart, M., Greiner, A., Wendroff, J. H. *Adv. Mater.* **2001**, *13*, (1), 70-72.

-
- (97) Srinivasarao, M., Collings, D., Philips, A., Patel, S. *Science* **2001**, *292*, (5514), 79-82.
- (98) Casper, C. L., Stephens, J. S., Tassi, N. G., Chase, D. B., Rabolt, J. F. *Macromolecules* **2004**, *37*, (2), 573-578.
- (99) Bognitzki, M., Frese, T., Steinhart, M., Greiner, A., Wendorff, J. H., Schaper, A., Hellwig, M. *Polym. Eng. Sci.* **2001**, *41*, (6), 982-989.
- (100) Li, D., Ouyang, G., McCann, J. T., Xia, Y. *Nano Lett.* **2005**, *5*, (5), 913-916.
- (101) Loscertales, I. G., Gomez, J. E. D., Lallave, M., Rosas, J. M., Bedia, J., Rodriguez-Mirasol, J., Cordero, T., Marquez, M., Shenoy, S., Wnek, G. E., Thorsen, T., Fernandez-Nieves, A., Barrero, A. *Mater. Res. Soc. Symp. Proc.* **2007**, *948E*, No pp. given, Paper #: 0948-B06-01.
- (102) Li, D., Xia, Y. *Nano Lett.* **2004**, *4*, (5), 933-938.
- (103) Loscertales, I. G., Barrero, A., Marquez, M., Spretz, R., Velarde-Ortiz, R., Larsen, G. *J. Am. Chem. Soc.* **2004**, *126*, (17), 5376-5377.
- (104) Kim, C., Kim, B., Sheikh, F. A., Lee, U., Khil, M., Kim, H. *Macromolecules* **2007**, *40*, (14), 4823-4828.
- (105) Kim, K., Luu, Y. K., Chang, C., Fang, D., Hsiao, B. S., Chu, B., Hadjiargyrou, M. *J. Controlled Release* **2004**, *98*, (1), 47-56.
- (106) Kim, H., Lee, H., Knowles, J. C. *J. Biomed. Mater. Res., Part A* **2006**, *79A*, (3), 643-649.
- (107) Xu, X., Yang, L., Xu, X., Wang, X., Chen, X., Liang, Q., Zeng, J., Jing, X. *J. Control. Release* **2005**, *108*, 33-42.
- (108) Xu, X., Zhuang, X., Chen, X., Wang, X., Yang, L., Jing, X. *Macromol. Rapid Comm.* **2006**, *27*, 1637-1642.
- (109) Lin, S., Cai, Q., Ji, J., Sui, G., Yu, Y., Yang, X., Ma, Q., Wei, Y., Deng, X. *Compos. Sci. Technol.* **2008**, *68*, (15-16), 3322-3329.
- (110) Hou, H., Jun, Z., Reuning, A., Schaper, A., Wendorff, J. H., Greiner, A. *Macromolecules* **2002**, *35*, (7), 2429-2431.
- (111) Hou, H., Reneker, D. H. *Adv. Mater.* **2004**, *16*, (1), 69-73.
- (112) Zhang, D., Karki, A. B., Rutman, D., Young, D. P., Wang, A., Cocke, D., Ho, T. H., Guo, Z. *Polymer* **2009**, *50*, (17), 4189-4198.
- (113) Sanders, E. H., Kloefkorn, R., Bowlin, G. L., Simpson, D. G., Wnek, G. E. *Macromolecules* **2003**, *36*, (11), 3803-3805.
- (114) Coleman, J. N., Khan, U., Blau, W. J., Gun'ko, Y. K. *Carbon* **2006**, *44*, (9), 1624-1652.
- (115) Chronakis, I. S. *J. Mater. Process. Technol* **2005**, *167*, (2-3), 283-293.
- (116) Breuer, O., Sundararaj, U. *Polym. Compos.* **2004**, *25*, (6), 630-645.
- (117) Caseri, W. R. *Mater. Sci. Technol.* **2006**, *22*, (7), 807-817.
- (118) Krishnamoorti, R., Vaia, R. A. *J. Polym. Sci., Part B: Polym. Phys.* **2007**, *45*, (24), 3252-3256.

-
- (119) Thostenson, E. T., Li, C., Chou, T. *Compos. Sci. Technol.* **2005**, *65*, (3-4), 491-516.
- (120) Jordan, J., Jacob, K. I., Tannenbaum, R., Sharaf, M. A., Jasiuk, I. *Mater. Sci. Eng., A* **2005**, *393*, 1-11.
- (121) Naganuma, T., Kagawa, Y. *Compos. Sci. Technol.* **2002**, *62*, (9), 1187-1189.
- (122) Zou, H., Wu, S., Shen, J. *Chem. Rev.* **2008**, *108*, (9), 3893-3957.
- (123) Singh, R. P., Zhang, M., Chan, D. *J. Mater. Sci.* **2002**, *37*, (4), 781-788.
- (124) Ash, B. J., Siegel, R. W., Schadler, L. S. *Macromolecules* **2004**, *37*, (4), 1358-1369.
- (125) Vollenberg, P. H. T., Heikens, D. *Polymer* **1989**, *30*, (9), 1656-1662.
- (126) Thompson, C. M., Herring, H. M., Gates, T. S., Connell, J. W. *Compos. Sci. Technol.* **2003**, *63*, (11), 1591-1598.
- (127) Chan, C., Wu, J., Li, J., Cheung, Y. *Polymer* **2002**, *43*, (10), 2981-2992.
- (128) Huang, J. *Adv. Polym. Technol.* **2002**, *21*, (4), 299-313.
- (129) Rong, M. Z., Zhang, M. Q., Zheng, Y. X., Zeng, H. M., Walter, R., Friedrich, K. *Polymer* **2000**, *42*, (1), 167-183.
- (130) Zhu, Y. G., Li, Z. Q., Zhang, D., Tanimoto, T. *J. Polym. Sci. Part B. Polym. Phys.* **2006**, *44*, (8), 1161-1167.
- (131) Zhu, Y. -, Li, Z. -, Zhang, D., Tanimoto, T. *J. Polym. Sci. Part B. Polym. Phys.* **2006**, *44*, (9), 1351-1356.
- (132) Castrillo, P. D., Olmos, D., Amador, D. R., Gonza'lez-Benito, J. *J. Colloid Interface Sci.* **2007**, *308*, (2), 318-324.
- (133) Patel, A. C., Lee, K. W. *Elastomerics* **1990**, *122*, (3), 14-18.
- (134) Tsubokawa, N. *Prog. Polym. Sci.* **1992**, *17*, (3), 417-470.
- (135) Ray, S. S., Okamoto, M. *Prog. Polym. Sci.* **2003**, *28*, (11), 1539-1641.
- (136) Gao, F. *Mater. Today* **2004**, *7*, (11), 50-55.
- (137) Alexandre, M., Dubois, P. *Mater. Sci. Eng., R* **2000**, *R28*, (1-2), 1-63.
- (138) Okada, A., Kawasumi, M., Usuki, A., Kojima, Y., Kurauchi, T., Kamigaito, O. *Mater. Res. Soc. Symp. Proc.* **1990**, *171*, 45-50.
- (139) Biswas, M., Ray, S. S. *Adv. Polym. Sci.* **2001**, *155*, 167-221.
- (140) Giannelis, E. P., Krishnamoorti, R., Manias, E. *Adv. Polym. Sci.* **1999**, *138*, 107-147.
- (141) Giannelis, E. P. *Adv. Mater.* **1996**, *8*, (1), 29-35.
- (142) Kiliaris, P., Papaspyrides, C. D. *Prog. Polym. Sci.* **2010**, *35*, (7), 902-958.
- (143) Giannelis, E. P. *Appl. Organomet. Chem.* **1998**, *12*, (10/11), 675-680.

-
- (144) Bharadwaj, R. K. *Macromolecules* **2001**, *34*, (26), 9189-9192.
- (145) Messersmith, P. B., Giannelis, E. P. *J. Polym. Sci., Part A: Polym. Chem.* **1995**, *33*, (7), 1047-1057.
- (146) Xu, R., Manias, E., Snyder, A. J., Runt, J. *Macromolecules* **2001**, *34*, (2), 337-339.
- (147) Ray, S. S., Yamada, K., Okamoto, M., Ueda, K. *Nano Lett.* **2002**, *2*, (10), 1093-1096.
- (148) Zheng, W., Lu, X., Wong, S. *J. Appl. Polym. Sci.* **2004**, *91*, (5), 2781-2788.
- (149) Krishnamoorti, R., Vaia, R. A., Giannelis, E. P. *Chem. Mater.* **1996**, *8*, (8), 1728-1734.
- (150) Samakande, A., Hartmann, P. C., Cloete, V., Sanderson, R. D. *Polymer* **2007**, *48*, (6), 1490-1499.
- (151) Samakande, A., Juodaityte, J. J., Sanderson, R. D., Hartmann, P. C. *Macromol. Mater. Eng.* **2008**, *293*, (5), 428-437.
- (152) Samakande, A., Sanderson, R. D., Hartmann, P. C. *J. Polym. Sci., Part A: Polym. Chem.* **2008**, *46*, (21), 7114-7126.
- (153) Qin, X., Wang, S. *Mater. Lett.* **2008**, *62*, (8-9), 1325-1327.
- (154) Mazinani, S., Aiji, A., Dubois, C. *Polymer* **2009**, *50*, 3329-3342.
- (155) Vaisman, L., Wachtel, E., Wagner, H. D., Marom, G. *Polymer* **2007**, *48*, (23), 6843-6854.
- (156) Titchenal, N.L., Naguib, N., Ye, H., Gogotsi, Y., Liu, J., Ko, F.K. *Abstracts of papers 226th ASC national meeting, NY, USA*, **2003**, 1-573.
- (157) Iijima, S. *Nature* **1991**, *354*, (6348), 56-58.
- (158) Moniruzzaman, M., Winey, K. I. *Macromolecules* **2006**, *39*, (16), 5194-5205.
- (159) Ajayan, P. M., Stephan, O., Colliex, C., Trauth, D. *Science* **1994**, *265*, (5176), 1212-1214.
- (160) Coleman, J. N., Khan, U., Gun'ko, Y. K. *Adv. Mater.* **2006**, *18*, (6), 689-706.
- (161) Moniruzzaman, M., Winey, K. I. *Macromolecules* **2006**, *39*, (16), 5194-5205.
- (162) Thostenson, E. T., Li, C., Chou, T. *Compos. Sci. Technol.* **2005**, *65*, (3-4), 491-516.
- (163) Xie, X., Mai, Y., Zhou, X. *Mater. Sci. Eng., R* **2005**, *R49*, (4), 89-112.
- (164) Thostenson, E. T., Ren, Z., Chou, T. *Compos. Sci. Technol.* **2001**, *61*, (13), 1899-1912.
- (165) Thostenson, E. T., Ren, Z., Chou, T. *Compos. Sci. Technol.* **2001**, *61*, (13), 1899-1912.
- (166) Odom, T. W., Huang, J., Kim, P., Lieber, C. M. *Nature* **1998**, *391*, (6662), 62-64.
- (167) Peigney, A., Laurent, C., Flahaut, E., Bacsa, R. R., Rousset, A. *Carbon* **2001**, *39*, (4), 507-514.
- (168) Awasthi, K., Srivastava, A., Srivastava, O. N. *J. Nanosci. Nanotechnol.* **2005**, *5*, (10), 1616-1636.

-
- (169) Guo, T., Nikolaev, P., Thess, A., Colbert, D. T., Smalley, R. E. *Chem. Phys. Lett.* **1995**, *243*, (1,2), 49-54.
- (170) Thess, A., Lee, R., Nikolaev, P., Dai, H., Petit, P., Robert, J., Xu, C., Lee, Y. H., Kim, S. G., et al. *Science* **1996**, *273*, (5274), 483-487.
- (171) Guo, T., Nikolaev, P., Rinzler, A. G., Tomanek, D., Colbert, D. T., Smalley, R. E. *J. Phys. Chem.* **1995**, *99*, (27), 10694-10697.
- (172) Shi, Z., Lian, Y., Zhou, X., Gu, Z., Zhang, Y., Iijima, S., Zhou, L., Yue, K. T., Zhang, S. *Carbon* **1999**, *37*, (9), 1449-1453.
- (173) Ebbesen, T. W., Ajayan, P. M. *Nature* **1992**, *358*, (6383), 220-222.
- (174) Bethune, D. S., Kiang, C. H., de Vries, M. S., Gorman, G., Savoy, R., Vazquez, J., Beyers, R. *Nature* **1993**, *363*, (6430), 605-607.
- (175) Endo, M., Takeuchi, K., Igarashi, S., Kobori, K., Shiraishi, M., Kroto, H. W. *J. Phys. Chem. Solids* **1993**, *54*, (12), 1841-1848.
- (176) Jose-Yacamán, M., Miki-Yoshida, M., Rendon, L., Santiesteban, J. G. *Appl. Phys. Lett.* **1993**, *62*, (6), 657-659.
- (177) Ando, Y., Zhao, X., Sugai, T., Kumar, M. *Mater. Today* **2004**, *7*, (10), 22-29.
- (178) Flahaut, E., Laurent, C., Peigney, A. *Carbon* **2005**, *43*, (2), 375-383.
- (179) Manchado, M. A. L., Valentini, L., Biagiotti, J., Kenny, J. M. *Carbon* **2005**, *43*, (7), 1499-1505.
- (180) Ajayan, P. M., Schadler, L. S., Giannaris, C., Rubio, A. *Adv. Mater.* **2000**, *12*, (10), 750-753.
- (181) Dyke, C. A., Tour, J. M. *J. Phys. Chem. A* **2004**, *108*, (51), 11151-11159.
- (182) Salvétat, J., Briggs, G. A. D., Bonard, J., Bacsá, R. R., Kulik, A. J., Stockli, T., Burnham, N. A., Forro, L. *Phys. Rev. Lett.* **1999**, *82*, (5), 944-947.
- (183) Niyogi, S., Hamon, M. A., Hu, H., Zhao, B., Bhowmik, P., Sen, R., Itkis, M. E., Haddon, R. C. *Acc Chem Res* **2002**, *35*, (12), 1105-1113.
- (184) Sun, Y., Fu, K., Lin, Y., Huang, W. *Acc. Chem. Res.* **2002**, *35*, (12), 1096-1104.
- (185) Dyke, C. A., Tour, J. M. *Chem.--Eur. J.* **2004**, *10*, (4), 812-817.
- (186) Hamon, M. A., Hu, H., Bhowmik, P., Niyogi, S., Zhao, B., Itkis, M. E., Haddon, R. C. *Chem. Phys. Lett.* **2001**, *347*, (1,2,3), 8-12.
- (187) Liu, J., Rinzler, A. G., Dai, H., Hafner, J. H., Bradley, R. K., Boul, P. J., Lu, A., Iverson, T., Shelimov, K., Huffman, C. B., Rodriguez-Macias, F., Shon, Y., Lee, T. R., Colbert, D. T., Smalley, R. E. *Science* **1998**, *280*, (5367), 1253-1256.
- (188) Riggs, J. E., Guo, Z., Carroll, D. L., Sun, Y. *J. Am. Chem. Soc.* **2000**, *122*, (24), 5879-5880.
- (189) Sun, Y., Huang, W., Lin, Y., Fu, K., Kitaygorodskiy, A., Riddle, L. A., Yu, Y. J., Carroll, D. L. *Chem. Mater.* **2001**, *13*, (9), 2864-2869.
- (190) Fu, K., Huang, W., Lin, Y., Riddle, L. A., Carroll, D. L., Sun, Y. *Nano Lett.* **2001**, *1*, (8), 439-441.

-
- (191) Ge, J. J., Hou, H., Li, Q., Graham, M. J., Greiner, A., Reneker, D. H., Harris, F. W., Cheng, S. *Z. D. J. Am. Chem. Soc.* **2004**, *126*, (48), 15754-15761.
- (192) Mickelson, E. T., Huffman, C. B., Rinzler, A. G., Smalley, R. E., Hauge, R. H., Margrave, J. L. *Chem. Phys. Lett.* **1998**, *296*, (1,2), 188-194.
- (193) Mickelson, E. T., Chiang, I. W., Zimmerman, J. L., Boul, P. J., Lozano, J., Liu, J., Smalley, R. E., Hauge, R. H., Margrave, J. L. *J. Phys. Chem. B* **1999**, *103*, (21), 4318-4322.
- (194) Pekker, S., Salvétat, J., Jakab, E., Bonard, J., Forro, L. *J. Phys. Chem. B* **2001**, *105*, (33), 7938-7943.
- (195) Georgakilas, V., Kordatos, K., Prato, M., Guldi, D. M., Holzinger, M., Hirsch, A. *J. Am. Chem. Soc.* **2002**, *124*, (5), 760-761.
- (196) Holzinger, M., Vostrowsky, O., Hirsch, A., Hennrich, F., Kappes, M., Weiss, R., Jellen, F. *Angew. Chem., Int. Ed.* **2001**, *40*, (21), 4002-4005.
- (197) O'Connell, M. J., Boul, P., Ericson, L. M., Huffman, C., Wang, Y., Haroz, E., Kuper, C., Tour, J., Ausman, K. D., Smalley, R. E. *Chem. Phys. Lett.* **2001**, *342*, (3,4), 265-271.
- (198) O'Connell, M. J., Bachilo, S. M., Huffman, C. B., Moore, V. C., Strano, M. S., Haroz, E. H., Rialon, K. L., Boul, P. J., Noon, W. H., Kittrell, C., Ma, J., Hauge, R. H., Weisman, R. B., Smalley, R. E. *Science* **2002**, *297*, (5581), 593-596.
- (199) Islam, M. F., Rojas, E., Bergey, D. M., Johnson, A. T., Yodh, A. G. *Nano Lett.* **2003**, *3*, (2), 269-273.
- (200) Meng, L., Fu, C., Lu, Q. *Prog. Nat. Sci.* **2009**, *19*, (7), 801-810.
- (201) Grady, B. P., Pompeo, F., Shambaugh, R. L., Resasco, D. E. *J. Phys. Chem. B* **2002**, *106*, (23), 5852-5858.
- (202) Andrews, R., Jacques, D., Minot, M., Rantell, T. *Macromol. Mater. Eng.* **2002**, *287*, (6), 395-403.
- (203) Schadler, L. S., Giannaris, S. C., Ajayan, P. M. *Appl. Phys. Lett.* **1998**, *73*, (26), 3842-3844.
- (204) Cooper, C. A., Ravich, D., Lips, D., Mayer, J., Wagner, H. D. *Compos. Sci. Technol.* **2002**, *62*, (7-8), 1105-1112.
- (205) Kearns, J. C., Shambaugh, R. L. *J. Appl. Polym. Sci.* **2002**, *86*, (8), 2079-2084.
- (206) Sennett, M., Welsh, E., Wright, J. B., Li, W. Z., Wen, J. G., Ren, Z. F. *Appl. Phys. A: Mater. Sci. Process.* **2003**, *76*, (1), 111-113.
- (207) Jin, Z., Pramoda, K. P., Xu, G., Goh, S. H. *Chem. Phys. Lett.* **2001**, *337*, (1,2,3), 43-47.
- (208) Jin, Z., Pramoda, K. P., Goh, S. H., Xu, G. *Mater. Res. Bull.* **2002**, *37*, (2), 271-278.
- (209) Andrews, R., Jacques, D., Qian, D., Rantell, T. *Acc. Chem. Res.* **2002**, *35*, (12), 1008-1017.
- (210) Zhang, W. D., Shen, L., Phang, I. Y., Liu, T. *Macromolecules* **2004**, *37*, (2), 256-259.
- (211) Liu, T., Phang, I. Y., Shen, L., Chow, S. Y., Zhang, W. *Macromolecules* **2004**, *37*, (19), 7214-7222.

-
- (212) Zhu, J., Kim, J., Peng, H., Margrave, J. L., Khabashesku, V. N., Barrera, E. V. *Nano Lett.* **2003**, *3*, (8), 1107-1113.
- (213) Zhu, J., Peng, H., Rodriguez-Macias, F., Margrave, J. L., Khabashesku, V. N., Imam, A. M., Lozano, K., Barrera, E. V. *Adv. Funct. Mater.* **2004**, *14*, (7), 643-648.
- (214) Gong, X., Liu, J., Baskaran, S., Voise, R. D., Young, J. S. *Chem. Mater.* **2000**, *12*, (4), 1049-1052.
- (215) Moniruzzaman, M., Du, F., Romero, N., Winey, K. I. *Polymer* **2006**, *47*, (1), 293-298.
- (216) Jia, Z. J., Wang, Z. J., Xu, C. L., Liang, J., Wei, B. Q., Wu, D. H., Zhu, S. W. *Mater. Sci. Eng., A: Struct.* **1999**, *271*, 395.
- (217) Velasco-Santos, C., Martinez-Hernandez, A. L., Fisher, F. T., Ruoff, R., Castano, V. M. *Chem. Mater.* **2003**, *15*, (23), 4470-4475.
- (218) Zhao, C., Hu, G., Justice, R., Schaefer, D. W., Zhang, S., Yang, M., Han, C. C. *Polymer* **2005**, *46*, (14), 5125-5132.
- (219) Badaire, S., Poulin, P., Maugey, M., Zakri, C. *Langmuir* **2004**, *20*, (24), 10367-10370.
- (220) Jin, L., Bower, C., Zhou, O. *Appl. Phys. Lett.* **1998**, *73*, (9), 1197-1199.
- (221) Qian, D., Dickey, E. C., Andrews, R., Rantell, T. *Appl. Phys. Lett.* **2000**, *76*, (20), 2868-2870.
- (222) Safadi, B., Andrews, R., Grulke, E. A. *J. Appl. Polym. Sci.* **2002**, *84*, (14), 2660-2669.
- (223) Ruan, S. L., Gao, P., Yang, X. G., Yu, T. X. *Polymer* **2003**, *44*, (19), 5643-5654.
- (224) Dufresne, A., Paillet, M., Putaux, J. L., Canet, R., Carmona, F., Delhaes, P., Cui, S. *J. Mater. Sci.* **2002**, *37*, (18), 3915-3923.
- (225) Dalmas, F., Chazeau, L., Gauthier, C., Masenelli-Varlot, K., Dendievel, R., Cavaille, J. Y., Forro, L. *J. Polym. Sci., Part B: Polym. Phys.* **2005**, *43*, (10), 1186-1197.
- (226) Probst, O., Moore, E. M., Resasco, D. E., Grady, B. P. *Polymer* **2004**, *45*, (13), 4437-4443.
- (227) Sundararajan, P. R., Singh, S., Moniruzzaman, M. *Macromolecules* **2004**, *37*, (26), 10208-10211.
- (228) Bryning, M. B., Milkie, D. E., Islam, M. F., Kikkawa, J. M., Yodh, A. G. *Appl. Phys. Lett.* **2005**, *87*, (16), 161909/1-161909/3.
- (229) Ago, H., Petritsch, K., Shaffer, M. S. P., Windle, A. H., Friend, R. H. *Adv. Mater.* **1999**, *11*, (15), 1281-1285.
- (230) De la Chapelle, M. L., Stephan, C., Nguyen, T. P., Lefrant, S., Journet, C., Bernier, P., Munoz, E., Benito, A., Maser, W. K., Martinez, M. T., De la Fuente, G. F., Guillard, T., Flamant, G., Alvarez, L., Laplaze, D. *Synth. Met.* **1999**, *103*, (1-3), 2510-2512.
- (231) Xu, X., Thwe, M. M., Shearwood, C., Liao, K. *Appl. Phys. Lett.* **2002**, *81*, (15), 2833-2835.
- (232) Benoit, J. -, Corraze, B., Lefrant, S., Blau, W. J., Bernier, P., Chauvet, O. *Synth. Met.* **2001**, *121*, (1-3), 1215-1216.
- (233) Singh, S., Pei, Y., Miller, R., Sundararajan, P. R. *Adv. Funct. Mater.* **2003**, *13*, (11), 868-872.

-
- (234) Du, F., Fischer, J. E., Winey, K. I. *J. Polym. Sci., Part B: Polym. Phys.* **2003**, *41*, (24), 3333-3338.
- (235) Xia, H., Wang, Q., Li, K., Hu, G. *J. Appl. Polym. Sci.* **2004**, *93*, (1), 378-386.
- (236) Werner, P., Altstaedt, V., Jaskulka, R., Jacobs, O., Sandler, J. K. W., Shaffer, M. S. P., Windle, A. H. *Wear* **2004**, *257*, (9-10), 1006-1014.
- (237) Regev, O., ElKati, P. N. B., Loos, J., Koning, C. E. *Adv. Mater.* **2004**, *16*, (3), 248-251.
- (238) Yu, J., Lu, K., Sourty, E., Grossiord, N., Koning, C. E., Loos, J. *Carbon* **2007**, *45*, (15), 2897-2903.
- (239) Grossiord, N., Wouters, M. E. L., Miltner, H. E., Lu, K., Loos, J., Van Mele, B., Koning, C. E. *Eur. Polym. J.* **2010**, *46*, (9), 1833-1843.
- (240) Miltner, H. E., Grossiord, N., Lu, K., Loos, J., Koning, C. E., Van Mele, B. *Macromolecules* **2008**, *41*, (15), 5753-5762.
- (241) Lu, K., Grossiord, N., Koning, C. E., Miltner, H. E., van Mele, B., Loos, J. *Macromolecules* **2008**, *41*, (21), 8081-8085.
- (242) Vigolo, B., Poulin, P., Lucas, M., Launois, P., Bernier, P. *Appl. Phys. Lett.* **2002**, *81*, (7), 1210-1212.
- (243) Ng, H. T., Foo, M. L., Fang, A., Li, J., Xu, G., Jaenicke, S., Chan, L., Li, S. F. Y. *Langmuir* **2002**, *18*, (1), 1-5.
- (244) Thostenson, E. T., Li, W. Z., Wang, D. Z., Ren, Z. F., Chou, T. W. *J. Appl. Phys.* **2002**, *91*, (9), 6034-6037.
- (245) Raravikar, N. R., Schadler, L. S., Vijayaraghavan, A., Zhao, Y., Wei, B., Ajayan, P. M. *Chem. Mater.* **2005**, *17*, (5), 974-983.
- (246) Kimura, T., Ago, H., Tobita, M., Ohshima, S., Kyotani, M., Yumura, M. *Adv. Mater.* **2002**, *14*, (19), 1380-1383.
- (247) Pradhan, B., Kohlmeyer, R. R., Chen, J. *Carbon* **2009**, *48*, (1), 217-222.
- (248) Yu, G., Cao, A., Lieber, C. M. *Nat. Nanotechnol.* **2007**, *2*, (6), 372-377.
- (249) Tian, X., Wang, Y., Xi, N., Dong, Z., Tung, S. *Chin. Sci. Bull.* **2008**, *53*, (22), 3590-3596.
- (250) Haggenueller, R., Gommans, H. H., Rinzler, A. G., Fischer, J. E., Winey, K. I. *Chem. Phys. Lett.* **2000**, *330*, (3,4), 219-225.
- (251) Haggenueller, R., Zhou, W., Fischer, J. E., Winey, K. I. *J. Nanosci. Nanotechnol.* **2003**, *3*, (1/2), 105-110.
- (252) Dror, Y., Salalha, W., Khalfin, R. L., Cohen, Y., Yarin, A. L., Zussman, E. *Langmuir* **2003**, *19*, (17), 7012-7020.
- (253) Ji, J., Sui, G., Yu, Y., Liu, Y., Lin, Y., Du, Z., Ryu, S., Yang, X. *J. Phys. Chem. C* **2009**, *113*, (12), 4779-4785.
- (254) Hou, H., Ge, J. J., Zeng, J., Li, Q., Reneker, D. H., Greiner, A., Cheng, S. Z. D. *Chem. Mater.* **2005**, *17*, (5), 967-973.

-
- (255) Salalha, W., Dror, Y., Khalfin, R. L., Cohen, Y., Yarin, A. L., Zussman, E. *Langmuir* **2004**, *20*, (22), 9852-9855.
- (256) Rosenhead L. *Laminar boundary layers* Oxford: Clarendon Press; **1963**, 144-150.
- (257) Lau, K., Hui, D. *Carbon* **2002**, *40*, (9), 1605-1606.
- (258) Dalton, A. B., Collins, S., Munoz, E., Razal, J. M., Ebron, V. H., Ferraris, J. P., Coleman, J. N., Kim, B. G., Baughman, R. H. *Nature* **2003**, *423*, (6941), 703.
- (259) Liao, K., Li, S. *Appl. Phys. Lett.* **2001**, *79*, (25), 4225-4227.
- (260) Geng, H., Rosen, R., Zheng, B., Shimoda, H., Fleming, L., Liu, J., Zhou, O. *Adv. Mater.* **2002**, *14*, (19), 1387-1390.
- (261) Gao, J., Itkis, M. E., Yu, A., Bekyarova, E., Zhao, B., Haddon, R. C. *J. Am. Chem. Soc.* **2005**, *127*, (11), 3847-3854.
- (262) Coleman, J. N., Cadek, M., Blake, R., Nicolosi, V., Ryan, K. P., Belton, C., Fonseca, A., Nagy, J. B., Gun'ko, Y. K., Blau, W. J. *Adv. Funct. Mater.* **2004**, *14*, (8), 791-798.
- (263) Lu, X., Chen, Z. *Chem. Rev.* **2005**, *105*, (10), 3643-3696.
- (264) Ju, Y., Choi, G., Jung, H., Lee, W. *Electrochim. Acta* **2008**, *53*, (19), 5796-5803.
- (265) Heikkila, P., Harlin, A. *Express Polym. Lett.* **2009**, *3*, (7), 437-445.
- (266) Ra, E. J., An, K. H., Kim, K. K., Jeong, S. Y., Lee, Y. H. *Chem. Phys. Lett.* **2005**, *413*, (1-3), 188-193.
- (267) Baughman, R. H., Zakhidov, A. A., de Heer, W. A. *Science* **2002**, *297*, (5582), 787-792.
- (268) Bai, J. B., Allaoui, A. *Composites, Part A* **2003**, *34A*, (8), 689-694.
- (269) Du, F., Fischer, J. E., Winey, K. I. *Phys. Rev. B: Condens. Matter Mater. Phys.* **2005**, *72*, (12), 121404/1-121404/4.
- (270) Ko, F., Gogotsi, Y., Ali, A., Naguib, N., Ye, H., Yang, G., Li, C., Willis, P. *Adv. Mater.* **2003**, *15*, (14), 1161-1165.
- (271) Sen, R., Zhao, B., Perea, D., Itkis, M. E., Hu, H., Love, J., Bekyarova, E., Haddon, R. C. *Nano Lett.* **2004**, *4*, (3), 459-464.
- (272) Chakrabarti, K., Nambissan, P. M. G., Mukherjee, C. D., Bardhan, K. K., Kim, C., Yang, K. S. *Carbon* **2006**, *44*, (5), 948-953.
- (273) Kim, J., Reneker, D. H. *Polym. Compos.* **1999**, *20*, (1), 124-131.
- (274) Bergshoef, M. M., Vancso, G. J. *Adv. Mater.* **1999**, *11*, (16), 1362-1365.
- (275) Tang, C., Liu, H. *Composites, Part A* **2008**, *39A*, (10), 1638-1643.
- (276) Chen, G., Liu, H. *J. Appl. Polym. Sci.* **2008**, *110*, (2), 641-646.
- (277) Pinho, E. D., Martins, A., Araujo, J. V., Reis, R. L., Neves, N. M. *Acta Biomater.* **2009**, *5*, (4), 1104-1114.

- (278) Fong, H. *Polymer* **2004**, *45*, (7), 2427-2432.
- (279) Dodiuk-Kenig, H., Lizenboim, K., Roth, S., Zalsman, B., McHale, W. A., Jaffe, M., Griswold, K. *J. Nanomater.* **2008**, 1-6.
- (280) Han, S. O., Son, W. K., Youk, J. H., Park, W. H. *J. Appl. Polym. Sci.* **2008**, *107*, (3), 1954-1959.
- (281) Neppalli, R., Marega, C., Marigo, A., Bajgai, M. P., Kim, H. Y., Causin, V. *Eur. Polym. J.* **2010**, *46*, 968-976.
- (282) Swart, M., Olsson, R. T., Hedenqvist, M. S., Mallon, P. E. *Polym. Eng. Sci.* **2010**, *50*, (11), 2143-2152.

Chapter 3

Experimental

3.1 Synthesis

The following section gives the experimental procedures followed in the synthesis and characterisation of the materials produced and tested in this work.

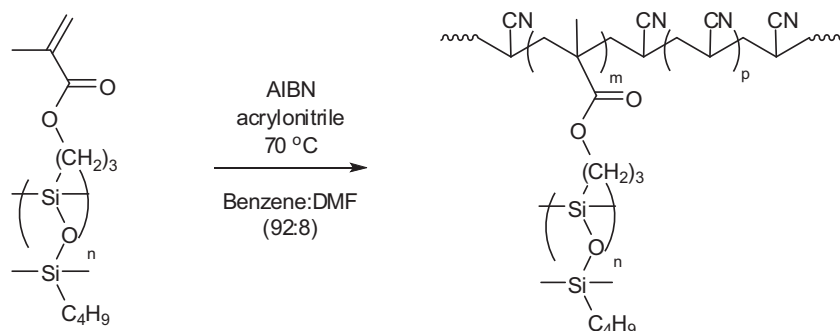
3.1.1 Materials

Mono-methacryloxypropyl terminated polydimethylsiloxane (MMP-PDMS, Gelest Inc., Mw: 10 000; 5 000; 1 800) were used as received. Acrylonitrile monomer (AN, Sigma-Aldrich, >99%) was passed through a monomethyl ether hydroquinone inhibitor removal column (Sigma-Aldrich) prior to polymerisation. Azobisisobutyronitrile (AIBN, Plascon) recrystallised from methanol prior to polymerisation was used as initiator. Methanol (MeOH, Sasol, Class 3) was used to precipitate out the synthesised polymer. Sodium nitrate (NaNO_3 , >99%); sulphuric acid (H_2SO_4 , purum 30% in H_2O); nitric acid (HNO_3 , ACS reagent 70%); potassium permanganate (KMnO_4 , >99%); benzene (benzene, 99.8% anhydrous) and hydrogen peroxide (H_2O_2 , 30 wt% in H_2O) all from Sigma-Aldrich, were used as received. Hexane (hexane, Sasol, Class 3) was used for MMP-PDMS extraction. Solvents for chromatography analysis were tetrahydrofuran (THF, Chromasolve plus[®] HPLC grade) and N,N dimethylformamide (DMF, Chromasolve plus[®] HPLC grade) both from Sigma-Aldrich. Silicone Dehesive 920 with 2.5 wt% crosslinker V24 and 1 wt% Catalyst C 05, Wacker, Germany.

3.1.2 Synthesis of polyacrylonitrile-graft-polydimethylsiloxane copolymers

Conventional free radical polymerisation was employed to synthesise the graft copolymers of polyacrylonitrile (PAN) and polydimethylsiloxane (PDMS). Due to the severe incompatibility between the two constituents of the graft copolymer, a solvent mixture of benzene and DMF was used as reaction medium. A 250 ml single necked round bottomed flask served as reaction vessel. The flask was charged with mono methyl methacrylate functional PDMS (MMA-PDMS) macromonomer and the solution of benzene:DMF (92:8). PDMS macromonomers with varying molecular weights ($1000 \text{ g}\cdot\text{mol}^{-1}$; $5000 \text{ g}\cdot\text{mol}^{-1}$; $10000 \text{ g}\cdot\text{mol}^{-1}$) were used. These components were added to give a 15 % solids content. A stirrer bar was added and the vessel was sealed with a rubber septum. N_2 gas was bubbled through the solution while stirring for approximately 10 min. Degassed acrylonitrile (AN) monomer was then introduced via a syringe. The amount of AN added depended on the weight ratio PDMS macromonomer desired in the final graft copolymer. This feed ratio was varied from a 5 wt% PDMS macromonomer to a 25 wt% PDMS macromonomer reaction with regards to the AN added. After adding the appropriate amount of AN monomer the solution was allowed to stir

for a further 15 min. Azobisisobutyronitrile (AIBN) initiator was then added to the reaction vessel in a ratio of 0.1 wt% with regards to the mol AN added in the feed. The reaction vessel was then placed in a temperature controlled oil bath set at 70 °C. The polymerisation reaction was left to proceed for 48 hrs where precipitation of the graft copolymer occurred after 24 hrs yielding a milky white solution. After reaction, the polymer solution was added to rapidly stirring excess methanol for complete precipitation. The solution was then filtered on a glass sinter filter and the product dried in a vacuum oven at room temperature until constant weight. The reaction scheme is illustrated below:



Scheme 3.1 : Synthesis of the novel PAN-g-PDMS copolymers via free radical copolymerisation.

3.1.3 Extraction of homo-PDMS

As with any conventional free radical copolymerisation reaction, the formation of homopolymer always occurs along with that of the copolymer due to reactivity ratio effects or the exclusion of macromonomer from copolymer chains¹. Sometimes it is necessary to remove these homopolymers as they may adversely affect future studies. An extraction step was needed to remove all unreacted PDMS macromonomer from the final copolymer product as PDMS does not readily electrospin. Homo-PAN was left with the copolymer product as it is difficult to extract and undergoes electrospinning readily. A simple hexane extraction was employed. After drying, the polymer blend was placed in excess hexane and stirred for 48hrs. The supernatant was then separated from the graft copolymer and homo-PAN using a vacuum sintered glass filter. The product was then placed in a vacuum oven and dried until a constant weight had been reached.

3.1.4 Modification of multi-walled carbon nanotubes

The following experimental procedure² describes the surface functionalisation of the multi-walled carbon nanotubes (MWCNT's) used in this project. The aim was to introduce carboxylic acid functionality via an acid oxidation procedure. The weight of MWCNT's functionalised was kept at 2 g each time. A 250 ml round bottomed flask was loaded with

MWCNT's and NaNO_3 powder in a weight ratio of 2 g : 1 g (MWCNT: NaNO_3). A stirrer bar was placed inside the flask which was then lowered into an ice bath. 46 ml of 90 wt% H_2SO_4 was then added carefully and the mixture was allowed to stand for approximately 10 min while stirring gently. After 10 min, 300 g KMNO_4 was added to the solution while stirring vigorously. Care was taken when adding the KMNO_4 and the temperature of the mixture was kept below 20 °C by slow addition. This mixture was then allowed to stir vigorously for a further 10 min. The reaction vessel was removed from the ice bath and placed on a heating stirrer plate, where it was heated to 98 °C. Once the solution had stopped effervescing and turned brown-grey in colour, 92 ml of distilled H_2O was slowly added. The solution was then kept at 98 °C for 15 min. A 3 wt% solution of H_2O_2 in distilled H_2O was then added to the reaction mixture to increase the volume of this solution to 200 ml. This final mixture was allowed to stir for 20 min. Finally, the MWCNT solution was neutralised by repeatedly diluting with distilled H_2O and centrifugation of the mixture. The supernatant was then decanted and additional H_2O was added and centrifugation repeated. This cycle was repeated until the pH of the MWCNT solution was found to be neutral. The MWCNT's were then freeze dried on a Christ Alpha 2-4 LD Freeze-drier.

3.1.5 Silicone matrix preparation and curing

The procedure for preparing the silicone matrix is as follows: 0.13 g of Crosslinker V24 is added to 5 g of Dehesive 920 silicone. The solution is then stirred vigorously with a glass rod. 0.05 g of Catalyst C 05 is then added and the solution is again stirred vigorously. The mixture is then placed under vacuum (for approximately 45 min) to remove any air bubbles trapped inside. After layering the fiber sheet into the resin, the uncured system is placed into a vacuum oven again. The sample is placed under vacuum for additional 45 min after which the resin is cured. The temperature profile used for curing was as follows: 75 °C for approximately 45 min, then raise the temperature to 120 °C for a further 45 min to 60 min.

3.2 Characterisation

This section describes the equipment, conditions and sample preparation used during analysis or characterisation of the synthesised polymer materials.

3.2.1 Size exclusion chromatography (SEC)

This chromatographic technique separates polymer molecules according to size, or more correctly hydrodynamic volume. Depending on whether the chromatographic medium is a gel or not, the technique is also referred to as gel permeation chromatography (GPC). The

SEC instrument used in this project comprised of the following units: Waters 1515 isocratic HPLC pump; Waters 717 plus Auto-sampler; Waters 2487 Dual λ Absorbance detector; Waters 2414 Refractive index (RI) detector at 30°C and data processing was performed using Breeze Version 3.30 SPA (Waters) software. Separation was achieved using two PL gel (Polymer Laboratories) 5 μ m Mixed-C (300 \times 7.5 mm) columns connected in series along with a PL gel 5 μ m guard column (50 \times 7.5 mm). The columns were kept at a constant temperature of 30 °C. DMF Chromasolve HPLC grade solvent (0.125 % LiCl) was used as mobile phase at a flow rate of 1 ml/min. Samples were dissolved in the DMF at a concentration of 5mg/ml and 100 μ l injection volumes were used. The system was calibrated using Polymer Laboratories PMMA Standards.

3.2.2 Gradient elution chromatography (GEC)

This technique is widely employed in the separation of polymers according to chemical composition³. This technique allows separation of block and graft copolymer molecules from their respective homopolymers. This is achieved by varying the mobile phase solvent composition. This technique was performed using a dual pump HPLC comprising of the following units: Waters 2690 Separations module (Alliance); Agilent 1100 series variable wavelength detector; PL-ELS 1000 detector and data was recorded and processed using PSS WinGPC unity (Build 2019) software. The mobile phase flow rate was maintained at 1ml/min and the composition varied as described in section 4.2.2.3. A bare silica column was used (Nucleosil 300Si 5 μ m 250 \times 0.46 mm Technokroma) at 30 °C. Samples were prepared in a solution of DMF (100 %), and at a concentration of 5mg/ml. The mobile phase consisted of a solvent gradient of DMF to THF, as discussed in chapter 4.

3.2.3 Nuclear magnetic resonance (NMR)

¹H-NMR and ¹³C-NMR were performed as routine analysis for the determination of molecular structure, and PDMS macromonomer incorporation efficiencies. Routine identification was achieved using a Varian VXR, 300MHz, Spectrometer. When precise integration data was needed the Varian ^{Unity} Inova, 400MHz or 600MHz was used. Samples were prepared in NMR borosilicate tubes. Typically, 60mg of sample was added to the sample tube, topped up with *d*-DMSO to the 5 mm height mark.

3.2.4 Static contact angle measurements

This technique was used to monitor the changes in hydrophobicity of the polymer samples and fibres. Analysis was performed at room temperature (23 °C), in a climate controlled laboratory (50 % RH). Measurements were conducted on a KSV instruments CAM 200,

equipped with a Basler A602f camera (100 frames per second). A 3 μ L droplet was placed on the sample surface with an automatic piston syringe and photographed. Contact angles were then determined using CAM software which fits the measured drop profile with a Young-Laplace equation. At least ten measurements were performed per sample for reproducibility. Figure 3.2 shows how the contact angles were calculated according to equation 3.1

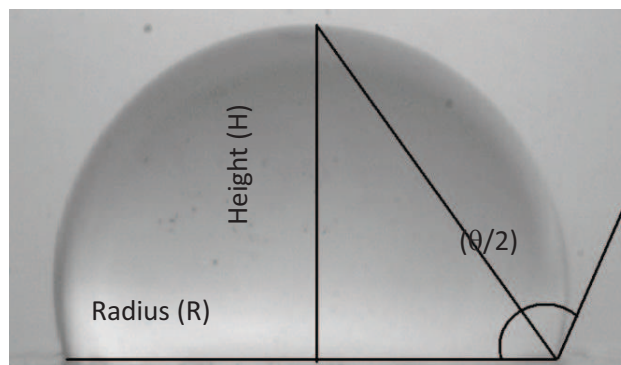


Figure 3.2 : Image of water drop showing the height and radius used in determination of the contact angle (θ).

$$\theta = 2 \times \tan^{-1}(H/R) \quad 3.1$$

3.2.5 Scanning electron microscopy (SEM) and field emission SEM (FE-SEM)

For SEM analysis the fibres were fastened onto SEM pegs and subsequently coated in gold sputter. Analysis was performed using a Leo 1430VP Scanning Electron Microscope fitted with Backscatter, Cathodoluminescence, Variable pressure and Energy Dispersive detectors, as well as a Link EDS system and software for microanalysis. For the FE-SEM, samples were kept in a dessicator for 48 hrs prior to use and then gold sputter coated (10 nm) using an AGAR high resolution sputter coater (model 208RH), equipped with a goal target/AGAR thickness monitor controller. Samples were then analysed on a Hitachi S-4800 FE-SEM.

3.2.6 Transmission electron microscopy (TEM)

This is an imaging technique whereby a beam of electrons is focused on a sample specimen. TEM images were obtained from a JEOL 1200 EXII instrument at the University of Cape Town's electron microscopy unit. Samples were prepared by casting a thin film from very dilute solution onto the Copper grid. This method allowed the preparation of films thin

enough for TEM analysis. Fibres were embedded in an epoxy resin and fine sections (approximately 90 to 120 nm thick), were microtomed for TEM analysis.

3.2.7 Attenuated total reflectance (ATR) fourier transform infra-red (FT-IR)

This technique allows FT-IR analysis of samples, without the need for strict sample preparation. FT-IR analysis was achieved using a Thermo Nicolet (Nexus model) instrument. The ATR attachment was a Smart Golden Gate accessory (ZnSe lenses) with diamond window.

3.2.8 Rheology measurements

Rheological analysis was performed on a Modular Compact Rheometer, Physica MCR 300 (Paar Physica) from Advanced Laboratory Solutions. The instrument was fitted with TEK 150 P-C (measuring cell) and Physica VT2 (temperature control). The data was collected and processed on Rheoplus / 32 V2.66 software from Anton Paar (Germany).

Oscillating rheological analysis was performed on a Anton Paar MCR501 Rheometer equipped with a plate measuring cell (PTD200/TG+H-PTD200) and plate geometry (PP25). All measurements were performed at 25°C. Amplitude sweep – constant frequency of 1Hz, amplitude ramped from 0.01 – 100% strain over 60s. Frequency sweep – constant amplitude of 1%, frequency ramped from 0.1 – 100Hz over 60s.

3.2.9 Mechanical testing on Instron

Tensile tests were carried out on an Instron 5567 universal testing machine, equipped with a 100 N load cell. All tests were carried out in a climate controlled room at a temperature of 25 °C and 50% RH. The sample specimens were clamped in place at a distance of 20 mm between each clamp. The samples were then subjected to a cross head speed of 10 mm/min. Between 7 and 9 sample specimens were punched from the each prepared silicone composites for reproducibility. Samples were dumbbell shaped with a length and width of the narrow section measuring 16 mm and 4 mm respectively. Samples were also conditioned for three days in the climate controlled room prior to testing.

3.2.10 Wide angle X-ray diffraction (WAXD)

The instrument used was a PANalytical X'Pert PRO MPD (Multi-Purpose Diffractometer) with X'Celerator detector and fixed divergence slits. The source: Cu K α radiation and optics: Fixed anti-scatter slits on incident and diffracted beams and Nickel filter and parallel plate collimator on diffracted beam optical attachments to allow parallel beam work. Cryostat: Anton Paar TTK450 (with automated sample height adjustment) for non-ambient

measurements from -193 °C to 450 °C in vacuum to -120 °C to 300 °C in inert gas. Sample fibres and powders were placed directly under the incident beam for analysis.

3.3 Electrospinning apparatus

The electrospinning setup was constructed “in-house” similarly to the usual setup as published in literature^{4,5}. The electrospinning apparatus consisted of a variable high voltage supply (built “in-house” and capable of up to 50 kV voltage) which was used to apply a potential difference between the spinneret and the grounded collector plate. A Hamilton SGE gas tight syringe used as the spinning solution reservoir was placed in a Kent Scientific (model: Genie Plus) pump which fed the polymer solution at a constant predetermined rate. Teflon tubing (60 cm length, Separations) equipped with luer-lock fittings connected the syringe reservoir to the stainless steel spinneret (22 gauge blunt nosed 50 mm needle) which allowed freedom to electrospun vertically, horizontally or any other angle as required. Aligned fibres were collected on an earthed high speed rotating drum (controlled by a Reliance Electric (model: E243) motor connected to an Eagle HP005B (model: HEP-613) variable power supply unit) revolving at approximately 5000 rpm.

3.4 References

- (1) Flory PJ. Copolymerization, Emulsion Polymerization, and Ionic Polymerization. Principles of Polymer Chemistry USA: Cornell University Press; **1953**, 178-230.
- (2) Hummers, W. S., Jr., Offeman, R. E. *J. Am. Chem. Soc.* **1958**, *80*, 1339.
- (3) Pasch, H., Trathnigg, B. *HPLC of Polymers*. Springer-Verlag: Berlin, **1998**.
- (4) Ramakrishna, S., Fujihara, K., Teo, W. E., Lim, T. C., Ma, Z. *An Introduction to Electrospinning and Nanofibers*. World Scientific: London, **2005**.
- (5) Reneker, D. H., Yarin, A. L. *Polymer* **2008**, *19*, 2387-2425.

Chapter 4

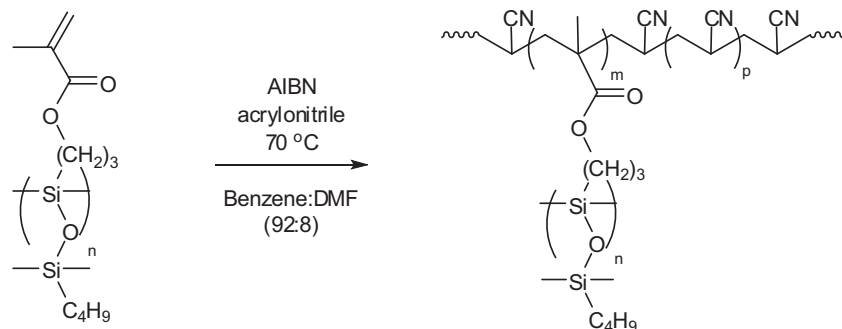
Fibre precursor synthesis and electrospinning

4.1 Novel PAN-graft-PDMS copolymer fibre filler precursor material

The synthesis of a novel copolymer was necessary to realise the fibre reinforced silicone composites prepared in this work. As has been discussed in the literature review, it is clear that for enhanced properties to be attained, sufficient distribution of the filler and interaction with the matrix is needed. Previous studies¹ have shown success when using PMMA based materials for silicone composite reinforcement. This study focused on using PAN based fibres, due to the excellent physical properties PAN offers. PAN-g-PDMS copolymers were synthesised to increase the compatibility between the PAN based fibres and the cross-linked silicone matrix. According to literature, this graft copolymer has not been synthesised before, and the following section discusses the synthesis of this novel copolymer.

4.1.1 Synthesis of the fibre filler precursor material

The severe incompatibility of the constituents in this novel graft copolymer made it essential to optimise the reaction conditions for this polymerisation with regards to solvent composition. The solvents chosen for this solution polymerisation were DMF (solvent for PAN) and benzene (solvent for PDMS). The “grafting through” or macromonomer copolymerisation technique employed acrylonitrile monomer, PDMS macromonomer as the co-monomer and AIBN as initiator. The reaction scheme is presented in Scheme 4.1.



Scheme 4.1 : Synthesis of the novel PAN-g-PDMS copolymers via free radical copolymerisation.

Various feed amounts of PDMS macromonomer were used (5 wt%, 10 wt%, 15 wt% and 25 wt%). The molecular weight of the PDMS macromonomer was also varied (1000 g.mol⁻¹, 5000 g.mol⁻¹). Two routes were initially studied in the synthesis of the copolymer, namely, a reaction solution with DMF as the major constituent and one with benzene as major constituent. With the first system, as the polymerisation continued, the resultant polymer was soluble in the reaction medium, but the initial PDMS macromonomer remained insoluble². and did not react readily with the acrylonitrile monomer. ¹H-NMR was performed on the

product after precipitation and hexane extraction of the unreacted PDMS macromonomer. It was found that little to no PDMS had been incorporated into the polymer chains using DMF as solvent medium, producing essentially PAN homopolymer. This result remained consistent in all the various PDMS feed amounts as well as molecular weights. The PDMS macromonomer has to be in solution to react with the growing polymer chains. Following the previous unsuccessful attempt, a reaction medium of 100 % benzene was investigated. PDMS is soluble and acrylonitrile (AN) is miscible with benzene, therefore, at the start of the reaction all constituents are in solution. After 1hr at 70 °C the reaction became milky, as the graft copolymer started precipitating out of solution, due to the high AN content. PAN is not soluble in benzene, which resulted in a heterogeneous polymerisation reaction³. After completion of the reaction, methanol precipitation and PDMS macromonomer hexane extraction, ¹H NMR showed much improved results with definite PDMS incorporation into the PAN backbone chains. The unreacted PDMS macromonomer was removed so as to avoid incorrect estimation of the final polymer composition. The percentage PDMS incorporated was calculated using ¹H-NMR and compared to the wt% PDMS added in the feed. This is represented in Table 4.1. Relatively good correlations were observed. The addition of DMF to the initial solvent medium showed increased PDMS incorporations up till a maximum of 10 v% DMF to benzene, after which a decrease in the PDMS incorporation occurred. At this point the PDMS macromonomer had difficulty remaining in solution at the start of the polymerisation reaction. ¹H NMR showed that optimum PDMS incorporation occurred at a solvent composition of 92 % benzene to 8 % DMF (v/v). In other words, the incorporated PDMS macromonomer most closely matched the initial feed ratio of PDMS macromonomer to acrylonitrile monomer at this solvent composition. It must be noted that a variety of different solvent compositions were studied and are not all presented in the table below. Table 4.1 simply compares the optimum solvent composition results to that of the 100 % benzene reaction medium.

SEC using LiCl stabilised DMF (mobile phase) was used to determine the molecular weights as described in the experimental chapter 3, according to PMMA standards. The molecular weights and polydispersity are typical of other uncontrolled free radical copolymerisations³. The PDI's range from 1.6 to 2.4 which is not unusual for uncontrolled polymerisations. The molecular weights are important, in that this precursor material will later be electrospun to produce the fibre fillers. The molecular weights are in the range of 69 000 to 110 000 g.mol⁻¹ which is sufficiently high for electrospinning.

Table 4.1 : PDMS macromonomer incorporation in the PAN-g-PDMS copolymers at different reaction medium compositions, and for different macromonomer lengths.

1000g.mol ⁻¹ PDMS						92 v% benzene to 8 v% DMF
Sample codes	homo-PAN	CP40	CP41	CP42	CP43	
PDMS Feed %wt	0	5	10	15	25	
PDMS ¹ H NMR %wt ^a	0	4.8	11.4	16.3	19.4	
M _n (g.mol ⁻¹) ^b	69300	69200	104300	102300	109400	
PDI ^b	2.35	1.59	1.68	1.67	1.62	
5000g.mol ⁻¹ PDMS						
Sample codes	homo-PAN	CP14	CP15	CP16	CP17	
PDMS Feed %wt	0	5	10	15	25	
PDMS ¹ H NMR %wt ^a	0	4.2	8.5	13.1	16.2	
M _n (g.mol ⁻¹) ^b	69400	78500	101300	108400	105500	
PDI ^b	2.35	1.84	1.59	1.64	1.68	
1000g.mol ⁻¹ PDMS						100 % benzene
	homo-PAN	CP34	CP35	CP36	CP37	
PDMS Feed %wt	0	5	10	15	25	
PDMS ¹ H NMR %wt ^a	0	3.2	8.5	13.1	17.4	
5000g.mol ⁻¹ PDMS						
	homo-PAN	CP10	CP11	CP12	CP13	
PDMS Feed %wt	0	5	10	15	25	
PDMS ¹ H NMR %wt ^a	0	3	7.4	10.8	14.1	

^(a) Determined using ¹H-NMR integration of PDMS peak (ppm) and PAN peak (ppm).

^(b) Determined according to PMMA standards on a mixed C styrene/divinylbenzene column (stationary phase) with DMF (mobile phase) at 1 ml.min⁻¹ and 30°C.

The PDMS incorporation in the table above appears to correlate fairly well with the feed ratios of the reaction comonomers. A decrease in the incorporation of the 1000 g.mol⁻¹ PDMS macromonomer is evident at the highest feed ratio of 25 wt% PDMS to AN monomer. The 5000 g.mol⁻¹ series deviates to a larger extent than the shorter PDMS macromonomer series. The 25 wt% feed ratio shows an incorporation of 16.2 wt%. The deviations are due to the steric and polarity effects of the comonomers in solution. The PDMS macromonomers are bulky in nature which results in a slower diffusion of these molecules throughout the reaction medium. Direct interaction with the growing polymer chain in solution is required to add the macromonomer. The larger PDMS macromonomers show decreased incorporation due to this fact that they are competing with the smaller AN monomers to add to the growing

polymer chain. The high feed ratios of PDMS results in a larger number of the bulky macromonomers competing to add to the polymer chain, which in turn results in a lower incorporation than the reactions with lower feed ratios. The grafting through approach used in this work, does have limitations when used in a conventional uncontrolled system. The incorporation is reliant on the reactivity ratios⁴ as discussed in Chapter 2. When the reactivity ratios approach zero, an alternating graft copolymer would be the most likely product. If one of the components have a significantly larger reactivity ratio than the other, a more random combination of various graft copolymers could form.

Methods exist where one can control the growth of the polymer chains using RAFT⁵ or ATRP⁶, which allows a better control of the incorporation and molecular weights of the polymer molecules. The focus in this work was not to control the synthesised material to such a large extent, but to simply obtain species with varying amounts of PDMS. Reactivity ratio determinations would be needed to gain a better understanding of the PDMS graft incorporation, but this was not performed in this project. The bulky nature of the PDMS macromonomer would suggest that it is feasible that this monomer unit would have a significantly lower reactivity ratio than the AN monomer. The fact that its incorporation is lower when the feed ratio is increased, as well as the macromonomer size, confirms this hypothesis. The incompatibility of the disparate moieties means that they are not soluble in a common solvent. Precipitation or heterogeneous polymerisation resulted as mentioned previously. Initially all components were in solution, but as the polymerisation proceeded, they precipitated out of solution resulting in heterogeneous system. The PDMS macromonomers remained soluble throughout the reaction. Work by Xu *et. al.*⁷ and Wan *et. al.*⁸ show uncontrolled precipitation copolymerisation to yield good comonomer incorporation (soluble comonomer as in our case). They reacted AN in water, together with water soluble comonomers, where all constituents were in solution at the start of the reaction. The conditions are very similar to those in this work. Their results did in fact show that the reactions proceeded better than the solution copolymerisation analogues. Good correlation between the feed ratios and incorporated monomers were also evident. During precipitation polymerisation, chain transfer and termination does not occur as readily as with solution polymerisations which can lead to increased yields and molecular weights. The NMR results clearly show that there is incorporation of PDMS macromonomer into the graft copolymer chain, however, other techniques were also used to confirm this and gain more insight into the synthesised graft copolymer.

4.1.2 Characterisation of the fibre filler precursor material

Further characterisation of the synthesised copolymers was performed to confirm successful synthesis of the novel PAN-g-PDMS graft copolymers used in this study. The results of this analysis are presented in this section.

4.1.2.1 Gradient chromatography

SEC was performed to determine the average molecular weight and molar mass distributions of the copolymers. However, this technique does not give an indication of the chemical composition distribution of the copolymers. Gradient elution chromatography⁹ (GEC) was chosen to gain insight into the material distribution. The gradient profile is presented below in Figure 4.2. The gradient chromatograms are shown below in Figure 4.3 (a) and (b). A solvent gradient consisting of DMF and THF was chosen as the mobile phase solvent, while a polar silica column (300Å, 5µm) was used as stationary phase.

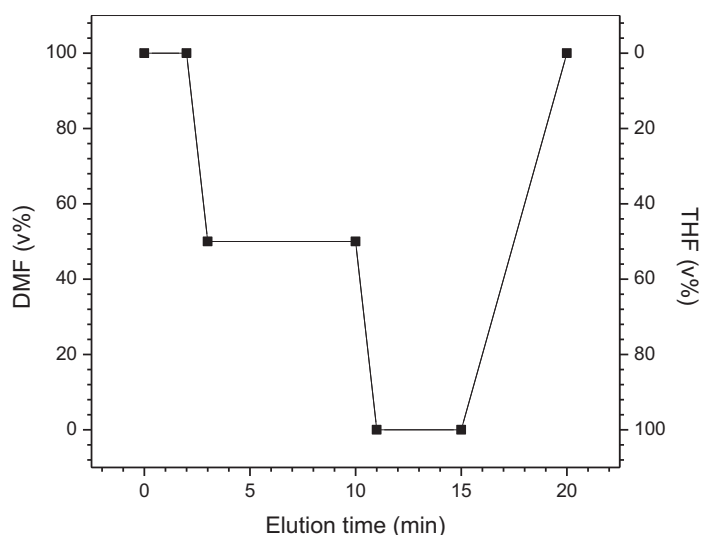


Figure 4.2 : Gradient profile of THF:DMF mobile phase vs. elution time for the gradient chromatographic separation of the PAN-g-PDMS copolymers. (DMF/THF mobile phase, Si 300 Å, 5 µm, 1 ml.min⁻¹, 30 °C)

The polarity of the polymer system under study would normally require a non-polar stationary phase if elution of the non-polar PDMS components at the end of the gradient profile is desired. A variety of different gradient profiles were examined, but it was found that the best separation occurred using a polar (silica) stationary phase. It is well known that in such uncontrolled free radical copolymerisations, there is always the possibility of homopolymer formation. In this case, we expect the formation of homo-PAN along with the

copolymer, as well as unreacted PDMS homopolymer (macromonomer). The homo-PDMS was successfully extracted as mentioned in the experimental chapter 3, as it is not electrospinnable and would hinder this process.

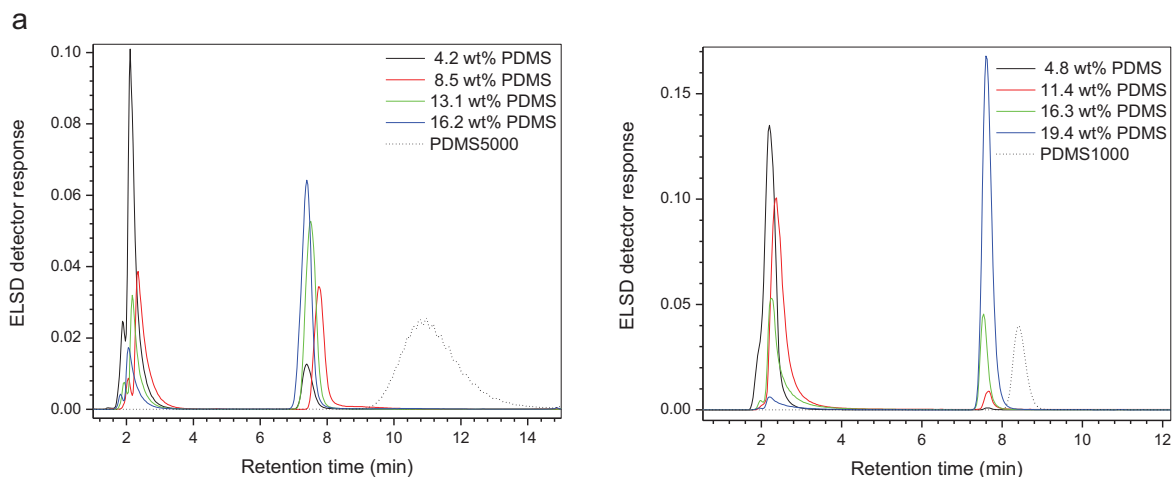


Figure 4.3 : Gradient elution chromatographic overlays of the various PAN-g-PDMS / homo-PAN polymer blend, where (a) shows the 1000g.mol^{-1} PDMS and (b) the 5000 g.mol^{-1} PDMS grafts. (DMF/THF mobile phase, Si 300 \AA , $5\text{ }\mu\text{m}$, 1 ml.min^{-1} , $30\text{ }^{\circ}\text{C}$)

Homo-PAN is desirable due to its excellent physical properties and ability to be electrospun into fibres. Figure 4.3 shows two distinct distributions. The first distribution, at low retention times is that of homo-PAN and the second is due to the graft copolymer. The initial gradient consists of 100% DMF, so the homo-PAN is completely soluble. The graft copolymer is not soluble due to the insoluble PDMS grafts causing precipitation onto the stationary phase. The homo-PAN, therefore, elutes first at approximately 2 min. The mobile phase is then changed to a 50/50 (v/v) DMF/THF mixture using a linear gradient, which enables the solubilisation of the graft copolymers and elution thereof at approximately 7 min. The graft material should elute according to the PDMS content relative to PAN in the polymer molecules. The higher the PDMS content, the longer the polymer takes to solubilise and elute through the column. Figure 4.3 shows that the graft copolymers all elute at roughly the same elution volume, indicating that the respective molecules contain similar amounts of PDMS graft incorporation. The relative intensity of the homo-PAN peak to the graft copolymer peak also change dramatically as the PDMS macromonomer content in the polymerisation feed changes. Increased PDMS macromonomer incorporation results in an increased copolymer peak and a decreased homo-PAN peak, yet no significant shift in the elution point of the graft material. However the amphiphilic nature of this copolymer complicates the situation greatly. Chromatography of amphiphiles is not a widely studied

field, and their self assembling nature in solution can result in a multitude of possibilities. This does make it difficult to extract too much more information from the above mentioned results pertaining to the gradient chromatograms. The increased PDMS macromonomer / AN feed ratio does, however, seem to indicate an increased number of graft copolymer molecules relative to homo-PAN molecules. The feed ratio does appear to affect the overall amount of graft copolymer molecules relative to homo-PAN molecules. It must be noted that the material precursor for the fibre fillers are indeed a blend of homo-PAN and PAN-g-PDMS copolymer, where the copolymer was chosen as a possible compatibiliser between the PAN and the silicone matrix. These qualitative results show a definite increase in the amount of graft copolymer to that of the homo-PAN as the PDMS content is increased. PDMS macromonomer was extracted, but as a control the elution profiles of both the PDMS macromonomers have been overlaid. It is clearly shown that the peaks are due to the presence of copolymer and not un-extracted PDMS homopolymer. In conclusion, the graft molecules were successfully synthesised but extracting more information from these results are complicated by the amphiphilic nature of the molecules in solution. The fibre filler precursor material synthesised does, however, contain varying amounts of graft copolymer to PAN homopolymer in the precursor blend.

4.1.2.2 WAXD of the fibre filler precursor material

PAN's good physical properties can be related to the crystalline nature of the material. The fibre filler precursor material studied in this work is, however, a multiphase system containing a blend of PAN homopolymer and PAN-g-PDMS graft copolymer. PDMS is a highly amorphous material and the question is, does the presence of the non-crystallisable PDMS grafts affect the crystallinity of the PAN segments? The group of Minagawa¹⁰⁻¹² have published a series of detailed studies on the crystallinity of PAN homopolymer. Interestingly, they found that the degree of crystallinity of PAN does not depend on the extent of stereo-regularity, in contrast to other crystalline materials. Tacticity was varied from 25 to 83 % and no change in the degree of crystallinity was observed. They did, however, find a shift in the main crystalline peak from 17.1° to 16.8° and a decrease in the peak width at half maximum from 1.7° to 0.97°, as the stereo-regularity was increased. PDMS, as mentioned earlier, is an amorphous polymer so it does not undergo crystallisation at room temperature. Wide angle X-ray diffraction (WAXD) was used to study the effect of PDMS content on the crystallinity of the prepared PAN-g-PDMS / PAN polymer blends. Various methods can be used to study the degree of crystallinity, including the methods by Hinrichsen¹³, Bell and Dumbleton¹⁴, and Gupta *et. al.*^{15,16} The methods differ according to the definition of the crystalline and

amorphous phases (after deconvolution of the XRD patterns)¹¹ and can result in differences of between 40 to 70 %. Figure 4.4 (a) below illustrates the methodology used by Gupta *et al.*^{15,16} which is the same approach used in this work. The WAXD pattern in Figure 4.4 (a) is that of homo-PAN synthesised according to the same procedure as the graft materials. There are two crystalline regions labelled Area C₁ (peak approximately 17°) and Area C₂ (peak approximately 29.5°).

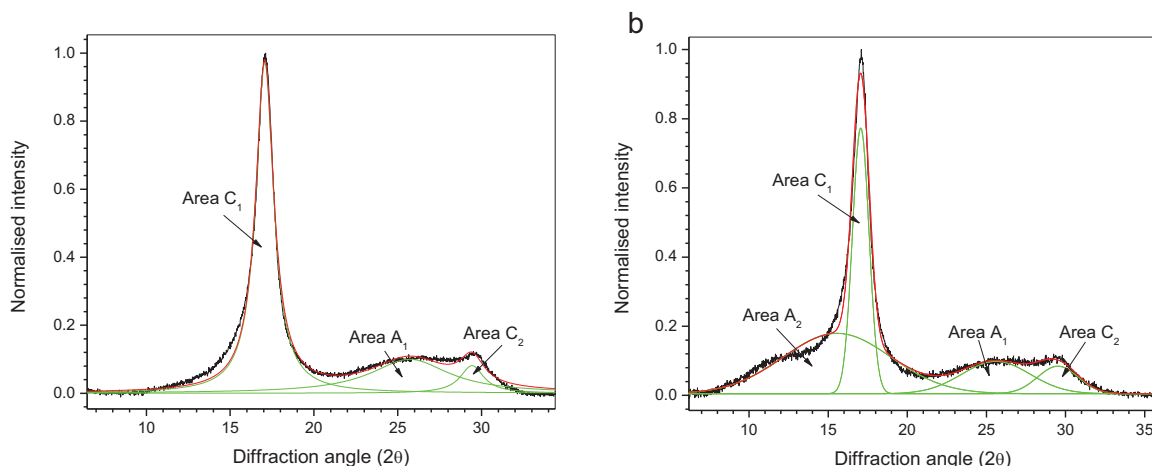


Figure 4.4 : WAXD patterns of (a) PAN and (b) PDMS-g-PAN / PAN blend with 25 wt% PDMS (19.4 wt%, 1000 g.mol⁻¹), highlighting the various crystalline and amorphous regions according to the Gupta *et al.*^{15,16} method.

It was found by Mingawa *et al.*¹¹ that the smaller crystal peak at 29.5° disappeared with decreasing stereo-regularity, hence assigning it to the diffraction of isotactic PAN crystal packing. From the geometric consideration of rod-like PAN molecules, it was further assigned to the [101] lattice plane ($d = 3.0\text{-}3.1 \text{ \AA}$) in the hexagonal packing of PAN. Comparison of the crystalline to amorphous areas yields the degree of crystallinity of the sample. Area A₁ highlights the amorphous halo of the PAN. The WAXD patterns become more complicated when moving to the PDMS containing graft copolymer blend material as shown in Figure 4.4 (b). PDMS contributes an additional amorphous halo found at approximately 12° and is highlighted in Figure 4.4 (b) as Area A₂. The degree of crystallinity of the various PDMS copolymer blends was calculated by taking the ratio between the crystalline regions and the sum of the crystalline and amorphous areas, as shown in equation 4.1.

$$D_{crystallisation} = \left(\frac{Area\ C_1 + Area\ C_2}{Area\ C_1 + Area\ C_2 + Area\ A_1 + Area\ A_2} \right) \times \frac{100}{W_{PAN}} \quad (4.1)$$

Where, W_{PAN} refers to the weight fraction of PAN material present in the copolymer blend (homo-PAN and PAN in the copolymers). The calculated $D_{\text{crystallisation}}$ values are presented in Table 4.2. An overlay of the WAXD patterns of the various PDMS (1000 g.mol^{-1}) containing copolymers are shown below in Figure 4.5. It is clear that the amorphous halo at approximately 12° due to the PDMS segments increases as the wt % PDMS in the samples increase. Great care must be taken when interpreting these results, as it is obvious that the amount of crystalline material would decrease as the presence of an amorphous species increases. Depending on the molecular arrangement of the non-crystallisable grafts along the PAN backbone, the degree of crystallinity of the crystallisable material may not be greatly affected. It is, therefore, necessary to calculate a degree of crystallinity weighted to the % crystallisable material in the polymer sample according to equation 4.1. The corrected degree of crystallisation values are also depicted graphically in Figure 4.6.

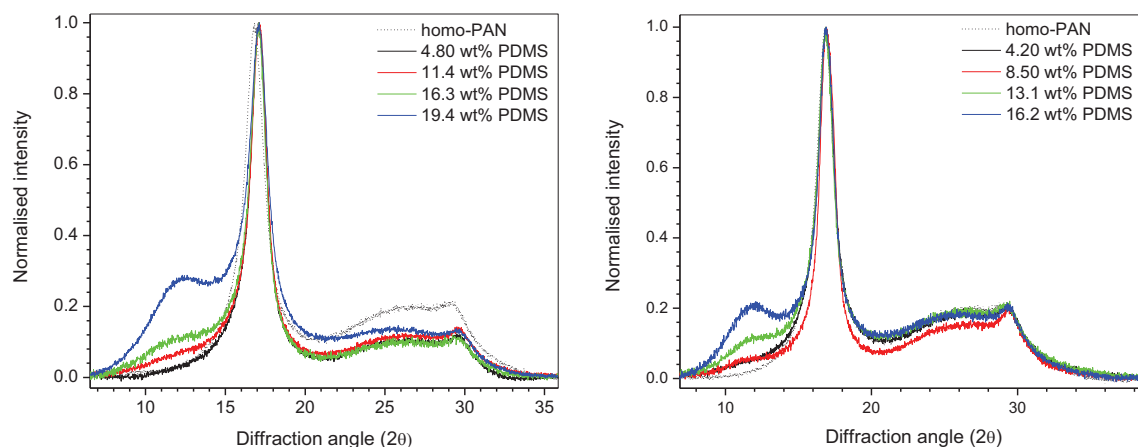


Figure 4.5 : WAXD patterns of the various (a) 1000 g.mol^{-1} and (b) 5000 g.mol^{-1} PDMS containing graft copolymer PAN-homopolymer blends.

The presence of PDMS does disrupt the crystallisability of the PAN molecules as evident in the significant lowering of the degree of crystallinity of the samples containing 4.8 to 16.3 wt% PDMS. There is, however, a large decrease in the degree of crystallisation of the PAN molecules in the 19.4 wt% PDMS (CP43) and the 16.2 wt% (CP17) content graft copolymer materials. The difference between the copolymer series prepared using the 1000 g.mol^{-1} and 5000 g.mol^{-1} PDMS macromonomers is also evident. The graft material containing the longer PDMS grafts have lower degrees of crystallinity compared to the shorter PDMS grafts.

The PAN material appears to crystallise, relatively unhindered by the presence of the PDMS components in the graft copolymer material. The slight decrease in crystallinity of the fibre precursor material blends is due to decreased crystallinity of the PAN-g-PDMS molecules present in the blend. The higher graft copolymer containing blends show a dramatically decreased degree of crystallinity which indicates that in these cases, the graft copolymer material appears to hinder the crystallisation of the PAN molecules to a significant extent. Ultimately, there is also less PAN homopolymer in the higher PDMS content blends as evident from the gradient chromatography results. The graft copolymer blends containing the longer PDMS grafts also appear to show a larger more significant decrease in crystallinity for the lower PDMS containing copolymers, as shown in Figure 4.6. This indicates that the longer PDMS grafts have a greater effect on the crystal packing of the PAN segments. The greater disruption of crystalline packing is due to the increased amount and length of the amorphous PDMS material. The impact of this decrease in crystallinity will be shown later to affect the mechanical properties of the prepared composites, but will not be discussed at this stage.

Table 4.2 : Summary of the crystalline and amorphous regions of a series of PDMS-g-PAN copolymer ($1000 \text{ g}\cdot\text{mol}^{-1}$ PDMS and $5000 \text{ g}\cdot\text{mol}^{-1}$) blends with PAN, the calculated degree of crystallinity, FWHM and the coherence length (L).

Sample	PDMS content (wt%)	Apparent $D_{\text{Crystallinity}}$	$D_{\text{crystallinity}}$ (%)	FWHM	L (nm)
Homo-PAN	0.00	57.46	57.46	1.13	70.52
CP40	4.80	53.54	56.24	1.15	68.92
CP41	11.40	47.79	53.94	1.17	67.89
CP42	16.30	42.49	50.77	1.21	65.66
CP43	19.40	20.04	24.86	1.41	56.19
CP14	4.20	44.94	46.92	1.19	66.64
CP15	8.50	38.29	41.85	1.29	61.58
CP16	13.10	36.19	41.64	1.30	61.29
CP17	16.20	19.99	23.86	1.42	56.10

The full width at half maximum (FWHM) is depicted in Figure 4.6 and can be used as a measure of the crystal sizes. The narrower the crystalline diffraction peak, the smaller the FWHM and the larger the individual crystals. The Scherrer equation can be used to determine the coherence length L, also known as the crystal size according to equation 4.2.

$$L = 0.89\lambda/B \cos \theta \quad (4.2)$$

Where L is the coherence length, λ is the x-ray wavelength (1.504 nm), B is the FWHM value and θ is the Bragg diffraction angle. The calculated values are summarised in Table 4.2. The crystal size will differ as the crystal packing and size of the PAN crystals is disrupted. This explains why there is a broadening of the (110) plane reflection at 17° . Table 4.2 clearly shows a decrease in the crystal thickness as the content of graft copolymer in the blend is increased relative to the homo-PAN control. Significant changes in crystal thickness for CP43 and CP17 in Table 4.2 relates back to the greater decrease in the $D_{\text{Crystallinity}}$ for these respective samples. This is further confirmation that the crystal structure is most perturbed by the highest PAN-g-PDMS containing copolymer blends. The graft copolymer series containing the longer PDMS grafts (5000 g.mol^{-1}) once again shows smaller crystal thicknesses as compared to the 1000 g.mol^{-1} PDMS analogues. A general decrease in crystal thicknesses remain between the other copolymers with lower PDMS content, although not as notable as for the higher content PDMS copolymer materials.

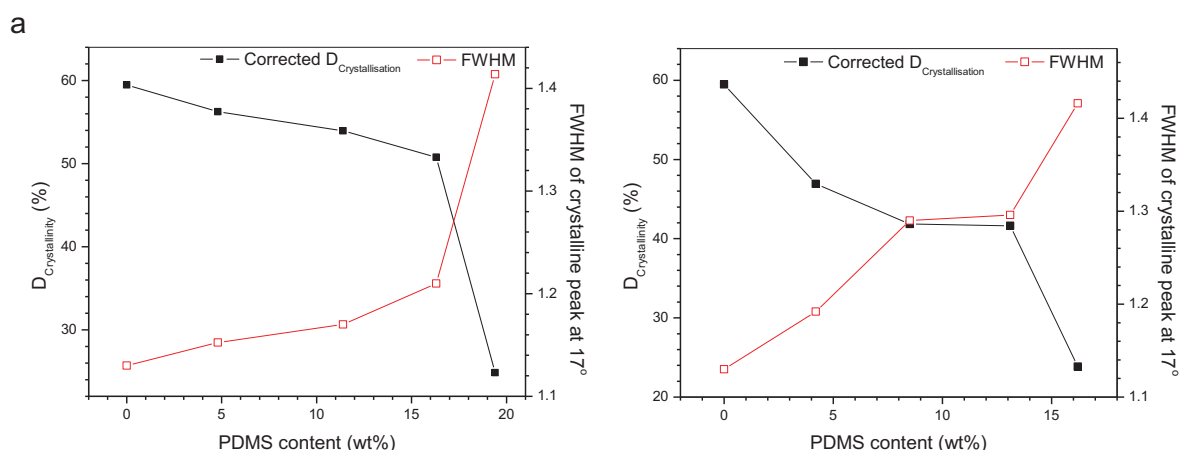


Figure 4.6 : Degree of crystallisation values as a function of PDMS content, overlaid with the FWHM of the dominant PAN crystallisation peak at 17° for (a) the 1000 g.mol^{-1} and (b) 5000 g.mol^{-1} PDMS series.

In conclusion, the WAXD results show that the presence of PDMS in these complex multiphase polymer systems does indeed affect the crystal packing of the PAN material. The degree of crystallinity does decrease as the graft copolymer content in the fibre precursor blend increases. Disruption of the crystal packing is also evident in increased FWHM values and the decreased crystal coherence length values of the PAN (110) reflection at 17° . The most significant effects are, however, observed for the fibre precursor blends containing the highest amount of PDMS graft copolymer (CP43 and CP17) as well as the copolymer blend series containing the longer PDMS grafts.

4.2 Production of the reinforcing fibre fillers via electrospinning

The previous section dealt with the synthesis of novel PAN-g-PDMS copolymer materials. This section focuses on using these polymers as the raw material for the production of electrospun fibres. A discussion in a later section will investigate how these fibres can be used as reinforcing fillers for silicone matrices. Electrospinning is generally used to prepare fibres with diameters in the nano-scale range, therefore below 100 nm in diameter. It has been argued in many papers that this upper limit of 100 nm does not always apply in terms of speaking about electrospun nanofibres. On occasion, this limit can be pushed as high as anything less than 1 μm . The fibres prepared in this work have a varied diameter distribution, as will be discussed, depending on the electrospinning conditions and copolymer composition. The variation in diameters from approximately 400 nm to as high as 3.5 μm for the electrospun fibres in this work denotes that the fibres in this work will not be referred to as “nano” but simply as electrospun fibres for the sake of consistency. Investigation of the electrospinning process variables on the various copolymers will be discussed in the following section along with the solution properties of this amphiphilic graft copolymer (in DMF) and how this affects the final fibre morphology.

4.2.1 Electrospinning procedure and resultant fibre morphological variation

There are many factors affecting the morphology of electrospun nanofibres, including¹⁷ : solution concentration (viscosity and surface tension of the solution), solution conductivity, voltage applied, tip to collector distance (TCD), feed-rate of solution, needle diameter, temperature and humidity. Variation of the different spinning parameters can be used to essentially vary the morphology of the fibres with regards to surface morphology, fibre diameter and uniformity of the fibres. In this study the solution solvent (100 % DMF), feed-rate (0.008 $\text{ml}\cdot\text{min}^{-1}$), needle diameter (gauge 26), ambient temperature ($\pm 25\text{-}30\text{ }^\circ\text{C}$) and humidity (RH $\pm 35\text{-}50\%$) (controlled using an IR lamp) were kept constant.

The electrospinning of PAN has been well documented in literature¹⁷⁻²⁰. The current study considers the electrospinning of a novel graft copolymer, namely, PAN-g-PDMS. As has been shown in the previous section, in reality the polymers are a blend of graft copolymer with PAN homopolymer as a result of the synthesis. Unlike the widely studied electrospinning of homopolymers, copolymer electrospinning has an additional parameter. The influence of the amphiphilic nature of the graft copolymers in DMF and the PDMS content on the fibre morphology, will also be considered / studied.

4.2.1.1 Effect of PDMS content on solution properties and final fibre morphology

In this study on the effects of PDMS content, all samples were electrospun at the following conditions: feed-rate ($0.008 \text{ ml}\cdot\text{min}^{-1}$), TCD (20 cm), voltage (15 kV) and concentration (15 wt%) so as to ascertain the effect of the PDMS content. The PDMS content in the graft copolymers was varied as discussed in the previous section. The PDMS incorporation can be viewed in Table 4.1. Two different molecular weights of PDMS macromonomer were also studied, namely, $1000 \text{ g}\cdot\text{mol}^{-1}$ and $5000 \text{ g}\cdot\text{mol}^{-1}$. As mentioned earlier and shown in Table 4.1, the actual PDMS incorporation closely matches the initial feed values. Increasing PDMS in the feed was shown to increase the amount of graft copolymer molecules in the PAN-g-PDMS, homo-PAN blend material. The electrospinning solvent used, as with PAN homopolymer as shown in literature, was 100 % DMF. Rheological analysis was performed using a rotational (cone-plate) viscometer. Figure 4.7 shows the plots and the increase in viscosity can be seen, as we move from 4.8 wt% PDMS ($1000 \text{ g}\cdot\text{mol}^{-1}$) to 19.4 wt% PDMS ($1000 \text{ g}\cdot\text{mol}^{-1}$) containing fibre precursor material.

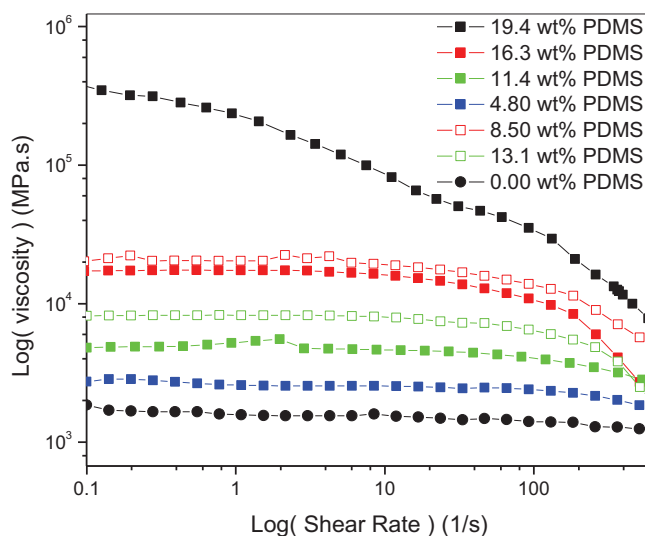


Figure 4.7 : Viscosity versus shear rate for the precursor PAN-g-PDMS / PAN copolymer blend materials in DMF (15 wt%) for the $1000 \text{ g}\cdot\text{mol}^{-1}$ (solid squares) series and two samples from the $5000 \text{ g}\cdot\text{mol}^{-1}$ PDMS series (open squares).

The concentration was kept at 15 wt% in DMF, as this was the concentration used for electrospinning of these copolymers. In all cases, shear thinning is shown to be the dominant rheological behaviour for these copolymer blends in DMF. The intonation point at which the shear thinning takes effect is shifted to higher shear rates as the PDMS content is decreased. The higher the PDMS content, the higher the viscosity values versus the shear

rate throughout the experiment. This can be ascribed to the fact that the PDMS remains insoluble in DMF while the PAN segments remain soluble. The graft material does dissolve in DMF, but behaves like an amphiphilic material in solution. The amphiphilic nature will be expanded on in a later section of this work, but it must be noted that self-assembly in solution is likely to cause these viscosity increasing effects. The viscosity behaviour is, therefore, not only attributed to solubility effects, but rather to the formation of aggregated structures in solutions. The large amount of copolymer relative to homo-PAN in the 19.4 wt% PDMS sample ($1000 \text{ g}\cdot\text{mol}^{-1}$) results in a material that is almost entirely graft copolymer as seen in the gradient chromatographic results. The increased viscosity can be attributed to larger aggregate formation in solution which relates to a larger hydrodynamic volume and increase in viscosity. Homo-PAN (0 wt% PDMS) follows a more Newtonian flow behaviour, owing to the fact that it has increased solubility and does not self-assemble due to amphiphilic character. Hence, a more “liquid-like” behaviour is observed. The 4.8 wt% PDMS solution also follows similar Newtonian flow behaviour as the PAN homopolymer as this sample contains a relatively small amount of the amphiphilic graft material. The incompatibility or insolubility of the PDMS components in the graft copolymer material, results in an increase in viscosity of the electrospinning solutions, irrespective of sample concentration. The differences in viscosity have a dramatic effect on the fibre diameters and uniformity.

Figure 4.8 shows the relationship between the mean fibre diameters and the wt% PDMS incorporated into the fibre precursor material. The two different PDMS graft lengths are also compared. It must be noted that the bars on the plot are not error bars, but standard deviations. The standard deviations are a measure of the uniformity of the mean fibre diameters and present a measure of the distribution of these diameters. There is a clear correlation between the measured fibre diameters and the PDMS content in both series. The mean fibre diameters increase steadily as the PDMS content is increased. The $1000 \text{ g}\cdot\text{mol}^{-1}$ PDMS series shows a point during which the increasing trend appears to “jump”, which is not as apparent in the $5000 \text{ g}\cdot\text{mol}^{-1}$ series. Both series do, however, follow a relatively linear trend. The change in uniformity of the fibres is evident as is seen by the increase in the standard deviation with increasing PDMS content. The $5000 \text{ g}\cdot\text{mol}^{-1}$ series also shows a higher average fibre diameter in all cases. This difference increases as the PDMS content increases. The increase in diameter and uniformity is not as large for the three lowest PDMS containing copolymer blends, however, a large increase is observed for the highest PDMS content materials. These results correspond well to the viscosity data presented earlier. Increased viscosity generally has the effect of increasing the diameter of electrospun fibres

due to greater difficulty in the stretching of the solution jet^{21,22}. This is most evident in the solutions containing the highest amount of PDMS, as was shown in Figure 4.7 where these solutions showed a dramatic increase in the solution viscosity. The increase in diameters can therefore, be ascribed to the increase in viscosity of the electrospinning solutions. This also explains why the 5000 g.mol⁻¹ series has increased diameters relative to the 1000 g.mol⁻¹ series for similar PDMS contents.

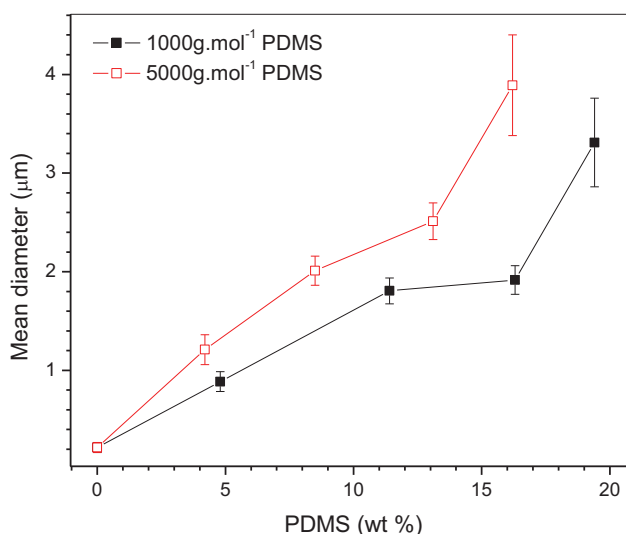


Figure 4.8 : Mean fibre diameter as a function of PDMS (wt%) content in the PAN-g-PDMS copolymer series for the 1000g.mol⁻¹ and 5000g.mol⁻¹ copolymer series.

4.2.1.2 Effect of PAN-g-PDMS Concentration

Concentration is usually a measure of the viscosity of the electrospinning solutions and is thus important in obtaining smooth fibres²³. Deitzel *et al*²⁴ found that when electrospinning PAN, 4 wt% polymer in DMF was the concentration limit at which smooth fibres were obtained mixed with beaded fibres. The surface tension of the liquid jet needs to be suppressed in order to prevent the formation of droplets which lead to beaded morphologies along the fibre axis^{17,19,21}. The main factors shown to suppress this are electrostatic repulsion forces between the charges on the jet surface as well as the viscoelastic force of the polymer solution which resists rapid change in shape. This balance of forces results in a stable Taylor cone which enables smooth fibres with little to no beading to persist^{17,25}. Generally, lower solution concentrations can lead to narrower fibre diameters as the whipping fibre jet can stretch more readily due to the lower viscosity of the solution^{17,21}. A minimum concentration is, however, reached where beaded morphologies persist due to

surface tension dominance as mentioned previously. Normal concentration ranges for PAN electrospinning range from 7 wt% to 15 wt%^{19,26,27} in 100% DMF. This is not the case for the polymers in this study, where heavy beading and electrospay appear to be the dominant morphology for the 10 wt% solutions. The differences in the surface tension between the homo-PAN and graft copolymer solutions in this study are what lead to the large differences in optimum solution concentrations. Figure 4.9 compares the graft copolymer (CP40) containing 4.8 wt% PDMS ($1000 \text{ g}\cdot\text{mol}^{-1}$) at various spinning solution concentrations.

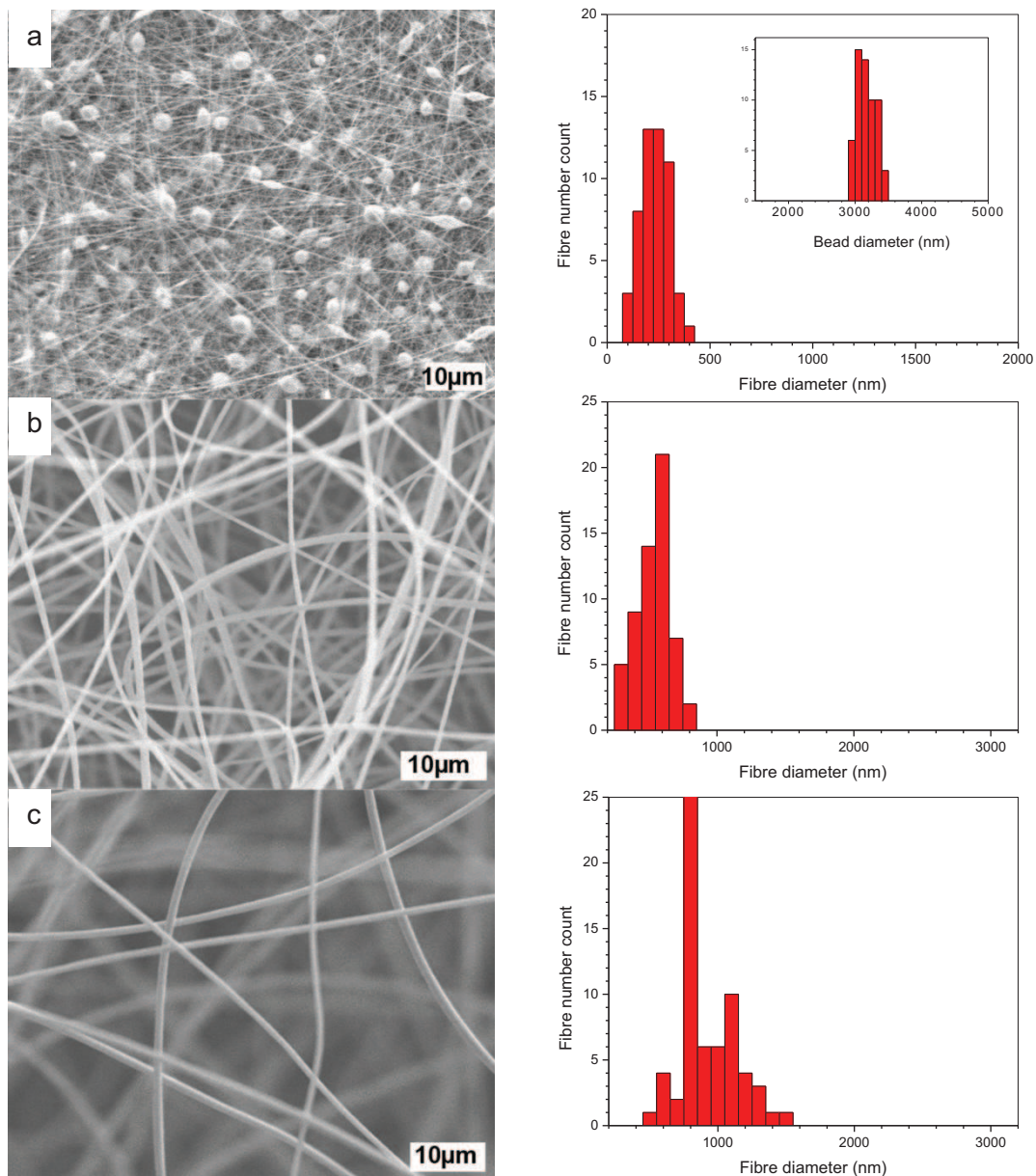


Figure 4.9 : SEM images and corresponding diameter distribution diagrams of (a) 13 wt% polymer, (b) 15 wt% polymer and (c) 18 wt% polymer ($4.8 \text{ wt}\% \text{ PDMS}$, $1000 \text{ g}\cdot\text{mol}^{-1}$) in DMF with the TCD (20 cm), feed-rate ($0.008 \text{ ml}\cdot\text{min}^{-1}$) and the voltage (15 kV) in all cases.

The 13 wt% solution presents a beaded type of morphology, while the 15 wt% solutions gave the smoothest fibres with the narrowest fibre diameter distribution. Figure 4.9 clearly shows that the 18 wt% solutions gave smooth fibres but they tended to be thicker than those obtained from the 15 wt% solutions. Concentrations above 18 wt% were too viscous to electrospin. This can be attributed to the severe insolubility of PDMS in DMF causing a dramatic increase in solution viscosity. The complex behaviour of these amphiphilic materials lead to “gel-like” character in solution. Concentrations above 18 wt% were too high to successfully electrospin the higher content PDMS grafts (19.4 wt%, CP43 and 16.2 wt% CP17) as they tended to form a highly viscous gel and the resultant solution was difficult to pump, drying at the needle tip. The effect of chain entanglements can also play a role in the case of these graft copolymers. Limited solubility could result in limited chain entanglement in solution as the graft copolymer molecules do not uncoil completely in the DMF solution. Although the viscosity of the solution appeared high, due to aggregate formation, the lack of chain entanglements leads to bead formation and at concentrations less than 10 wt%, electrospinning. This chain entanglement effect was studied in work by Shenoy *et al.*²² where they showed that insufficient chain entanglement can result in electrospinning if the solution concentrations were not high enough. Higher concentrations of these graft copolymer PAN blend materials were, therefore, needed to successfully achieve smooth fibres as compared to conventional homo-PAN. The 15 wt% solution was found to be the optimum concentration for the electrospinning of these novel graft copolymers yielding the most uniform fibres with the narrowest diameters.

4.2.1.3 Voltage and tip-to-collector distance effects

The final fibre morphology is also affected greatly by voltage and tip-to-collector (TCD) distance, although to a lesser extent than the solution concentration. The voltages investigated in the present study were varied between 7.5 kV, 10 kV, 15 kV and 20 kV. Voltages lower than 7.5 kV were unable to distort the droplet into the formation of a stable Taylor cone in most cases and therefore could not be electrospun. While studying the voltage and distance effects on the electrospun fibre morphology the solution concentration was held constant at 15 wt% due to solubility and viscosity restraints. Figure 4.10 compares the fibre diameters as a function of TCD for three different graft copolymers (11.4 wt%, 16.3 wt% and 19.4 wt%) of the 1000g.mol⁻¹ PDMS series and (4.2 wt%, 8.5 wt% and 16.2 wt%) of the 5000 g.mol⁻¹ PDMS series respectively. The TCD distance is varied from 8 cm to 20 cm at a fixed voltage of 15 kV. The figure shows there is a definite narrowing of the fibre diameter as well as a more uniform distribution of diameters (as indicated by the standard deviation bar) with increasing TCD distance. (Note that the standard deviation bar

represents the fibre uniformity or distribution around the mean average) Decreasing the TCD distance reduces the flight time of the fibres, resulting in less stretching of the fibres, evaporation of solvent and thicker fibre formation. The flight time of the fibre solution jet is very important, as the stretching and thinning of the fibres occur at this stage^{17,28,29}. The bending instability associated with the high voltage charge gradient across the tip to collector plate causes intense and rapid whipping and stretching of the solution jet. The PDMS content greatly affects the final fibre morphology as mentioned previously and this trend continues when studying these parameters. Figure 4.10 shows that although the diameters of the 11.4 and 16.3 wt% PDMS copolymer fibres differ (PDMS content effect) they still follow a similar trend, where the diameters gradually decrease as the TCD distance increases to 20 cm. This trend is expected due to the longer flight times as mentioned earlier. The 19.4 wt% PDMS copolymer also decreases in diameter up until a TCD of 16 cm, after which it appears to increase in the case of the 1000 g.mol⁻¹ PDMS series. The mean fibre diameters obtained after electrospinning of the different precursor materials results in noticeable differences between the materials. The higher the PDMS content in the graft copolymer blend, the thicker the fibre diameter.

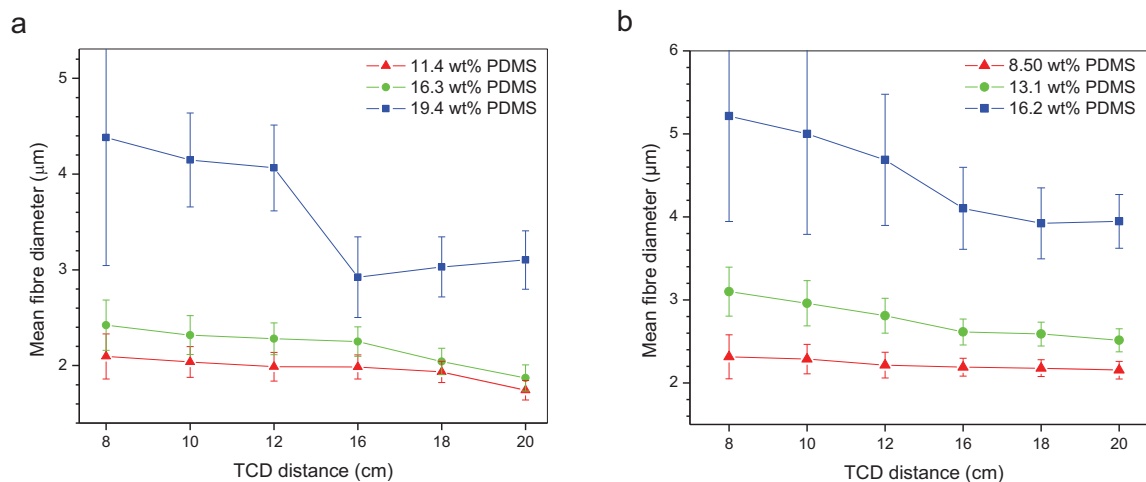


Figure 4.10 : Mean fibre diameter as a function of PDMS content (wt%) and TCD distance for (a) the 1000 g.mol⁻¹ PDMS and (b) the 5000 g.mol⁻¹ PDMS series.

A similar trend is visible in the 5000 g.mol⁻¹ series. The lower PDMS content graft copolymer blends (8.5 and 13.1 wt%) show a general decrease in the fibre diameter as the TCD distance is increased. The same trend can be seen for the highest PDMS content material at 16.2 wt% PDMS (5000 g.mol⁻¹). At distances larger than 16 cm there is, however, a levelling off and slight increase in the mean fibre diameters. The slight increase in diameter is seen in both series for the highest PDMS content copolymer blends as we move from 16 cm to 20

cm. However, a noticeable difference between the first three TCD distances and the last three exists. This suggests that the stretching of the fibres in the case of the high PDMS content copolymers is restricted as a result of the material properties in solution and not the actual TCD distance, as is the case with the lower PDMS content copolymers. The high PDMS content graft materials are mostly graft copolymer, compared to the other samples and the “gel-like” behaviour of these amphiphilic graft materials in DMF limits the stretching of the fibres after a certain TCD (16 cm). This is an effect not readily found with electrospun homopolymers or blends. The concentration was held at 15 wt% when studying these effects, and it is interesting to notice that no visible beading was obtained in the ranges investigated. The differences in diameters of the various graft copolymer blends can again be related to viscosity issues as presented in the previous sections, where increased PDMS content was shown to lead to increased average fibre diameters. It has, however, been suggested by Deitzel *et al*²⁴ that at higher voltages, bead formation is likely to occur.

Figure 4.11 (a) and (b) show a plot of varying voltage at a constant TCD of 18 cm and concentration of 15 wt% polymer in DMF for the 1000 g.mol⁻¹ and 5000 g.mol⁻¹ PDMS series respectively. A general increase in fibre diameter is apparent moving from 7.5 kV to 20 kV at a tip-to-collector distance of 18 cm.

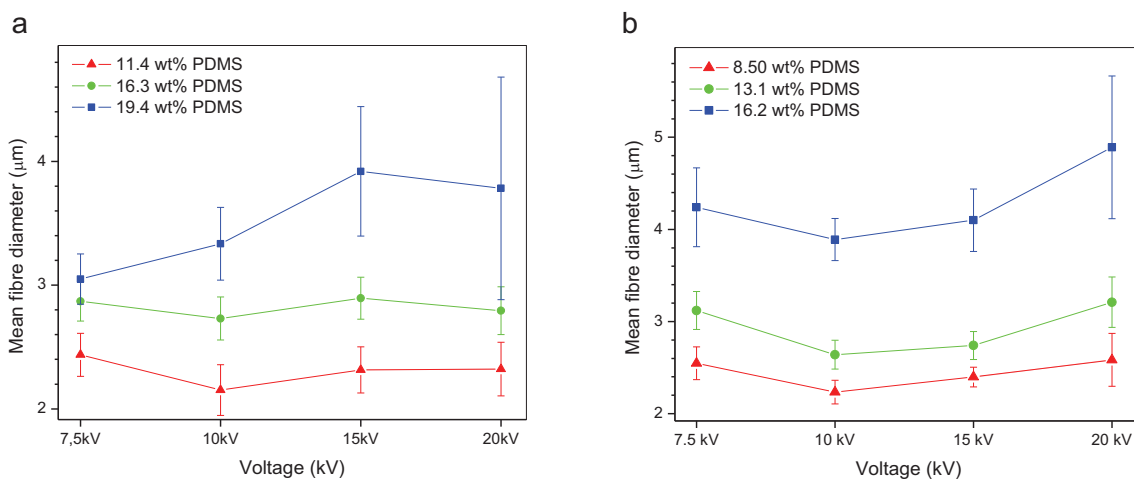


Figure 4.11 : Mean fibre diameter as a function of PDMS content (wt %) and potential voltage applied for (a) the 1000 g.mol⁻¹ and (b) the 5000 g.mol⁻¹ PDMS series.

The increased electric field strength results in greater acceleration of the fibre jet to the ground plate, giving it less time to stretch and thin. The 7.5kV voltage was too low to produce a completely stable Taylor cone. This resulted in poor fibre formation and an increased fibre diameter as the field was too weak to fully stretch the solution jet. The effects of voltage and working distance are linked in that decreasing of the tip-to-collector distance

mimics the effect of increasing the applied voltage. This phenomenon was shown in work by Li *et al*²¹ as well as Demir and co-workers³⁰. The trends are similar to those observed in Figure 4.10 where the two lower PDMS content copolymer blends show the same expected tendencies as the voltage is varied. The 19.4 wt% (1000 g.mol⁻¹ PDMS) and 16.2 wt% (5000 g.mol⁻¹ PDMS) copolymers, once again, show larger fibre diameter distributions. There is a noticeable difference between the two lower and two higher voltages as seen in Figure 4.11. This further confirms the fact that at high PDMS contents, the solution properties of the molecules in DMF dominate the achievable fibre diameters.

4.2.1.4 Amphiphilic solution effects on porous fibre filler morphology

The nature of the prepared graft copolymers and their behaviour in solution lend them interesting properties. The copolymers are electrospun from a 100 % DMF solution as mentioned earlier. The implications of this on the molecular behaviour of the disparate components of the graft copolymer in the solution are major, as PDMS is insoluble whereas PAN is soluble in the spinning solvent. The copolymers in this study are, therefore, amphiphilic in nature due to the solvent incompatibilities of the constituent moieties. In Chapter 2 it was discussed how amphiphilic copolymers have the ability to self-assemble into a variety of structures in solution. Amphiphilic block copolymers³¹ have received much attention due to the ability to control the formation of various aggregate structures, from micelles to vesicles and liposomes for emulsions and use in medicinal chemistry. Graft copolymers have not received as much attention as their aggregation and solution behaviour tends to be more complex than their block copolymer counterparts. However, it has been shown that similar structures can be achieved using this class of copolymers³²⁻³⁵. The behaviour of these graft copolymer blends are highly complex with competing effects. Electrospinning of these solutions are not simply achieved by evaporation of solvent and development of fibres. Rapid evaporation and stretching of the solution jet is only one mechanism affecting the fibre morphology. The amphiphilic nature of the graft copolymer molecules induce phase segregation and self-assembly of the material molecules in solution. The fact that PAN is a crystalline material also plays a role, as the fibres undergo rapid crystallisation during the evaporation and stretching process. All these factors play a role in thermodynamic versus kinetic morphology of the final electrospun fibres.

Figure 4.12 (a) to (d) show TEM images of the graft copolymer blend materials in dilute solution (DMF). Casting the polymer from very dilute solution and allowing the solvent to evaporate was done in an attempt to mimic the effect of the electrospinning process, although the evaporation process is considerably slower. The TEM images are by no means

assumed to represent the actual self-assembled structure of the molecules in solution, but used to gain insight into possible amphiphilic phase separation of the material in solution. Cryo-TEM would be needed to examine the actual structure in solution. A complex network structure of interconnected cylinders is evident in the TEM images. The PDMS content in the graft copolymer material is increased moving from Figure 4.12 (a) to (d), and a noticeable increase in the diameter of the interconnected cylinders / rod-like particles is visible. Unfortunately the phase separation between the PAN and PDMS domains are not readily visible in the TEM images, possibly due to similarities in the electron densities of the disparate components. Attempts were made to capture images showing the phase segregation of the immiscible PAN and PDMS moieties, but proved to be unsuccessful.

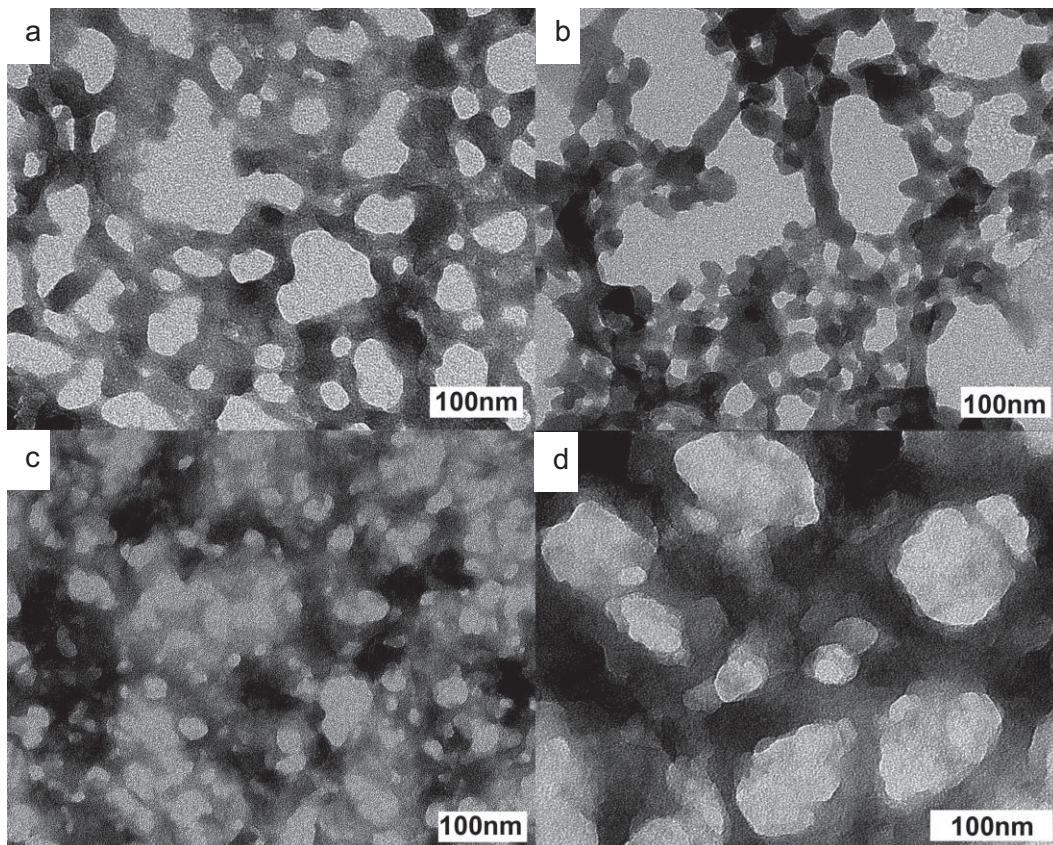


Figure 4.12 : Typical TEM images obtained from identical dilute concentration solutions in DMF of various PAN-g-PDMS fibre precursor materials (a) 4.8 wt% PDMS ($1000 \text{ g}\cdot\text{mol}^{-1}$), (b) 11.4 wt% PDMS ($1000 \text{ g}\cdot\text{mol}^{-1}$), (c) 16.3 wt% PDMS ($1000 \text{ g}\cdot\text{mol}^{-1}$) and (d) 19.4 wt% PDMS ($1000 \text{ g}\cdot\text{mol}^{-1}$).

Kikuchi and Nose^{36,37} have studied and modelled the behaviour of sparsely grafted (short grafts) amphiphilic copolymers where the backbone is in solution and the grafts not, and vice versa. The materials under study in this work are similar to the polymer system studied by

Kikutchi and Nose, where the current polymers have short sparsely grafted PDMS units that are not soluble in the solution medium while the backbone (PAN) is soluble. The graft copolymers in this study are expected to form structures where the PDMS segments group together as a solvent immiscible core, and the PAN acts as the solvent miscible outer shell.

The images in Figure 4.12 do not appear to indicate the formation of defined particles or micelles, but instead a complicated network structure possibly due to the absence of long range order. Similar results have been seen in work by Wang *et.al.*³⁸ where they looked at graft copolymers of chitooligosaccharides as backbones and polycaprolactones as branches. They found that by varying the branch lengths and the solvent composition they were able to create spherical micelles, petal-like spheres, vesicles and then the same network of cylinders that we observed in our graft copolymers (Figure 4.12). The long PAN segments in the case of our graft copolymers achieve similar results where the cylinders in solution tend to fuse together causing a network via aggregation. Work by Zhang *et. al.*³⁹ once again showed the same network of cylinders in their copolymers of a polyphosphazene backbone with tryptophan ethyl ester (EtTrp) as hydrophobic groups and oligomer poly(N-isopropylacrylamide) (PNIPAm) as hydrophilic segments using various solvents. They showed that by varying the copolymer composition and solvent conditions, various morphologies could be achieved. The polymer material under study in this work differs from those in literature as it is a blend of graft copolymer and homo-PAN, with the exception of the highest PDMS content materials which consists mainly out of graft material. The presence of the homo-PAN disrupts the formation of possible micelles or rod-like particles that one could expect from such amphiphilic graft copolymers. If we were to relate the TEM images obtained in Figure 4.12 to possible solution properties we would expect the formation of a lightly cross-linked gel due to the aggregation of the amphiphilic molecules in solution.

Figure 4.13 illustrates a typical result of oscillating rheological analysis. This technique was chosen as it can supply more information on the properties of the molecules in solution including possible gel formation due to the self-assembling of molecules in solution. The technique yields information on the viscoelastic behaviour of the polymer solutions by studying the storage (G') and loss (G'') moduli. Additional analysis can be found in the appendix. The solution presents itself as a viscoelastic solid, as the storage modulus exceeds the loss modulus. The shape of the curve is also reminiscent of a lightly cross-linked gel in solution. The gel-like behaviour ties in well with the TEM images obtained in Figure 4.12, where we appear to have possible formation of a “gel-like” network via self-assembly.

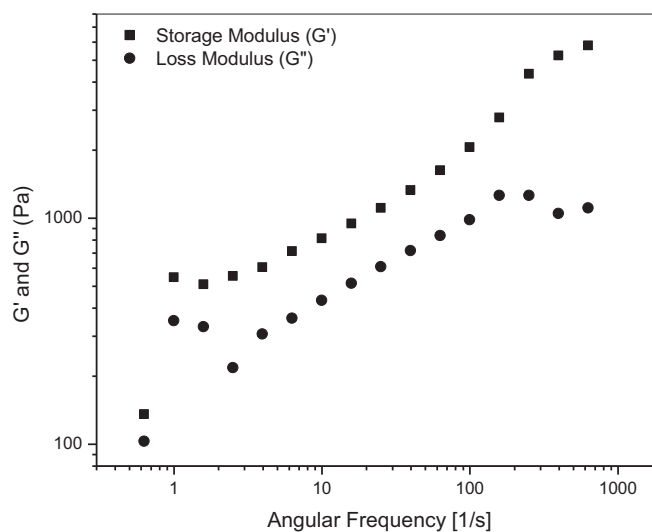


Figure 4.13 : Oscillating rheological analysis of the 19.3 wt% PDMS (1000 g.mol^{-1}) fibre precursor material, presenting the typical storage (G') and loss moduli (G'') obtained as a function of angular frequency (ω).

It is clear from these analyses that the behaviour of these amphiphilic copolymers in solution is highly complex. Obtaining a full understanding of the nature of these solutions would require the variation of additional properties such as the solution concentrations as well as temperature, as these all affect the aggregation of amphiphiles in solution. For example, the gel point (crossing of G' and G'') of each graft copolymer type in DMF could be found by varying the concentration of each copolymer solution. This was outside the scope of this work, but presents itself as an extremely interesting avenue to pursue in future investigations. The focus of this work was to have a basic understanding of the solutions used for electrospinning, hence fixed concentrations and temperatures (room temperature). In summary, the amphiphilic nature of the graft materials prepared in this work present complex solution behaviours, evident from the above results. The phase segregation and self-assembly behaviour of the materials in DMF will have a significant effect on the fibre morphology.

Figure 4.14 shows the FE-SEM images of the fibres electrospun from the amphiphilic solutions discussed previously. The insets correspond to the TEM images of the respective fibre precursor material are dried from dilute solution (DMF) set on the same length scale. A striking resemblance exists between the observed surface fibre morphology and the TEM images. The complicated network assembly of the graft copolymer “cylinders” in solution as

discussed previously presents itself dramatically in the actual structure of the electrospun nanofibres as can be seen in Figure 4.14.

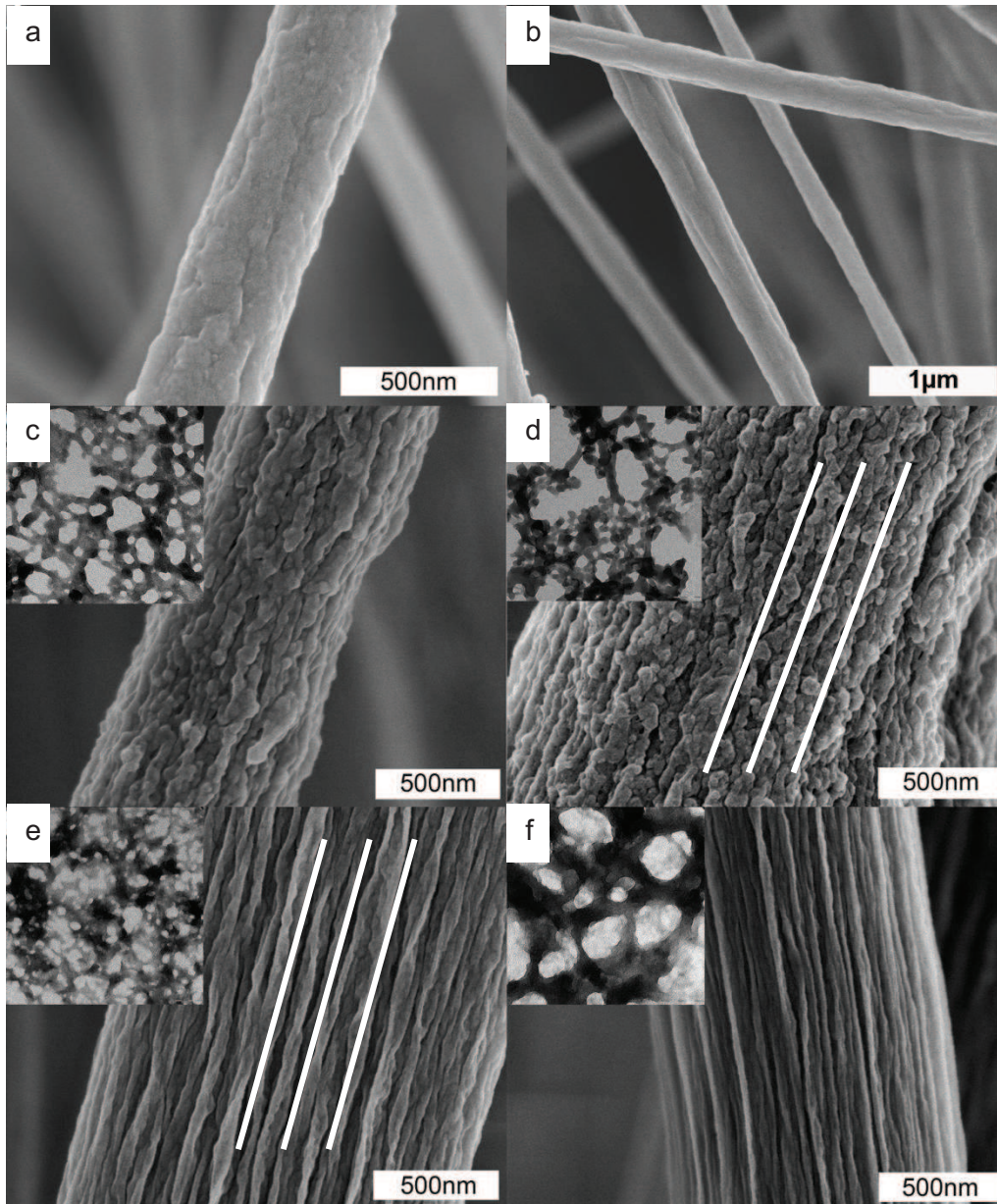


Figure 4.14 : FE-SEM images of (a) homo-PAN, (b) homo-PAN, (c) 4.8 wt% PDMS (1000 g.mol^{-1}), (d) 11.4 wt% PDMS (1000 g.mol^{-1}), (e) 16.3 wt% PDMS (1000 g.mol^{-1}) and (f) 19.4 wt% PDMS (1000 g.mol^{-1}), corresponding TEM images obtained from evaporation from dilute solution (100% DMF) as insets set on the same scale.

The fibres have distinctly rough and porous type morphology, due to the fact that they seem to be “assembled” from an aggregated network of fused cylinders. Direct comparison of the TEM insets with the fibre morphology is not strictly correct as during electrospinning the

concentration is higher and the evaporation does occur more rapidly. The basic principle is the same and one can clearly see the direct relationship between the TEM insets and the respective FE-SEM fibre images. This is particularly the case for the 4.8 and 11.4 wt% PDMS copolymer materials. Figure 4.14 (a) shows that the electrospun homo-PAN has a much smoother surface, with no evidence of the aggregated cylindrical network structure as observed in the graft copolymers. Comparing the images of the copolymer fibres we do see a difference moving from the 4.8 wt% PDMS copolymer to the 19.4 wt% PDMS copolymer. The rough surface morphology of the 4.8 wt% and 11.4 wt% graft copolymers (Figure 4.14 (c) and (d)) change to a more regular “fibrillar-like” patterning on the surface of the 16.3 wt% and 19.4 wt% PDMS copolymer (Figure 4.14 (e) and (f)) fibres. The TEM inserts also show a distinct difference between these two sets of copolymers. It is clear that the diameters of the aggregated cylinders become much larger for the higher PDMS content copolymers. A similar change in aggregate structure was also observed in work by Zhang *et. al.*³⁹, but in their case the polymer was cast from different solutions, thus changing the self-assembly and molecular morphology. The polymer solutions in this study are not cast from different solutions, however, the graft copolymer material does vary with PDMS content. The increasing graft copolymer content provides changes in the morphology similar to the effect of changing the solvent or temperature, as these all affect the molecular behaviour in solution. The finer aggregate structural detail is lost due to the increase in diameter of the cylinders, and after the electrospinning procedure this results in a seemingly more uniform surface structure. Comparing the lower content PDMS graft copolymers shows that there is some form of “fibrillar-like” arrangement of ridges on the surfaces of these fibres as indicated by the white bars in Figure 4.14 (d) and (e). This arrangement is, however, masked by the presence of the finer surface detail, which as mentioned earlier is lacking in the higher PDMS content copolymers. The fibrillar arrangement is due to the electrospinning procedure as we have stretching of the polymer jet during electrospinning. As is the case with the alignment of fibre mats due to mechanical drawing of non-woven fibres, it is possible that the random network of aggregates is oriented during the powerful stretching of the polymer jet. Not much work has been performed on the electrospinning of amphiphilic graft copolymers, or in fact, the multiple morphological behaviour of graft copolymers in solution. This work shows that by electrospinning amphiphilic graft copolymers with different arrangements of aggregate structure in solution, we can manipulate the final fibre morphology, from smooth exteriors (homo-PAN) to rough, random or even patterned surfaces. The 5000 g.mol⁻¹ PDMS series show very similar trends regarding the fibre surface roughness as shown in Figure 4.15. The two samples are the (a) and (b) 8.5 wt% PDMS-g-PAN copolymer and the (b) and (c) 13.1 wt% PDMS-g-PAN copolymer fibres. These fibres were also used to prepare the

silicone composites discussed in chapter 5. The fine detailed structure on the surface is again lost moving to the higher PDMS content copolymer fibres, where a “fibrillar-like” structure persists across the fibre surface.

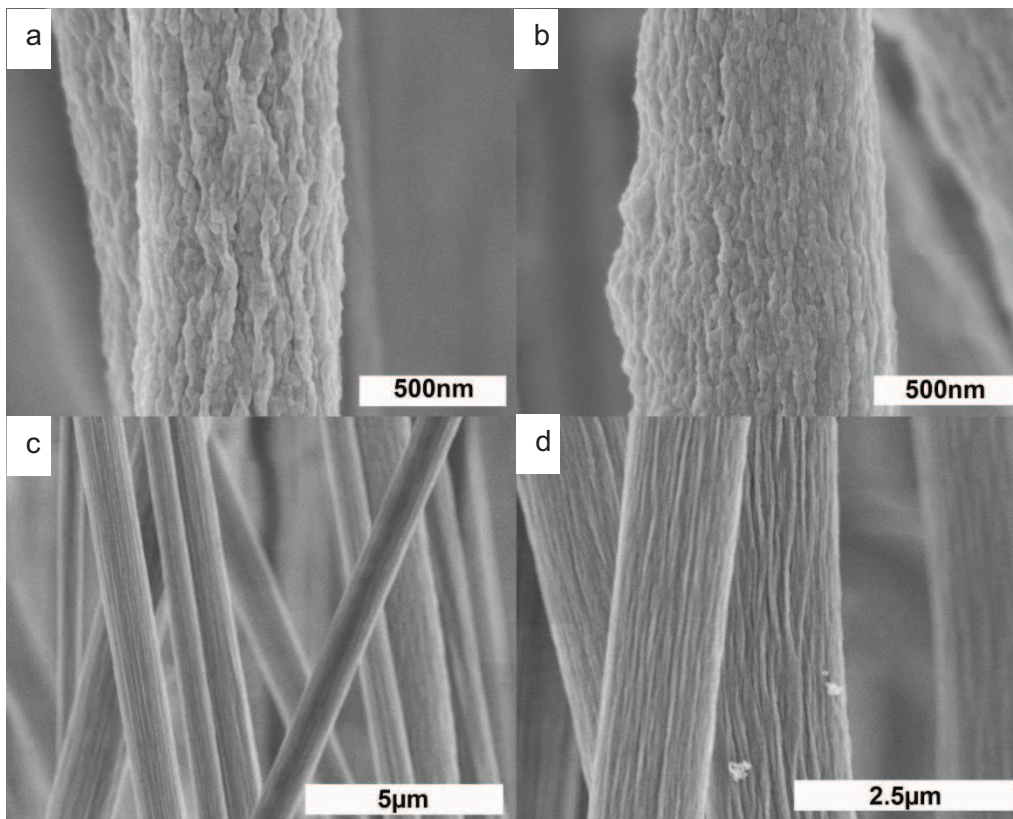


Figure 4.15 : FE-SEM images of (a) 8.5 wt% PDMS (5000 g.mol^{-1}), (b) 8.5 wt% PDMS (5000 g.mol^{-1}), (c) 13.1 wt% PDMS (5000 g.mol^{-1}) and (d) 13.1 wt% PDMS (5000 g.mol^{-1}), corresponding TEM images obtained from evaporation from dilute solution (100% DMF) as insets.

Figure 4.16 shows the cross-section of the electrospun fibre precursor material containing 11.4 wt% PDMS (1000 g.mol^{-1}). The previous discussion focused on the rough and porous surface character of the electrospun fibres, but it is clear in the cross-sectional views of the fibres that the porous nature persists throughout the bulk of the electrospun fibres. This exciting result presents an alternative route to the production of electrospun fibres that are fully porous. The electrospinning of the self-assembled molecules in solution result in a fibre that is constructed of a network-like structure of the precursor material as discussed previously. Pore formation on the surface of electrospun nanofibres is a fairly common occurrence that has been shown to occur due to humid environments. Casper *et. al.*⁴⁰ studied polystyrene electrospun from THF at different humidities. They found that smooth fibre surfaces persisted at humidities lower than 25%, while above 30% pore formation occurred. Megelski and colleagues⁴¹ studied four different polymer types, which they

electrospun from a variety of solvents with different vapour pressures. The use of less volatile solvents such as dimethyl formamide (DMF) resulted in a decrease in pore formation. They also found that the humidity played an important role in the formation of pores on the surface. Rapid evaporation of the solvent and the accompanying cooling effect as the fibre travels from the spinneret to the collector allowed for moisture in the atmosphere to condense on the fibre surface creating breathe figures (imprints on the fibre surface after evaporation of condensed water droplets). As the fibres dry and solidify the water droplets leave behind physical imprints on the surface of the fibres⁴².

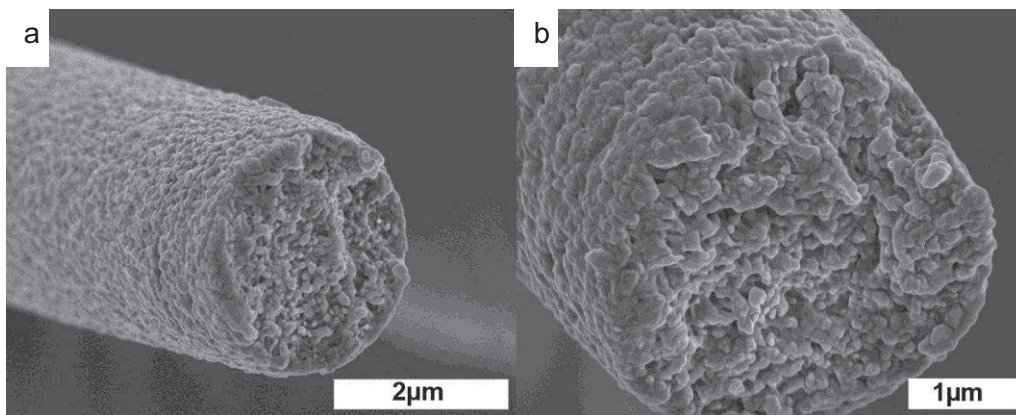


Figure 4.16 : Cross-sectional views of an 11.4 wt% PDMS (1000g.mol^{-1}) containing electrospun fibre.

Porosity in these cases are limited to the surface of the fibres only. Fully porous fibres are more difficult to produce and can be achieved by the electrospinning of two different polymer types followed by removal of one of the phases. Wendorff *et. al.*⁴³ studied blends of polylactic acid (PLA) with PVP, where they selectively removed one of the components after fibre production. The polymer materials in this study allow the direct formation of fully porous electrospun fibres, without the need for controlling the ambient atmosphere, or selective removal of a component. The phase separation behaviour of the materials in DMF present a unique and novel way to produce fully porous fibres.

The discussion above, shows that the effect of phase segregation together with the rapid solvent evaporation and stretching of the solution jets has a dramatic effect on the non-equilibrium morphology of the final electrospun fibres. The drive for crystallisation of the PAN segments also serves to affect the final fibre morphology. WAXD patterns of the electrospun fibres are shown below in Figure 4.17. Distinct differences to the patterns obtained from the unprocessed precursor material (Figure 4.5) are evident.

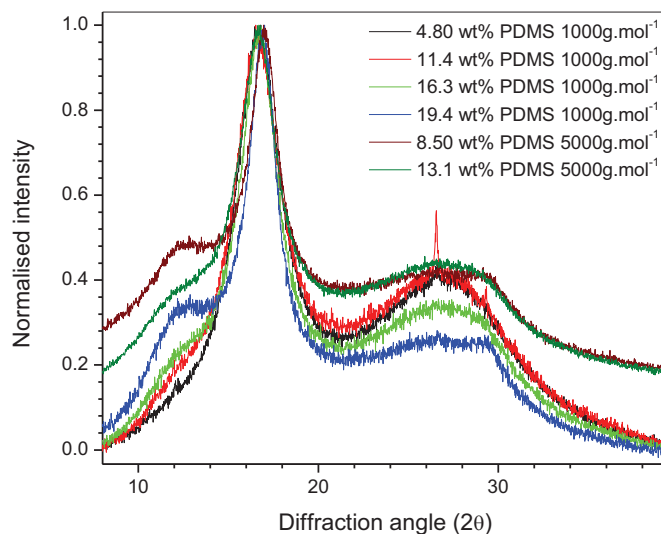


Figure 4.17 : WAXD diffraction patterns of the electrospun fibres of PAN-g-PDMS/PAN copolymer blends for the 1000 g.mol⁻¹ series and two 5000 g.mol⁻¹ samples used for filler production.

The first detail one notices is the disappearance of the weak crystalline peak at 29.5°. Mingawa *et. al.*¹¹ found that the smaller crystal peak at 29.5° disappeared with decreasing stereo-regularity, hence assigning it to the diffraction of isotactic PAN crystal packing. The PAN crystalline reflection peak at 17° shows a definite broadening as the PDMS content is increased. The broadening of the main PAN crystalline peak shows a decrease in the crystallite coherence length as calculated using the Scherrer equation (4.2) and shown in Table 4.3. The degree of crystallisation is also presented in Table 4.3 and calculated according to equation 4.1. The crystallinity and crystal thickness is shown to decrease as the PDMS content in the fibre precursor material is increased. The largest deviations are evident for the fibres containing the highest percentage PDMS content.

Table 4.3 : Summary of the crystalline and amorphous regions of a series of electrospun fibres of PDMS-g-PAN copolymer (1000 g.mol⁻¹ PDMS) blends with PAN, the calculated degree of crystallinity and the coherence length (L).

Sample	PDMS content (wt%)	Apparent $D_{\text{Crystallinity}}$	$D_{\text{crystallinity}}$ (%)	FWHM	L (nm)
Homo-PAN	0.00	51.04	51.04	1.45	54.89
CP40	4.80	37.24	39.20	2.24	35.53
CP41	11.40	29.98	33.31	2.57	30.92
CP42	16.30	29.40	34.59	2.68	29.66
CP43	19.40	20.44	27.25	2.96	26.84

These results are in line with the WAXD patterns of the raw precursor material, where the amorphous PDMS grafts disrupt the crystal packing of the PAN molecules. Figure 4.18 shows a direct comparison of a typical WAXD pattern overlay of the fibre precursor material and its corresponding electrospun fibre.

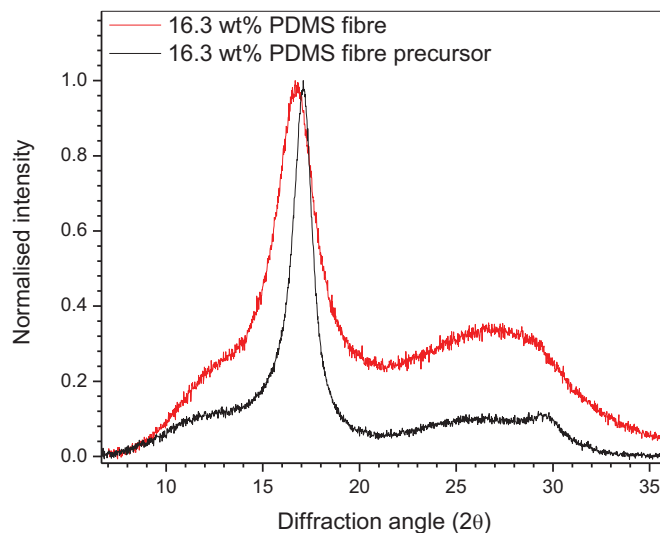


Figure 4.18 : WAXD overlays of the 16.3 wt% PDMS ($1000 \text{ g}\cdot\text{mol}^{-1}$) in fibre form and fibre precursor powder form (normalized to the 17° peak).

A clear broadening of the crystalline reflection (17°) is evident after the material has been electrospun. The small crystalline reflection at 29.5° related to the isotactic PAN crystal regions also disappears. Mingawa¹², has shown that when casting from solvents such as DMF and dimethylsulfoxide (DMSO), there is a change in the packing of the crystalline regions¹². Figure 4.19 shows plots comparing the degree of crystallinity (a) and FWHM values (b) of the fibres and the fibre precursor material before processing. There is a clear difference in the degree of crystallinity in all cases. The electrospun homo-PAN differs significantly from the unprocessed precursor material, but the difference increases as the PDMS content increases. Interestingly, the two highest PDMS content fibres show smaller crystallinity differences to the unprocessed material. The FWHM values in Figure 4.19 (b) show a large difference throughout, with the broadness increasing as the PDMS content increases. The crystal sizes according to the coherence lengths are greatly reduced in the processed fibres as compared to the precursor material. During the electrospinning procedure, there is a rapid evaporation process occurring along with phase segregation of the disparate graft components and crystallisation of the PAN molecules. Work by Zhang *et al.*¹⁹ has shown similar results where the electrospinning process results in the formation of

smaller crystal thicknesses for PAN homopolymer. Ge and colleagues⁴⁴ also showed that the orientation of the crystals tend to align in the direction of the electrospinning jet.

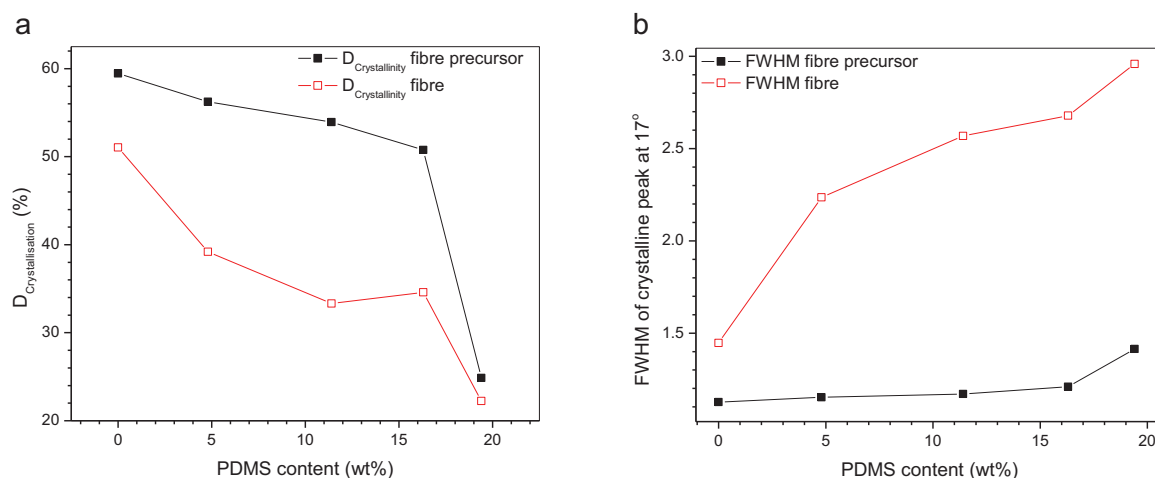


Figure 4.19 : Comparison of (a) the degree of crystallinity and (b) the FWHM values of the electrospun fibres and the fibre precursor materials (1000 g.mol⁻¹ PDMS series).

The PDMS content has an obvious effect on the crystallinity of the electrospun fibres as is the case with the fibre precursor material due to the material phase segregation. The additional effect of the electrospinning procedure (rapid evaporation and stretching) is shown to have a dramatic effect on the crystallisation of the PAN components. In conclusion, the electrospinning of the polymer materials synthesised and studied in this work are highly complex. The various effects contributed by the phase segregation of the material in DMF, the crystallisation behaviour of the material and the rapid evaporation and stretching of the polymer solution jet all combine to produce fibres with highly non-equilibrium morphology. Unique, highly porous fibres are obtained with “fibrillar-like” arrangements of ultra-fine surface structure. The rapid crystallisation of the PAN segments during the electrospinning process “freezes in” the unique porous structure. The crystallinity behaviour of the fibres are also markedly different from that of the precursor material, as the crystallisation of the PAN segments occurs in a highly stressed environment, where the material is being stretched and oriented during the evaporation of the solvent.

4.2.1.5 Effect of MWCNTs on the electrospun amphiphilic solutions.

MWCNTs are widely used as reinforcing fillers in the nanocomposite field. MWCNTs lend composite materials improved physical and functional properties, as long as they are well dispersed throughout the composite⁴⁵. In this study the inclusion of these nano-fillers into the electrospun fibres was done so as to indirectly incorporate nanotubes into the silicone matrix. This section studies the effect that the MWCNTs have on the electrospinning

solutions as well as the final fibre filler materials. The behaviour of these materials in amphiphilic copolymer blends will also be discussed. Various PAN-g-PDMS copolymer blends were electrospun with varying amounts of MWCNTs. MWCNT incorporation was varied according to the weight percentage graft copolymer (2 wt%; 4 wt%; 8 wt%; 16 wt% and 32 wt%). The choice of MWCNT filler amounts will be discussed in Chapter 5. Agglomeration of these nano-fillers can lead to poorer material performance. Surface modification of MWCNTs is a widely used technique in improving the dispersion of these nano-fillers^{26,45,44} and is the strategy that was utilised in this project. The aim was to oxidise the MWCNTs so as to incorporate carboxylic acid (-COOH) groups along the surface of the nano-tubes. The procedure used is discussed in the experimental section of this paper. The (-COOH) functional groups interact with the DMF solvent molecules⁴⁴. This interaction aids in the dispersion of the nano-tubes after ultra-sonication without the need for various surfactants to stop nano-tube agglomeration. The appropriate concentrations of functionalised MWCNTs were therefore well dispersed in DMF before addition to the graft copolymer. Addition of the MWCNT solutions to the copolymer material resulted in the interaction between the solvent molecules and the (-COOH) groups being replaced by an interaction between the (-COOH) groups and the nitrile groups on the PAN backbone. Ge and co-workers⁴⁴ used UV/vis spectroscopy and suggested that this interaction with the PAN is due to the formation of a charge transfer complex between the surface oxidised MWCNTs and the PAN molecules through delocalisation of the π -electrons along the conjugated sequence. The interaction allows for good dispersion of the MWCNTs in the electrospinning solution, as well as an interaction between the polymer chains and filler particles. This interaction had a dramatic effect on the electrospinning of these solutions. The following section focuses on the effects that the nanotube addition had on the electrospinning of the fibres as an additional parameter along with the solution viscosity, TCD and voltage effects.

4.2.1.5.1 Electrospinning of the MWCNT filled PAN-g-PDMS solutions:

Different parameters affecting the electrospinning of the PAN-g-PDMS copolymers were varied (concentration, voltage, TCD distance) and discussed in the previous section. The same parameters were varied with the MWCNT containing analogues, producing similar trends in morphological properties. The concentration of these solutions and its effect on the fibre morphology was, however, markedly different and this section will focus on this parameter. The optimum concentration for the electrospinning of these copolymers is 15 wt%. Upon the addition of the MWCNTs, these 15 wt% solutions became unspinnable due to a dramatic increase in viscosity. Five MWCNT concentrations were studied: 2 wt%, 4 wt%, 8 wt%, 16 wt% and 32 wt% relative to the mass copolymer in the solution. Even for the

solutions containing 2 wt% MWCNTs, the solutions formed a viscous gel-like material. Gelation can be attributed to the interaction between the functionalised MWCNTs and the nitrile groups of the PAN-g-PDMS copolymer. The MWCNTs seem to behave as physical cross-linking points between the graft copolymer molecules, thus producing a gel-like material. Lowering the concentration of the polymer solutions enabled the development of readily spinnable solutions. Figure 4.20 plots the mean fibre diameter as a function of different MWCNT content at their respective optimum solution concentrations.

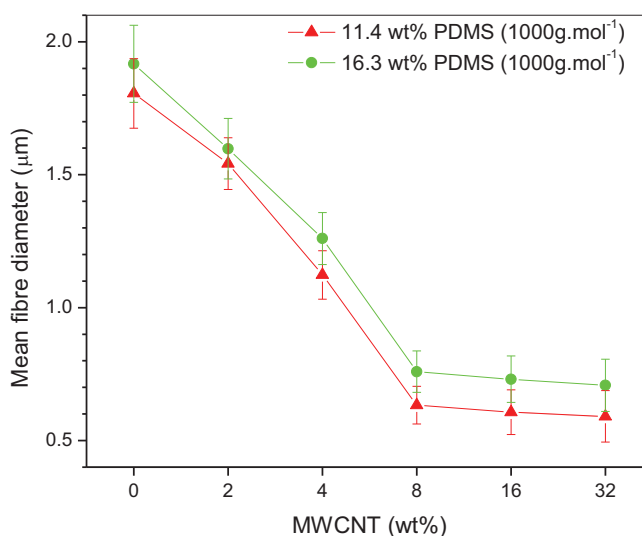


Figure 4.20 : Mean fibre diameter as a function of MWCNT content (wt%) for two different PDMS content copolymer blends (11.4 and 16.3 wt% PDMS, 1000 g.mol⁻¹), spun at optimum concentrations: 13.5 wt% PAN-g-PDMS (2 wt% MWCNT), 12 wt% PAN-g-PDMS (4 wt% MWCNT), 10 wt% PAN-g-PDMS (8 wt% MWCNT) and 8,5 wt% PAN-g-PDMS (16 and 32 wt% MWCNT) in DMF.

Optimum electrospinning concentrations for the five different MWCNT containing solutions were as follows: 13.5 wt% PAN-g-PDMS (2 wt% MWCNT), 12 wt% PAN-g-PDMS (4 wt% MWCNT), 10 wt% PAN-g-PDMS (8 wt% MWCNT) and 8,5 wt% PAN-g-PDMS (16 and 32 wt% MWCNT). The higher the MWCNT concentration, the more dilute the polymer solution must be in order to produce a solution that can be electrospun. The mean fibre diameters are shown to decrease as the MWCNT content is increased. It must be noted that the concentration of polymer in the electrospun solutions also decreased resulting in an overall drop in the viscosity of the electrospun solutions. The viscosity or concentration could not be held constant as there were limited ranges over which the MWCNT containing solutions were electrospinnable. The steady decrease in the diameter from 0 to 8 wt% MWCNT incorporation, levels off, at contents above 8 wt% nanotubes. The concentrations for these samples were relatively similar which could lead to this result. The nature of this graft

copolymer and the lack of solubility in DMF of the PDMS segments lead to the need for relatively high concentrations of the polymer material in DMF to produce solutions that can be electrospun. Sufficient chain entanglements are needed to produce smooth fibres as discussed previously. The cross-linking effect of the MWCNTs allows the polymer to be electrospun at lower concentrations (viscosities) where the lack of chain entanglements of the unfilled solutions resulted in electrospaying. The concentrations used for the electrospinning of the MWCNT containing solutions produced an electrospay in the unfilled solutions. The lower viscosities of these MWCNT filled solutions enable the fibre jet to stretch more readily producing fibres with narrower diameters¹⁷. It must be noted that the presence of the electrically conductive MWCNTs also increased the conductivity of the spinning solutions. This can in turn lead to an increase in the charges carried by the electrospinning jet and thus an increase in fibre stretching. Increased solution conductivity helps eliminate beading as well as facilitating generation of fibres with narrower diameters⁴⁶. Figure 4.20, as mentioned before does show that the increased MWCNT content did result in narrower fibre distributions. The increased conductivity with increased MWCNT content leads to the slightly narrower fibre diameters of the 16 and 32 wt% MWCNT containing fibres, as the concentrations are relatively similar.

The PDMS content was varied in the same way as mentioned earlier for the unfilled fibres. Figure 4.21 (a) and (b) shows a plot of this behaviour. All samples were electrospun at the following conditions: feed-rate (0.008 ml/min), TCD (20 cm), voltage (15 kV), concentration (10 wt%) and MWCNT content (8 wt% to polymer in solution).

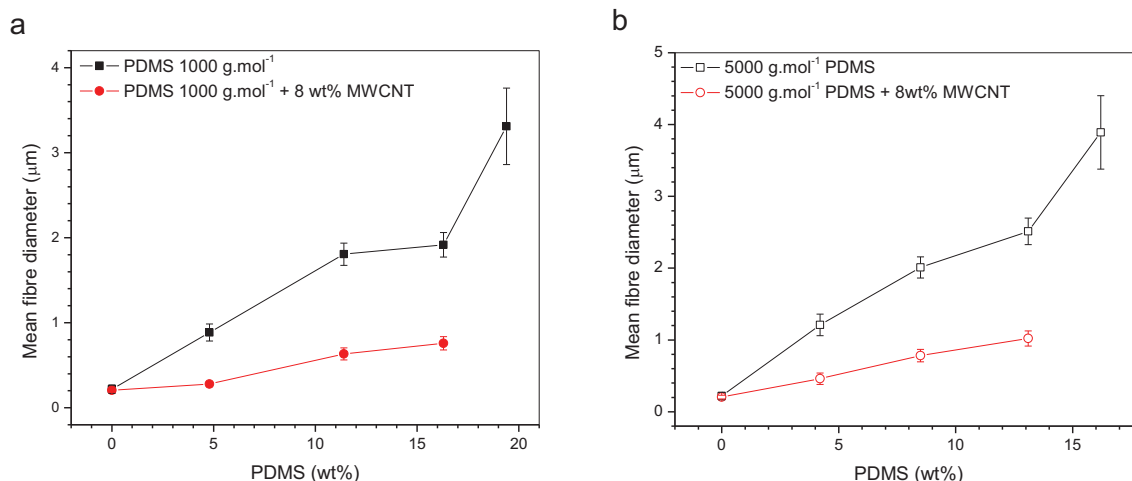


Figure 4.21 : Mean fibre diameter as a function of PDMS content (wt%) in the copolymer blends containing 8 wt% MWCNTs for (a) the 1000 g.mol⁻¹ and (b) 5000 g.mol⁻¹ series.

Figure 4.21 only highlights the 8 wt% MWCNT containing fibres, as this concentration was chosen as the base for the MWCNT filled fibre composites. The plots show the difference in average fibre diameter between the filled and unfilled fibres, where the nanotubes filled fibres are in the order of 2.5 times narrower. The uniformity of the fibres containing MWCNTs are also narrower as indicated by the standard deviation bars associated with the plot points. The clear increase in fibre diameter as the PDMS content is increased is evident. All spinning parameters were held constant except for the concentration which was kept at 10 wt% polymer in DMF for the filled fibres and 15 wt% for the unfilled analogues. The effect of the amphiphilic aggregation causes the same increase in fibre diameter as was discussed previously for the MWCNT unfilled analogues. The highest PDMS content materials (19.4 and 16.2 wt% PDMS, 1000 g.mol⁻¹ and 5000 g.mol⁻¹ respectively) were too “gel-like” and viscous to electrospin with the addition of 8 wt% MWCNTs. The aggregation due to the amphiphilic nature of the high PDMS content copolymers, along with the cross-linking effect of the nanotubes lead to highly “gel-like” solutions that could not be successfully electrospun. The marked decrease in average fibre diameters of the MWCNT containing fibres is due to the lower concentration needed to electrospin the nanotube filled solutions. The increased conductivity of these solutions also leads to increased stretching and the development of fibres with increased uniformity. The effect of MWCNTs is clear from these results, showing that they allow the production of fibres with narrower diameters and increased uniformity.

4.2.1.5.2 Porous morphology of the MWCNT filled PAN-g-PDMS solutions

The development of porous morphology as found in the unfilled fibres was investigated in the nanotube filled analogues. The behaviour of these solutions during electrospinning undergo the same effects of segregation and segmental crystallisation during the rapid solvent evaporation and stretching of the fibre jets. The previous discussion on these parameters promoting non-equilibrium morphology will not be repeated in this section. The effect and behaviour of the MWCNTs will, however, be highlighted here. Figure 4.22 (a) to (d) shows the TEM images from dilute solution of the PAN-g-PDMS copolymer blend containing 8 wt% MWCNTs. The same complex network of cylinders is apparent as with the unfilled material blends. MWCNTs are clearly visible throughout the network structure. The nanotubes are situated along the cylinder-like material paths. There is no apparent agglomeration of the nanotubes either, highlighting the efficient interaction between the nanotubes and the polymer matrix. The functional nanotubes interact with the PAN molecules which indicate that the cylinder-like interconnecting material appears to be rich in PAN material. To our knowledge, images like this showing the clear dispersion of nanotubes in a amphiphilic phase segregated system have not been published to date. The polymer

appears to be “wrapped” around the MWCNTs. The usual coiling up of the nanotubes also appears limited, indicating that the nanotubes are situated in the polymer material network structure, and are not forcing the network structure themselves. The electrospinning of these solutions used much higher solids content than was used to obtain the TEM images above, however, similar porous network like structure was obtained in the fibres.

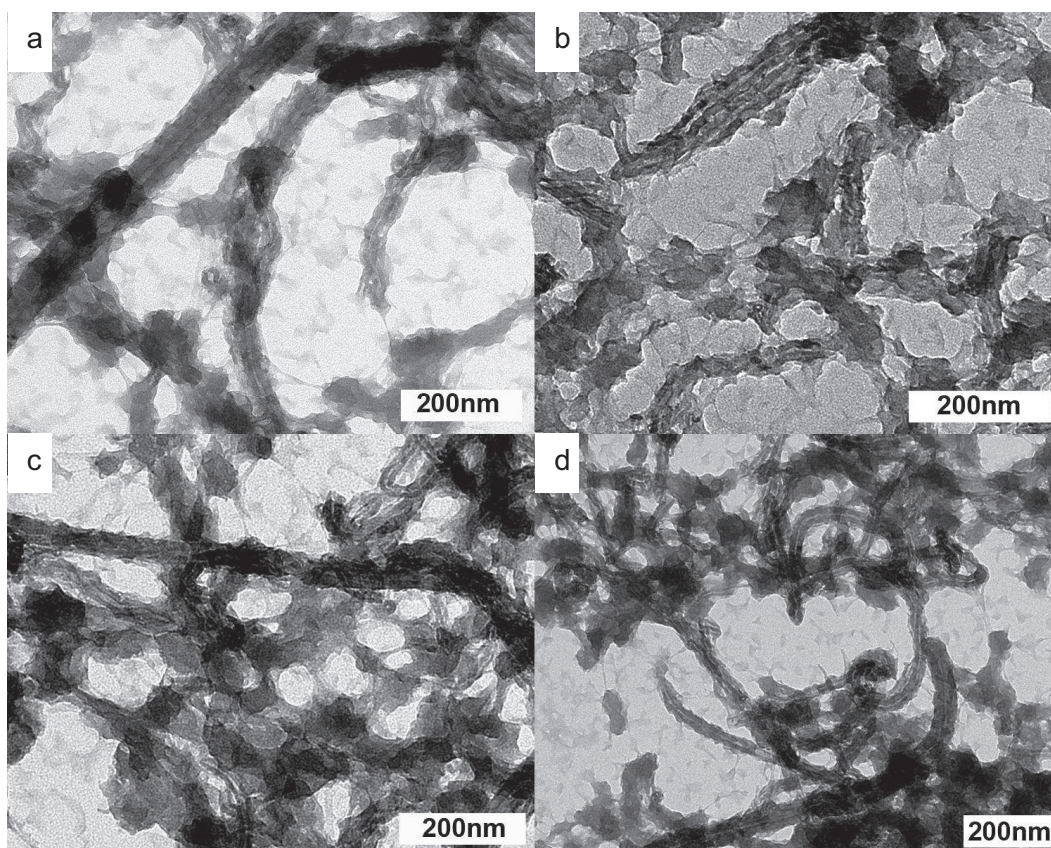


Figure 4.22 : Typical TEM images obtained from dilute solution in DMF of various PAN-g-PDMS copolymers (a) 4.8 wt% PDMS (1000 g.mol^{-1}), (b) 11.4 wt% PDMS (1000 g.mol^{-1}), (c) 16.3 wt% PDMS (1000 g.mol^{-1}) and (d) 19.4 wt% PDMS (1000 g.mol^{-1}) containing 8 wt% MWCNTs.

Figure 4.23 (a) to (d) shows the FE-SEM images of a series of fibres electrospun from graft copolymer blends containing various amounts of PDMS as indicated. MWCNTs have been included in an 8 wt% ratio to the polymer material, and the TEM images of the composite materials in DMF are added as insets. The same rough porous type morphology as was seen with the unfilled fibres is again evident in the fibres above. The highest PDMS content fibre (16.3 wt%) presents a more linear arrangement of rough ridges as was seen and discussed in the previous section focusing on the unfilled fibres. The presence of the nanotubes in the network structure, as shown in the TEM images, suggests that they are situated within the same porous network throughout the fibres. No apparent disruptions due

to the presence of the nanotubes are visible either. TEM images were obtained from cross-sections through the fibres to ascertain where the nanotubes are situated and how they are positioned in the fibres. Work on the electrospinning of nanotube containing solutions has been published^{44,47,48} showing that nanotubes tend to align in the direction of the electrospinning jet due to Hamel flow as shown in work by Dror *et. al.*⁴⁹. The materials in this case are, however, markedly different, as they are amphiphilic and behave completely differently to completely soluble materials. The question was, do the nanotubes still align in the direction of the fibres and what implications does this pose.

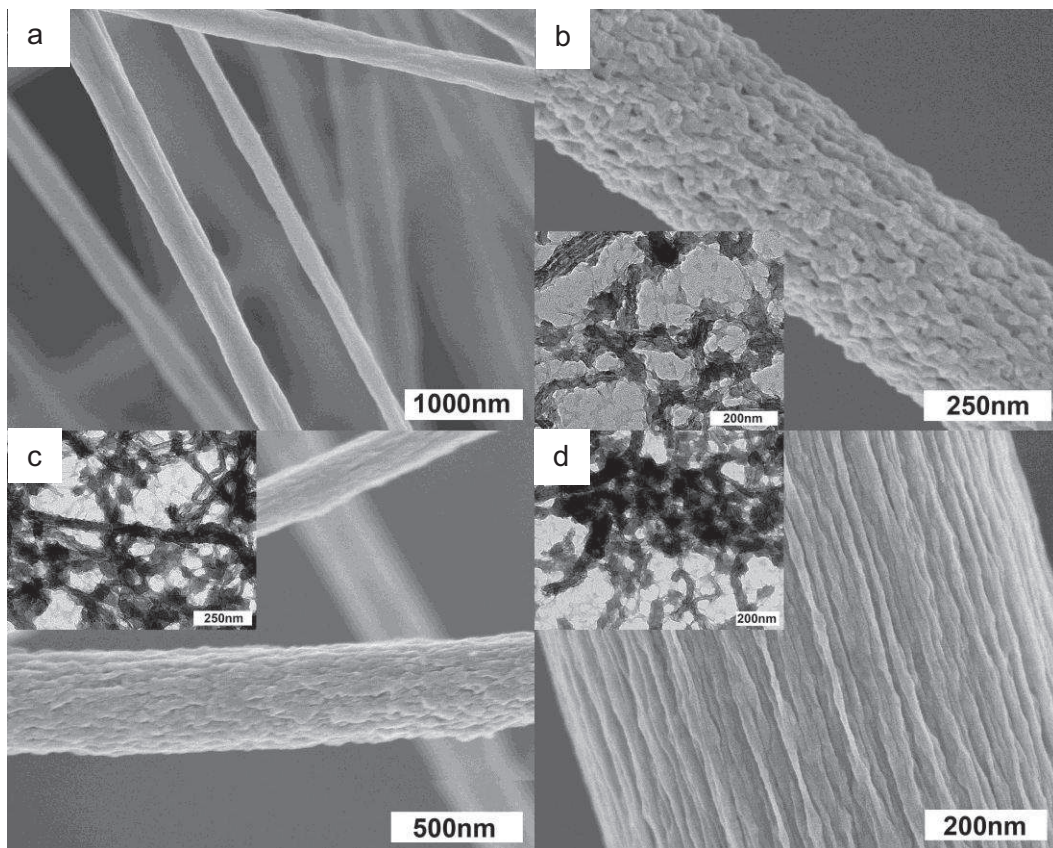


Figure 4.23 : FE-SEM images of (a) homo-PAN, (b) 4.8 wt% PDMS (1000 g.mol^{-1}), (c) 11.4 wt% PDMS (1000 g.mol^{-1}) and (d) 16.3 wt% PDMS (1000 g.mol^{-1}), all containing 8 wt% MWCNTs, corresponding TEM images obtained from evaporation from dilute solution (100% DMF) as insets.

The TEM images obtained from microtomed cross-sections of the fibres are shown in Figure 4.24 (a), (b), (c) and (d). The MWCNTs tend to align along the fibre axis as indicated by the directional arrows. Figure 4.24 (b) shows a cross-section through a fibre and one can see the “end on” view of the MWCNTs which appear as darker rings. The nanotubes appear to be aligned in the direction of the fibre axis as literature would suggest. The complicated

network and porous structure of the amphiphilic copolymer material does not appear to influence the orientation of the nanotubes during the electrospinning procedure.

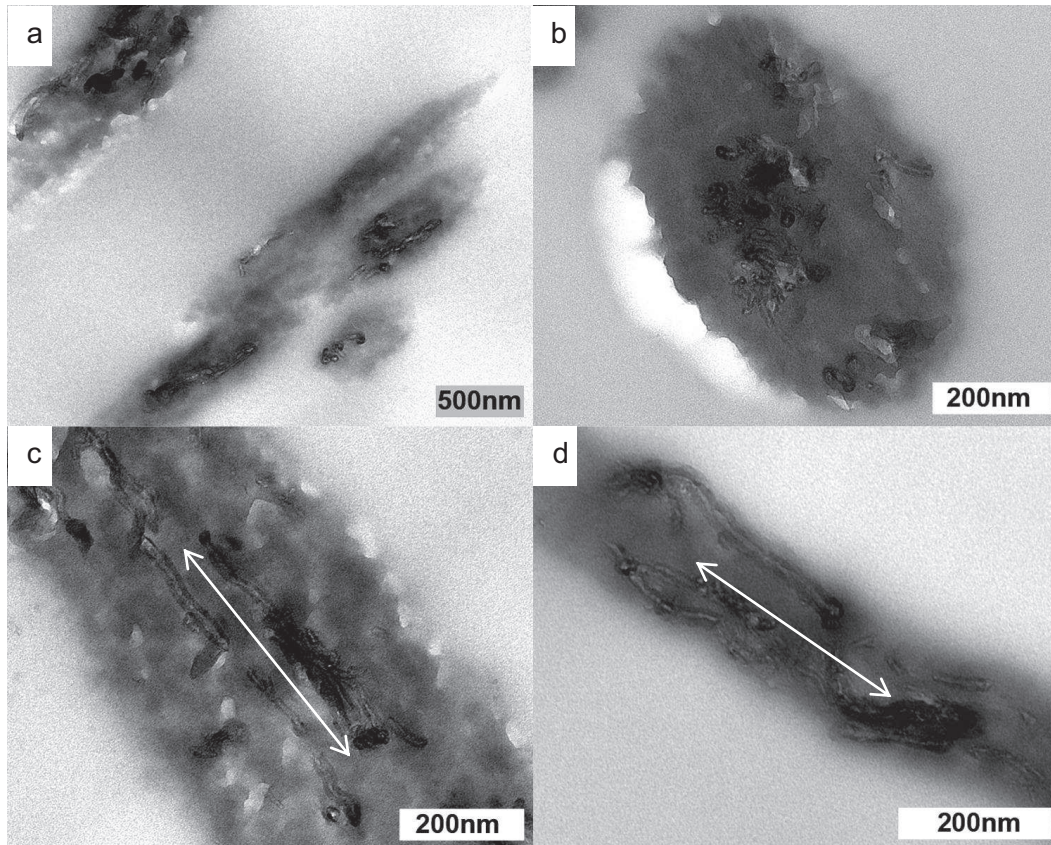


Figure 4.24 : TEM images obtained from MWCNT containing fibres (8 wt%) embedded in an epoxy resin and then microtomed showing the MWCNT dispersion.

Alignment of the nanotubes indirectly shows that the porous network-like structure is also stretched and aligned in the direction of the fibre axis. This result corresponds well with the FE-SEM images that indicate a “fibrillar-like” arrangement of the fine surface detail along the fibre surfaces. The intense stretching of the electrospun fibres during the electrospinning process causes the nanotubes to align along with the complex porous network structure of the fibre matrix polymer. The uneven colouration of the TEM fibre regions is due to the uneven thicknesses of the various areas as a result of the porous nature of the fibre matrix. Agglomeration and entangling of inadequately dispersed carbon nano-tubes leads to poor nanotubes alignment with the electrospun fibre as studied in work by Dror *et. al.*⁴⁹ Images obtained on these fibre composites show very little to no agglomeration of the MWCNTs which further suggests that the modification of the nano-tubes successfully allowed interaction with the graft copolymer and excellent dispersion.

Crystallisation of the PAN segments is a further factor influencing the electrospinning of these MWCNT filled solutions. The crystallisation effect was discussed for the unfilled analogues in a previous section of this work. WAXD analysis was performed on the samples and an overlay of the raw fibre precursor compared to the filled and unfilled electrospun fibres is presented in Figure 4.25. The filled fibre follows an almost identical trace to that of the unfilled fibre material. The same disappearance of the isotactic PAN crystalline peak at 29.5° is also evident.

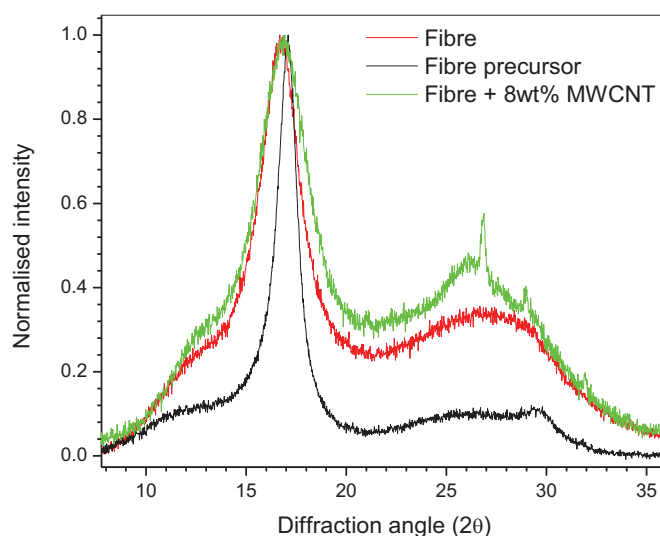


Figure 4.25 : WAXD pattern overlays of the raw fibre precursor, electrospun fibre and electrospun fibre filled with 8 wt% MWCNTs for the 16.3 wt% PDMS copolymer blend (1000 g.mol^{-1} PDMS).

The same broadening of the main PAN crystalline reflection at 17° is also evident along with a slight shift in the peak maximum to approximately 16.9° for the MWCNT filled nanocomposite fibre. The additional reflection at 27.2° is assigned to the (002) crystal planes of the MWCNTs. The (020) crystal plane of the MWCNT presents another peak at approximately 29.6° . The WAXD patterns of the MWCNT filled composites prove the presence of these nano-fillers due to the unique diffraction pattern as indicated above⁴⁹. MWCNTs retain their crystallinity even after functionalisation and dispersion in the nanofibres as expected. The overlaying of the MWCNT diffraction peaks makes deconvolution of the diffraction patterns too complex. It would appear that the presence of the MWCNTs do not disrupt the crystallinity of the fibre to a large extent as seen by the overlay of the filled and unfilled fibre patterns. The dominant effect on the crystallisation is still the electrospinning process and the behaviour of the materials in solution.

This section on the synthesis and electrospinning of the novel PAN-g-PDMS copolymer blend materials is now concluded. Successful synthesis of the materials was achieved as discussed. The production of a blend of PAN homopolymer and graft copolymer was evident from the characterisation of these materials. The PDMS content was varied in the feed which allowed the incorporation of varying amounts of PDMS into the fibre precursor material. The increase in PDMS feed ratio did not lead to the production of more densely grafted chains, but instead created more grafted molecules containing approximately the same amount of graft per molecule during the precipitation polymerisation. The electrospinning of these materials revealed highly complex and interesting results due to the amphiphilic nature of these graft copolymer blend materials in the chosen electrospinning solvent (DMF). The amphiphilic nature was shown to induce phase segregation and agglomeration behaviour of the molecules dried from solution. The competing mechanistic and thermodynamic effects of the phase segregation, crystallisation of the PAN segments as well as the rapid evaporation and stretching of the fibres during electrospinning, lead to the development of complex fibre morphology. The work presents a unique route to the synthesis of fully porous fibres by electrospinning amphiphilic solutions. The rapid stretching was also shown to align not only the MWCNT fillers, but also the agglomerated network structure to a certain extent. The electrospinning of the amphiphilic materials studied in this work, unlike conventional electrospinning using homopolymers or homopolymer blends, was shown to be affected by a number of additional parameters. The PDMS content for instance had a great effect on the optimisation of the electrospinning parameters and in some cases was shown to limit the effects of changing these parameters. The following chapter will focus on using these electrospun fibres and MWCNT fibre nanocomposites as reinforcing fillers for silicone matrices.

4.3 References

- (1) Swart, M., Olsson, R. T., Hedenqvist, M. S., Mallon, P. E. *Polym. Eng. Sci.* **2010**, *50*, (11), 2143-2152.
- (2) Flory PJ. Copolymerization, Emulsion Polymerization, and Ionic Polymerization. Principles of Polymer Chemistry USA: Cornell University Press; **1953**, 178-230.
- (3) Nuyken O. Polymers and their derivatives. In: Kricheldorf HR, Nuyken O, Swift G, editors. Handbook of Polymer Synthesis. 2nd ed. New York: Marcel Dekker, 290-328.
- (4) Chonnowski, J., Cypryk, M., Fortuniak, W., Rozga-Wijas, K., Scibiorek, M. *Polymer* **2002**, *43*, 1993-2001.
- (5) Shinoda, H., Matyjaszewski, K. *Macromolecules* **2003**, *36*, 4772-4778.
- (6) Shinoda, H., Miller, P.J., Matyjaszewski K. *Macromolecules* **2001**, *34*, 3186-3194.
- (7) Xu, Z., Kou, R., Liu, Z., Nie, F., Xu, Y. *Macromolecules* **2003**, *36*, (7), 2441-2447.
- (8) Wan, L., Xu, Z., Huang, X., Wang, Z., Wang, J. *Polymer* **2005**, *46*, (18), 7715-7723.
- (9) Pasch, H., Trathnigg, B. *HPLC of Polymers*. Springer-Verlag: Berlin, **1998**.
- (10) Minagawa, M., Taira, T., Kondo, K., Yamamoto, S., Sato, E., Yoshii, F. *Macromolecules* **2000**, *33*, (12), 4526-4531.
- (11) Minagawa, M., Taira, T., Yabuta, Y., Nozaki, K., Yoshii, F. *Macromolecules* **2001**, *34*, (11), 3679-3683.
- (12) Minagawa, M., Yoshida, W., Kurita, S., Takada, S., Yoshii, F. *Macromolecules* **1997**, *30*, (6), 1782-1786.
- (13) Hinrichsen, G. *J. Polym. Sci., Part C* **1972**, No. 38, 303-314.
- (14) Bell, J. P., Dumbleton, J. H. *Text. Res. J.* **1971**, *41*, (3), 196-203.
- (15) Gupta, A. K., Chand, N. *J. Polym. Sci., Polym. Phys. Ed.* **1980**, *18*, (5), 1125-1136.
- (16) Gupta, A. K., Singhal, R. P. *J. Polym. Sci., Polym. Phys. Ed.* **1983**, *21*, (11), 2243-2262.
- (17) Ramakrishna, S., Fujihara, K., Teo, W. E., Lim, T. C., Ma, Z. *An Introduction to Electrospinning and Nanofibres*. World Scientific: London, **2005**.
- (18) Fennessey, S. F., Farris, R. J. *Polymer* **2004**, *45*, (12), 4217-4225.
- (19) Zhang, D., Karki, A. B., Rutman, D., Young, D. P., Wang, A., Cocke, D., Ho, T. H., Guo, Z. *Polymer* **2009**, *50*, (17), 4189-4198.
- (20) Zhang, W., Wang, Y., Sun, C. *J. Polym. Res.* **2007**, *14*, (6), 467-474.
- (21) Li, D., Xia, Y. *Adv. Mater.* **2004**, *16*, (14), 1151-1170.
- (22) Shenoy, S. L., Bates, W. D., Frisch, H. L., Wnek, G. E. *Polymer* **2005**, *46*, (10), 3372-3384.
- (23) Fong, H., Chun, I., Reneker, D. H. *Polymer* **1999**, *40*, (16), 4585-4592.

-
- (24) Deitzel, J. M., Kleinmeyer, J., Harris, D., Beck Tan, N. C. *Polymer* **2001**, *42*, (1), 261-272.
- (25) Subbiah, T., Bhat, G. S., Tock, R. W., Parameswaran, S., Ramkumar, S. S. *J. Appl. Polym. Sci.* **2005**, *96*, (2), 557-569.
- (26) Hou, H., Ge, J. J., Zeng, J., Li, Q., Reneker, D. H., Greiner, A., Cheng, S. Z. D. *Chem. Mater.* **2005**, *17*, (5), 967-973.
- (27) Heikkila, P., Harlin, A. *Express Polym. Lett.* **2009**, *3*, (7), 437-445.
- (28) Reneker, D. H., Yarin, A. L. *Polymer* **2008**, *19*, 2387-2425.
- (29) Reneker, D. H., Chun, I. *Nanotech.* **1996**, *7*, (3), 216-223.
- (30) Demir, M. M., Yilgor, I., Yilgor, E., Erman, B. *Polymer* **2002**, *43*, (11), 3303-3309.
- (31) Letchford, K., Burt, H. *Eur. J. Pharm. Biopharm.* **2007**, *65*, (3), 259-269.
- (32) Borisov, O. V., Zhulina, E. B. *Macromolecules* **2005**, *38*, (6), 2506-2514.
- (33) Hiwatari, K., Serizawa, T., Seto, F., Kishida, A., Muraoka, Y., Akashi, M. *Polym. J.* **2001**, *33*, (9), 669-675.
- (34) Zhang, L., Lin, J., Lin, S. *J. Phys. Chem. B* **2007**, *111*, (31), 9209-9217.
- (35) Duan, H., Kuang, M., Wang, J., Chen, D., Jiang, M. *J. Phys. Chem. B* **2004**, *108*, (2), 550-555.
- (36) Kikuchi, A., Nose, T. *Macromolecules* **1996**, *29*, (21), 6770-6777.
- (37) Kikuchi, A., Nose, T. *Polymer* **1996**, *37*, (26), 5889-5896.
- (38) Wang, C., Li, G., Guo, R. *Chem. Commun.* **2005**, (28), 3591-3593.
- (39) Zhang, J. X., Qiu, L. Y., Zhu, K. J. *Macromol. Rapid Commun.* **2005**, *26*, (21), 1716-1723.
- (40) Casper, C. L., Stephens, J. S., Tassi, N. G., Chase, D. B., Rabolt, J. F. *Macromolecules* **2004**, *37*, (2), 573-578.
- (41) Megelski, S., Stephens, J. S., Chase, D. B., Rabolt, J. F. *Macromolecules* **2002**, *35*, (22), 8456-8466.
- (42) Srinivasarao, M., Collings, D., Philips, A., Patel, S. *Science* **2001**, *292*, (5514), 79-82.
- (43) Bognitzki, M., Frese, T., Steinhart, M., Greiner, A., Wendorff, J. H., Schaper, A., Hellwig, M. *Polym. Eng. Sci.* **2001**, *41*, (6), 982-989.
- (44) Ge, J. J., Hou, H., Li, Q., Graham, M. J., Greiner, A., Reneker, D. H., Harris, F. W., Cheng, S. Z. D. *J. Am. Chem. Soc.* **2004**, *126*, (48), 15754-15761.
- (45) Meng, L., Fu, C., Lu, Q. *Prog. Nat. Sci.* **2009**, *19*, (7), 801-810.
- (46) Zong, X., Kim, K., Fang, D., Ran, S., Hsiao, B. S., Chu, B. *Polymer* **2002**, *43*, (16), 4403-4412.
- (47) Ji, J., Sui, G., Yu, Y., Liu, Y., Lin, Y., Du, Z., Ryu, S., Yang, X. *J. Phys. Chem. C* **2009**, *113*, (12), 4779-4785.

- (48) Ko, F., Gogotsi, Y., Ali, A., Naguib, N., Ye, H., Yang, G., Li, C., Willis, P. *Adv. Mater.* **2003**, *15*, (14), 1161-1165.
- (49) Dror, Y., Salalha, W., Khalfin, R. L., Cohen, Y., Yarin, A. L., Zussman, E. *Langmuir* **2003**, *19*, (17), 7012-7020.

Chapter 5

Composite fabrication and mechanical testing

5.1 Preparation of the fibre filled silicone nano/composites

This section presents the production of the silicone composites filled with the electrospun fibres prepared from the novel PAN-g-PDMS copolymer blends. The synthesis and electrospinning of the MWCNT filled and unfilled PAN-g-PDMS copolymer fibres are discussed in the previous Chapter 4. The term silicone nano/composite is used. The unfilled fibres are of too large a diameter to be considered nano-metric, however, the MWCNT filled fibres are of smaller diameters and inherently nanocomposite fibres, as they contain MWCNTs.

5.1.1 Choice of PAN-g-PDMS copolymers as filler materials

The synthesis of these novel amphiphilic graft copolymers, as well as their properties in solution, are discussed in detail in chapter 4 of this work. Table 4.1 in chapter 4 summarises the copolymers prepared including the molecular weights of the materials relative to PMMA standards. The copolymers have been labelled CP40-CP43 and CP14-CP17 depending on the PDMS incorporation. The weight percentages of the PDMS graft components as well as the molecular weights of the grafts were varied accordingly. PAN is a robust semi-crystalline material with excellent physical properties which lends it applications as fibres in hot gas filtration systems, outdoor awnings, sails for yachts, and even fibre reinforced concrete¹⁻³. PAN is also a precursor for carbon fibre¹. These properties lend it applications in the field of polymer composites as reinforcing fibre fillers. Most of the research to date has looked at using carbon fibres derived from oxidised PAN fibres as filler materials due to the extremely enhanced physical and structural properties of this material^{4,5}. This work, however, looks at using unoxidised electrospun PAN fibres as reinforcing fillers for silicone matrices. Most fillers, especially nano-fibres, require sufficient interaction between the matrix and filler material. Agglomeration of filler fibres and poor interaction with the matrix can lead to decreased performance of the composite material. This led to the concept of covalently incorporating PDMS graft polymer components that allowed interaction between the PAN fibres and the silicone matrices. The immiscibility of the polymer components induces nano-phase segregation and with its lower surface energy, PDMS tends to surface segregate^{6,7}. This lends the advantage of interaction and improved dispersion of the PAN based fibres to the silicone matrices. The PDMS domains act as compatibilisers between the PAN fibres and the silicone matrix. Variation of the PDMS graft content will be studied by investigating the changes in the reinforcing properties of the electrospun fibre fillers.

Further improvement of the physical properties of the electrospun PAN-g-PDMS fibres, was investigated by incorporating MWCNTs into the fibres. MWCNTs lend composite materials

improved physical and functional properties, as long as they are well dispersed throughout the composite⁸. Agglomeration of these nano-fillers can lead to poorer material performance. Surface modification of MWCNTs is a widely used technique in improving the dispersion of these nano-fillers^{9,8,10} and is the strategy that was utilised in this project. The aim was to oxidise the MWCNTs so as to incorporate carboxylic acid (-COOH) groups along the surface of the nano-tubes. The procedure used is discussed in the experimental section of this chapter. Ge and co-workers¹⁰ used UV/vis spectroscopy and suggested that the interaction between the MWCNTs and PAN molecules is due to the formation of a charge transfer complex between the surface oxidised MWCNTs and the PAN molecules through delocalisation of the π -electrons along the conjugated sequence. This allowed good dispersion and interaction of our MWCNTs in the electrospinning solution, as discussed in Chapter 4.

5.1.2 Summary of the fibre fillers prepared

A detailed study on the electrospinning of these novel graft copolymer materials was presented in Chapter 4 of this work and is not discussed in detail here. The optimum conditions for the electrospinning of these reinforcing fibres are presented as summaries in Table 5.1 which compares the filled and unfilled fibres.

Table 5.1 : Comparison of electrospinning conditions for the respective unfilled PAN-g-PDMS and MWCNT filled graft copolymers, including the mean fibre diameters obtained.

Samples (codes)	PDMS (wt%)	$D_{\text{crystallin}}$ (%)	Mean fibre diameters (μm)				
			Unfilled	MWCNT (8 wt%)	MWCNT (16 wt%)	MWCNT (32 wt%)	
PDMS short	PAN	0.0	57	0.22 \pm 0.05	0.21 \pm 0.03		
	CP40	4.8	56	0.89 \pm 0.10	0.28 \pm 0.03		
	CP41	11.4	53	1.81 \pm 0.13	0.63 \pm 0.07	0.69 \pm 0.10	0.73 \pm 0.12
	CP42	16.3	50	1.92 \pm 0.15	0.76 \pm 0.08	0.74 \pm 0.09	0.84 \pm 0.07
	CP43	19.4	24	3.31 \pm 0.45			
PDMS long	CP14	4.2	46	1.21 \pm 0.15	0.46 \pm 0.08		
	CP15	8.5	41	2.01 \pm 0.15	0.78 \pm 0.08		
	CP16	13.1	41	2.51 \pm 0.19	1.02 \pm 0.11		
	CP17	16.2	23	3.89 \pm 0.51			

All samples were electrospun at the following conditions: 0.008 ml.min⁻¹ feed-rate; 18 cm tip-to-collector distance; 12.5 kV

^a Degree of crystallinity of the copolymer powders prior electrospinning determined using WAXD

^b Electrospinning solution concentration of 15 wt%

^c Electrospinning solution concentration of 10 wt%

^d Electrospinning solution concentration of 9.5 wt%

^e Electrospinning solution concentration of 9.0 wt%

^f PDMS grafts with a molecular weight of 1000 g.mol⁻¹

^g PDMS grafts with a molecular weight of 5000 g.mol⁻¹

It must be noted that optimisation of the electrospinning procedure for these MWCNT filled and unfilled polymer fibres was needed. All conditions were kept constant, except for the electrospinning solution concentrations of the MWCNT filled polymer solutions. The reasons for this were discussed in Chapter 4. Table 5.1 also shows the average fibre diameters achieved for the various electrospun fibres. The higher the PDMS content the thicker the fibres. The same is true for the MWCNT filled fibres, however, the diameters as compared to their unfilled analogues are significantly smaller. The reasons for this relate to the electrospinning solution viscosity as discussed previously. Before production of the filled silicone composites, it was necessary to investigate whether or not successful surface segregation of the PDMS domains to the surface of the fibres took place, so as to improve interaction with the silicone matrix.

5.1.3 Contact angle determinations of the fibre fillers

PDMS is known, from literature^{6,7}, to preferentially surface segregate, due to its lower surface energy. Contact angle measurements are a useful way to determine whether or not PDMS surface segregation has taken place, as PDMS is a highly hydrophobic material and tends to result in higher contact angles. This lends interesting hydrophobic properties to the electrospun fibres. Figure 5.1 (a) and (b) show the three dimensional plots that compare the contact angle data with the PDMS content and fibre diameter values, of both the filled and unfilled electrospun fibres. The contact angle is shown to increase as the PDMS content in the graft copolymer blend material is increased. Mean fibre diameters also increase as the PDMS content is increased. A contradictory result is that of the increasing contact angle as the fibre diameter increases. There are two possible physical effects that influence the hydrophobicity and hence the contact angle: these are known as the Wenzel or Cassie state¹¹. Increased surface area (as is the case for the fibres) amplifies the natural hydrophobicity of the material. The “rougher” the surface the higher the contact angle. Thicker fibres would normally result in lower surface roughness thus lower contact angle values. Competing against this is the fact that the hydrophobic PDMS content is increasing which should result in higher contact angle values. The results clearly show that the PDMS content is the dominant factor governing the hydrophobicity of the fibre mats, as the contact angles increase with an increase in PDMS content but decrease with a decrease in fibre diameter. Similar behaviour was reported in the work of Swart and Mallon¹² where the polymers under study were graft copolymers of poly(methyl methacrylate) and PDMS. The inherent surface porosity of the fibres themselves, also lend additional “nano-surface roughness” to the fibres. The two degrees of surface roughness are related to the micro-

texture of the fibres and the nano-texture of the porous fibre surfaces, much like that of the lotus leaf. The hydrophobicity of the lotus leaf (lotus effect¹³) is due not only to the waxy surface, but the micro-monoliths along the surface, which are in turn covered in nano-protrusions. The surface roughness aspect of our fibres together with the PDMS hydrophobicity allows the achievement of contact angles in excess of 140°. This is remarkable considering the majority of the fibre matrix material consists of PAN which is not known for its hydrophobicity. Increasing of the contact angle as the PDMS content increases is due to the increased presence of PDMS domains at the surface of the fibre fillers and the nano-texture.

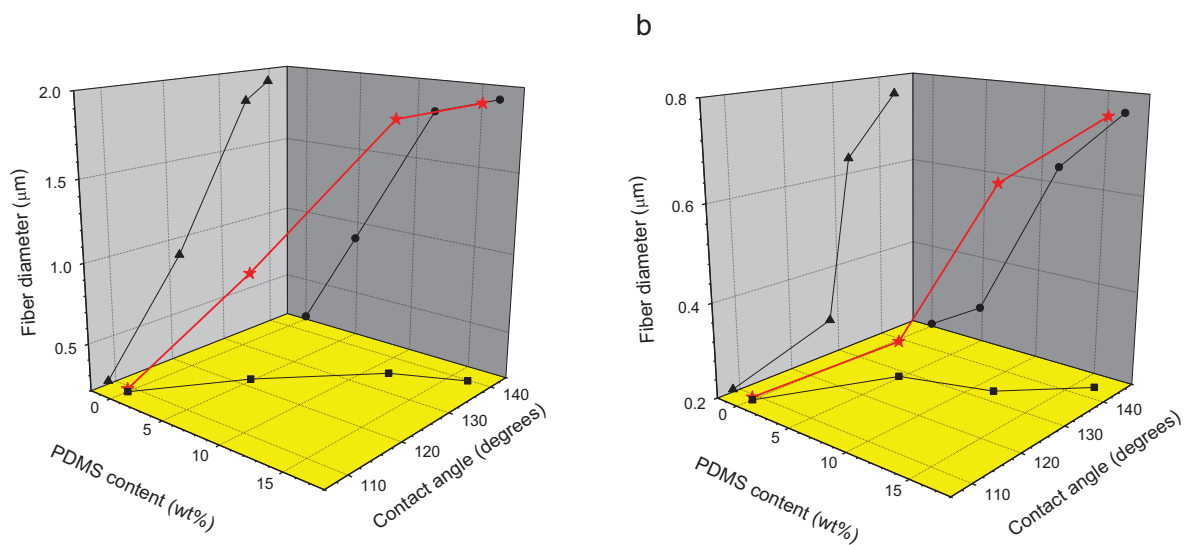


Figure 5.1 : Mean fibre diameter and contact angle as a function of PDMS incorporation for (a) the unfilled fibres and (b) the MWCNT (8 wt%) filled fibres.

The discussion of the fibre morphology in Chapter 4, highlighted that the amphiphilic nature of the graft copolymer material resulted in very complex behaviours. Imaging of the PAN and PDMS phases via TEM proved unsuccessful. The increase in contact angle does, however, suggest that PDMS domains do segregate to the surface even after the electrospinning procedure. The amount or extent of surface segregation is not clear, but as the PDMS content is increased there is a definite increase in the PDMS surface domains. This successful result should prove to have a significant effect on the reinforcing properties of these electrospun fibre filler materials. Enhanced dispersion of the prepared fibre fillers is essential in preparing silicone composites with improved physical properties. The nanotube containing fibres have higher contact angles, as the average fibre diameters are markedly smaller than the unfilled analogues. The fibres, after having shown successful PDMS

surface segregation, were then used to develop a series of composites to study the effects of the various filler compositions.

5.1.4 Variables studied in the production of the fibre filled silicone composites

A series of graft copolymer fibres were electrospun with and without MWCNTs. The fibre mats were then tested as reinforcing fillers for silicone films. The preparation of non-woven mats as well as aligned fibre mats of these various electrospun materials was included as an additional parameter. For clarity, Table 5.2 has been included as a summary, highlighting the various fibre fillers produced to test as reinforcing agents for the silicone matrices.

Table 5.2 : A summary of the various composites prepared in this work, where (NW) refers to the non-woven mats and (Ali) refers to the Aligned fibre mats. The columns and rows highlighted from A - G are added to clarify the variables studied.

	Fibres (wt% PDMS)		MWCNT filled fibres (wt% PDMS)						
	0 wt% MWCNT		8 wt% MWCNT		16 wt% MWCNT		32 wt% MWCNT		
NW*	NW	Ali	NW	Ali	NW	Ali	NW	Ali	
-	0	-	-	-	-	-	-	-	
-	4.8	4.8	4.8	4.8	-	-	-	-	
8.5	11.4	11.4	11.4	11.4	11.4	11.4	11.4	11.4	E
13.1	16.3	16.3	16.3	16.3	16.3	16.3	16.3	16.3	F
G	A	B	C	D					

* These samples contain 5000 g.mol^{-1} PDMS while the others all contain 1000 g.mol^{-1} variant.

The series was chosen so as to ascertain which filler variables lent the most improved mechanical properties to the final silicone composites. It must be noted that there are a plethora of parameters one can vary to study the various aspects affecting the composites prepared in this work. The following were chosen as a systematic series to obtain the most information without having to prepare so many composites as to exceed the time-scale of this project.

As can be seen on Table 5.2, the highlighted columns and rows indicate the variables studied as follows:

- Column (A) looks at the influence of PDMS content on reinforcement efficiency as we move from homo-PAN (0 wt% PDMS) to CP42 (16.3 wt% PDMS) for silicone composites filled with non-woven fibre mats.

- Column (B) looks at the influence of PDMS content on reinforcement efficiency as we move from CP40 (5 wt% PDMS) to CP42 (16.3 wt% PDMS) for silicone composites filled with aligned fibre mats.
- Column (C) investigates the same PDMS content influence as with column (A), but this material contains 8 wt% MWCNT and is also present in the composite as a non-woven mat filler.
- Column (D) relates to column (B), where the PDMS influence is studied for the aligned fibre mat fillers, but these fibres also contain 8 wt% MWCNT.
- Row (E) studies the influence of MWCNT (0, 8, 16 and 32 wt%) content for the 10 wt% PDMS containing copolymers and how this relates to the composite reinforcement.
- Row (F) once again studies the influence of MWCNT (0, 8, 16 and 32 wt%) content, but in this case we look at the effect on a copolymer fibre with higher PDMS content (ie: 16.3 wt% PDMS).
- Column (G) compares the 5000 g.mol⁻¹ PDMS to the 1000 analogues in column A, to study the macromonomer length influence.

The MWCNT content appears rather high in contrast to the amounts normally added to composite materials as found in literature. The reason for this is the fact that the MWCNTs are filling fibres which are in turn filling the silicone composites. The fibre content is already a 12.5 wt% incorporation in the silicone. The nanotube content has to be higher in the fibres so that any property effects due to its presence can be seen in the composite behaviour. The 8 wt% MWCNT containing fibres correspond to a 1 wt% of MWCNTs in the silicone film. The concentrations of nanotubes relative to the silicone matrix are in fact in line with the amounts generally used in literature. Upon establishment of the parameters under study, the next section discusses the actual preparation of the silicone composites.

5.1.5 Production of the filled silicone composites

The technique used to create the composites is relatively simple and involves the layering of the fibre mat, be it non-woven or aligned, into a mould containing the uncured silicone resin. The difference between the non-woven and aligned fibre mats was purely due to the collection of the fibres. The non-woven fibres were collected on a stationary grounded collector plate, while the aligned fibres were collected on a high speed rotating drum. There are many ways in which to align electrospun fibres, a comprehensive review on this subject is given by Teo and Ramakrishna¹⁴.

5.1.5.1 Aligned fibre filler collection

The rotating drum method proved to produce well aligned fibres in the large yields necessary for the preparation of the composites. Figure 5.2 shows SEM images of the non-woven mats and their aligned analogues highlighting the success of using the rotating drum method to have long range alignment of the fibre mats.

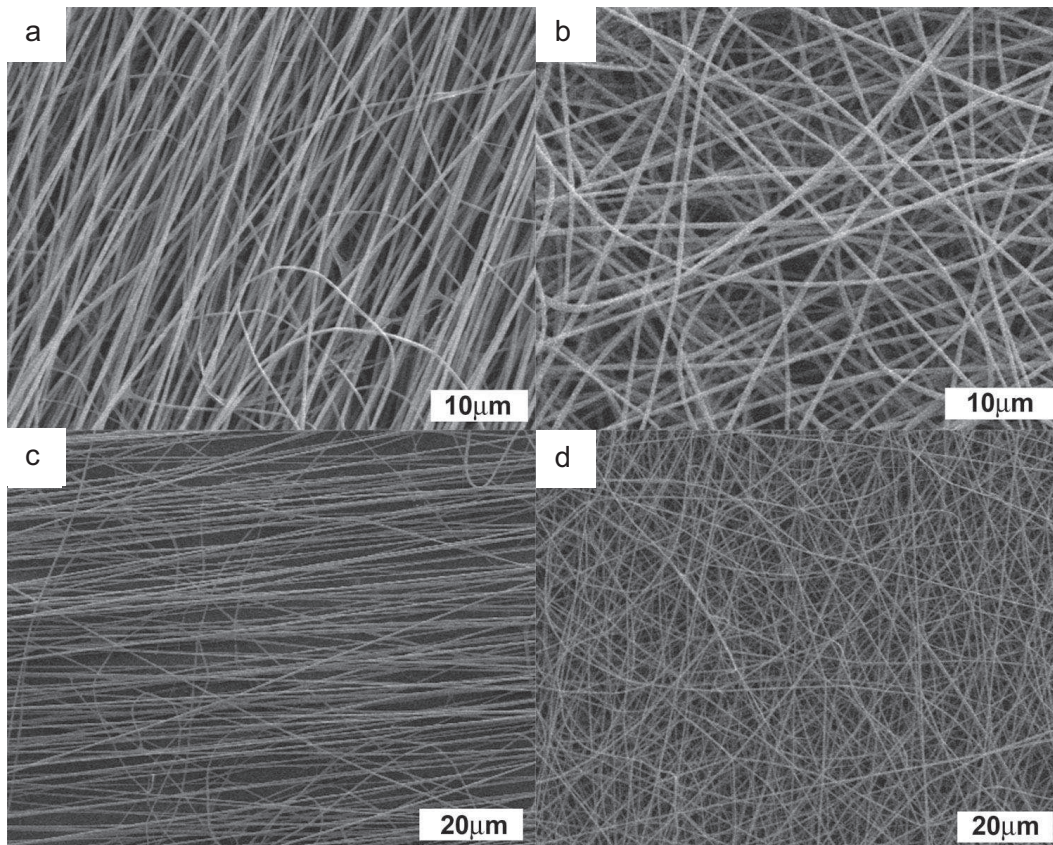


Figure 5.2 : SEM images of (a) aligned fibre mat of 4.8 wt% PDMS unfilled, (b) non-woven mat of 4.8 wt% PDMS unfilled, (c) aligned mat of 4.8 wt% PDMS (8 wt% MWCNT) and (d) non-woven mat of 4.8 wt% PDMS (8 wt% MWCNT) electrospun fibres (1000 g.mol^{-1} PDMS).

The alignment is certainly not 100%, but the differences between the two fibre collection procedures are clearly evident. Later discussions will show the dramatic impact that the alignment of the fibres has on the composite properties, even at the level of alignment as seen here. The procedure used to prepare the uncured silicone is discussed in the experimental section. All the fibres were collected prior to deposition in the uncured silicone and allowed to dry in a vacuum oven at 90°C . This was to ensure removal of any residual DMF. The collection of the fibres on a rotating drum is known to have an influence on the diameters of the electrospun fibres, depending on the drawing speed of the collector drum.

Figure 5.3 illustrates the effect that the high-speed rotating collector drum has on the diameters of the collected fibres. There is generally a narrowing of the fibre diameters, as expected. Additional stretching can lead to fibres of smaller diameters than those collected on a stationary collector. The difference in diameters is, however, not significantly different in most samples. The differences as evident in the plots below are relatively small as compared to the variations in diameters achieved by varying the electrospinning parameters as discussed in Chapter 4. The effect of additional stretching due to the collection of the aligned fibres was, therefore, considered to be negligible relative to the other fibre properties.

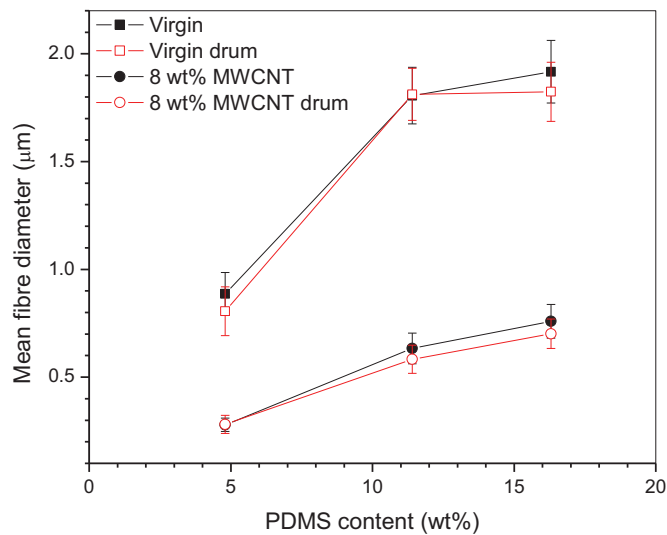


Figure 5.3 : Mean fibre diameter of filled and unfilled fibres collected on the rotating drum versus the stationary collector.

5.1.5.2 Composite preparation and curing

The fibres were not impregnated with silicone *in situ*, but first collected in the form of fibre mats, dried in vacuum and then further used to produce the composites as explained in the following procedure and illustrated in Figure 5.4. The *in situ* composite fabrication method was tested but proved unsuccessful due to the effect of the electric field on the uncured silicone in the grounded mould. The mould containing the silicone was grounded (electrically conductive aluminium mould) which caused problems upon application of the high voltage field. The silicone tended to “creep” out of the mould, making it difficult to have an accurate estimation of the fibre to matrix content. This effect was enhanced when using nanotube filled spinning solutions. Obtaining aligned fibre mats in uncured silicone resin was also not possible using the rotating drum collector. The fibres had to be collected on the drum and

then immersed in the silicone resin. Consistency dictated that the non-woven mats should be prepared in the same manner. Direct deposition of the fibres into the uncured silicone matrix also did not allow the complete drying of the electrospun fibres to remove any traces of DMF.

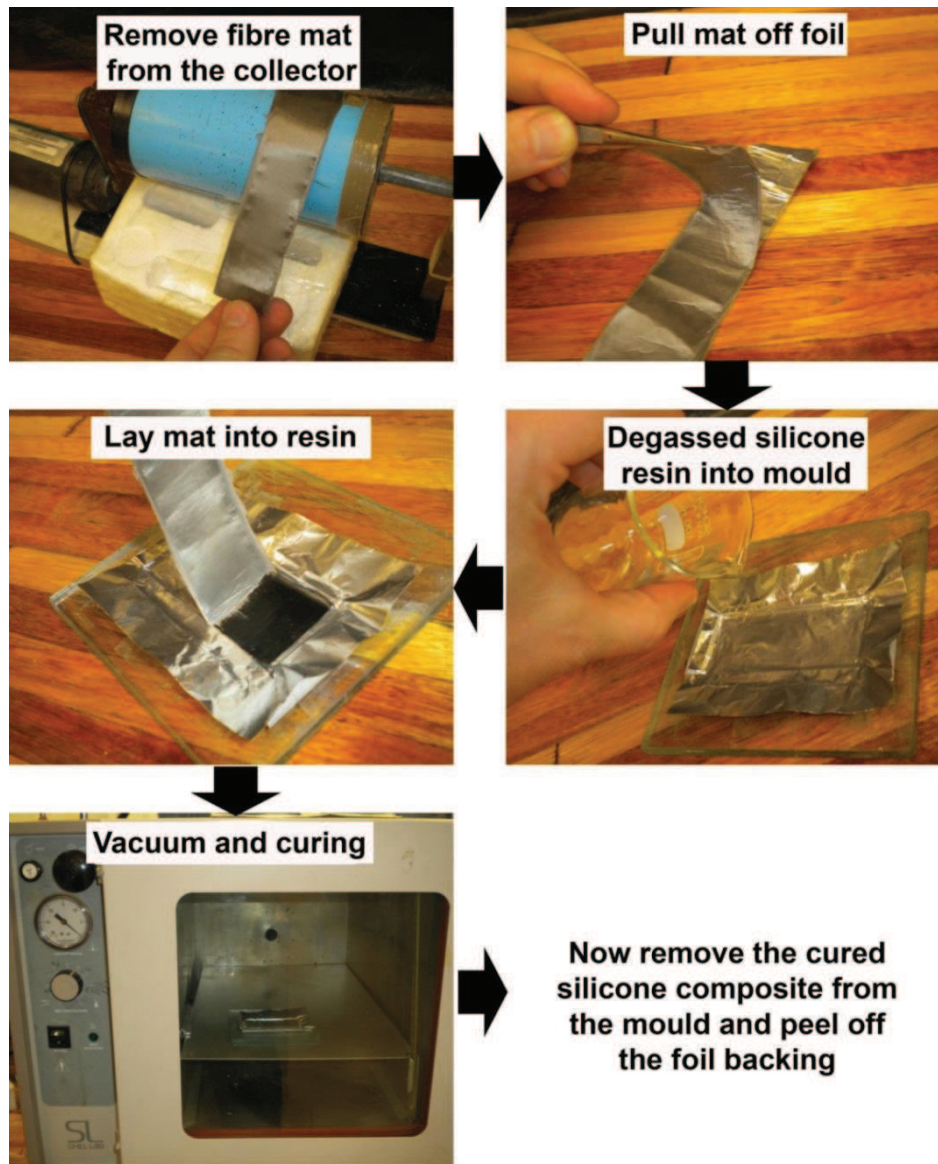


Figure 5.4 : Stepwise guide of how the silicone elastomer composites were prepared.

- Step 1: collection of the electrospun fibres on the stationary collector or the rotating drum. (Note the use of aluminium foil as the grounding collector sheet)
- Step 2: once the required volume of solution has been electrospun, the fibre mats are gently peeled off of the aluminium foil and weighed. The amount of fibres collected per sample was aimed at approximately 250mg.

- Step 3: the degassed pre-weighed (2g) silicone resin (prepared as per mentioned in the experimental section) is placed into an aluminium foil lined mould.
- Step 4: the fibre mats are gently placed into the silicone resin, but to limit the formation of bubbles, the silicone was allowed to gradually wet the fibre and slowly soak them into the uncured resin. The ability of the fibre mats to essentially soak up the silicone is already an excellent indication that the fibres have good interaction with the silicone matrix.
- Step 5: the uncured and filled silicone resin is placed in vacuum for approximately 60 min to remove any trapped air-bubbles.
- Step 6: curing of the filled silicone resin according to the temperature profile mentioned in the experimental section allows the production of smooth silicone films.

The importance of keeping track of the weight of the silicone to the weight of the fibre fillers is important for consistency. A variation in filler content would mask any changes in reinforcement efficiency induced by the properties of the various filler materials under study. Every 2 g silicone resin required the addition of 250 mg fibres, giving a constant filler content of 12.5 wt% for all composites under study. Figure 5.5 (b) and (c) shows optical images of the prepared composites. Figure 5.5 (a) shows the poor distribution of nanotubes incorporated directly into the silicone matrix after mechanical mixing. Note the even distribution of nanotubes evident by the even colour of the composite in Figure 5.5 (c).

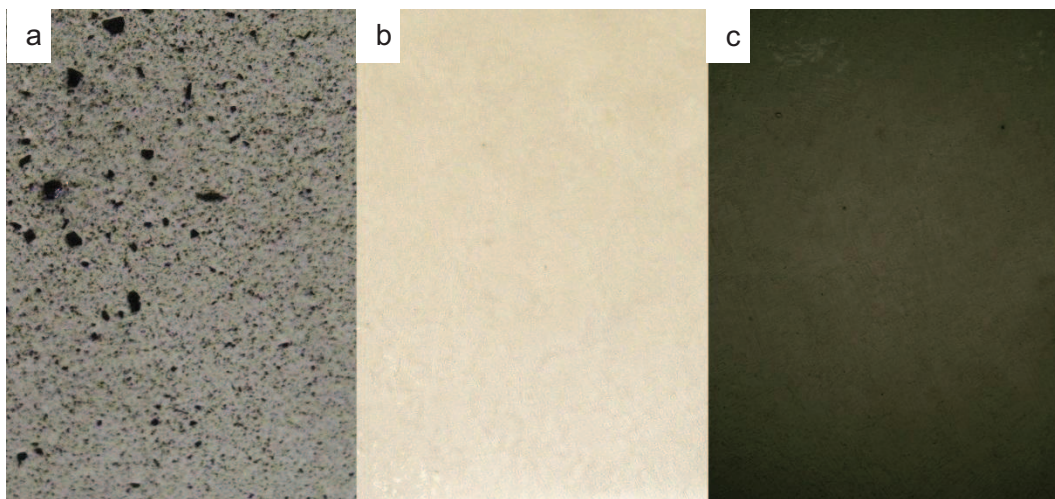


Figure 5.5 : Typical optical images of (a) MWCNTs directly added to the silicone film, (b) fibre filled silicone composite and (c) fibre filled silicone composite with 8 wt% MWCNTs in the fibre fillers and 1.2 wt% to the silicone matrix.

5.1.6 Investigation of fibre distribution in the silicone elastomer composites

It is very important to have a good distribution of the fibres in the silicone matrix, as agglomeration or sedimentation of the fibres in the silicone elastomers can lead to uneven load distribution and a decrease in the physical properties of the composite. This is why it was decided to use a PAN-g-PDMS / PAN blended polymer to produce the fibres as the PDMS components aid in the distribution of the filler fibres. Figure 5.6 (a) and (b) was obtained after slicing through the middle of a prepared composite using a scalpel, and then investigating the cut surface using SEM. The images shown are typical of what was seen for all of the prepared composites. Figure 5.6 shows a remarkably uniform distribution of the fibres in the silicone matrices with little to no agglomeration of the fibres. There are also little to no observable voids in the matrix between the fibres. The biggest challenge in using micro or even nano scaled fillers is the dispersion and successful interaction of the materials with the matrix. The image below shows excellent dispersion of the fibres highlighting the positive effect the incorporation of PDMS segments has on the compatibility between the PAN based fibres and the silicone matrix. It must be mentioned that the silicone matrix also allows the dispersion of the fibres in its uncured form. The uncured resin is a viscous liquid which makes it simpler to disperse a material before curing. The dispersion of the MWCNTs in the composite fibres must also be sufficient so as to improve the physical properties of the fibres. This has been discussed in chapter 4 of this work and the TEM results presented in that section showed the excellent distribution and alignment of the MWCNTs in the fibre fillers. After the preparation of these well dispersed silicone composites, mechanical testing was performed to study the reinforcement characteristics.

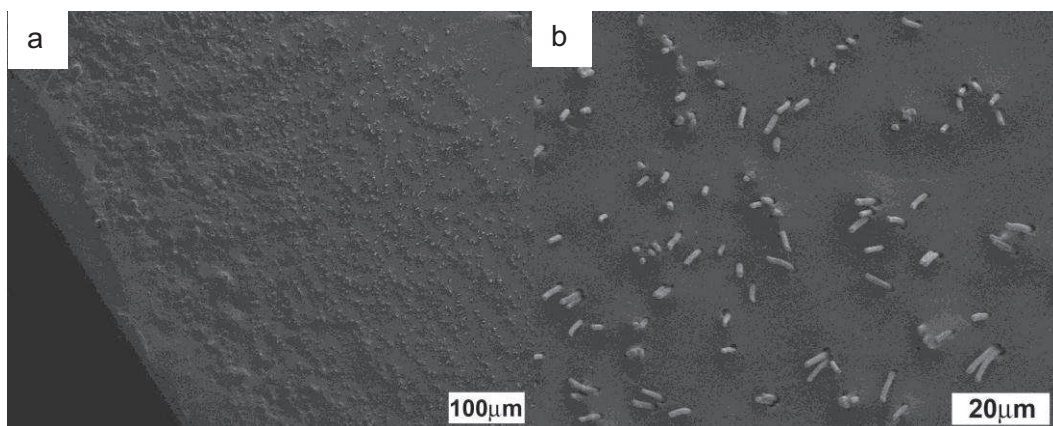


Figure 5.6 : Typical fibre distribution in the silicone elastomer matrix observed using SEM at two different magnifications (a) and (b).

5.1.7 Mechanical properties of the filled silicone elastomer composites

Conventional tensile testing was performed on the composite test pieces. Table 5.2 presents a summary of the composite specimens analysed in this work. The mechanical properties reported are also compared to the FE-SEM images of the fracture surfaces of the respective composite specimens. The mechanical results together with the FE-SEM images work concurrently when describing the mechanical behaviour of the filled silicone elastomer composites. Stress-strain curves were analysed to determine the mechanical and reinforcement behaviour of the various silicone composites prepared. Figure 5.7 shows the enhanced physical properties of four of the composites. The composites were chosen as they represent the differences between the main filler variations.

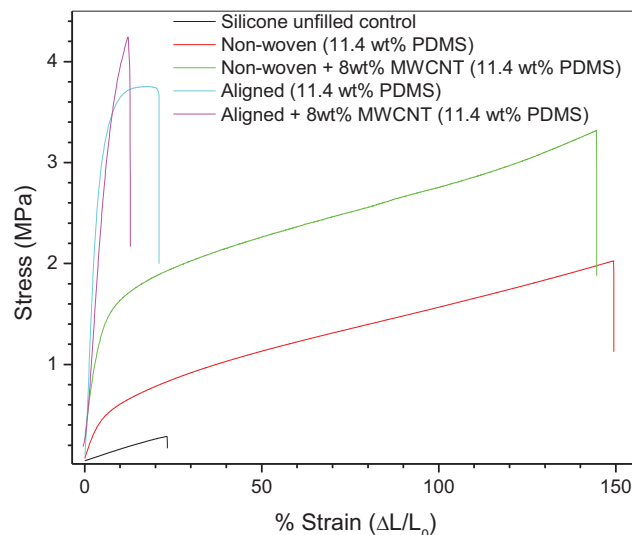


Figure 5.7 : Summary of the tensile stress-strain curves of the 11.4 wt% PDMS (1000 g.mol^{-1}) nonwoven and aligned fibre composites with and without 8 wt% MWCNTs.

Significant differences are visible between the non-woven and aligned fibre mats, as well as those fibres filled with MWCNTs and those without. The differences between the behaviour of the various composites are remarkable and the reasons for this are discussed in the following section. The non-woven mat fillers lend dramatic increases in the strain of the silicone composites as opposed to the aligned fibre fillers. This large increase in strain is not commonly seen in such fibre filled composites which is a highly significant result. The aligned fibres show much larger stiffness behaviour. The MWCNT containing fibres also appear much stiffer than the unfilled analogues and have higher tensile strengths. Figure 5.8 (a) to (e) shows a comparison of the different tensile samples at the point just before composite failure. Note the extreme increase in elongation at break for the non-woven mat

fibre filled samples (d and e). The non-woven nanotube filled sample (d) appears lighter in colour compared to the aligned nanotube filled sample (c). This shows how much more the non-woven composite is being stretched and thinned.

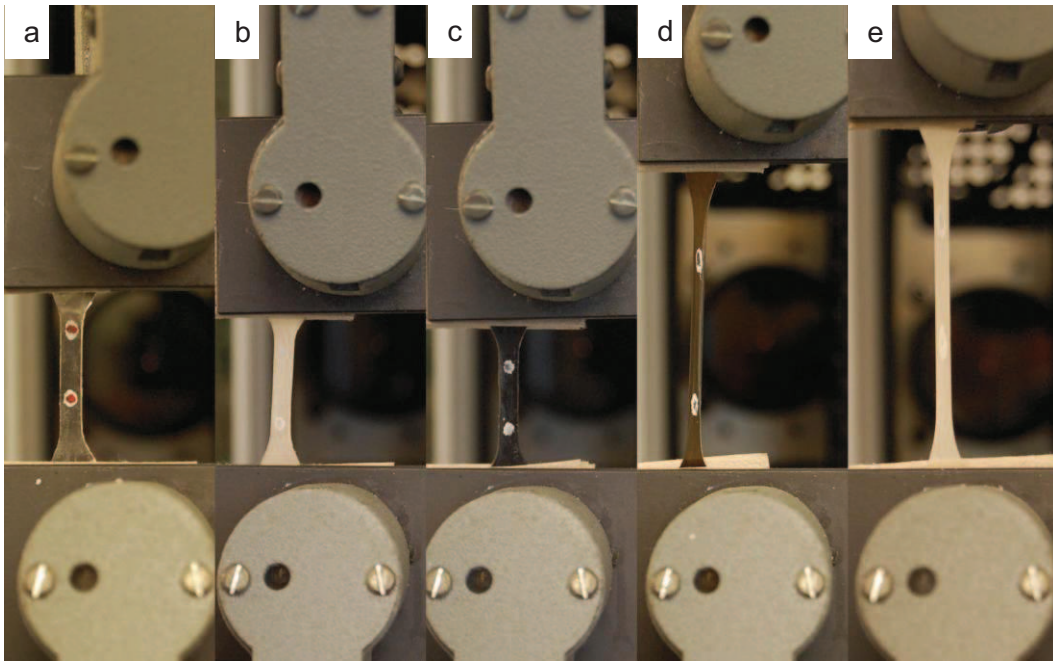


Figure 5.8 : Comparison of the tensile test specimens just prior to fracture for (a) unfilled silicone, (b) aligned fibre filler, (c) aligned fibre filler with 8 wt% MWCNT, (d) non-woven fibre filler with 8 wt% MWCNT and (e) non-woven fibre filler, with all the fibres containing (11.4 wt% PDMS, 1000 g.mol⁻¹).

Figures A.1 to A.8 in appendix A present a graphical summary of all the mechanical properties including the standard deviations. Tabulated results are, however, used to compare the various composite behaviours in the following section. Tables 5.3 and 5.4 summarise the mechanical properties of the silicone films reinforced with electrospun fibres (unfilled and 8 wt% MWCNT filled).

For all the composite types there tends to be an increase in the maximum strain at break ϵ_{max} values as the PDMS content increases from 0 wt% (PAN) to 16.3 wt% (CP42, 1000 g.mol⁻¹ PDMS series). The increased interaction of the higher content PDMS fibres with the silicone matrix causes this improvement. The better interfacial interaction leads to improved load transfer between the matrix and the fibre fillers. It must be noted that the smaller the diameters of the fibres the larger the interfacial area between the filler and matrix, resulting in improved properties. Increasing the PDMS content led to an increase in the fibre diameters. The increased PDMS content has a greater influence than the corresponding

increase in diameter of the fibre fillers as there is improvement in the properties despite the fact that the fibres are increasing in diameter.

Table 5.3: A summary of the mechanical properties of the reinforced silicone films, filled with non-woven as well as aligned fibre mats, prepared by the electrospinning of PAN-g-PDMS copolymer with varying PDMS content and 0 wt% MWCNT.

Samples containing 0 wt% MWCNT					
Samples		Non-Woven			
PDMS (wt%) ^c	σ_{\max} (MPa)	ϵ_{\max} ($\Delta L/L_0$)	W_{\max} (MPa.mm)	E (MPa) ($\times 10^{-3}$)	
Silicone ^d	0.3 ± 0.17	0.31 ± 0.17	1.1 ± 0.3	47 ± 4	
0.0	1.3 ± 0.21	1.13 ± 0.25	17.7 ± 3.1	57 ± 5	
^a 4.8	1.4 ± 0.23	0.94 ± 0.31	14.1 ± 3.2	113 ± 15	
^a 11.4	1.8 ± 0.18	1.47 ± 0.15	31.7 ± 2.4	101 ± 25	
^a 16.3	1.7 ± 0.06	1.37 ± 0.18	24.6 ± 2.9	190 ± 14	
^b 8.5	1.6 ± 0.09	1.32 ± 0.12	23.5 ± 1.9	149 ± 20	
^b 13.1	1.5 ± 0.11	1.24 ± 0.10	20.2 ± 2.0	119 ± 28	
Samples		Aligned			
PDMS (wt%)	σ_{\max} (MPa)	ϵ_{\max} ($\Delta L/L_0$)	W_{\max} (MPa.mm)	E (MPa) ($\times 10^{-3}$)	
Silicone ^d	0.3 ± 0.17	0.31 ± 0.02	1.1 ± 0.3	47 ± 4	
^a 4.8	2.3 ± 0.52	0.10 ± 0.02	2.3 ± 0.2	598 ± 10	
^a 11.4	3.0 ± 0.63	0.11 ± 0.02	2.5 ± 0.2	633 ± 11	
^a 16.3	2.9 ± 0.58	0.13 ± 0.04	4.3 ± 0.3	758 ± 19	
^b 8.5	2.7 ± 0.53	0.12 ± 0.03	3.1 ± 0.2	687 ± 24	
^b 13.1	2.3 ± 0.50	0.12 ± 0.02	3.1 ± 0.2	674 ± 18	

^a PDMS pendant group (1000 g.mol⁻¹)

^b PDMS pendant group (5000 g.mol⁻¹)

^c The wt% PDMS in the copolymer fibre fillers

^d Silicone control sample, therefore no fibre fillers present

The highest content PDMS fibres (16.3 wt%) do, however, show a decrease in ϵ_{\max} . This can be attributed to three main effects. The first effect is the large increase in PDMS content. PDMS is a soft, weak material, and will lead to a decrease in fibre strength when used as a filler at too high concentrations. The second effect is the decreased crystallinity (as shown in Table 5.1) which will also impact on the strength of the fibres. The 16.6 wt% PDMS fibres showed a significantly lower degree of crystallinity than the other fibre fillers. The third effect can be related to the large increase in fibre diameter relative to the other fibre fillers (as seen in Table 5.1). The larger diameters, in this case, lead to a significantly lower interfacial adhesion area between the matrix and filler. These three effects all contribute to weakening the highest content PDMS fibre fillers, which overrides the fact that these fibres should have better interaction due to their increased PDMS content.

Table 5.4: A summary of the mechanical properties of the reinforced silicone films, filled with non-woven as well as aligned fibre mats, prepared by the electrospinning of PAN-g-PDMS copolymer with varying PDMS content and 8 wt% MWCNT.

Samples containing 8 wt% MWCNT					
Samples		Non-woven			
PDMS (wt%) ^a	σ_{\max} (MPa)	ϵ_{\max} ($\Delta L/L_0$)	W_{\max} (MPa.mm)	E (MPa) ($\times 10^{-3}$)	
Silicone ^b	0.3 ± 0.17	0.31 ± 0.17	1.1 ± 0.3	47 ± 4	
4.8	1.5 ± 0.19	0.45 ± 0.16	6.9 ± 1.3	354 ± 37	
11.4	2.7 ± 0.16	1.35 ± 0.18	23.3 ± 1.5	327 ± 17	
16.3	3.4 ± 0.32	1.27 ± 0.17	18.7 ± 1.3	322 ± 9	
Samples		Aligned			
PDMS (wt%) ^a	σ_{\max} (MPa)	ϵ_{\max} ($\Delta L/L_0$)	W_{\max} (MPa.mm)	E (MPa) ($\times 10^{-3}$)	
Silicone ^b	0.3 ± 0.17	0.31 ± 0.02	1.1 ± 0.3	47 ± 4	
4.8	3.7 ± 0.62	0.10 ± 0.02	1.6 ± 0.5	568 ± 9	
11.4	3.3 ± 0.58	0.21 ± 0.04	4.7 ± 0.9	603 ± 9	
16.3	3.3 ± 0.77	0.23 ± 0.03	5.5 ± 1.2	510 ± 13	

^a The wt% PDMS in the copolymer fibre fillers

^b Silicone control sample, therefore no fibre fillers present

The two composites of the 5000 g.mol⁻¹ PDMS series (8.5 wt% PDMS and 13.1 wt% PDMS) both showed improved strain relative to the lower content (4.8 wt%, 1000 g.mol⁻¹) PDMS fibres. These strain values were, however, lower than those of the corresponding higher content (11.4 wt% and 16.3 wt%, 1000 g.mol⁻¹) PDMS fibres. These fibres did, however, show decreased crystallinity compared to those in the 1000 g.mol⁻¹ series, as well as larger mean fibre diameters. This explains the lower strain performance of these fibres relative to the other PDMS series. The MWCNT filled and unfilled aligned fibre composites present ϵ_{\max} values that are lower than the unfilled silicone control sample. However, the non-woven mat filled composites show dramatic improvement in extensibility. In both the unfilled and MWCNT filled non-woven mat series, the ϵ_{\max} values far outperform those of the unfilled silicone control sample and that of the aligned fibre samples. It can be seen that the composite containing 11.4 wt% PDMS (CP41) (unfilled, non-woven) an elongation of 147% is achieved, as compared to the 31% of unfilled silicone. This is a 470% improvement in the extensibility. The corresponding MWCNT filled non-woven fibre mats (11.4 wt% PDMS) also proved to perform remarkably well, with a maximum ϵ_{\max} value of 135%. The maximum stress values at break (σ_{\max}) must be studied before explaining the differences in behaviour between the non-woven and aligned fibre mats. The σ_{\max} relates to the strength of the material and the values are included in Tables 5.3 and 5.4.

The increasing σ_{\max} values correspond to an increasing PDMS content. This once again highlights the increased compatibility between the filler and the matrix due to the PDMS

compatibilising components. The best performing composites (strength-wise) are those containing the 4.8 wt% and 11.4 wt% PDMS graft copolymer (1000 g.mol⁻¹ PDMS, CP40 and CP41) fibre fillers. This can also be ascribed to the increased fibre diameter and decreased crystallinity. The strength of the filled silicone composites outperforms the unfilled silicone control sample in all cases, as opposed to the strain values where the aligned samples present lower extensibility. A “reversal” in the behaviour is also evident in Tables 5.3 and 5.4, where the aligned fibre fillers are presenting higher σ_{\max} values than their non-woven analogues. The 8 wt% MWCNT filled aligned fibre filler of 4.8 wt% PDMS (CP40) presents a value of 3.71 MPa, compared to that of 0.33 MPa for the unfilled silicone elastomer. This is an 1100% improvement in the stress at break of the silicone composite. The samples containing 4.8 wt% and 11.4 wt% PDMS (CP41 and CP42) (MWCNT filled) as well as their unfilled analogues all have vastly improved σ_{\max} values. The fibres of the 5000 g.mol⁻¹ PDMS series, show very similar behaviour to the 1000 g.mol⁻¹ analogues. The σ_{\max} values are, however, slightly lower for these two composites (Table 5.3, the 8.5 and 13.1 wt% PDMS composites with 5000 g.mol⁻¹ PDMS). The decreased crystallinity and increased diameters of these fibres are responsible for this decrease in strength relative to the 1000 g.mol⁻¹ PDMS analogues.

Figure 5.9 shows the fracture surfaces of a non-woven mat containing no MWCNTs. The fibres exhibit ductile behaviour, and yielding and necking of the fibre fillers is clearly visible. The lower PDMS content fibres (4.8 wt%) do not exhibit the same dramatic ductile yielding as the 11.4 wt% and 16.3 wt% PDMS (1000 g.mol⁻¹) containing fibre fillers. The tapering of the fractured fibres in the 4.8 wt% sample towards the fractured tip does, however, present a ductile failure pattern. PAN fibres are known to present a more ductile failure pattern prior to oxidation to form carbon fibres^{15,16}. Ji *et.al.*¹⁵ compared PAN precursor fibre fracture surfaces to the surfaces of fibres oxidised at different stages. The precursor fibres presented a rough, granular fracture surface consistent with ductile failure. The elongation at break was shown to be about 9.8% for the unoxidised fibres. They found no evidence for fibre necking as observed in the FE-SEM images of our fibres. The remarkable strain enhancements of our non-woven fibre composites (MWCNT filled and unfilled) is a highly significant result, and requires special attention. The contrasting behaviour of the aligned fibre composites will be discussed later.

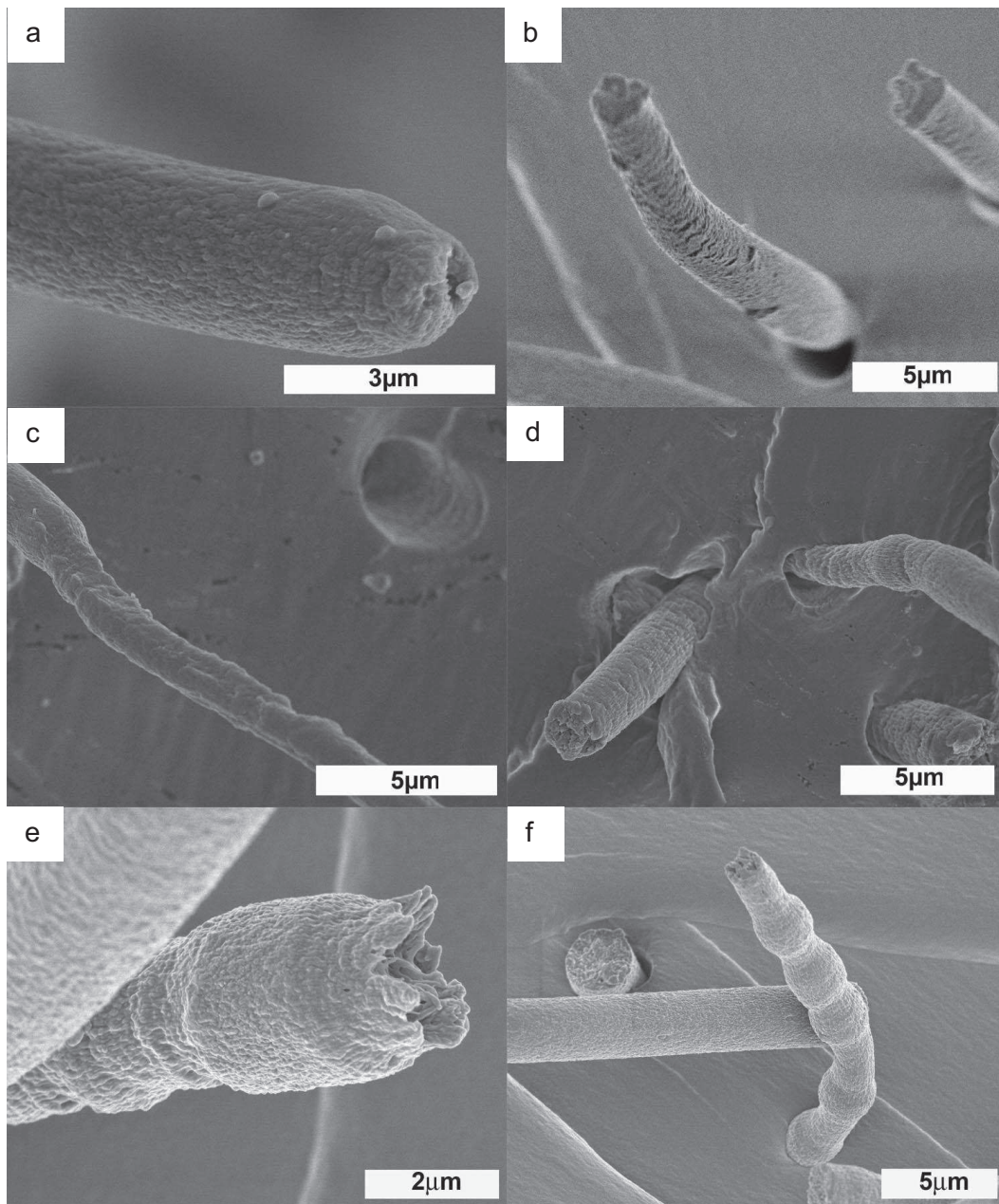


Figure 5.9 : FE-SEM images of non-woven fibre filled silicone composite fracture surfaces of (a) and (b) 4.8 wt% PDMS, (c) and (d) 11.4 wt% PDMS and (e) and (f) 16.3 wt% PDMS containing copolymer fibres (1000 g.mol^{-1}) after tensile failure.

The enhanced strain properties are partly due to the notably ductile behaviour of these fibres. The ductile behaviour, presented as yielding and necking of the fibres, is necessary for the uptake of mechanical stress from the composite matrix to the reinforcing fillers. Interfacial bonding between the fibre filler and the matrix is essential in the transfer of load to the deforming fibres. The mechanism of the composite failure greatly affects the strain

behaviour. The ductile behaviour of the non-woven fibre fillers, and then the mechanism of sample failure are now discussed.

The increased ductility of the non-woven fibres (Figure 5.9) is related to the PDMS content of the fibre precursor material as well as the porous structure that the amphiphilic material affords the electrospun fibres. The visibly nanoporous structure of the fibres has been discussed in detail in Chapter 4 of this work. Work by Kim *et. al.*¹⁷ studied electrospun fibres of PMMA with Na-MMT clay particles and showed that the electrospun nanocomposite fibres undergo ductile failure as opposed to the brittle failure of conventional fibre composites. The dramatic increase in fibre elongation and necking achieved in their work is ascribed to the porous nature of the nanofibres. The pores act as stress concentrators during the deformation. *In situ* TEM images on the stressed fibres show that the pores lead to stress concentration and overlapping of the stress fields which, suppress craze formation and lead to necking of the nanofibres. The diameters of the fibres in our study are indeed larger than those in the study of Kim *et. al.*¹⁷, but remained highly porous. The porosity of the fibres in our study was as a result of the amphiphilic nature of the precursor material.

Pull-out of the fibres from the matrix is also clearly evident in Figure 5.9. Hsueh¹⁸ modelled the pull-out of ductile fibres from a brittle matrix using a shear lag model. Figure 5.10 obtained from reference¹⁸ shows the diagrammatic representation of the shear lag model proposed.

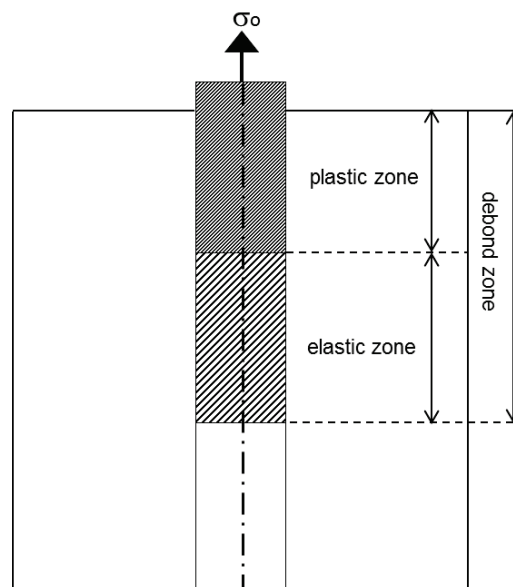


Figure 5.10 : Diagrammatic representation of the shear lag model for modeling the pull-out behaviour of a ductile fibre in a brittle matrix as proposed in work by Hsueh¹⁸.

Tardiff¹⁹ also modelled the behaviour of ductile fibres in a brittle matrix by studying crack formation and the closing strength of the crack by embedded fibre fillers. Hsueh considered both Poisson's contraction of the fibre and Coulomb friction of the debonded interface. He found that when the fibre has a finite embedded length, necking prior to full pull-out of the fibre was required to optimise the toughening of a brittle matrix due to plastic deformation of the fibres. The fibre debonding from the matrix occurs when the applied stress overcomes the interfacial bond strength between the matrix and the fibre. The debonding length increases as the stress on the specimen increases until the fibre yields. Necking commences once the stress reaches a critical level. This model can be used to explain the increase in strain of the composites before failure, although the matrix used in our study was not brittle. However, "brittle-like" failure of the silicone matrix was still observed (low elongations and stress due to the weakness of the material).

The porous surface morphology of the fibre fillers is also clearly evident in Figure 5.9. This is probably due to the amphiphilic nature of these electrospun solutions. More importantly, one can see a "templating effect" between the fibres and the matrix, where the matrix has a surface morphology identical to that of the fibres. This excellent result once again indicates a close interaction between the fibre fillers and the silicon matrix, resulting in total wetting of the fillers and prevention of void formation. Hsueh¹⁸ also reported that coulomb friction upon interfacial debonding contributes to the increased mechanical properties of the sample. The energy required to "pull-out" a rough fibre, like those prepared in this study, from the matrix would require more frictional force than a smooth fibre, which also contribute to the improved mechanical properties. Tardiff¹⁹ noted that two significant factors affecting the composite reinforcement were the strength and ductility or uniform elongation of the fibres.

Figure 5.11 shows the FE-SEM images of the fracture surface of a MWCNT containing non-woven mat filled silicone composite. The fracture showed slight differences compared to the unfilled compound. No visible indications of the same necking and yielding mechanisms present in the samples shown in Figure 5.9 are evident in this case. Slight necking is indicated in Figure 5.11 (circle marked B) for some of the fibres. This is related to the MWCNTs which, while they increase the strength of the fibres, they make them much stiffer, which hinders the ductile failure mechanism. The non-woven mats without MWCNTs, therefore, have better strain properties than the MWCNT filled non-woven mats. The presence of fibre "pull-out", as mentioned earlier, still lends high strain values to the nanotube filled composites. The "templating effect" of the porous fibres on the silicone matrix is again evident in these samples. The increased stiffness due to the nanotubes also lends increased "brittle-like" behaviour to these fibres, evident from the snapped fibre indicated in

Figure 5.11 (circle marked A). The bright white spots present across the fibre fracture surfaces are due to the MWCNTs. They appear as very bright granules on the FE-SEM images.

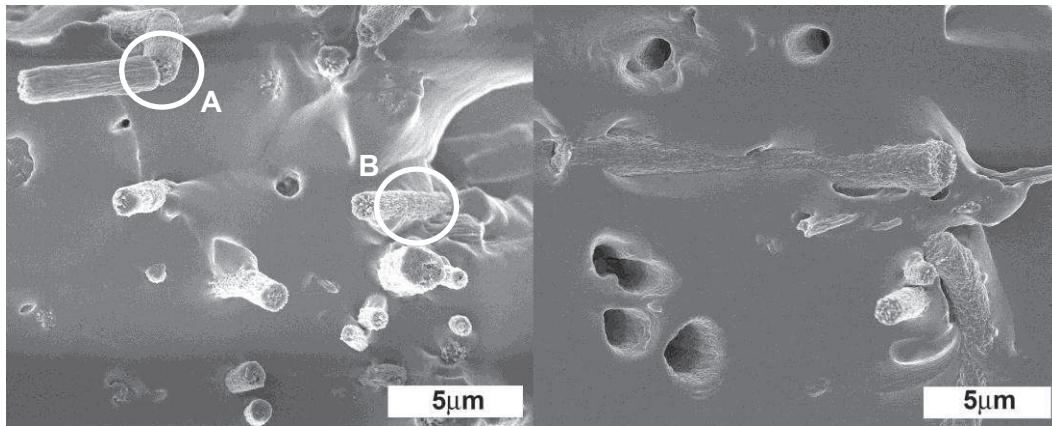


Figure 5.11 : FE-SEM images of non-woven fibre filled silicone composite fracture surfaces of 11.4 wt% PDMS containing copolymer fibres ($1000 \text{ g}\cdot\text{mol}^{-1}$) containing 8 wt% MWCNT after tensile failure.

The fibre filler behaviour contributes greatly to the increased elongation properties of these composites, but the mechanism of failure also plays a large role. The unfilled silicone fails at very low extensions. The fibre ductility alone is unable to fully explain why such large strain enhancements are possible. The extremely enhanced strain properties suggest that the composites do not simply fracture in one place, and remain intact by bridging of the fibre fillers in simply one fracture zone. The more likely scenario is that of multiple fracture sites occurring throughout the composite tensile specimen. Figure 5.12 shows optical microscopy images (light microscope) of a tensile test specimen after fracture. In Figure 5.12 (c) and (d) the entire length of the sample specimen neck shows an underlying network of failure plains (indicated by the arrows). These network structures were not as evident on the unstressed test specimens (no evidence) or the aligned specimens (very little evidence) as shown typically in Figure 5.12 (a) and (b). Interestingly, the samples appear smooth when imaged using SEM, confirming that the fracture network is present within the composite sample.

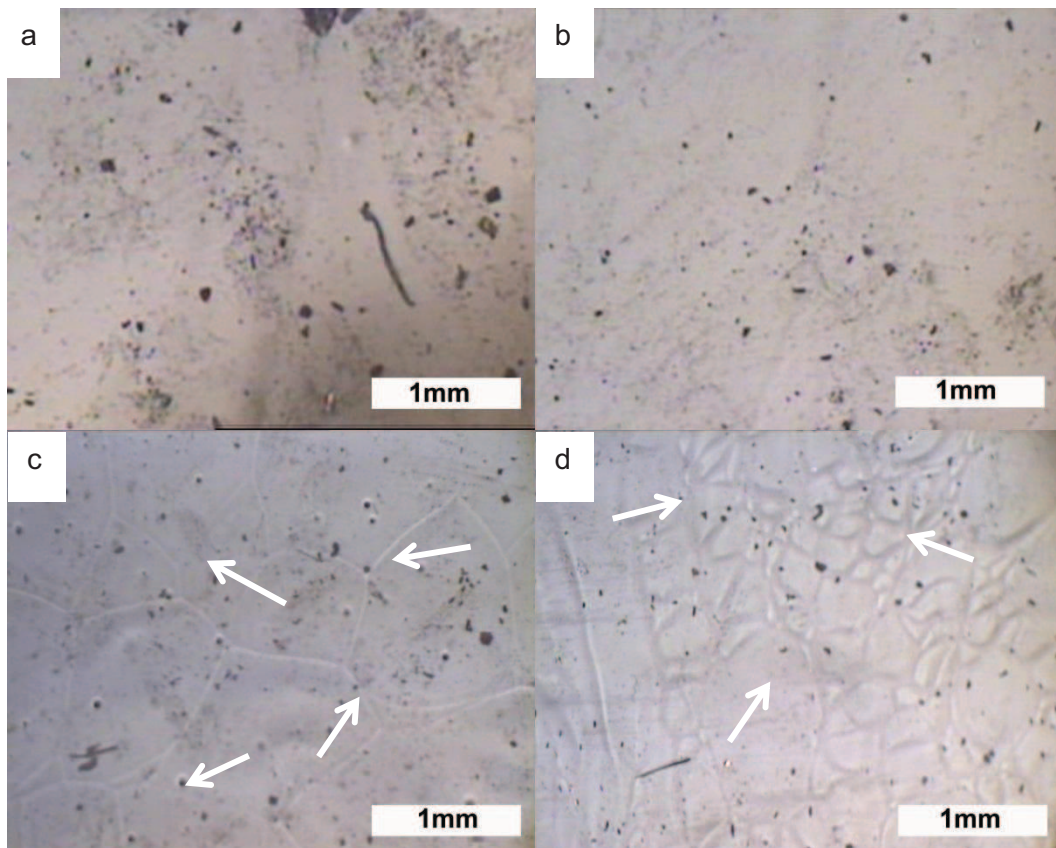


Figure 5.12 : Typical optical microscopy images of (a) and (b) tensile fractured unfilled silicone composites and (c) and (d) tensile fractured non-woven composite sample specimen.

Figure 5.13 shows the SEM images of a surface crack that was found on one of the tensile fractured samples. The crack appears shallow in certain regions. The appearance of protruding fibres (indicated by arrows) was evidence of bridging fibres and the associated absorbance of energy of the advancing crack. This result suggests that as the non-woven mat filled silicon films are stressed, the fibres are continually absorbing the applied stress and hindering crack propagation. The fibres are aligned randomly, which makes them more effective in countering the propagation of the fracture planes and bridging the advancing gaps. After failure of a fibre there are others, as yet unstressed, that are capable of taking over the load. Therefore, as fibres fail, there are others that can “replace” them and continue countering the strain. This continual fibre “fracture and replacement” occurs over a longer period due to the random arrangement of the fibres, allowing more time for the ductile yielding and necking of the fibre fillers. The entire sample is undergoing fracture at multiple sites throughout the sample, as evidenced by the network of lines in Figure 5.12 (a) and (b). The fibres are capable of preventing complete failure at these multiple sites due to their ductile nature, strength and random arrangement. At some point one of the fracture areas

will not have sufficient fibre fillers present to continue keeping the composite specimen intact, and final sample failure occurs. The behaviour of these non-woven composites shows a highly complex failure mechanism, which helps to explain the extreme strain enhancements of the non-woven mat filled silicone films.

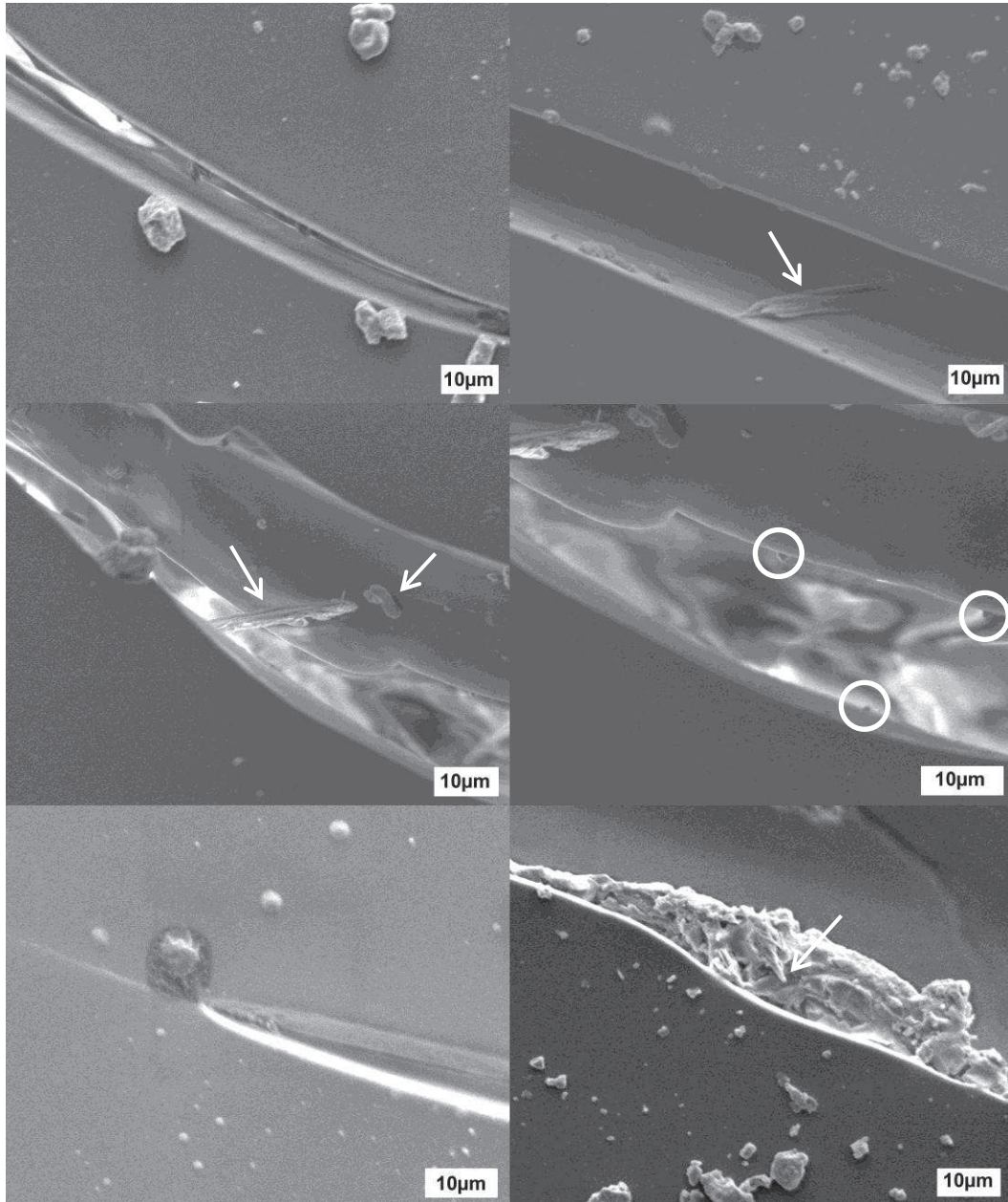


Figure 5.13 : SEM images of a surface crack present on a tensile fractured non-woven sample specimen at different magnifications.

The behaviour of the aligned composites as mentioned earlier was markedly different from the non-woven mat filled composites. The samples showed increased strength in most

cases, but dramatic decreases in elongation. Data for the stiffness of the aligned fibres are also presented in Tables 5.3 and 5.4. There is a dramatic difference in the stiffness of the aligned fibre and the non-woven fibre composites; the aligned fibre composites tend to be twice as stiff as the MWCNT filled non-woven mats and approximately 400% as stiff as the unfilled non-woven mats. The increased stiffness of these fibres relates to their arrangement within the matrix. The mechanism of failure in the case of the aligned composite differs from that of the non-woven analogues, resulting in elongations lower than in the unfilled silicone matrix in some cases.

The fact that the aligned fibres are aligned in the direction of the applied stress allows for a much stiffer composite. The MWCNT filled non-woven composites are slightly stiffer due to the presence of the aligned MWCNT particles, which are known to stiffen composites^{9,20,21}. Figure 5.14 and Figure 5.15 show FE-SEM images of the fracture surfaces of the aligned fibre composites. Figure 5.14 shows the unfilled fibres and Figure 5.15 shows the MWCNT filled fibres.

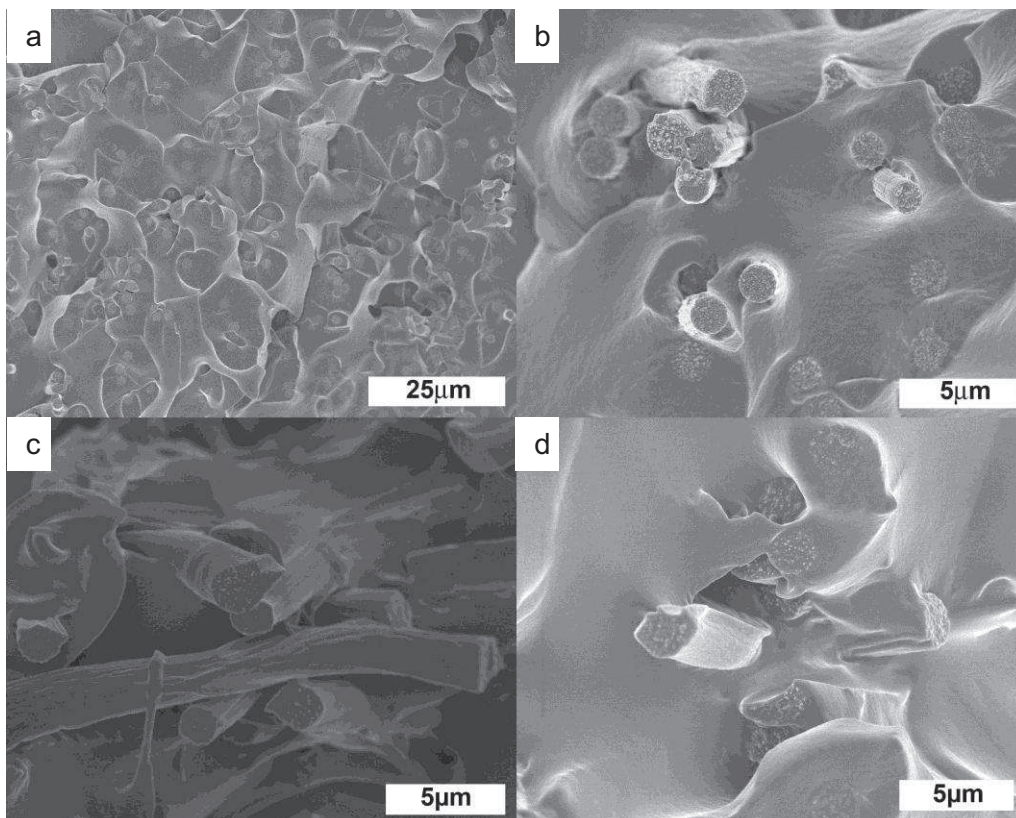


Figure 5.14 : FE-SEM images of aligned fibre filled silicone composite fracture surfaces of (a) and (b) 11.4 wt% PDMS and (c) and (d) 16.3 wt% PDMS containing copolymer fibres ($1000 \text{ g}\cdot\text{mol}^{-1}$ series) after tensile failure.

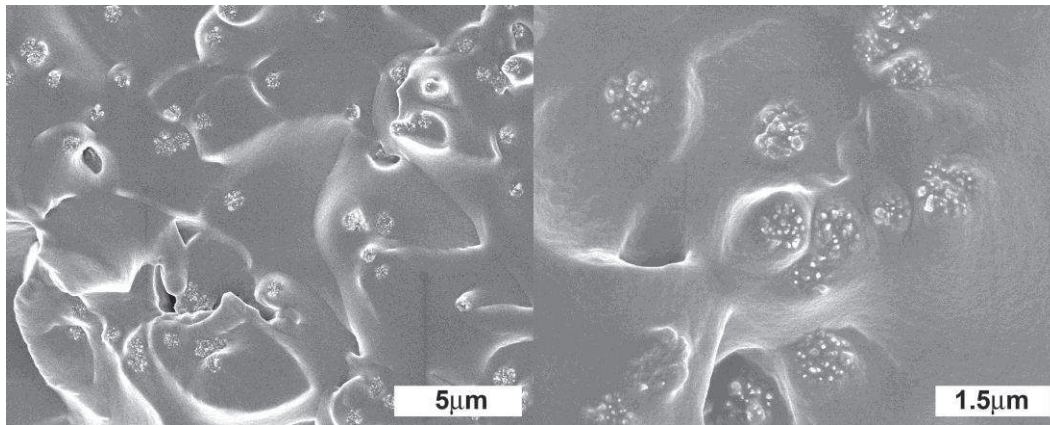


Figure 5.15 : FE-SEM images of aligned fibre filled silicone composite fracture surfaces of 11.4 wt% PDMS containing fibres ($1000 \text{ g}\cdot\text{mol}^{-1}$) with 8wt% MWCNTs after tensile failure.

Noticeable differences to the fracture surfaces of the non-woven analogues are evident in these images. Little to no fibre “pull-out” is evident. No indication of necking or yielding mechanisms is clear. The silicone matrix is weak yet elastomeric in nature, which has implications on the failure mechanism of the aligned fibre composites. The poor elongation properties as well as the fracture surface analysis in Figure 5.14 and Figure 5.15 suggest that the fibres fail prior to total failure of the silicone matrix.

The silicone matrix is capable of elastically distorting (at very low extensions), until a critical point, at which the matrix fails. The stiff fibre fillers are arranged in the direction of the applied stress and more fibres undergo load at the same time, as for the randomly oriented non-wovens. It is not unclear whether all fibres undergo stress simultaneously, as it is unlikely that the aligned fibres span the entire length of the tensile specimens. The increased uniformity of these fibres relative to the non-woven mats does, however, dramatically increase the strength and stiffness of the composite. The matrix, capable of elastic behaviour, stretches to a certain point. The fibres appear to fracture within the silicone matrix as it stretches. The fibres fracture at approximately the same time due to their uniaxial arrangement within the composite specimen. The silicone fractures shortly after, resulting in elongations that are lower than those of the unfilled silicone specimens. The internal fibre fracture mechanism results in the lack of fibre “pull-out”, consistently shown in the non-woven analogues. The fast and simultaneous fracture of the fibres does not allow the same ductile yielding to occur as is evident in the non-woven composites. The inherent fibre filler material is, therefore, not the only parameter that determines the final composite properties. The failure mechanism, as related to the arrangement of the fibre fillers in the matrix, is extremely important in understanding the mechanical behaviour of these composite

materials. The aligned fibres containing 8 wt% MWCNTs as shown in Figure 5.15 present the same “in plane” fracture surfaces of the fibres in the silicone matrix. The nanotubes are visible as bright white granules in the FE-SEM images. The indirect distribution of the nanotubes in the matrix is evident as they appear consistently in the fracture planes of the fibres.

The maximum energy (W_{max}) results in Tables 5.3 and 5.4 were also used as a measure of the toughness of the composites. This energy value is determined from the area below the stress strain curve. It appears that the non-woven filled materials outperform the aligned counterparts in this respect. The unfilled non-woven fibre composites showed the highest toughness where the sample containing 11.4 wt% PDMS (CP41) at 0.127 J showed a 3 100% improvement, compared to the 0.004 J for the unfilled silicone elastomer. The significant enhancement in the strain values of the non-woven composites lend very high toughness to these reinforced silicone specimens. The increase in PDMS content of the copolymer has a corresponding increase in the W_{max} values. This confirms the excellent distributive and compatibilising properties of the PDMS components of the copolymer fibres once again.

Finally we looked at the series of MWCNT composites, where we varied the content of MWCNT filler from 8 wt% to 32 wt% (refer to Tables 5.4, 5.5 and 5.6).

Table 5.5: Summary of the mechanical properties of the reinforced silicone films, filled with non-woven as well as aligned fibre mats, prepared by the electrospinning of PAN-g-PDMS copolymer with varying PDMS content and 16 wt% MWCNTs.

Samples containing 16 wt% MWCNT					
Samples		Non-woven			
PDMS (wt%) ^a	σ_{max} (MPa)	ϵ_{max} ($\Delta L/L_0$)	W_{max} (MPa.mm)	E (MPa) ($\times 10^{-3}$)	
Silicone ^b	0.3 \pm 0.17	0.31 \pm 0.17	1.1 \pm 0.3	47 \pm 4	
11.4	0.9 \pm 0.25	0.20 \pm 0.03	2.8 \pm 0.4	258.55 \pm 1.89	
16.3	1.4 \pm 0.27	0.29 \pm 0.01	3.4 \pm 0.4	601.71 \pm 0.91	
Samples		Aligned			
PDMS (wt%) ^a	σ_{max} (MPa)	ϵ_{max} ($\Delta L/L_0$)	W_{max} (MPa.mm)	E (MPa) ($\times 10^{-3}$)	
Silicone ^b	0.3 \pm 0.17	0.31 \pm 0.02	1.1 \pm 0.3	47 \pm 4	
11.4	1.9 \pm 0.27	0.14 \pm 0.02	2.9 \pm 0.3	744 \pm 18	
16.3	1.0 \pm 0.23	0.10 \pm 0.01	1.5 \pm 0.1	815 \pm 20	

^a The wt% PDMS in the copolymer fibre fillers

^b Silicone control sample, therefore no fibre fillers present

The strain results show a decrease in values as the MWCNT content is increased for the non-woven mat filled composites. The non-nanotube containing composites present the

highest strain values, and the 8 wt% MWCNT filled composites show only a slight decrease in the strain behaviour. The 16 wt% and 32 wt% MWCNT filled composites show similar strain values, although significantly lower than for the 0 and 8 wt% composites. As mentioned earlier, this is due to an increase in the stiffness of the material. The strength (σ_{\max}) improved as the MWCNT content increased from 0 to 8 wt% in the fibre fillers, but decreased when moving to the 16 and 32 wt%. Again, the 16 and 32 wt% MWCNT filled composites presented similar values. Possible aggregation of the filler particles due to overloading of the composite fibres most likely resulted in these decreased values. This, in turn, affects the toughness of the composites, which decreases when moving from the 0 to the 8 wt% nanotube filled composites. The 16 and 32 wt% nanotube composites show a significant drop in toughness. This is expected, due to the strain and strength values. Note that these results apply to the non-woven mat filled composites only.

Table 5.6: Summary of the mechanical properties of the reinforced silicone films, filled with non-woven as well as aligned fibre mats, prepared by the electrospinning of PAN-g-PDMS copolymer with varying PDMS content and 32 wt% MWCNTs.

Samples containing 32 wt% MWCNT				
Samples		Non-woven		
PDMS (wt%) ^a	σ_{\max} (MPa)	ϵ_{\max} ($\Delta L/L_0$)	W_{\max} (MPa.mm)	E (MPa) ($\times 10^{-3}$)
Silicone ^b	0.3 ± 0.17	0.31 ± 0.17	1.1 ± 0.3	47 ± 4
11.4	0.9 ± 0.05	0.21 ± 0.02	3.37 ± 0.27	133.94 ± 2.08
16.3	1.3 ± 0.14	0.45 ± 0.01	6.97 ± 0.46	328.43 ± 0.94
Samples		Aligned		
PDMS (wt%) ^a	σ_{\max} (MPa)	ϵ_{\max} ($\Delta L/L_0$)	W_{\max} (MPa.mm)	E (MPa) ($\times 10^{-3}$)
Silicone ^b	0.3 ± 0.17	0.31 ± 0.02	1.1 ± 0.	47 ± 4
11.4	3.1 ± 0.34	0.14 ± 0.02	4.53 ± 0.46	811 ± 19
16.3	1.6 ± 0.46	0.17 ± 0.03	2.94 ± 0.35	395 ± 16

^a The wt% PDMS in the copolymer fibre fillers

^b Silicone control sample, therefore no fibre fillers present

The aligned fibre composites present a different behaviour to the non-woven analogues. It appears that the alignment of the nanofibres has a greater effect than the inclusion of nanotubes on the strength and strain properties of the composites. In the cases of the aligned composites the strain values are dramatically lower than for the non-wovens as explained earlier. There does not appear to be significant differences in the strain values reported for the different nanotube loadings compared to the non-nanotube filled composites. There is, however, a slight increase moving to the 8 wt% nanotube filled

samples but then a decrease moving to the 16 and 32 wt% nanotube composites. The σ_{\max} shows a similar trend, there is an initial increase in strength moving from the 0 to 8 wt% nanotube loading, followed by a significant decrease moving to the 16 and 32 wt% samples. It must be noted that the 11.4 wt% PDMS fibre filler containing 32 wt% nanotubes offshoots this trend, showing a high σ_{\max} value. It would appear that this sample has less agglomeration of nanotubes than the other high nanotube containing composites. The reason for this is unclear at this stage and could be anomalous, due to the erratic distribution of nanotubes at such high loadings.

The stiffness did, however, increase significantly, as presented in Tables 5.4, 5.5 and 5.6 for the nonwoven mat composites from the 0 to 16 wt% nanotube loaded composites. This is expected due to the increased stiffness that nanotubes are known to impart on composite specimens. The 32 wt% sample shows a marked decrease in stiffness, compared to the 8 and 16 wt% specimens. This can again be attributed to an increase in filler agglomeration at these high loadings. The aligned fibre composites, as discussed earlier, show dramatically higher stiffness values than the non-woven composites. It would appear that the alignment of the fibres dominates the increase in modulus attributed to the presence of nanotubes. The 0 and 8 wt% nanotube composites present modulus values similar to those of the aligned fibre composites. There is, however, a small increase in modulus moving to the 16 and 32 wt% MWCNT containing composites, which can be attributed to the stiff nanotube fillers. The 16.3 wt% PDMS composite fibre containing 32 wt% MWCNT shows a deviation from the trend once again. It would appear that at such high loadings, the distribution of nanotubes is highly erratic, resulting in composites with deviating physical properties.

A dramatic increase in stiffness as the MWCNT content increased for the aligned fibre mat composites is evident. The non-woven mats show slightly decreased stiffness relative to the aligned fibres. The increases in stiffness of these materials are, however, still significant. The stiffening effect of the MWCNTs plays a larger role when studying the aligned fibre mats. This could be related to the fact that the MWCNTs are aligned in the direction of the electrospun fibre axis, therefore, additionally in the direction of load on the test specimen.

5.1.8 Summary of the silicone nano/composites and comparison to literature

PDMS does not possess very good mechanical properties and tends to be reinforced with filler material. In most cases PDMS is filled with materials such as carbon black and silica²²⁻²⁴ at relatively high filler contents. There is not much information available in literature on the production of silicone nanocomposites other than the traditionally filled silicones as

mentioned. The *in situ* precipitation of silica via the sol-gel process is most widely used for reinforcing PDMS films. Using functionalised silica particles also aids in the interaction between the matrix and filler particles²⁵. Polymerising a glassy polymer such as PS²⁶ can also yield reinforced materials with increased properties. Some reported silicone nanocomposites include using HTiNbO₅ inorganic fillers²⁷, layered mica silicates²⁸, nano-clay dispersion using supercritical CO₂ dispersion²⁹ or intercalation of montmorillonite clay and even MWCNTs³⁰. A brief summary of the best performing composites is presented in this section along with a comparison to electrospun fibre filled composites prepared in literature. Literature on these types of materials is very limited and was presented in Chapter 2. This section serves to put the composites prepared in this work in perspective to others. It is difficult to do this directly as the polymer matrices and fillers differ, but there are a few key differences in the mechanical properties that should be highlighted. The composites produced in this project showed vast improvements in various properties depending on the type of composite (nonwoven/aligned or MWCNT filled or unfilled) the properties are summarised briefly in Table 5.. It is clear from the rest of the data, that the best performing composite prepared in this work was that of non-woven unfilled fibre filled material (CP41). In most cases the aligned composites filled with MWCNTs showed the best improvement in tensile strength and modulus, but a major decrease in strain and additionally material toughness (W_{max}). These results are similar to those obtained from previous composites as shown in literature. In this study, however, the aligned nanotube filled composites still presented dramatic increases in the tensile strength and stiffness values. In the work of Kim and Reneker³¹, Bergshoef and Vasco³², Tang and Liu³³, Pinho *et. al.*³⁴, Fong and colleagues³⁵, and Lin *et. al.*³⁶ the same decrease in strain at break were evident, with smaller increases in strength at break, stiffness and toughness.

Table 5.7 : Summation of the best performing silicone nano/composites prepared in this project according to the measured mechanical results after tensile testing.

Silicone composite film			Mechanical properties % increase ^a			
Fibre material	Mat type	MWCNT	σ_{max}	E	ϵ_{max}	W_{max}
CP41	non-woven	0 wt%	558%	214%	470%	3100%
CP40	aligned	8 wt%	1100%	1200%	-310%	175%
CP42	aligned	16 wt%	655%	1700%	-330%	164%

^a The percentage increase is that of the composite relative to that of an unfilled PDMS film.

The nylon-6 reinforced epoxy resins of Bergshoef and Vancso³² showed the most dramatic increases in stiffness (3640% increase) and tensile strength (290% increase). This was

obtained at a fibre filler content of 3.9 wt%. The elongation at break did, however, decrease from 80% to 3% (2666% decrease). Only two works published by Causin and co-workers³⁷ and Swart *et. al.*³⁸ showed increased mechanical properties including an increase in elongation at break. Causin³⁷ showed a 128% increase in ϵ_{\max} as well as 150% increase in stiffness and a 113% increase in σ_{\max} . Swart *et. al.*³⁸ showed an increase in ϵ_{\max} of 271% and a 1137% increase in W_{\max} . Composite CP41 shown in Table 5. presented an even more dramatic increase in the ϵ_{\max} of 470% increase over the unfilled material which is a highly significant result relative to others in published literature. The corresponding increase in toughness by 3100% is also what sets this composite apart from the others. Significant increases in the σ_{\max} and stiffness are accompanied by dramatically enhanced ϵ_{\max} and W_{\max} values.

5.2 References

- (1) Hughes, J. D. H. *Compos. Sci. Technol.* **1991**, *41*, (1), 13-45.
- (2) Chen, P. W., Chung, D. D. L. *Composites* **1993**, *24*, (1), 33-52.
- (3) Donnet, J. B., Ehrburger, P. *Carbon* **1977**, *15*, (3), 143-152.
- (4) Fennessey, S. F., Farris, R. J. *Polymer* **2004**, *45*, (12), 4217-4225.
- (5) Zussman, E., Chen, X., Ding, W., Calabri, L., Dikin, D. A., Quintana, J. P., Ruoff, R. S. *Carbon* **2005**, *43*, (10), 2175-2185.
- (6) Chen, X., Gardella Jr, J.A., Kumler, P.L. *Macromolecules* **1993**, *26*, 3778-3783.
- (7) Chen, X., Gardella Jr, J.A., Kumler, P.L. *Macromolecules* **1992**, *25*, 6631-6637.
- (8) Meng, L., Fu, C., Lu, Q. *Prog. Nat. Sci.* **2009**, *19*, (7), 801-810.
- (9) Hou, H., Ge, J. J., Zeng, J., Li, Q., Reneker, D. H., Greiner, A., Cheng, S. Z. D. *Chem. Mater.* **2005**, *17*, (5), 967-973.
- (10) Ge, J. J., Hou, H., Li, Q., Graham, M. J., Greiner, A., Reneker, D. H., Harris, F. W., Cheng, S. Z. D. *J. Am. Chem. Soc.* **2004**, *126*, (48), 15754-15761.
- (11) Callies, M., Quere, D. *Soft Matter* **2005**, *1*, (1), 55-61.
- (12) Swart, M., Mallon, P. E. *Pure Appl. Chem.* **2009**, *81*, (3), 495-511.
- (13) Marmur, A. *Langmuir* **2004**, *20*, (9), 3517-3519.
- (14) Teo, W. E., Ramakrishna, S. *Nanotechnology* **2006**, *17*, (14), R89-R106.
- (15) Ji, M., Wang, C., Bai, Y., Yu, M., Wang, Y. *Polym. Bull.* **2007**, *59*, (4), 527-536.

- (16) Ji, M., Wang, C., Bai, Y., Yu, M., Wang, Y. *Polym. Bull.* **2007**, *59*, (3), 381-390.
- (17) Kim, G., Lach, R., Michler, G. H., Chang, Y. *Macromol. Rapid Commun.* **2005**, *26*, (9), 728-733.
- (18) Hsueh, C. *J. Mater. Sci.* **1994**, *29*, (18), 4793-4801.
- (19) Tardiff, G. *Engineer. fracture mech.* **1973**, *5*, 1-10.
- (20) Ji, J., Sui, G., Yu, Y., Liu, Y., Lin, Y., Du, Z., Ryu, S., Yang, X. *J. Phys. Chem. C* **2009**, *113*, (12), 4779-4785.
- (21) Moniruzzaman, M., Winey, K. I. *Macromolecules* **2006**, *39*, (16), 5194-5205.
- (22) Kurian, T., De, P. P., Khastgir, D., Tripathy, D. K., De, S. K., Peiffer, D. G. *Polymer* **1995**, *36*, (20), 3875-3884.
- (23) Yatsuyanagi, F., Suzuki, N., Ito, M., Kaidou, H. *Polymer* **2001**, *42*, (23), 9523-9529.
- (24) Mark, J. E. *Acc. Chem. Res.* **2006**, *39*, (12), 881-888.
- (25) Jia, L., Du, Z., Zhang, C., Li, C., Li, H. *Polym. Eng. Sci.* **2007**, *48*, (1), 74-79.
- (26) Fu, F. S., Mark, J. E. *J. Appl. Polym. Sci.* **1989**, *37*, (9), 2757-2766.
- (27) Beigbeder, A., Bruzaud, S., Mederic, P., Aubry, T., Grohens, Y. *Polymer* **2005**, *46*, (26), 12279-12286.
- (28) Burnside, S. D., Giannelis, E. P. *Chem. Mater.* **1995**, *7*, (9), 1597-1600.
- (29) Horsch, S., Serhatkulu, G., Gulari, E., Kannan, R. M. *Polymer* **2006**, *47*, (21), 7485-7496.
- (30) Beigbeder, A., Linares, M., Devalckenaere, M., Degee, P., Claes, M., Beljonne, D., Lazzaroni, R., Dubois, P. *Adv. Mater.* **2008**, *20*, (5), 1003-1007.
- (31) Kim, J., Reneker, D. H. *Polym. Compos.* **1999**, *20*, (1), 124-131.

- (32) Bergshoef, M. M., Vancso, G. J. *Adv. Mater.* **1999**, *11*, (16), 1362-1365.
- (33) Tang, C., Liu, H. *Composites, Part A* **2008**, *39A*, (10), 1638-1643.
- (34) Pinho, E. D., Martins, A., Araujo, J. V., Reis, R. L., Neves, N. M. *Acta Biomater.* **2009**, *5*, (4), 1104-1114.
- (35) Fong, H. *Polymer* **2004**, *45*, (7), 2427-2432.
- (36) Lin, S., Cai, Q., Ji, J., Sui, G., Yu, Y., Yang, X., Ma, Q., Wei, Y., Deng, X. *Compos. Sci. Technol.* **2008**, *68*, (15-16), 3322-3329.
- (37) Neppalli, R., Marega, C., Marigo, A., Bajgai, M. P., Kim, H. Y., Causin, V. *Eur. Polym. J.* **2010**, *46*, 968-976.
- (38) Swart, M., Olsson, R. T., Hedenqvist, M. S., Mallon, P. E. *Polym. Eng. Sci.* **2010**,.

Chapter 6

Conclusions and future prospects

6.1 Conclusions

The first main objective entailed the synthesis of novel precursor materials for the electrospinning of fibre fillers for the reinforcement of silicone matrices. Novel amphiphilic graft copolymers of PAN-g-PDMS were successfully synthesised using conventional free radical copolymerisation via the grafting through (macromonomer) technique. A series of materials were synthesised with a varying amount of PDMS macromonomer in the feed. PDMS macromonomers of two different molecular weights were also used ($1000 \text{ g}\cdot\text{mol}^{-1}$ and $5000 \text{ g}\cdot\text{mol}^{-1}$). The reaction conditions were optimised for the precipitation polymerisation reaction. $^1\text{H-NMR}$ was used to determine the successful incorporation and amount of PDMS incorporated into the synthesised precursor material. Chromatographic (SEC) results indicated that the molecular weights obtained were typical of an uncontrolled free radical polymerisation. The molecular weights achieved were also in line with those needed for successful electrospinning of the material. Homo-PDMS (unreacted PDMS macromonomer) was successfully extracted from the graft material and homo-PAN. A gradient elution chromatographic profile was successfully optimised for the separation of the graft copolymer from the PAN-homopolymer material. It was found that the amount of PDMS incorporated into the graft molecules did not vary to a large degree as the feed ratio of PDMS was increased. Increasing PDMS feed content led to an increase in the number of graft molecules relative to homo-PAN. The series of graft material was therefore a blend of PAN-g-PDMS and homo-PAN, where the graft material increased relative to homo-PAN according to the feed ratio of PDMS to AN. The highest content PDMS graft copolymer materials, contained essentially graft molecules with very little homo-PAN. The graft copolymer molecules, however, contained approximately the same amount of PDMS grafts irrespective of the initial feed ratio. The PDMS content was found to affect the crystallisation of the PAN segments and led to a decrease in crystallinity as the PDMS content increased.

The electrospinning of these novel graft copolymer blends in DMF resulted in amphiphilic electrospinning solutions. The homo-PAN and PAN segments in the graft copolymer are soluble in DMF, but the PDMS is not. This resulted in phase separation and aggregation of the molecules in solution to produce “gel-like” electrospinning solutions. Successful electrospinning of homopolymers or homopolymer blends have been widely studied. The electrospinning of copolymers have not received as much attention, were electrospinning of amphiphilic copolymers is relatively unheard of. The nature of the solutions required a study of the electrospinning parameters and how the aggregation of the molecules affected the morphological properties of the final fibres. Conventional electrospinning is affected by various parameters including applied voltage, TCD, solution concentrations and so on. The

amphiphilic character introduces another variable affecting the fibre morphology. The “gel-like” character was found to limit the stretching of the fibres at high PDMS content, where the material was essentially PAN-g-PDMS copolymer only. The crystalline nature of the PAN segments lent additional complexity to the electrospinning of these copolymer materials. During electrospinning there is a rapid stretching of the solution jet and evaporation of the solvent, resulting in a highly non-equilibrium morphology of the fibres. The inherent phase separated and aggregated structure of the molecules in solution along with the rapid crystallisation of the PAN segments also has a dramatic influence on the fibre morphology. Together with the rapid stretching and solvent evaporation during electrospinning, the self-assembled aggregates resulted in the formation of highly porous fibres with a rough surface morphology. The rapid crystallisation helps “freeze-in” this morphology. “Fibrillar-like” morphologies were found as the rapid stretching elongated the aggregate structures aligning them in the direction of the fibre axis. The electrospinning of these novel amphiphilic solutions present a novel route to the fabrication of fully and highly porous electrospun fibres. Variation of the copolymer content can be used to vary the fibre surface morphology as well as the pore structure of the fibres. The crystallinity of the fibre fillers were shown to decrease as the PDMS content increased and interfered with the crystal packing of the PAN segments. The electrospinning procedure also led to a further decrease in the crystallinity of the copolymer material. The phase segregated morphologies and rapid electrospinning process led to lowering of the degree of crystallinity of the fibre fillers. It was shown that MWCNTs could be successfully incorporated into the electrospun fibres. Successful surface oxidation of the nanotubes allowed interaction with the PAN segments and excellent dispersion of the MWCNTs in the fibre material. The MWCNTs acted as cross-links between the molecules. This greater degree of interaction as well as the conductivity increase due to the nanotubes, allowed the production of fibres with smaller diameters and narrower diameter distributions. The nanotubes were shown to distribute themselves in the aggregated polymer solutions and undergo alignment in the direction of the fibre axis. The electrospinning process allows the alignment of nanotubes in the direction of the electrospinning jet. Unlike conventional electrospinning of homopolymers, the nanotubes in this study are situated in the aggregated polymer structures. The rapid stretching of the solution did, however, still allow for the alignment of the nanotubes in these amphiphilic solutions.

The production of reinforced silicone composites using the electrospun fibres was the final aim of this work. PAN is a strong robust, semi crystalline material often used as reinforcing fillers in its carbonised form. Distribution of the electrospun fibre in the matrix is essential in

producing reinforced composites. The synthesis of the novel copolymers was aimed at introducing a moiety that was compatible with the silicone matrix, hence the synthesis of the PAN-g-PDMS graft copolymers. It is known that PDMS tends to surface segregate due to its lower surface energy. Contact angle measurements confirmed the segregation of PDMS domains to the surface of the fibres as indicated by the increase in hydrophobicity of the fibre mats. The rough fibre micro-texture and surface nano-texture together with the PDMS hydrophobicity led to fibres with contact angles in excess of 140° . This makes these materials viable candidates for the fabrication of super-hydrophobic self-cleaning materials. MWCNTs are difficult to disperse in silicone matrices and require surface functionalisation or challenging mechanical dispersion methods. This project aimed at introducing MWCNTs into the silicone matrix indirectly, by dispersing them in the fibre fillers. Excellent dispersion in the fibre fillers was achieved as mentioned earlier. Composites reinforced with electrospun fibres have not been widely studied. Current literature results indicate improvements in tensile strength and stiffness, but a general reduction in strain properties. Depending on the fibre material and arrangement in the silicone, it was possible to obtain composites with vastly improved mechanical properties in this study.

Composites containing aligned fibre mats and non-woven fibre mats were successfully obtained using a rotating and static collectors respectively. The collected fibre mats were removed from the collectors and impregnated into uncured silicone resin. Excellent dispersion of the nanofibres throughout the silicone matrix was achieved. The PDMS components as well as the nature of the uncured resin allowed facile dispersion of the fibres in the silicone matrix. The composite properties were found to be affected by a number of factors. The increase in PDMS content led to a general increase in the mechanical properties, due to increased dispersion and interaction with the silicone matrix. At the higher PDMS contents properties were shown to decrease. This is attributed to the increase in PDMS content, which is a weak soft amorphous material. The PDMS content was also shown to disrupt the crystallisation of the PAN segments, leading to fibres with decreased crystallinity. Finally, as the PDMS content increased a corresponding increase in the fibre diameter was obtained. Larger fibre diameters lead to decreased fibre filler surface area. The decrease in interfacial area also contributes to the decrease in mechanical properties observed for the high PDMS content fibres.

One of the most significant results was that of the differences between the aligned and non-woven fibre fillers. The aligned fibres showed dramatic improvements in stiffness and tensile strength, however, the strain at break was lower than that of the unfilled silicone. This result is in line with those from literature. The non-woven composites showed a highly significant

result, where it was possible to obtain simultaneous increases in the stiffness, strength and elongation at break. Increases in strain at break of up to 470 % were obtained. This was shown to be as a result of the arrangement of the fibres in the silicone matrix, allowing continuous fibre failure and replacement as the matrix failed. The failure mechanism of the non-woven silicone composite was shown to exhibit multiple fracture sites along the entire sample specimen. The fibres were shown to prevent complete failure at the multitude of fracture zones, allowing a dramatic increase in the elongation at break. The fibres also displayed necking and yielding mechanisms along with a large amount of fibre “pull-out” from the silicone matrix. The necking and yielding was found to increase with PDMS content, due to an increase in the ductility of the material. The porous nature of the fibres allowed the deformation of the fibres via stress concentration and deformation of the network assembled fibre material between the pores. All these factors contributed to the dramatically enhanced strain properties of these materials, which are not often seen in literature. The aligned fibres appeared to fail inside the silicone matrix, prior to failure of the elastomeric matrix. The uniaxial arrangement of the fibres, allowed dramatic increases in the stiffness and strength, but failed swiftly at approximately the same time resulting in less fibre deformation and “pull-out” from the matrix. The nanotubes were found to increase the stiffness of the fibre fillers as well as the strength. Nanotube filled non-woven composites still showed excellent strain properties, although not as high as for the unfilled analogues.

In summation, the production of the novel copolymer fibre precursors was successfully achieved. The nature of the amphiphilic copolymers were found to have a dramatic effect on the electrospinning of these materials, allowing the production of highly porous fibres. MWCNTs were shown to be well distributed throughout the electrospun fibre fillers. The nanotubes allowed the production of fibres with decreased diameters, and still aligned in the direction of the electrospun fibre axis. The fibres were shown to disperse well in the silicone matrix and indirectly disperse the nanotubes thoroughly throughout the matrix. Enhanced properties were achieved by the introduction of these novel copolymer fibres, with the most significant improvement being that of the elongation at break for the non-woven mat filled silicone composites.

6.2 Prospects for future work

Certain aspects of this study open the door to additional investigations feasible for future projects. The electrospinning of amphiphilic copolymers is one of the avenues to be studied. The field of electrospinning is extremely wide, however, the electrospinning of copolymers

with covalently bonded moieties is a relatively new area. Amphiphilic graft copolymers are themselves a relatively unstudied field, which is gaining in importance at the moment. The self-assembling ability of amphiphilic materials (network structures, micelles, lysosomes, etc.) lend them applications in the field of medicinal/drug release and micro-reactor chemistry. Electrospinning is currently being studied for applications in tissue scaffolding and wound dressings. Combining the self-assembling nature of amphiphilic copolymers with the production of electrospun fibres allows one to tailor make fibres with a plethora of morphologies. These factors make this a field that justifies further research and development in the production of cutting edge materials capable of improving on existing ones. The ability to produce fibres that have the encapsulation and slow drug release mechanism inherent to the structure of existing amphiphilic materials is an exciting area with viable medical applications.

The inclusion of MWCNTs in the case of this project was to study whether these fillers could be incorporated successfully into the silicone matrices using the electrospun fibres as carriers. The reinforcement effect of these materials was then studied. It would, however, be remiss not to mention the conductive properties of the MWCNTs. MWCNTs are widely used in the production of conductive polymer materials. Their high aspect ratios mean that very little material is needed to impart conductivity to conventionally insulating materials. This lends a multitude of applications in the field of smart polymer composites. It has already been shown in literature that one can produce composites capable of being used as gas, pressure and tension sensors. The materials in this project present a possible route to the production of **flexible and conductive silicone composites**. Possible applications of this material in the sensor field are wide. Nanotubes are difficult to disperse well in silicone matrices, but this indirect technique presents a facile route to obtain aligned MWCNTs in a silicone matrix. Preliminary studies were performed on these materials, however, with limited success. The main challenges in this regard relate to the modification and fabrication of the composites. Firstly, the severe surface oxidation treatment of the nanotubes leads to damaging of the nanotube network structure and π -conjugation sequence which is the source of the conductivity. The surface oxidation and sonication prior to electrospinning solution preparation, also leads to shearing of the MWCNTs and a lowering in the aspect ratios. The excellent interaction of the nanotubes with the matrix also results in an increase in the percolation threshold, as the nanotubes are “wrapped closely” in insulating polymer material. Finally the alignment of nanotubes during electrospinning induces a level of order in the MWCNT arrangement and a decrease in contacts between adjacent fillers. All these factors result in an increase in the percolation threshold and very low conductivities. It must

be mentioned that films of the materials in this study (loaded with nanotubes, 8 wt%) were shown to be conductive, but the electrospun fibres were not as successful. Investigation of conductivity still warrants further study due to the possible excellent applications. The materials also need to be optimised in this regards, where the filler loading should be varied along with the modification procedures. Less severe surface modification procedures can be followed. The sonication time can be shortened/optimised. Nanotubes with higher aspect ratios (longer nanotubes) should also be studied as alternatives to the nanotubes in this project. The work in this project has shown that fibres with high MWCNT content (32 wt%) can be successfully electrospun. Increasing the amount of nanotubes in the electrospun fibres can definitely aid in reducing the percolation threshold and achieving conductive composite materials. High nanotube loadings, although not affecting the mechanical properties to a significant extent, allow one to drastically increase the number of contacts between adjacent nanotubes in the electrospun fibre. It is clear that slight optimisation of the techniques presented in this project can enable the production of flexible, conductive silicone composites with excellent mechanical properties (including outstanding strain and toughness values).

Appendix A

Appendix A

Appendix A

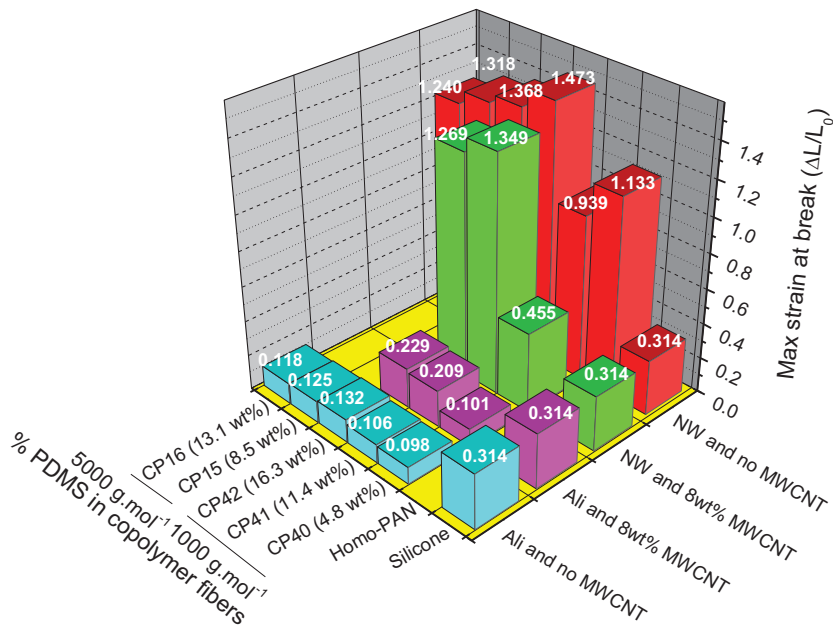


Figure A.1: Maximum strain at break ($\Delta L/L_0$) (ϵ_{max}) for the various composites, where the x-axis represents the PDMS content variation and the y-axis represents the filled, unfilled, non-woven and aligned fibre composites.

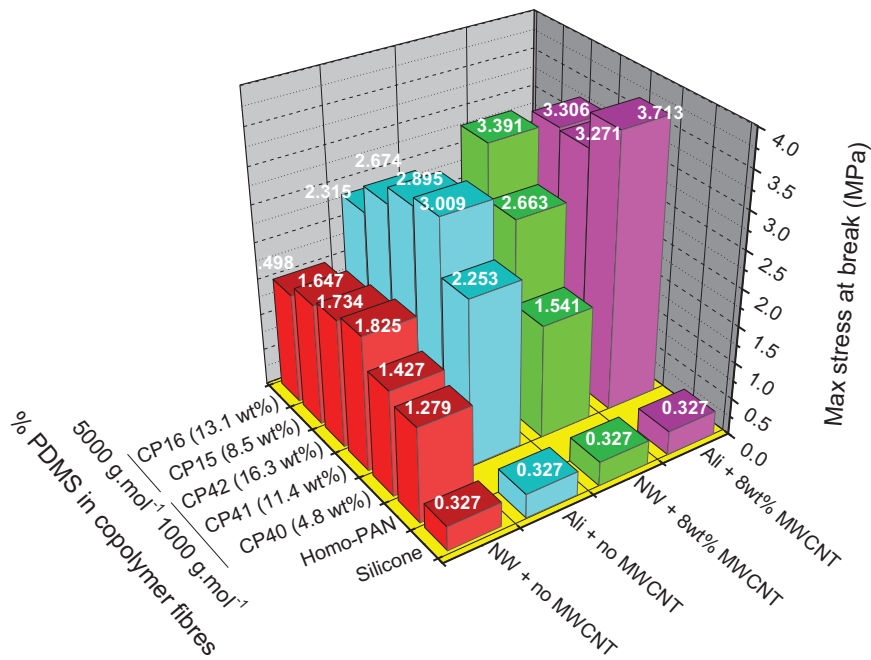


Figure A.2: Maximum stress at break (σ_{max}) (MPa) for the various composites, where the x-axis represents the PDMS content variation and the y-axis represents the filled, unfilled, non-woven and aligned fibre composites.

Appendix A

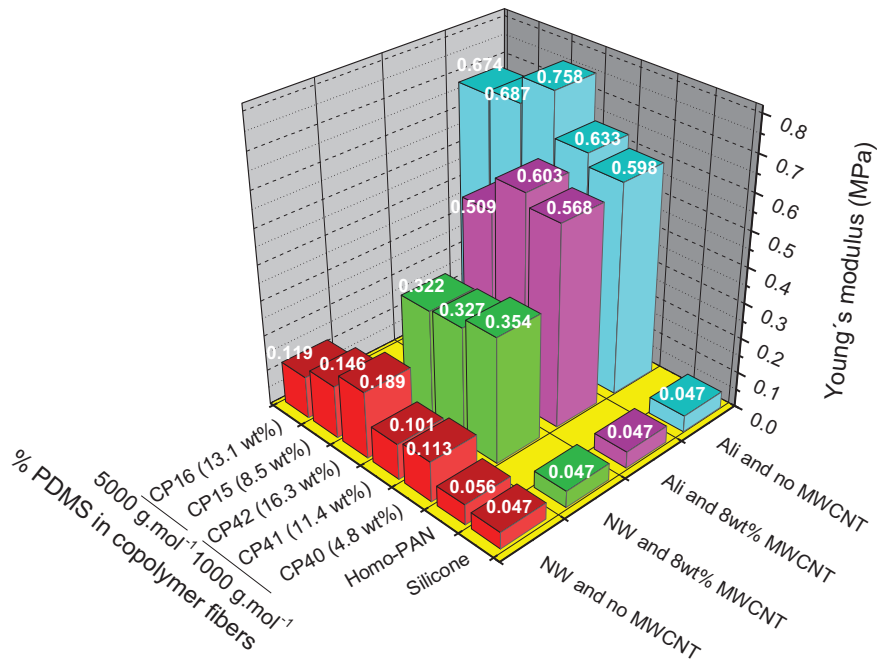


Figure A.3: Young's modulus or stiffness (E) (MPa) for the various composites, where the x-axis represents the PDMS content variation and the y-axis represents the filled, unfilled, non-woven and aligned fibre composites.

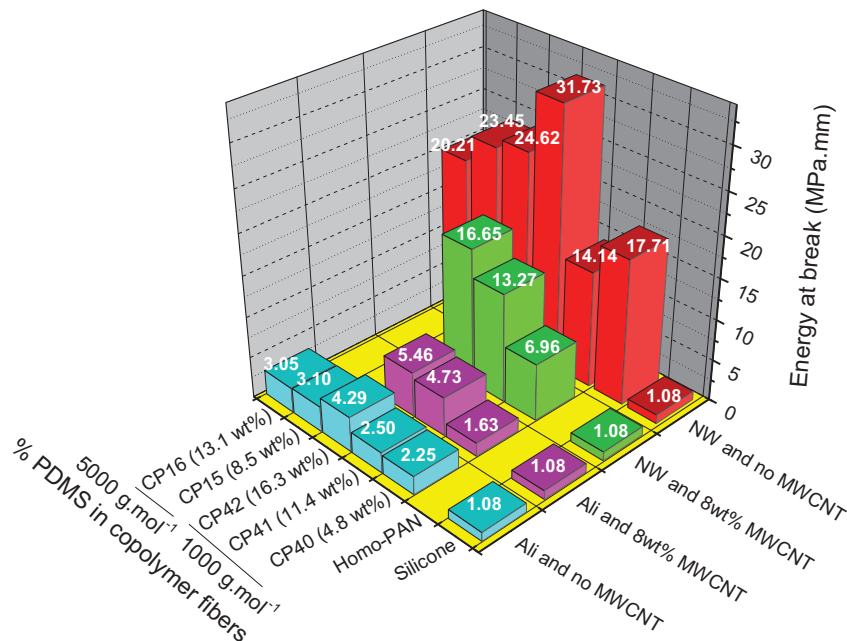


Figure A.4: Maximum energy (toughness) at break (J) for the various composites, where the x-axis represents the PDMS content variation and the y-axis represents the filled, unfilled, non-woven and aligned fibre composites.

Appendix A

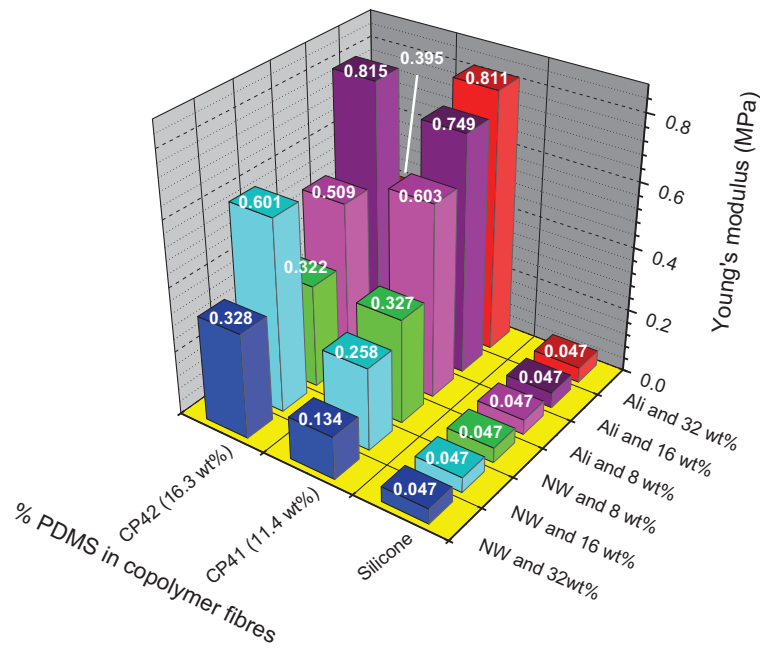


Figure A.5: Young's modulus (stiffness) (MPa) for the various composites, where the x-axis represents the PDMS content variation and the y-axis represents the MWCNT filled (8 wt%, 16 wt% and 32 wt%) non-woven and aligned fibre composites.

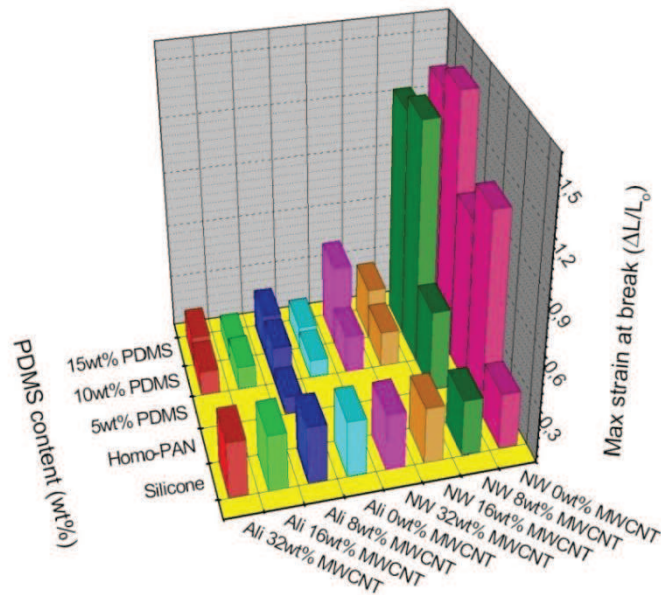


Figure A.6 : Maximum strain at break ($\Delta L/L_0$) (ϵ_{max}) for the various MWCNT containing composites, where the x-axis represents the PDMS content variation and the y-axis represents the various MWCNT filled, non-woven and aligned fibre composites.

Appendix A

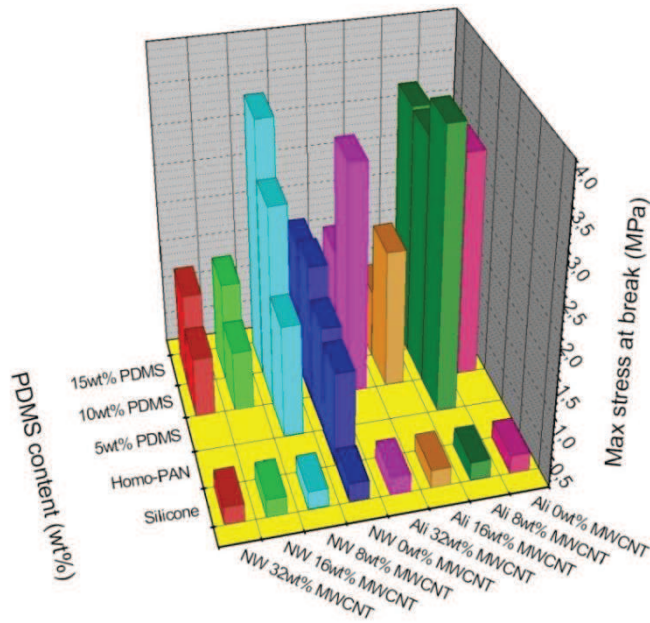


Figure A.7 : Maximum stress at break (σ_{max}) (MPa) for the various MWCNT containing composites, where the x-axis represents the PDMS content variation and the y-axis represents the various MWCNT filled, non-woven and aligned fibre composites.

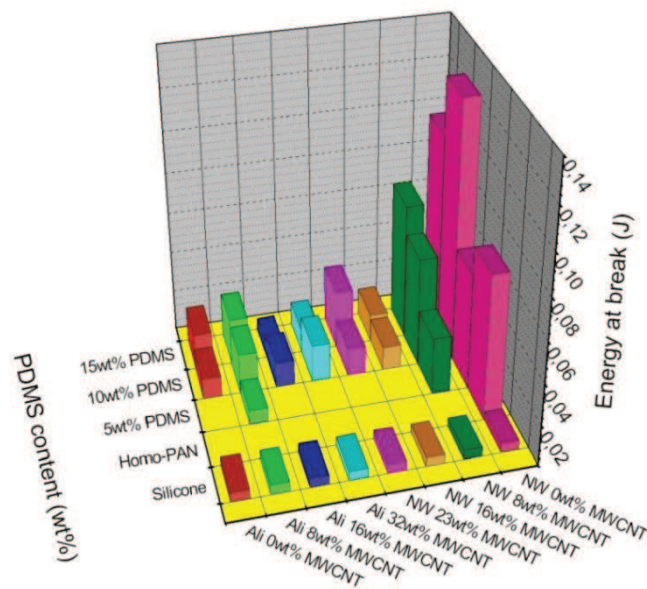


Figure A.8 : Maximum energy (toughness) at break (J) for the various MWCNT containing composites, where the x-axis represents the PDMS content variation and the y-axis represents the various MWCNT filled, non-woven and aligned fibre composites.

Appendix A

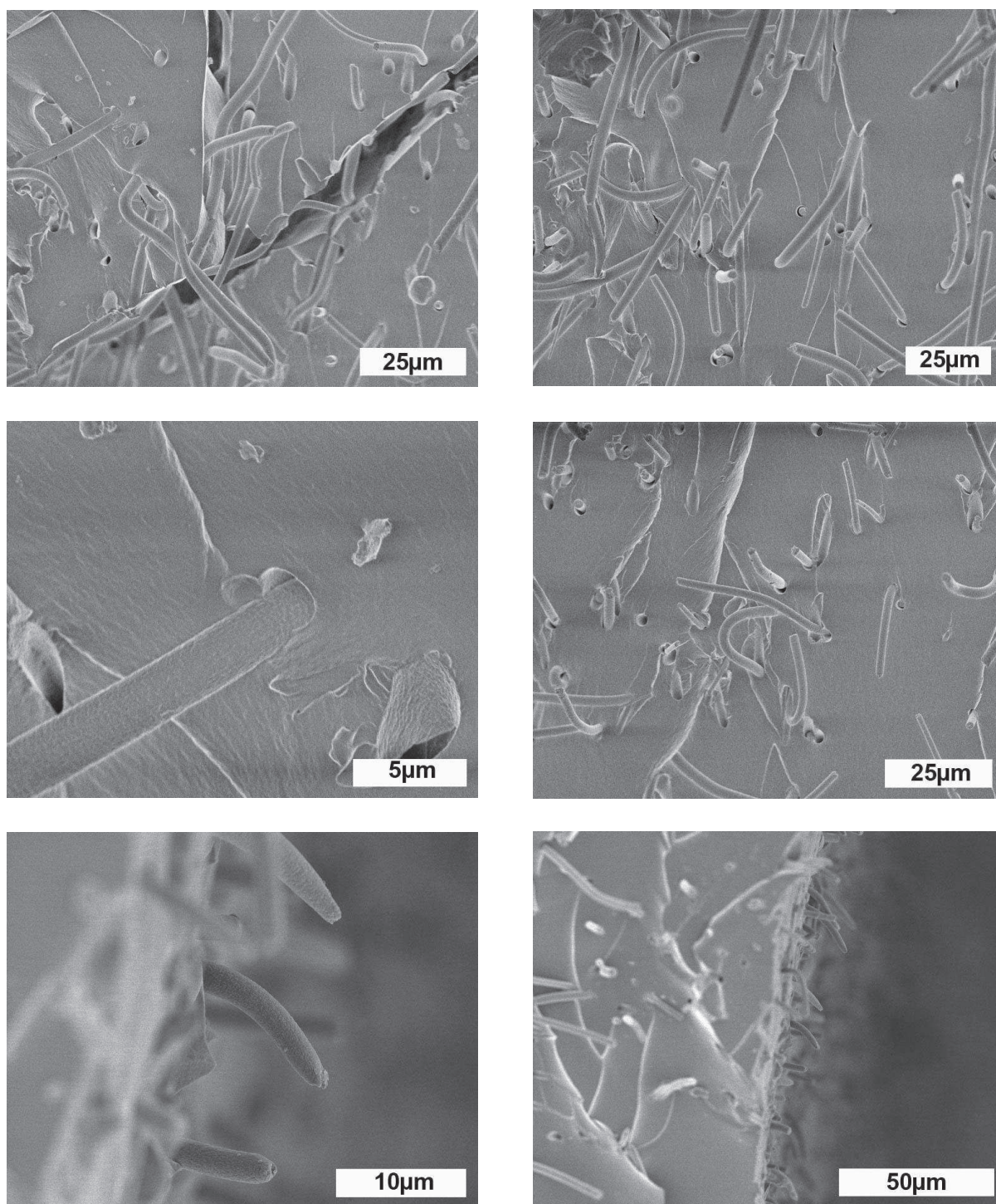


Figure A.9 : FE-SEM images of the tensile fracture surface of 4.8 wt% ($1000 \text{ g}\cdot\text{mol}^{-1}$) PDMS content non-woven fibre filled silicone composites.

Appendix A

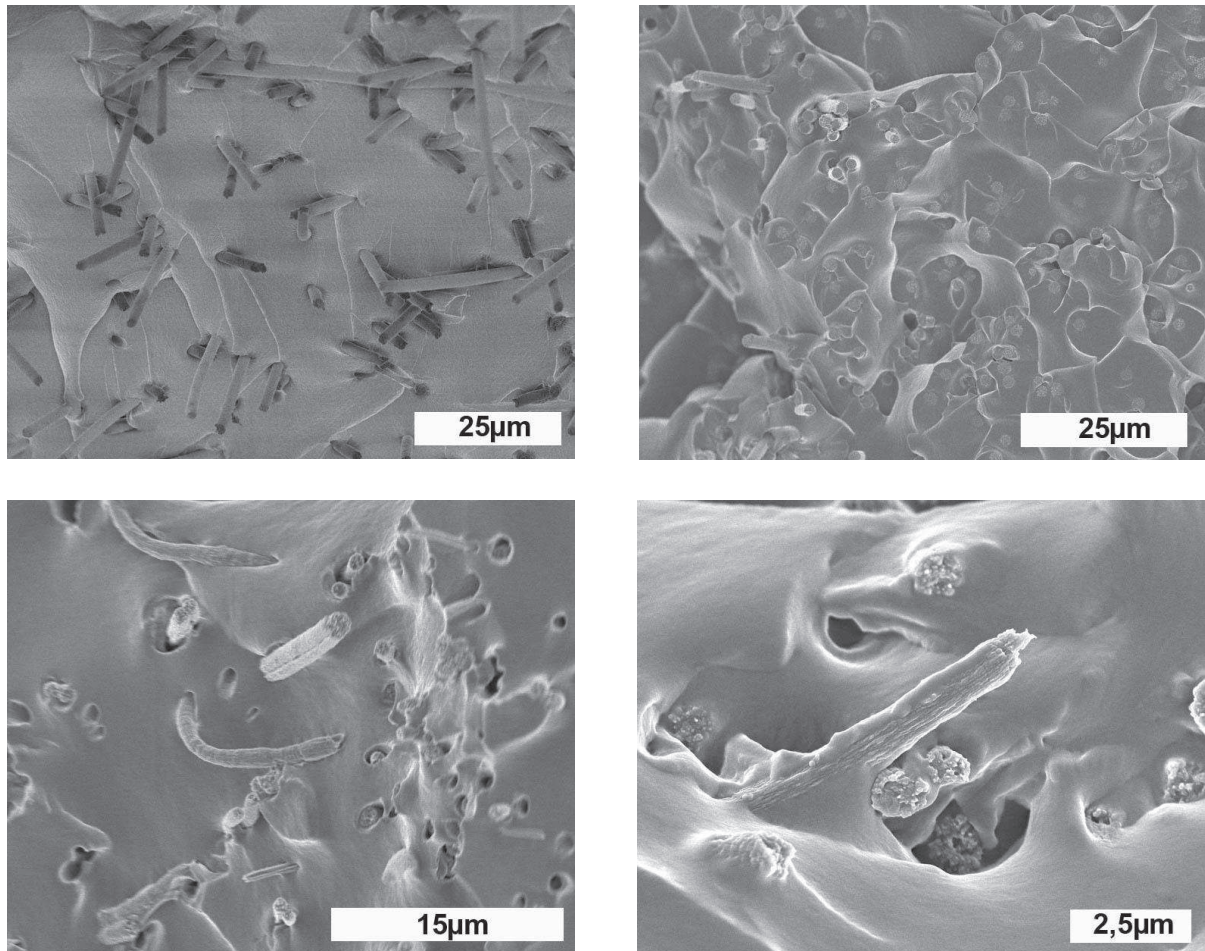


Figure A.10 : FE-SEM images of the tensile fracture surface of 4.8 wt% ($1000 \text{ g}\cdot\text{mol}^{-1}$) PDMS content aligned fibre filled silicone composites.

Appendix A

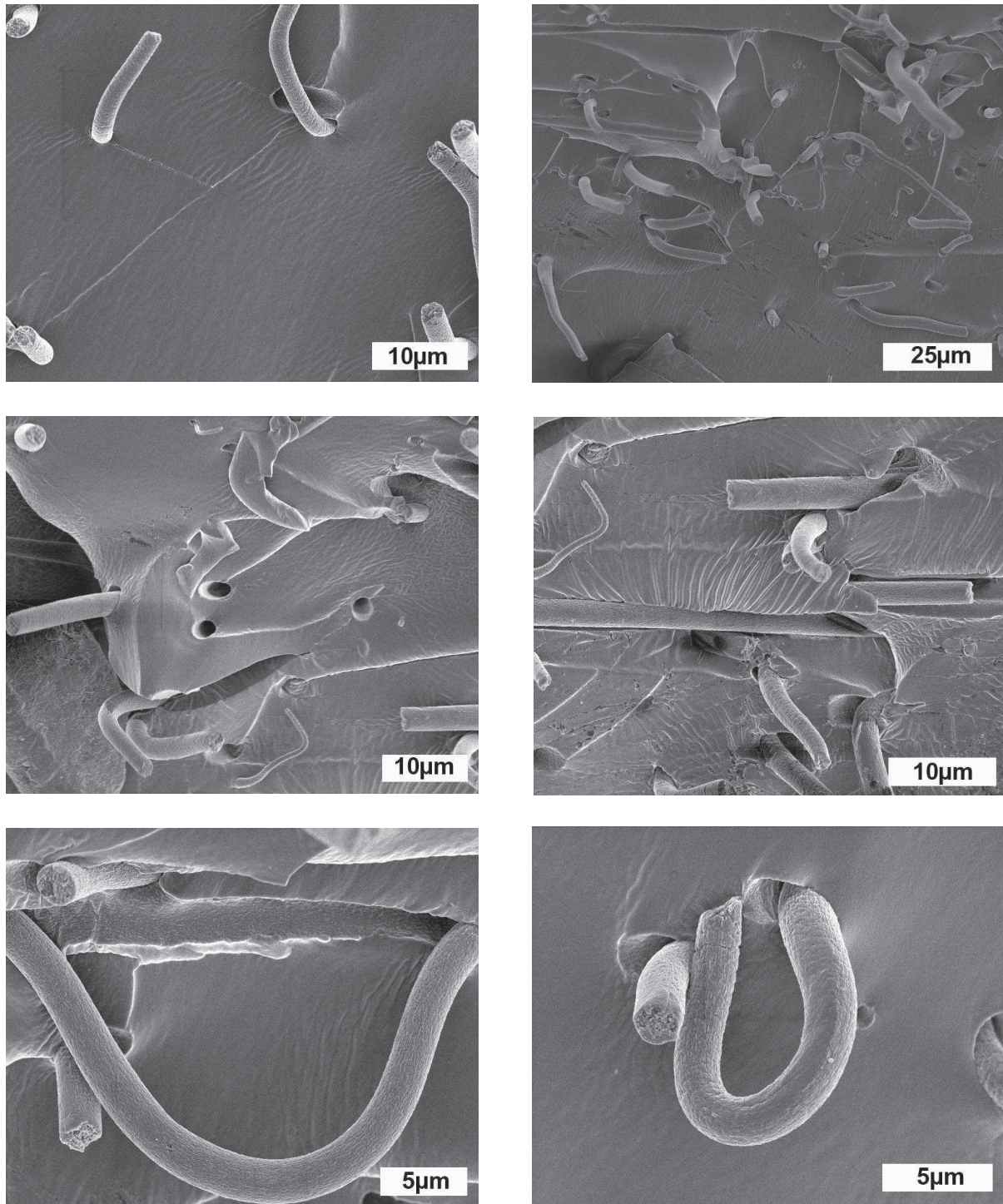


Figure A.11 : FE-SEM images of the tensile fracture surface of 11.4 wt% (1000 g.mol⁻¹) PDMS content non-woven fibre filled silicone composites.

Appendix A

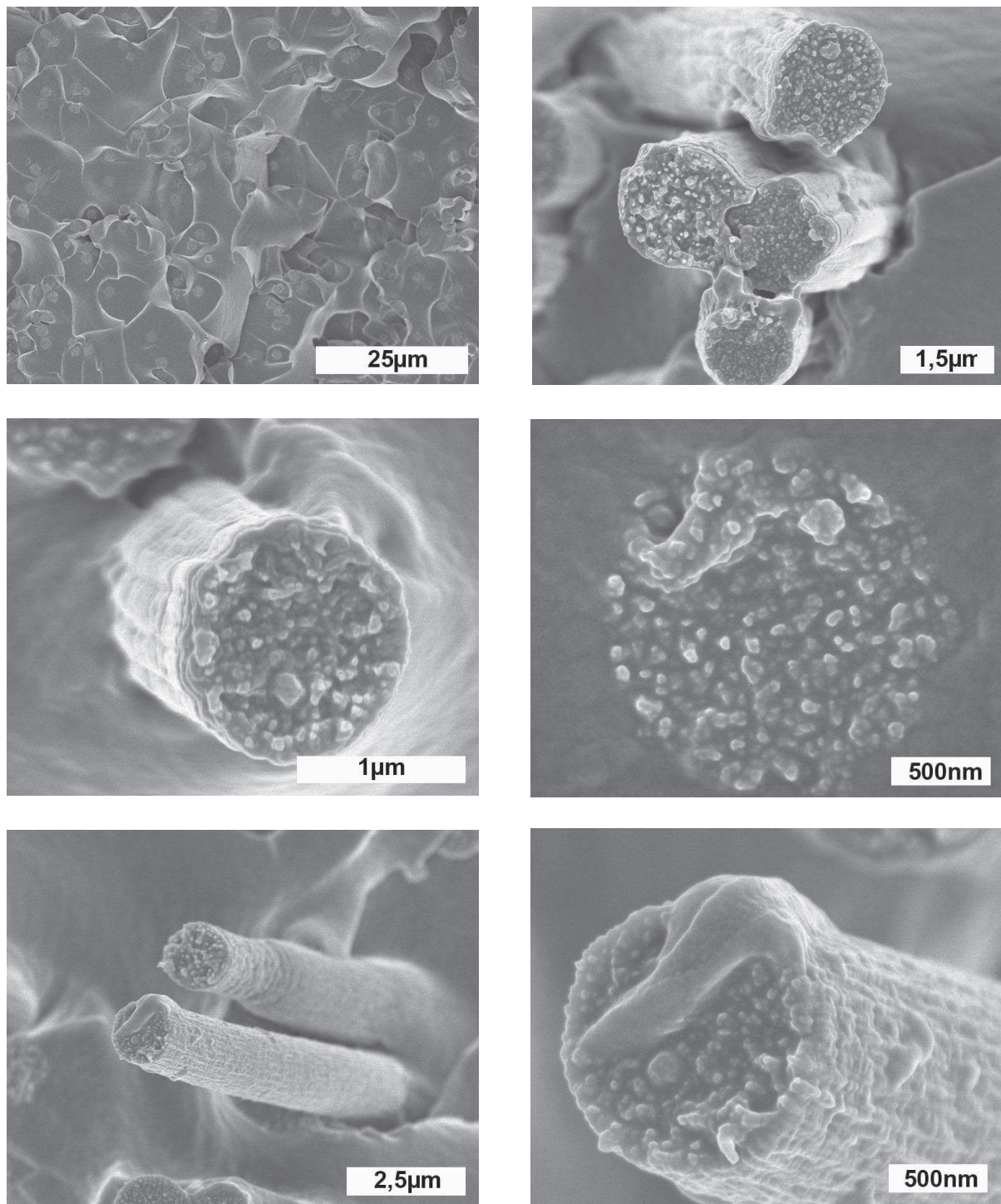


Figure A.12 : FE-SEM images of the tensile fracture surface of 11.4 wt% (1000 g.mol⁻¹) PDMS content aligned fibre filled silicone composites.

Appendix A

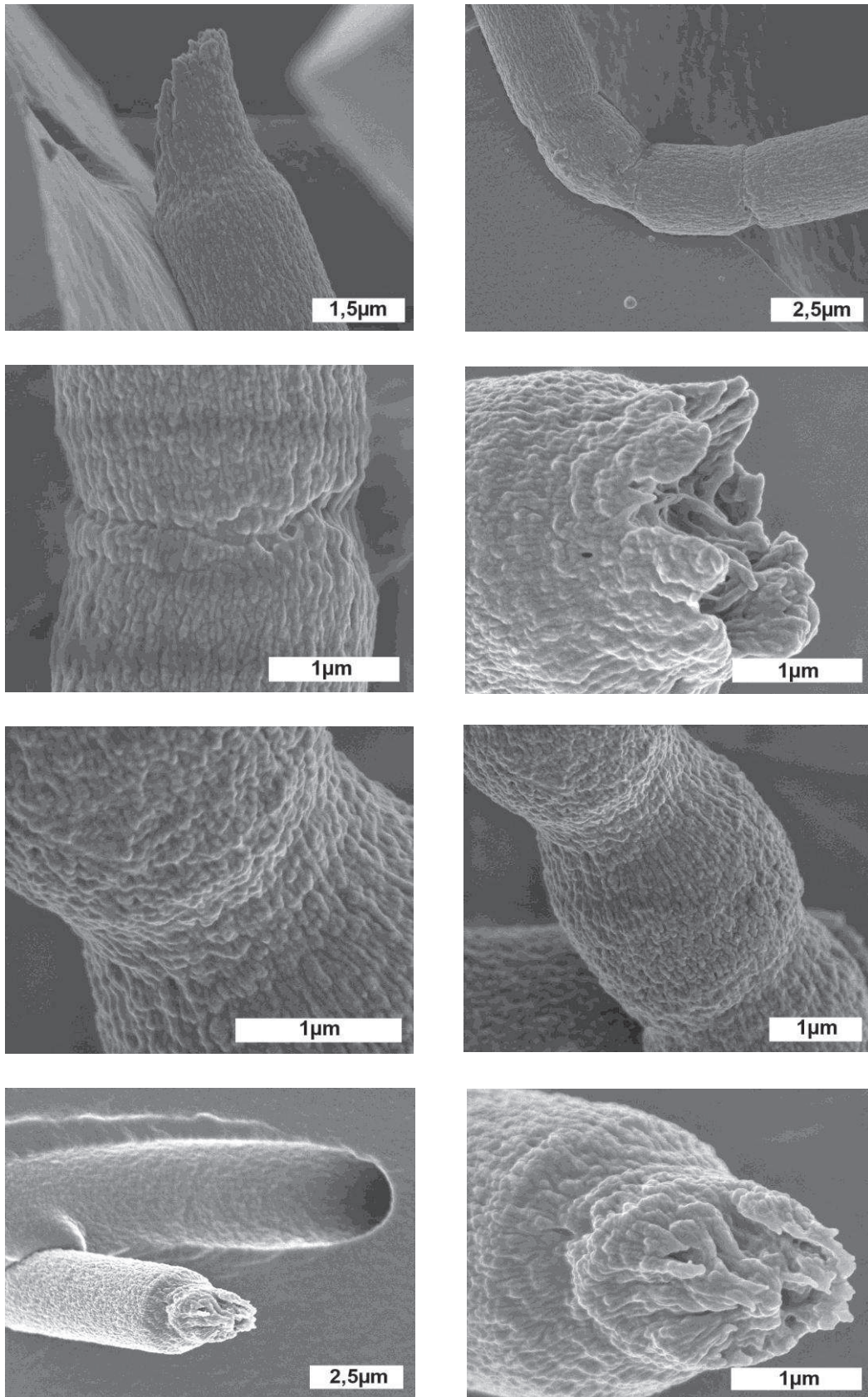


Figure A.13 : FE-SEM images of the tensile fracture surface of 16.3 wt% (1000 g.mol^{-1}) PDMS content non-woven fibre filled silicone composites.

Appendix A

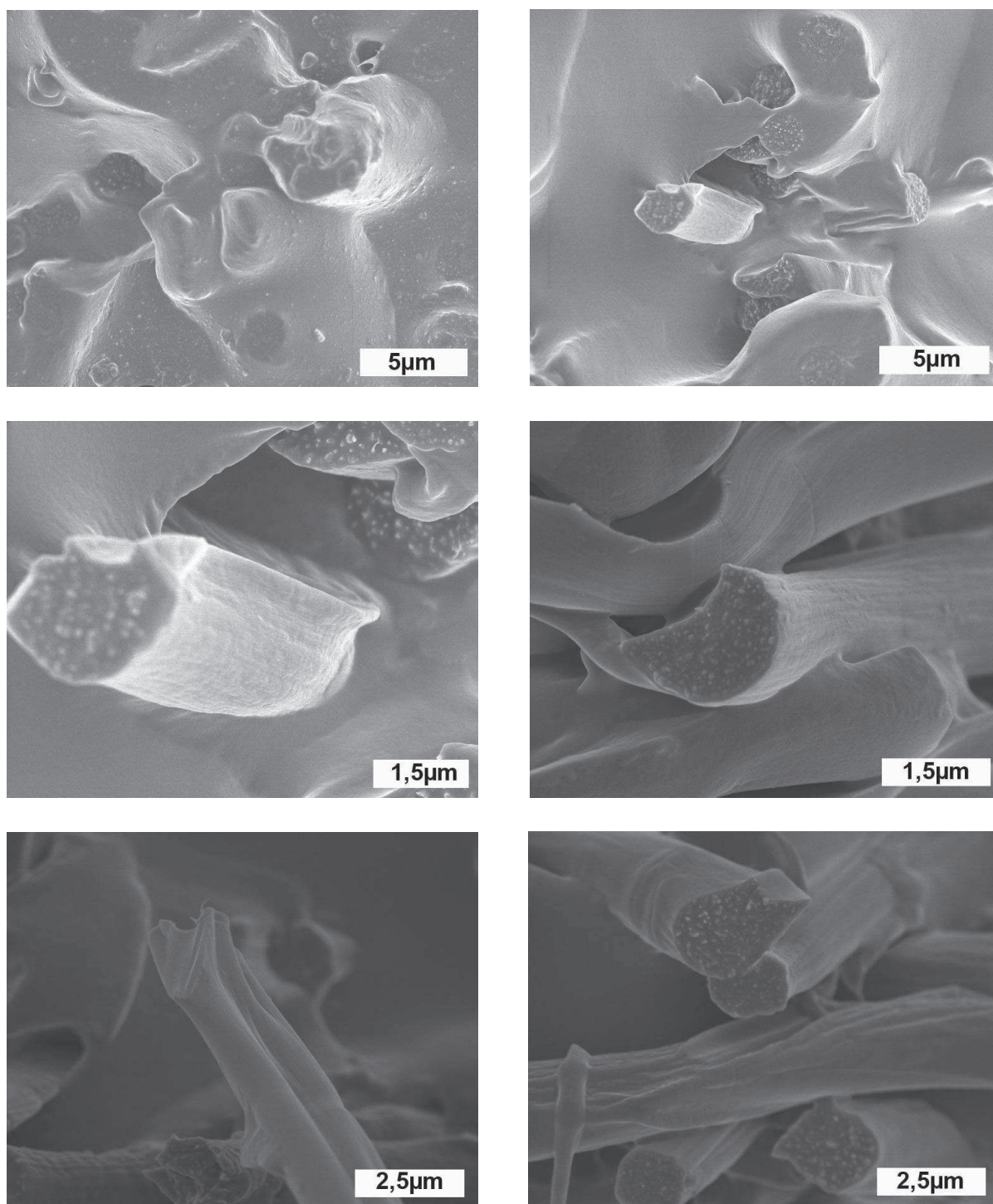


Figure A.14 : FE-SEM images of the tensile fracture surface of 11.4 wt% (1000 g.mol⁻¹) PDMS content aligned fibre filled silicone composites.

Appendix A

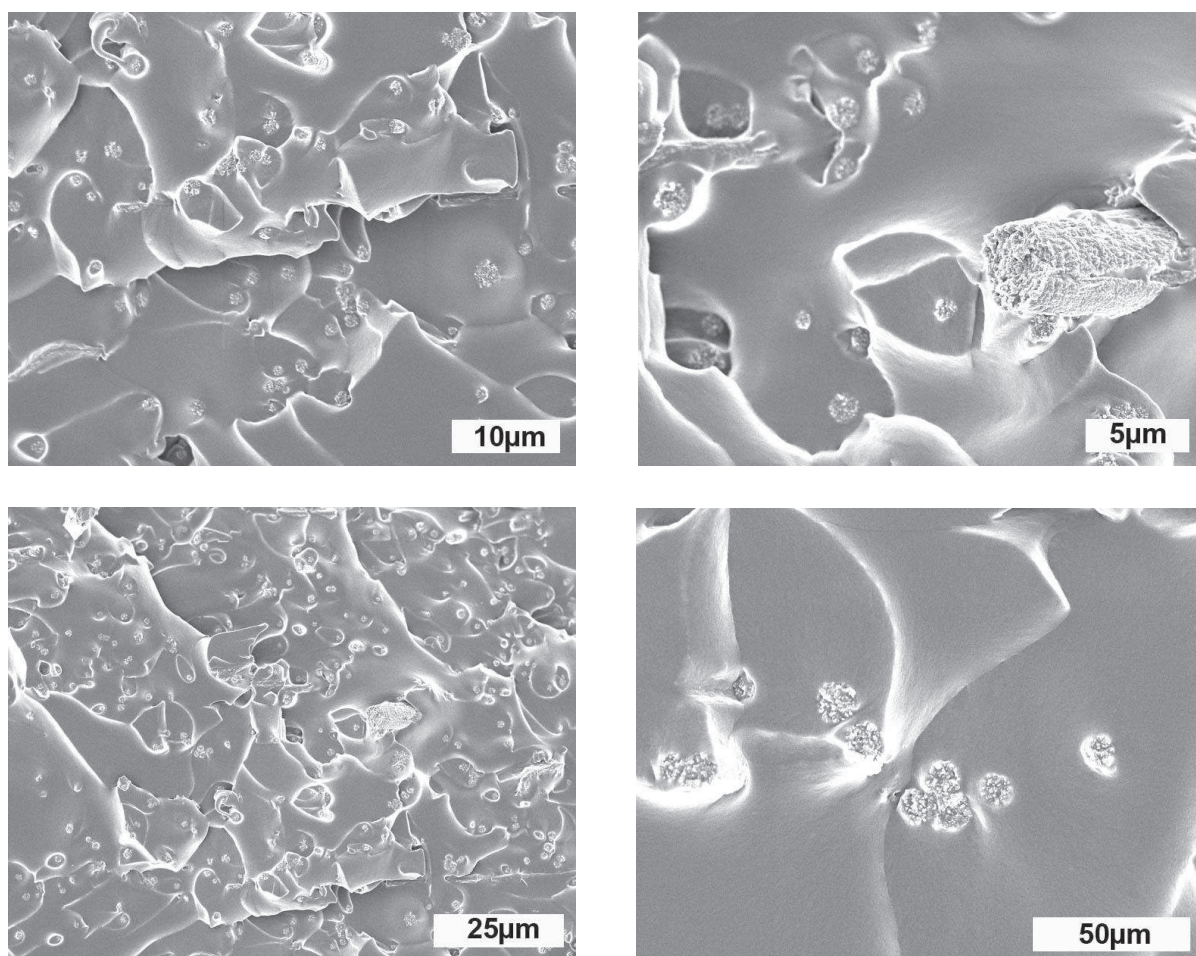


Figure A.15 : FE-SEM images of the tensile fracture surface of 4.8 wt% ($1000 \text{ g}\cdot\text{mol}^{-1}$) PDMS content non-woven fibre filled silicone composite (with 8 wt% MWCNTs in the fibres).

Appendix A

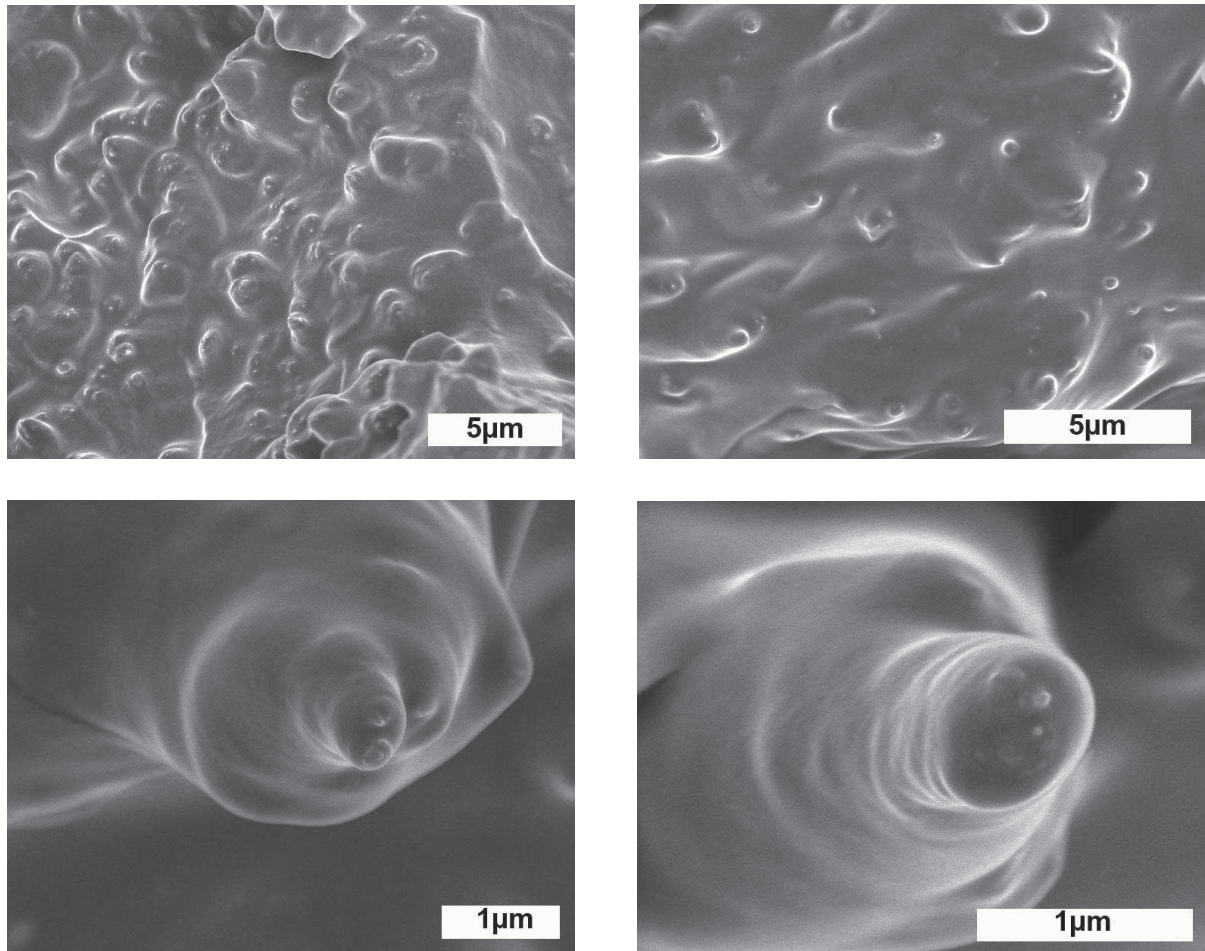


Figure A.16 : FE-SEM images of the tensile fracture surface of 4.8 wt% ($1000 \text{ g}\cdot\text{mol}^{-1}$) PDMS content aligned fibre filled silicone composite (with 8 wt% MWCNTs in the fibres).

Appendix A

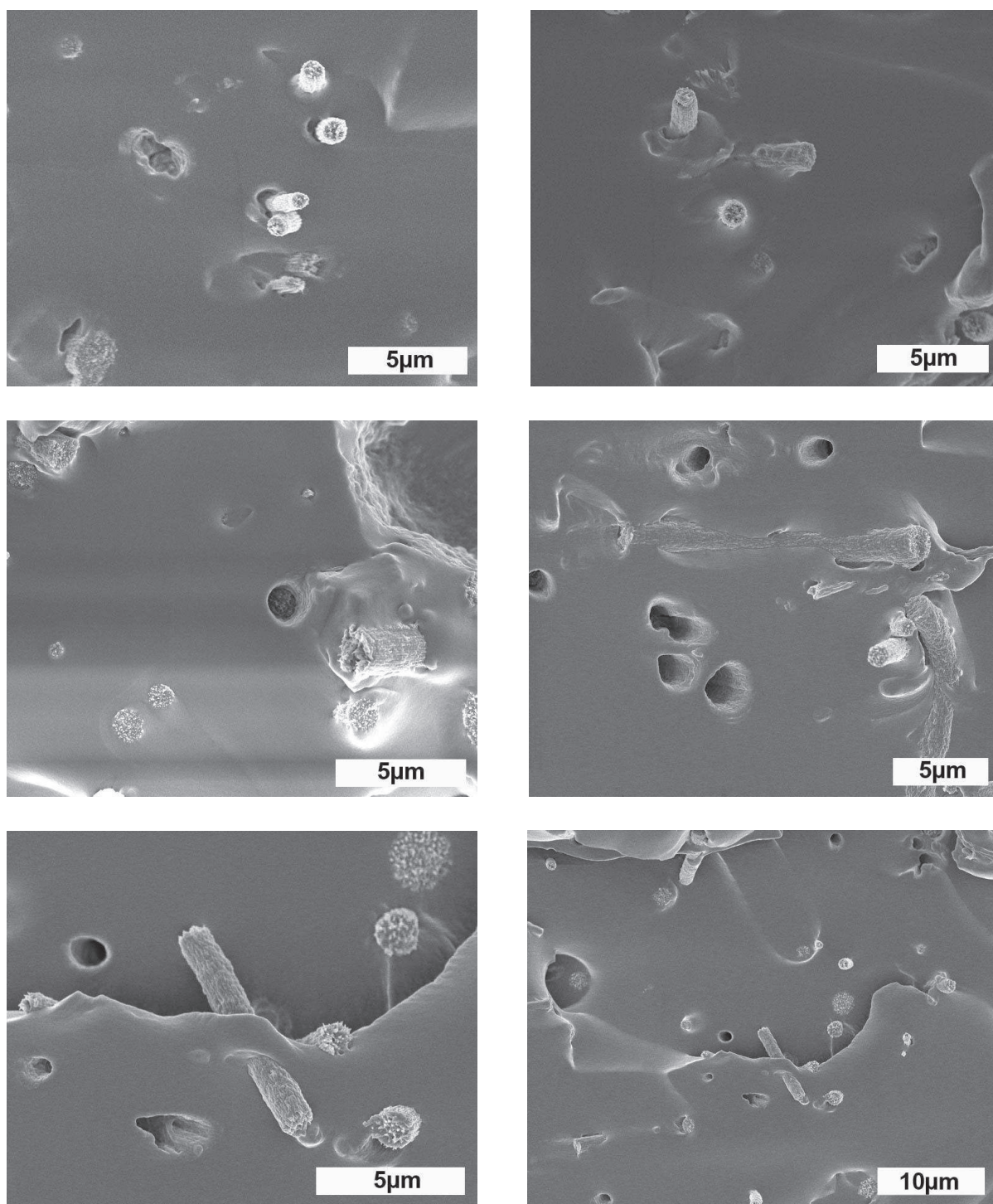


Figure A.17 : FE-SEM images of the tensile fracture surface of 11.4 wt% ($1000 \text{ g}\cdot\text{mol}^{-1}$) PDMS content non-woven fibre filled silicone composite (with 8 wt% MWCNTs in the fibres).

Appendix A

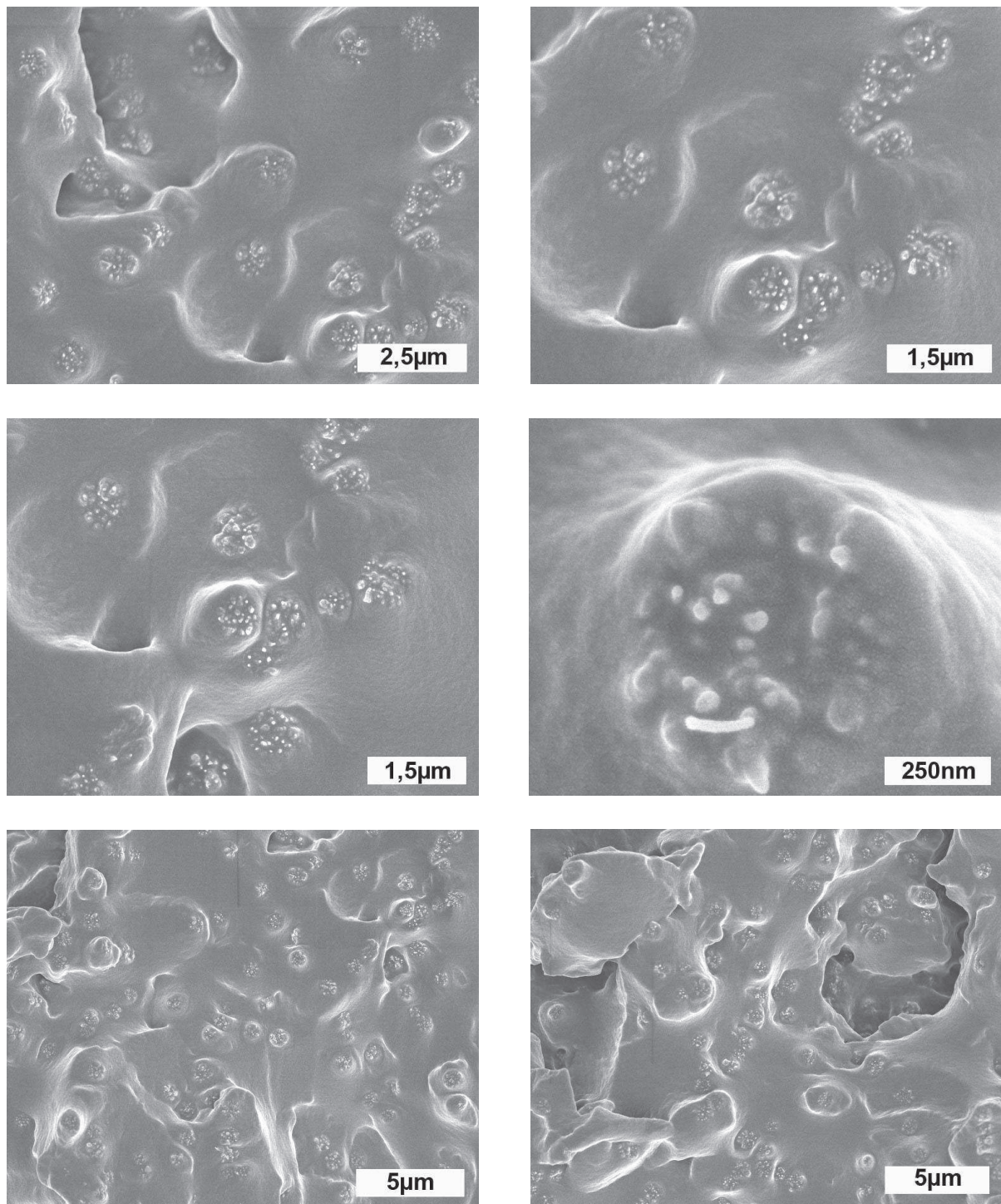


Figure A.18 : FE-SEM images of the tensile fracture surface of 11.4 wt% ($1000 \text{ g}\cdot\text{mol}^{-1}$) PDMS content aligned fibre filled silicone composite (with 8 wt% MWCNTs in the fibres).

Appendix A

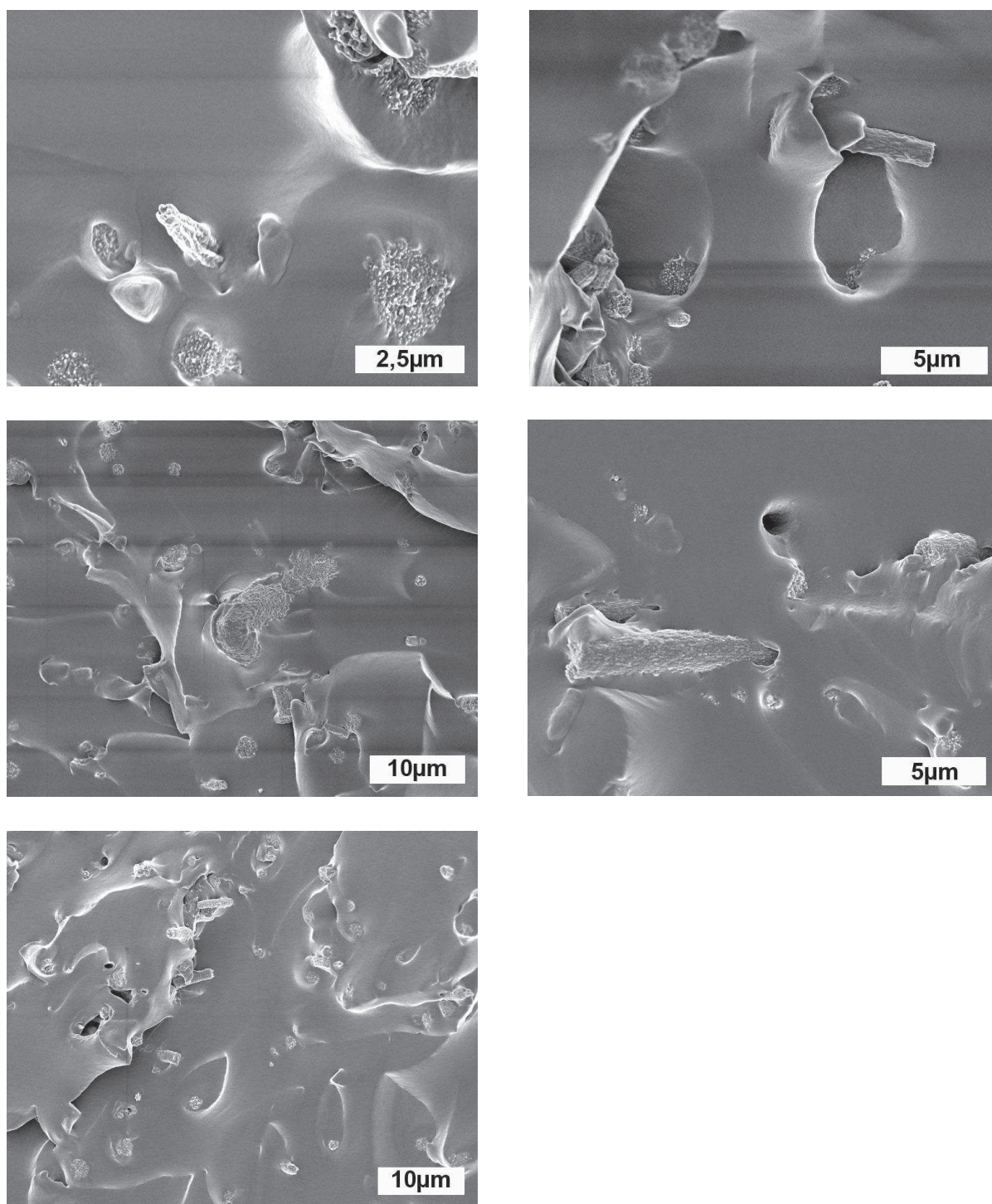


Figure A.19 : FE-SEM images of the tensile fracture surface of 16.3 wt% ($1000 \text{ g}\cdot\text{mol}^{-1}$) PDMS content non-woven fibre filled silicone composite (with 8 wt% MWCNTs in the fibres).

Appendix A

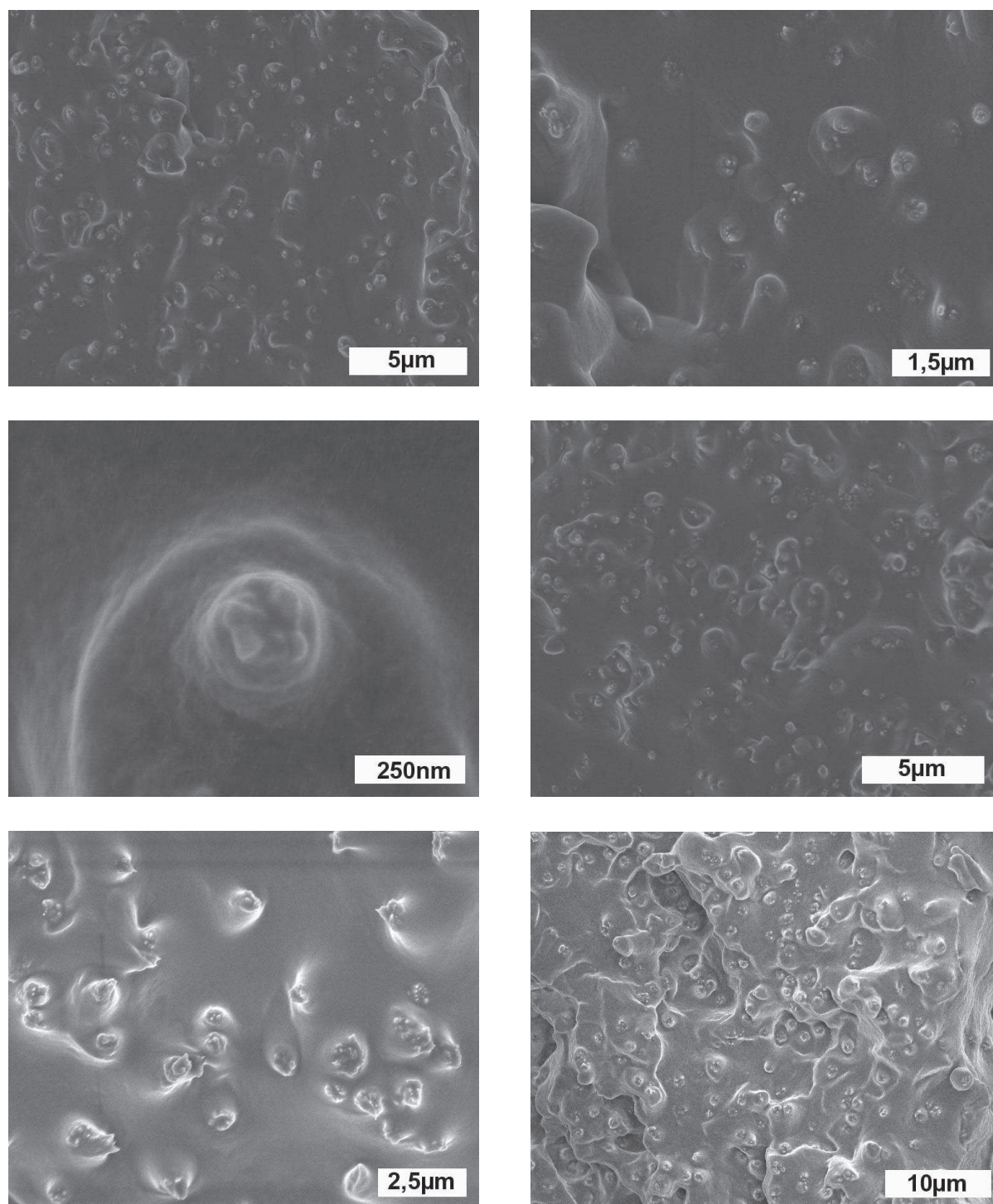


Figure A.20 : FE-SEM images of the tensile fracture surface of 16.3 wt% (1000 g.mol^{-1}) PDMS content aligned fibre filled silicone composite (with 8 wt% MWCNTs in the fibres).